Controlled/living Radical Polymerization of Multi-vinyl Monomer towards Hyperbranched Polymers for Biomedical Applications

Tianyu Zhao, BA, MA

UCD student number: 13209378

The thesis is submitted to University College Dublin in fulfilment of the requirements for the degree of Doctor of Philosophy

Charles Institute of Dermatology

School of Medicine and Medical Science

Head of School: Professor Patrick Murray

Principal Supervisor: Doctor Wenxin Wang

May/2015

TABLE OF CONTENTS

Table of Contents……..ii

List of Appendices……..vii

List of Figures…….....viii

List of Tables…….xvii

Acknowledgements……xix

Abbreviations……..xx

Abstract ……....xxiv

Statement of Original Authorship…….xxv

Chapter One Introduction.....1

1.1 Controlled/living Radical Polymerization 2

1.1.1 Free Radical Polymerization.....2

1.1.2 Controlled/living Radical Polymerization 4

1.2 Atom Transfer Radical Polymerization.....11

1.2.1 From ATRA to ATRP 12

1.2.2 Mechanism of ATRP 12

1.2.3 ISET vs OSET.....14

1.2.4 Components and Kinetics 15

1.2.5 ATRP Initiation Systems 17

1.2.6 Deactivation Enhanced ATRP.....21

1.3 Hyperbranched Polymers.....28

1.3.1 Concept and History 28

1.3.2 Degree of Branching.....31

1.3.3 Synthesis Methodology of HBP.....33

1.3.4 Biomedical Application of HBP 46

1.4 Aims and Objectives of This Thesis 55

1.5 References.....56

Chapter Two Optimizing Atom Transfer Radical Addition towards Good Kinetical Control of Homopolymerization of Multi-vinyl Monomers 73

2.1 Introduction 74

2.1.1 Atom Transfer Radical Addition 74

2.1.2 Effect of Kinetical Control on Polymer Architecture 77

2.2 Experimental 82

2.2.1 Materials 82

2.2.2 Characterization Method 82

2.2.3 Reaction Procedure 83

2.3 Results and Discussions 85

2.3.1 Evaluation of Different ATRA Systems 85

2.3.2 Synthesis and Characterization of HBPs through the *in situ* DE-ATRA System 98

2.4 Conclusions 106

2.5 References 107

Chapter Three Controlled Homopolymerization of Multi-vinyl Monomer through Vinyl Oligomer Combination as a Universal Approach to Hyperbranched Architectures 110

3.1 Introduction 111

3.1.1 Previous Methods to Synthesize HBPs 111

3.1.2 Polymerization Mechanism 112

3.1.3 Preparation of Hyperbranched Polymers via *in situ* DE-ATRP Method 116

3.2 Experimental 117

3.2.1 Materials 117

3.2.2 Characterization method 117

3.2.3 Reaction Procedure 118

3.3 Results and Discussions 120

3.3.1 Evaluation of *in situ* DE-ATRP of Methyl Acrylate 120

3.3.2 Homopolymerization of BDA via *in situ* DE-ATRP 122

3.3.3 Homopolymerization of Other Divinyl Monomers 138

3.3.4 Homopolymerization of a Disulfide Divinyl Monomer towards a Reductively Degradable HBP 140

3.3.5 Discussions 148

3.4 Conclusions 150

3.5 References 151

Chapter Four Synthesis of Water Soluble PEG-based Hyperbranched Polymers through Vinyl Oligomer Combination towards Biocompatible Hydrogels 155

4.1 Introduction 156

4.1.1 Hydrogels for Wound Healing 156

4.1.2 PEG-based Hydrogels 157

4.1.3 Aims and Hypotheses 160

4.2 Experimental 162

4.2.1 Materials 162

4.2.2 Synthesis of Hyperbranched Poly(PEGDA)s 162

4.2.3 Characterization Method 162

4.2.4 Preparation of Photo-crosslinked Hydrogels 163

4.2.5 Cytotoxicity Assessment 164

4.2.6 Statistical Analysis 164

4.3 Results and Discussions 164

4.3.1 Synthesis and Characterization of The PEG-based HBPs 164

4.3.2 Thermoresponsive Behavior of Poly($PEGDA_{575}$) 174

4.3.3 Photo-crosslinked Hydrogels and Cytotoxicity Assessment 177

4.4 Conclusions 179

4.5 References 179

Chapter Five Synthesis of Highly Branched Degradable Functional Poly(dimethylaminoethyl methacrylate-co-bis(2-acryloyl)oxyethyl disulphide) as Efficient Gene Vector 182

5.1 Introduction 183

5.1.1 Poly(dimethylaminoethyl methacrylate) Based Polymers as Gene Vectors 183

5.1.2 Aims and Hypotheses 184

5.2 Experimental 185

5.2.1 Materials 185

5.2.2 Preparation of The Bis(2-acryloyl)oxyethyl Disulfide (DSDA) Monomer 185

5.2.3 Synthesis and Functionalization of The Poly(DMAEMA-co-DSDA) (PD-DS) Polymers 186

5.2.4 Polymer Characterization Method 186

5.2.5 Polyplex Characterization 187

5.2.6 Cell Culture 187

5.2.7 Luciferase Transfection and AlamarBlue® Reduction 188

5.2.8 Green Fluorescent Protein (GFP) Expression 189

5.2.9 Statistical Analyses 189

5.3 Results and Discussions 190

5.3.1 Synthesis and Characterization of The Poly(DMAEMA-co-DSDA) Polymers 190

5.3.2 Degradation Test of The Poly(DMAEMA-co-DSDA) Polymers 197

5.3.3 Characterization of the polymer/DNA complexes 198

5.3.4 Transfection and cell viability study 200

5.4 Conclusions 207

5.5 References 208

Chapter Six Summary and Future Directions 211

6.1 Summary 212

6.1.1 ATRA Reaction Study for Good Kinetical Control of Homopolymerization of Multi-vinyl Monomer 212

6.1.2 Development of The Vinyl Oligomer Combination Strategy as a Universal Approach to HBPs 213

6.1.3 Synthesis of PEG-based HBPs by Vinyl Oligomer Combination towards Photo-crosslinkable Hydrogels 214

6.1.4 Synthesis of Highly Branched Degradable Cationic Polymers by Vinyl Oligomer Combination towards Efficient Gene Delivery Agents 215

6.2 Limitations 216

6.3 Future Directions 218

6.3.1 Kinetic Modeling and Simulation of Vinyl Oligomer Combination... 218

6.3.2 Bioactive Modification of PEG-based Hydrogels 218

6.3.3 Optimizing Polymeric Vectors for Better Transfection 219
6.4 References.....212

LIST OF APPENDICES

Appendices.....222

A. Sample Preparation for Gel Permeation Chromatography 223

B. Sample Preparation for Proton Nuclear Magnetic Resonance 223

C. Sample Preparation for Zetasizer 223

D. Experimental Protocol for Agarose Gel Electrophoresis 224

E. Experimental Protocol for Cell Splitting.....225

F. Experiemental Protocol for Cell Freezing and Thawing 225

G. Experimental Protocol for 2D Cell Seeding on Hydrogel Surface.....225

H. Experimental Protocol for Transfection of Cultured Cells: (96-well Plate) ..226

I. Experimental Protocol for AlamarBlue® Protocol for Cell Viability: (96-well Plate) 226

J. Conference Proceedings 227

K. Peer-reviewed Articles 227

LIST OF FIGURES

Figure 1.1 The general steps of FRP, including decomposition, initiation, propagation, and termination. 2

Figure 1.2 The kinetic plots of ln([M]$_0$/M]) versus time in a normal controlled/living radical polymerization and other situations. The scheme is redrawn from the original picture in the reference paper.....6

Figure 1.3 Plots of molecular weights versus conversion in an ideal controlled/living radical polymerization, as well as the effects of slow initiation, coupling and chain transfer on the molecular weight evolution. The scheme is redrawn from the original picture in the original paper 7

Figure 1.4 Main precision controls provided by controlled/living radical polymerizations, including (a) composition, (b) architecture or (c) functionality. 8

Figure 1.5 Dynamic equilibriums existed in (a) ATRP, (b) RAFT and (c) NMP systems. 10

Figure 1.6 Evaluation and comparison of ATRP, RAFT and NMP in different areas in the year 2002 and 2006, showing the evolution and development of CRP techniques. 10

Figure 1.7 General steps happened in atom transfer radical polymerization (ATRP). 13

Figure 1.8 Comparison of ISET and OSET mechanism in the reaction of copper complex with alkyl halides 15

Figure 1.9 General initiation mechanisms of normal ATRP, reverse ATRP, SR&NI ATRP reaction, ICAR ATRP, AGET ATRP and ARGET ATRP.....18

Figure 1.10 Simulated concentrations of all species (solid lines) and all rates (broken lines) for normal ATRP and DE-ATRP of styrene at 90°C, showing the concentrations of all species in DE-ATRP are almost constant during the whole polymerization. 22

Figure 1.11 Scheme of different units in dendrimer, hyperbranched polymer and linear polymer. The different degree of branching values were given according to two different definitions ($DB_{Frechet}$ and DB_{Frey}). 32

Figure 1.12 Hyperbranched polymer prepared by AB_2 type monomer. 34

Figure 1.13 Hyperbranched polymer prepared by A_2+B_3 methodology. 34

Figure 1.14 Hyperbranched polymer prepared by AB_2 and B_3 type monomer. 35

Figure 1.15 Hyperbranched polymer prepared by AA’ + B’B_2 approach or couple-monomer methodology (CMM).....36

Figure 1.16 Schematic representation of the self-condensing vinyl polymerization (SCVP) of an AB* monomer to give a hyperbranched vinyl polymer. 38

Figure 1.17 Monomers of nitroxide SCVP to create HBP. 39

Figure 1.18 Monomers used for ATRP SCVP to create HBP.....40

Figure 1.19 Monomers used for RAFT SCVP to create HBP.....41

Figure 1.20 Synthesis of branched vinyl polymers using a combination of multi-vinyl monomer and radical transfer agent (Strathclyde synthesis). 43

Figure 1.21 Example of HPG-CP for tissue adhesive: (a) multivalent HPG structures with CP end groups linked by 1,2,3-triazol units; (b) SEM images (5,000) of red blood cells forming aggregates in saline solution as a result of cell adhesion; (c) the mechanism of the biomembrane adhesion interaction.....48

Figure 1.22 Schematic representation of bioreducible SS-HPEI-mediated intracellular siRNA delivery.....53

Figure 2.1 Basic steps in Kharasch addition. 74

Figure 2.2 Basic steps in transition metal catalyzed ATRA. 75

Figure 2.4 Mechanism of a well-controlled ATRA for achieving highly branched polymer in the homopolymerization of divinyl monomer. In contrast, the free radical polymerization (FRP) or the normal ATRP reaction will lead to less branched polymers and low conversion before gelation. 78

Figure 2.5 Different gelation processes of the homopolymerization of divinyl monomer between FRP, normal ATRP and well-controlled ATRA. In the well-controlled ATRA, gelation can be postponed until high yield. Whereas the FRP and normal ATRP will lead to gelation at low or moderate yield due to the lack of kinetical control and the high polydispersity of the primary chains. 79

Figure 2.6 Proposed mechanism for copper-catalyzed ATRA. 81

Figure 2.7 ATRA reactions of chloroform with two mono-vinyl monomers (styrene and methyl methacrylate). The kinetic chain length (v) can be indirectly reflected by the monoadduct yield of products at a certain chloroform/ mono-vinyl monomer ratio...86

Figure 2.8 The difference between ARGET ATRP and *in situ* DE-ATRA. For ARGET ATRA, excess AA was used that reduces not only the initial Cu^{II} but also the newly formed Cu^{II}, while for *in situ* DE-ATRA, the Cu^{II} is partially reduced, leaving higher amounts of the deactivating Cu^{II}. The scheme shows that monoadduct formation is largely dependent on the Cu^{I} to Cu^{II} ratio. 87

Figure 2.9 GPC traces for FRP of styrene (entry 1, Table 2.1). Only polymers with high molecular weight were produced and the molecular weight did not significantly change from 1 hour to 4 hour. 89

Figure 2.10 GPC traces for ARGET-ATRA1 of styrene with molar ratio of [Styrene]:[$CHCl_3$]:[Cu^{II}]:[AA]=1000:4000:1:10 (entry 2 in Table 2.1). Polymer rather than monoadduct was produced after 24 hours reaction time.....89

Figure 2.11 GPC traces for ARGET-ATRA2 of styrene with molar ratio of [Styrene]:[$CHCl_3$]:[Cu^{II}]:[PMDETA]:[AA]=1000:4000:4:4:4 (entry 3, Table 2.1). Multimodal peaks of oligomer and polymer were observed. The result shows the monoadduct yield was increased compared to the ARGET-ATRA1. 90

Figure 2.12 GPC traces for ATRA1 of styrene with molar ratio of [Styrene]:[$CHCl_3$]:[Cu^{I}] =1000:4000:4 (entry 4, Table 2.1). Only peaks of monoadduct and oligomer were observed. 91

Figure 2.13 ^{1}H NMR spectrum of ATRA1 reaction of styrene (entry 4, Table 2.1), indicating low vinyl conversions and increased monoadduct yields with time.....91

Figure 2.14 GPC traces for *in situ* DE-ATRA1 of styrene with molar ratio of [Styrene]:[$CHCl_3$]:[Cu^{II}]:[AA] = 1000:4000:6:1.2. (entry 5 in Table 2.1). A notable peak of the monoadduct appeared after 24 hours. 93

Figure 2.15 GPC traces for *in situ* DE-ATRA2 of styrene with molar ratio of [Styrene]:[$CHCl_3$]:[Cu^{II}]:[AA] = 1000:4000:10:2. (entry 6 in Table 2.1). The peak of the monoadduct is more significant compared to in situ DE-ATRA1. 93

Figure 2.16 ^{1}H NMR spectrum of in situ DE-ATRA1 and in situ DE-ATRA2 of styrene (entry 5 and 6 in Table 2.1), indicating high vinyl conversions and high monoadduct yields. 94

Figure 2.17 GPC traces for the reactions of MMA. (a) FRP [I]:[M]:[ACCN]= 4: 1: 0.004 no copper catalyst, [I]=2.5 M; (b) ATRA1 [I]:[M]:[CuCl]= 4: 1: 0.004, [I]=2.5 M; (c) ATRA2 [I]:[M]:[CuCl]= 4: 1: 0.008, [I]=2.5 M; (d) *in situ* DE-ATRA [I]:[M]:[$CuCl_2$]:[AA]= 4: 1: 0.025: 0.00188, [I]=2.5 M; In all reaction I= $CHCl_3$, T=60^{o}C, [CuCl] or [$CuCl_2$]: [PMDETA]=1:1, 2-butanone was used as the solvent for the reaction. Molecular weight and PDI were characterized by GPC equipped with RI detector. No monoadducts were obtained in FRP, whilst oligomer and monoadduct were obtained in ATRA and *in situ* DE-ATRA. The *in situ* DE-ATRA showed highest monoadduct yield among all the reaction systems. 96

Figure 2.18 ^{1}H NMR spectrum of *in situ* DE-ATRA reaction of MMA. (entry 4 in Table 2.2), indicating high vinyl conversions and high monoadduct yields.....97

Figure 2.19 GPC traces for *in situ* DE-ATRA of EGDMA. (Table 2.3), showing that the EGDMA firstly undergo a linear propagation (<0.5h) followed by oligomer combination. (>0.5h).....99

Figure 2.20 Kinetic studies for *in situ* DE-ATRA of EGDMA (Table 2.3), include (a) plots of $\ln([V]_0/[V])$ versus time ([V] is the mole concentration of the vinyl group in the system) and (b) M_w and PDI versus vinyl conversion. 100

Figure 2.21 Scheme of *in situ* DE-ATRA of EGDMA and ^{1}H NMR results for the final product, the results indicate the purified polyEGDMA contains 28% branched EGDMA unit. 102

Figure 2.22 Plot of intrinsic viscosity *versus* molecular weight for hyperbranched

polyEGDMA and linear PMMA standards. The intrinsic viscosities [η] of the hyperbranched polyEGDMA are much lower than those of linear PMMA. MHS exponent α= 0.70 for PMMA versus 0.25 for the hyperbranched polyEGDMA. (Table 2.3) 104

Figure 2.23 GPC traces for *in situ* DE-ATRA of DVB, showing that the DVB monomers firstly undergo a linear propagation (<1h) followed by oligomer combination. (>1h)..... 105

Figure 2.24 Plot of intrinsic viscosity *versus* molecular weight for hyperbranched polyDVB and linear poly(styrene) standards. The intrinsic viscosities [η] of the hyperbranched polyDVB are much lower than those of linear poly(styrene). MHS exponent α= 0.71 for poly(styrene) versus 0.21 for the hyperbranched polyDVB (Table 2.3) 105

Figure 2.25 The plot of the gyration radius versus Log MW of *in situ* DE-ATRA of DVB (Figure 2.21) using GPC equipped with light scattering detector. 106

Figure 3.1 Previous copolymerization of multi-vinyl monomer and mono-vinyl monomer: (a) Cross-linked structure formed by combination of long linear polymer chain through FRP; (b) Branched structure consisting of a large proportion of mono-vinyl monomer and a small amount of multi-vinyl monomer (MVM) as crosslinkers through controlled/living radical copolymerization. The polymers usually have a low density of branching. 112

Figure 3.2 The scheme of the four different processes which involved in the homopolymerization of divinyl monomers..... 114

Figure 3.3 Homopolymerization of multi-vinyl monomer (MVM) via deactivation enhanced atom transfer radical polymerization (DE-ATRP) with different strategies leading to either cyclized or hyperbranched structures. (a) Under the condition of a restricted growth boundary (short kinetic chain length), cyclized structures are formed through the strategy of intra-enhanced propagation. The intramolecular cyclization is enhanced due to the high local/spatial vinyl concentration within the growth boundary. (b) Hyperbranched structures are formed under the strategy of vinyl oligomer combination. The intermolecular reaction is facilitated from early reaction stages when numerous oligomers are formed and become the predominant species in the reaction system. In this situation, the intramolecular cyclization is suppressed due to the short chain length during the linear growth period. 115

Figure 3.4 GPC traces of polymerization of methyl acrylate (MA) with a high initiator to monomer ratio (1:4) via *in situ* DE-ATRP (30mol% AA of Cu^{II}). The result shows a characteristic of living polymerization, which indicates that the kinetics chain length of *in situ* DE-ATRP can be diminished to an extremely low level..... 122

Figure 3.5 Time dependence of the composition of the polymerization mixtures monitored by GPC equipped with a refractive index (RI) detector, showing the reaction pathway that the divinyl monomer firstly underwent a large-scale linear

oligomerization (<1h) followed by oligomer combination. (>1h).....123

Figure 3.6 GC for the samples from the early period of polymerization of hyperbranched polyBDA, showing the composition evolution within the polymerization system: (a) GC of 0h sample in Figure 3.5; (b) GC of 0.5h sample in Figure 3.5; (c) GC of 1h sample in in Figure 3.5.....125

Figure 3.7 Mass spectrum for the samples from early period of polymerization of hyperbranched polyBDA, showing the chemical composition within the polymerization system: (a) Mass spectrum of 0.5h sample in Figure 3.5; (b) Mass spectrum of 1h's sample in Figure 3.5. The number gap between each major peak is exactly the molecular weight of BDA, which indicates that the molecular weight increases by 1 monomer unit and the vinyl groups of the divinyl monomer are mainly consumed on one side instead of on both sides at the beginning period. 126

Figure 3.8 ^{1}H NMR spectrum of different periods of polymerization of 1,3-butanediol diacrylate (BDA) towards hyperbranched structure via *in situ* DE-ATRP (30% AA of Cu^{II}). The vinyl conversion is defined as the ratio of consumed vinyl groups to all the original vinyl groups, as shown in Eq. 3.1.....127

Figure 3.9 Kinetic plot of $\ln([V]_0/[V])$ versus time for the *in situ* DE-ATRP of BDA ([V] is the concentration of vinyl groups in the reaction).....128

Figure 3.10 Comparison of theoretical and experimental results of branch ratio versus time. Theoretical curve was described according to eq. 3.2. Constant k is calculated based on the line slope in Figure 3.9.....130

Figure 3.11 ^{1}H NMR spectra of purified polymer hyperbranched polyBDA (3.5h product in Figure 3.5). The component ratio of the different units was calculated by eq. 3.3-eq. 3.5 and summarized in Table 3.2. The branched ratio is defined as the ratio of branched BDA units to all the BDA units, as shown in eq. 3.6. 131

Figure 3.12 The molecular structure in polyBDA. The ratio of branched units to initiators should below 1 in the ideal hyperbranched polymer. Also, this ratio will be higher than 1 for the cyclic or intramolecular crosslinked polymers.....132

Figure 3.13 Mechanism of an ideal hyperbranched polymer formation and the relationship between branched units and initiators. The ratio of branched units to initiators is lower than 1 in an ideal hyperbranched polymer ($N_{branched\ units} < N_{initiators}$). 133

Figure 3.14 Mechanism of the cyclic polymer/intramolecular crosslinks formation and the relationship between branched units and initiators. The ratio of branched units to initiator is higher than 1 in cyclic polymer due to the unavoidable intramolecular crosslinks ($N_{branched\ units} \geq N_{initiators}$).....134

Figure 3.15 Time dependence of the composition of the polymerization mixtures monitored by GPC equipped with a refractive index (RI) detector, showing the unimodal peaks typically at initial stages (<5h) and multimodal peaks appearing later

(>5h).....136

Figure 3.16 ^{1}H NMR spectra of purified cyclized polyBDA (5h product in Figure 3.15). The component ratio of the different units was calculated by eq. 3.3-eq. 3.5 and summarized in Table 3.4. The branched ratio is defined as the ratio of branched BDA units to all the BDA units, as shown in eq. 3.6. 137

Figure 3.17 GPC trace evolution for polymerizations from different types of divinyl monomers: (a) Polymerization of DEGDA; (b) Polymerization of EGDMA; (c) Polymerization of DVB. 139

Figure 3.18 Time dependence of the composition of the polymerization mixtures monitored by GPC equipped with a RI detector, indicating that the divinyl monomer firstly underwent a large-scale linear oligomerization (<1.5h) followed by oligomer combination (>1.5h).....142

Figure 3.19 ^{1}H NMR spectrum of different periods of polymerization of disulfide-based diacrylate (DSDA) towards hyperbranched structure via in situ DE-ATRP (30% AA of Cu^{II}). The vinyl conversion is defined as the ratio of consumed vinyl groups to all the original vinyl groups, as shown in Eq. 3.11.....142

Figure 3.20 ^{1}H NMR spectroscopy of purified hyperbranched polyDSDA (10h product in Figure 3.18). The branched ratio is defined as the ratio of branched DSDA units to all the DSDA units, as shown in Eq. 3.12.....143

Figure 3.21 Schematic representation of the degradation from polymer to linear primary chains by disulfide bond cleavage, showing that the molecular weight and hydrodynamic size of polymer chains will decrease significantly in hyperbranched polymers, but will only change slightly in single cyclized polymer.....144

Figure 3.22 GPC trace of the degradation from polymers to linear primary chains by reduction of disulfide bond using tributylphosphine (Bu_3P): (a) Degradation of hyperbranched polyDSDA (synthesized with 1:2 initiator to monomer ratio, purified 10h's polymer in Figure 3.18); (b) Degradation of 'single cyclized' polyDSDA (synthesized with 1:100 initiator to monomer ratio). The GPC trace before and after cleavage of polyDSDA synthesized with a high initiator to monomer ratio proves the hyperbranched structure because the M_w and hydrodynamic size substantially decreased after cleavage (from 31.9 kDa to 1.1 kDa), in contrast, the polyDSDA synthesized with a low initiator to monomer ratio demonstrates only a slight reduction (from 4.2kDa to 3.3 kDa). The vastly different degradation behaviors confirm the large variance between the polymer structures.....145

Figure 3.23 ^{1}H NMR spectrums before and after cleavage of the purified hyperbranched and cyclized polyDSDA. The disulfide bond was completely cleaved after 2 h, since the resonance of proton (2.9 ppm) completely disappeared. Peaks of vinyl groups also disappeared, since the vinyl groups were consumed by the newly generated -SH groups.....147

Figure 3.24 Formation of different structures via *in situ* DE-ATRP: (a) Formation of

hyperbranched structure; (b) Formation of 'single cyclized' structure. Three parameters are considered: the growth boundary (dotted circle), chain dimension (red shaded part) and chain concentration. The growth boundary, which confines the possible number of vinyl groups reacted within its active lifetime during the propagation process, could change the selectivity of vinyl groups attacked by the propagation centre. The probability of intermolecular combination decreases with distance between an active propagation centre and another polymer chain, which is strongly dependent on the chain dimension and chain concentration 149

Figure 4.1 (a) Simplified crosslinked hydrogel structure. Black dots represent crosslinking point; ξ represents mesh size of the gel. (b) Hydrogel property as a function of gel crosslinking density. 157

Figure 4.2 Schematic structures of PEG hydrogels formed via: (a) chain-growth, (b) step-growth, and (c) mixed-mode step and chain growth polymerization.....158

Figure 4.3 Homopolymerization of poly(ethylene glycol) diacrylate through vinyl oligomer combination strategy and a schematic mechanism of the reaction towards a hyperbranched structure. 161

Figure 4.4 Time dependence of the composition of the polymerization mixture for the poly($PEGDA_{575}$) syntheses, as monitored by GPC. The inserts are the GPC traces of the final product after purification. 167

Figure 4.5 Time dependence of the composition of the polymerization mixture for the poly($PEGDA_{700}$) syntheses, as monitored by GPC. The inserts are the GPC traces of the final product after purification. 168

Figure 4.6 Mark-Houwink plots for the polymers obtained by homopolymerization of (a) $PEGDA_{575}$ and (b) $PEGDA_{700}$ with different initiator-to-monomer ratios. The Mark-Houwink plots of a linear polymer from ATRP of poly(ethylene glycol) methyl ether acrylate (polyPEGMA, M_n=48k, PDI=1.24) is given for comparison. The Mark-Houwink exponents of poly(PEGDA)s are significantly low (α=0.3~0.4), indicating a more compact dense structure compared to the linear analogue.....171

Figure 4.7 ^{1}H NMR spectroscopy of purified polymers obtained by homopolymerization of $PEGDA_{575}$ with different initiator-to-monomer ratios. The poly(PEGDA)s composition was determined by integrating a, d, d' and g peaks (Figure 4.7). Eq. 4.3-4.5 outline the calculations. 173

Figure 4.8 ^{1}H NMR spectroscopy of purified polymers obtained by homopolymerization of $PEGDA_{700}$ with different initiator-to-monomer ratios. The poly(PEGDA)s composition was determined by integrating a, d, d' and g peaks (Figure 4.8). Eq. 4.3-4.5 outline the calculations. 174

Figure 4.9 Thermoresponsive properties of the obtained homopolymers of $PEGDA_{575}$: (a) Phase transition temperature of the poly($PEGDA_{575}$)s in distilled water at different concentrations. (b) Comparison of phase transition temperature of the poly($PEGDA_{575}$)s 1:4 obtained at different times of polymerization with different

molecular weight. 176

Figure 4.10 Cell metabolic activity assessment of 3T3 cells after one, three and five days 2D culture on poly(PEGDA) photo-crosslinked hydrogels using alamarBlue® assay. Cells on the blank culture plate were used as the control. The cell concentration was 5,000 per well on the 96-well plate. Note: there is significant difference of cell viability between the control and the hydrogels but no significant difference was found between the hydrogels crosslinked from different polymers after one, three and five days (mean ± SD, n = 3, $p < 0.05$). 178

Figure 5.1 Illustration of the controlled radical crosslinking copolymerization via *in situ* DE-ATRP and a post-functionalization process, alongside a graphical representation of the formation of structures of different branching degrees. The efficacy of functionalization depends on the content of the pendent vinyl groups.... 191

Figure 5.2 Time dependence of the composition of the polymerization mixtures for the three PDx-DSy syntheses, monitored by GPC equipped with a refractive index (RI) detector, showing subtly different reaction pathways. 192

Figure 5.3 GPC traces of the three PD_x-DS_y polymers obtained at different time point with similar M_w. 194

Figure 5.4 ^{1}H NMR spectrum of the three PD_x-DS_y polymers products, showing certain amount of vinyl groups left in those polymers. 194

Figure 5.5 ^{1}H NMR spectrum of PD_8-$DS_{2.5}$ before and after Michael addition of the primary amine on the MPA and vinyl group on the polymer, showing a successful functionalization 197

Figure 5.6 Degradation of the three PD_x-DS_y polymers: (a) Graphical representations of the degradations of structures with different branching degrees; (b) GPC traces of the three PD_x-DS_y polymers before and after 1 hours treatment of 20mM glutathione, showing a significant molecular weight reduction 198

Figure 5.7 The polymer/DNA interaction characterization by gel electrophoresis, showing that (a) PD_{32}-$DS_{1.5}$ complexes DNA at a ratio of 0.4:1 (w/w); (b) PD_{16}-DS_2 complexes DNA at a ratio of 0.6:1 (w/w) and (c) PD_8-$DS_{2.5}$ complexes DNA at a ratio of 0.8:1 (w/w)..... 199

Figure 5.8 Size and surface potential of the three PD_x-DS_y/DNA polyplexes at different weight ratios: (a) particle size; (b) surface potential. As the weight ratio of polymer/DNA increases, the particle size decreases and the surface potential increases for all the polyplexes..... 200

Figure 5.9 G-luciferase transfection and cytotoxicity analysis on HeLa cells after 48 hours incubation: The branched PD_x-DS_y polymers manifest more favorable transfection properties in terms of transfection ability (a) and cytotoxicity (b) than the linear PDMAEMA (n=6, 5,000 cells and 1μg of pDNA per well, error bars indicate ± standard deviation, and asterisks indicate a significant difference from linear

PDMAEMA). 202

Figure 5.10 Cytotoxicity analysis by alamarBlue assay on NHK (a) and hADSC (b) cells after 48 hours incubation, error bars indicate ± standard deviation. 203

Figure 5.11 Fluorescent microscopy images of HeLa cells incubated for 48 h with GFP polyplexes comprised of the three PD_x-DS_y polymers in comparison to the linear PDMAEMA (44kDa) and non-degradable branched PD_8-$E_{2.5}$ as well as the commercial 25kDa bPEI. The ratios embedded in the photos stand for the polymer/DNA weight ratio. 205

Figure 5.12 Fluorescent microscopy images of NHK cells incubated for 96 h with GFP polyplexes comprised of the three PD_x-DS_y polymers in comparison to the linear PDMAEMA (44kDa) and non-degradable branched PD_8-$E_{2.5}$ as well as the commercial 25kDa bPEI. The ratios embedded in the photos stand for the polymer/DNA weight ratio. 206

Figure 5.13 Fluorescent microscopy images of hADSC cells incubated for 96 h with GFP polyplexes comprised of the three PD_x-DS_y polymers in comparison to the linear PDMAEMA (44kDa) and non-degradable branched PD_8-$E_{2.5}$ as well as the commercial 25kDa bPEI. The ratios embedded in the photos stand for the polymer/DNA weight ratio. 207

LIST OF TABLES

Table 1.1 Rate constant values of normal ATRP and DE-ATRP of styrene. $[M]_0/[I]_0/[Cu^I]_0/[Cu^{II}]_0/[L]_0$=100/1/1/x/1, I=PEBr (l-phenylethyl bromide), L=PMDETA (N,N,N'N'N''-pentamethyldiethylenetriamine, $[M]_0$=2.5 M; $[I]_0$=0.025 M, T=90 °C. The rate constants values were taken from references.....23

Table 1.2 The Summary results of kinetics calculation in the polymerization of styrene by normal ATRP and DE-ATRP reaction (Eq.1.16 - Eq.1.28). ATRP reaction conditions: T=90 °C, $[M]_0/[I]_0/[Cu^I]_0/[L]_0$=100/1/1/1, I=PEBr, L=PMDETA, $[M]_0$=2.5 M; $[I]_0$=0.025 M; DE-ATRP reaction conditions: T=90 °C, $[M]_0/[I]_0/[Cu^I]_0/[Cu^{II}]_0/[L]_0$= 100/1/1/0.3/1.3, I=PEBr, L=PMDETA, $[M]_0$=2.5 M; $[I]_0$=0.025 M.....28

Table 1.3 History of hyperbranched polymers.....31

Table 2.1 Reaction results for ATRA of styrene. 88

Table 2.2 Reaction results for ATRA of MMA. 95

Table 2.3 Detailed information of polyDVB and polyEGDMA via *in situ* DE-ATRA reaction.....99

Table 3.1 Polymerization conditions and molecular weight characteristics of the hyperbranched polyBDA 124

Table 3.2 The component ratio of the different units in the purified 3.5h's sample polyBDA by ^{1}H NMR spectroscopy analysis 132

Table 3.3 Polymerization conditions and molecular weight characteristics of the cyclized polyBDA.....135

Table 3.4 The component ratio of the different units in the purified 5h's sample of cyclized polyBDA by ^{1}H NMR spectroscopy analysis.....137

Table 3.5 Polymerization conditions and molecular weight characteristics of polymerizations from different divinyl monomers. 140

Table 3.6 Polymerization conditions and molecular weight characteristics of the hyperbranched polyDSDA.....141

Table 4.1 Molecular weight of poly(PEGDA)s at different time points during the polymerization processes, monitored by GPC RI detector. 166

Table 4.2 Homopolymerization of PEGDA via in situ DE-ATRP, using tert-Butyl α-bromoisobutyrate as initiator and 2-butanone as solvent with a diacrylate concentration of 60% w/v at 50˚C. 169

Table 4.3 Molecular weight of purified poly($PEGDA_{575}$) 1:4 at different reaction time, monitored by GPC-RI detector. These polymers were used for the phase transition study. 177

Table 5.2 The composition of the three PD_x-DS_y polymers can be varied by adjusting the monomer feed ratios of the simple “One-Pot” reaction, with high percentage of branching unit and functional vinyl groups. 196

ACKNOWLEDGEMENTS

I would like to express my sincere gratitude to my supervisor Dr. Wenxin Wang for his invaluable guidance and immense support throughout my PhD study. He helped me develop my research skills, guided me in times of uncertainty, and encouraged my confidence and growth. His influence has allowed me to develop as a researcher and a scientist. Without his guidance and inspiration, this work and thesis could not be successfully completed.

I am grateful to all the staffs and students of the Charles Institute of Dermatology, especially Prof Frank Powell, Prof Martin Steinhoff and Dr Ruth Foley for their help and support during our group's moving in.

I further express my thanks to all the former and current postdocs in our group for all their professional advice and support to my research. Special thanks are due to Dr Yu Zheng for helping me develop my research skills in many areas, Dr. Dezhong Zhou and Dr. Yixiao Dong for their directions on my research, Dr. Ben Newland for his help on my biological experiment, and Dr. Udo Greiser for lots of help on my thesis and manuscripts preparations.

My thanks also goes my fellow labmates Lara Cutlar, Ahmed Aied, Ligia Bre, Robert Kennedy, Yongsheng Gao, Sean MC. Mahon, Zehua Li, Yue Qin, Fatma Alshehri, Jonathan O'Keeffe Ahern, Qian Xu, Sigen A, for the stimulating discussions, for the sleepless nights we were working together before deadlines, and for all the fun we have had in the last four years.

I would also like to thank National University of Ireland, Galway, Science Foundation Ireland, DEBRA Ireland for providing the funds and supports for this project.

I would like to thank all the members of the Network of Excellence for Functional Biomaterials (NFB), past and present, whose contribution to my project and thesis was substantial. I would like to specifically thank Doctor Oliver Carroll (the Laboratory manager at the NFB) for providing the necessary tools and expertise for majority of the project's experiments.

My gratitude is also extended to Dr. Hongyun Tai in Bangor University, UK for her exceptional help, support and encouragement over these four years.

Finally, my deepest appreciation goes to my family who give me much love and warmth. Thanks to my wife Hong Zhang for accompanying me during the toughest time. Thanks to the 'Brothers' in my house, Mingchuan, Jun, Weitao and Yan. Thank you all for so much support, love and understanding.

Tianyu Zhao
January 2015

ABBREVIATIONS

ν_{FRP}	Kinetics chain length in free radical polymerization
ν_{ATRP}	Kinetics chain length in atom transfer radical polymerization
τ	Life-time of radicals in free radical polymerization
τ'	Actual life-time of the radicals in atom transfer radical polymerization
τ_{act}	Time span of activation in atom transfer radical polymerization
τ_{deact}	Time span of deactivation in atom transfer radical polymerization
2D	Two-dimensional
3D	Three-dimensional
AA	L-ascorbic acid
AGET	Activator generated by electron transfer
AIBN	2,2'-Azobis(isobutyronitrile)
ACCN	1,1'-Azobis(cyclohexane-1-carbonitrile)
ARGET	Activator regenerated by electron transfer
ATRA	Atom transfer radical addition
ATRP	Atom transfer radical polymerization
BOD	4,4’-bioxepanyl-7,7-dione
Bpy	2,2'-bipyridine
CCTP	Cobalt catalytic transfer polymerization
$CDCl_3$	Deuterated chloroform
$CHCl_3$	Chloroform
Conv.	Conversion
CRCC	Controlled radical crosslinking copolymerization
CRP	Controlled/living radical polymerization
°C	Degrees celsius
DB	Degree of branching
DE-ATRP	Deactivation enhanced ATRP
DLS	Dynamic light scattering
DMAEMA	2-Dimethylaminoethyl methacrylate

DMF	N,N-dimethylformamide
DMSO	Dimethyl sulfoxide
dNbpy	4,4'-dinonyl-2,2'-bipyridine
DP_n	Degree of polymerization
DSC	Differential scanning calorimetry
DVB	Divinylbenzene
EBIB	ethylbromoisobutyrate
EGDMA	Ethylene glycol dimethacrylate
FDA	Food and drug administration
FRP	Free radical polymerization
GPC	Gel permeation chromatography
HA	Hyaluronic acid
hADSCs	human adipose-derived stem cells
HBP	Hyperbranched Polymer
HeLa	Henrietta lacks cells (cervical cancer cell line)
HPAE	Hyperbranched poly (β-amino esters)
IFIRP	Initiator-fragment incorporation radical polymerization
k_{act}	Activation rate in atom transfer radical polymerization
k_{deact}	Deactivation rate in atom transfer radical polymerization
K_{ATRP}	Equilibrium constant for atom transfer radical polymerization
K_{BO}	Bond dissociation energy of the alkyl halide
kDa	kilo Daltons
K_{EA}	Electron affinity of the halogen
K_{ET}	Equilibrium constants for electron transfer of metal complexes
K_X	Equilibrium constant for the heterolytic cleavage of the Cu^{II}-X bond
LSCT	Lower critical solution temperature
LRP	Living radical polymerization
Me_6-TREN	Tris[(2-dimethylamino)ethyl]amine
MeOH	Methanol
MMA	Methyl methacrylate

M_n	Number average molecular weight
MVM	Multi-vinyl monomer
MW	Molecular weight
M_w	Weight average molecular weight
NHK	Normal human keratinocytes
NMP	Nitroxide mediated polymerization
NMR	Nuclear magnetic resonance
N/P	Nitrogen to phosphate ratio
PAMAM	Poly (amidoamine)
PBS	Phosphate buffered saline
PCL	Poly(caprolactone)
PDI	Polydispersity Index
PDMAEMA	Poly(2-(diethylamino)ethyl methacrylate)
PE	Polyethylene
PEG	Polyethylene glycol
PEI	Polyethyleneimine
PMDETA	*N*,*N*,*N'*,*N''*,*N''*-pentamethyldiethylenetriamine
PMMA	Poly(methyl methacrylate)
PP	Polypropylene
PRE	Persistent radical effect
PS	Polystyrene
PSD	Particle size distribution
PVA	Poly(vinyl alcohol)
PVAc	Poly(vinyl acetate)
RAFT	Reversible addition fragmentation chain transfer
R_g	Gyration radius
R_h	Hydrodynamic radius
RI	Refractive index
ROP	Ring-Opening Polymerization
rpm	Rotations per minute

SCVP	Self-condensation vinyl polymerization
SEC	Size exclusion chromatography
SET	Single electron transfer
SR&NI	Simultaneous reverse and normal initiation
Tg	Glass transition temperature
THF	Tetrahydrofuran
T_m	Melting temperature
UV-vis	Ultraviolet-visible
wt%	Weight %

ABSTRACT

This thesis describes a novel route for the preparation of hyperbranched polymers. The aim is to produce veritable hyperbranched polymers from commercially available multi-vinyl monomers via *in situ* deactivation-enhanced ATRP at high conversion without crosslinking. The strategy is to alter the growth manner of polymerization by controlling the kinetic chain length together with manipulating chain growth conditions to achieve facile syntheses of 3D structured multifunctional materials.

Chapter 1 provides a general introduction to the controlled/living radical polymerization, basic concepts of hyperbranched polymers, their preparation methods and their applications in biomedical field.

Chapter 2 focuses on the study of different ATRA reaction system, including normal ATRA, ARGET ATRA and *in situ* DE-ATRA, for a better kinetic control of the polymerization of multi-vinyl monomers.

Chapter 3 covers the hyperbranched homopolymers prepared by in situ enhanced deactivation ATRP, illustrating the 'vinyl oligomer combination' strategy as a universal approach towards hyperbranched polymers.

Chapter 4 focuses on the synthesis of hyperbranched poly(PEGDA) as an efficient photo-crosslinked hydrogel.

Chapter 5 demonstrates the synthesis of degradable cationic hyperbranched copolymers as efficient gene transfection agent. Also the significance of branching on transfection is explored.

Chapter 6 summarises all the research presented in this thesis. Moreover, some possible research routes for the investigation in the future are listed in this part.

STATEMENT OF ORIGINAL AUTHORSHIP

I hereby certify that the submitted work is my own work, was completed while registered as a candidate for the degree stated on the Title Page, and I have not obtained a degree elsewhere on the basis of the research presented in this submitted work.

Chapter One

Introduction

Parts of this chapter have been published in:

Wang, D., **Zhao, T.**, Zhu, X., Yan, D., Wang, W. 'Bioapplications of hyperbranched polymers' *CHEMICAL SOCIETY REVIEWS*, **2015**, Advance Article, DOI: 10.1039/C4CS00229F

1.1 Controlled/living Radical Polymerization

1.1.1 Free Radical Polymerization

Free radical polymerization (FRP) has been an important polymerization method widely used since 1940s and remains one of the most heavily used organic processes, and millions of tons of polymers including polyethylene (PE), polypropylene (PP), polystyrene (PS), poly(vinyl chloride) (PVC), poly(vinyl acetate) (PVAC), poly(methyl methacrylate) (PMMA) and polyacrylonitrile (PAN), are produced by this route every year.

As a type of chain-growth polymerization, FRP is based on the continuous addition of vinyl monomers to a free radical which is a molecule with an unpaired electron.[1, 2] The whole process begins with initiator decomposition that can release radicals, followed by the addition of vinyl monomer units to the free radicals of growing chains. The chain growth is finally terminated by combination or disproportionation or chain transfer of the propagating radicals to form polymer molecules,[3] as shown in Figure 1.1.

Overal formulation of chain-growth polymerization

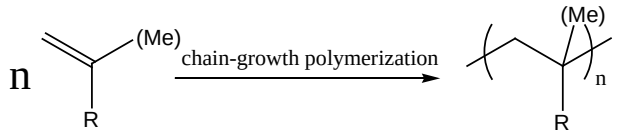

Steps of free radical polymerization

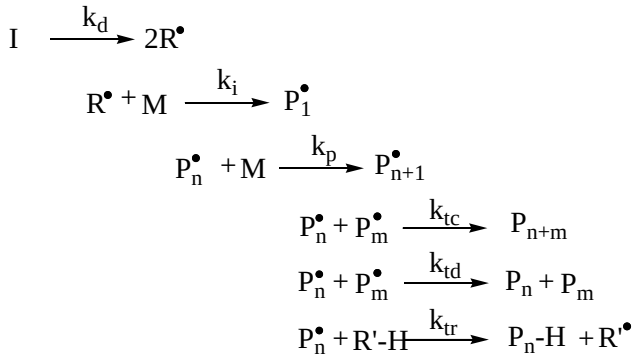

Figure 1.1 The general steps of FRP, including decomposition, initiation, propagation, and termination.

Eq. 1.1, 1.2 and 1.3 gives the kinetic formulation of rates of initiation, propagation and termination, respectively.[1] (R_i: the rate of initiation; R_p: the rate of propagation; R_t: the rate of termination; [M]: the mole concentration of monomer; [I]: the mole concentration of initiator; f: the efficiency of an initiator I; k_p: the rate constant for propagation for a monomer M; k_t: the rate constant for termination and $k_t = k_{tc} + k_{td}$

$$R_i = \frac{d[R^\bullet]}{dt} = 2k_d f[I] \qquad \text{Eq. 1.1}$$

$$R_p = -\frac{d[M]}{dt} = k_p[P^\bullet][M] \qquad \text{Eq. 1.2}$$

$$R_t = \frac{d[P^\bullet]}{dt} = 2k_t[P^\bullet]^2 \qquad \text{Eq. 1.3}$$

By assuming all vinyl groups have the same reactivity and the radical concentration become constant when the initiation rate is equal to the termination rate, the rate of polymerization can be derived as Eq. 1.4. The efficiency of an initiator f is defined as $[P_1^\bullet]/[R^\bullet]$, which is normally in the range of 0.3-0.8, since a proportion of primary radicals that are produced by the decomposition of initiator do not initiated with the monomer due to the 'cage' effect[4]. This kinetics equation can successfully describe most of the FRP processes.

$$R_p = -\frac{d[M]}{dt} = k_p\left(\frac{k_d f[I]}{k_t}\right)^{1/2}[M] \qquad \text{Eq. 1.4}$$

The characters of FRP can be concluded as 1) slow initiation, 2) fast propagation and 3) rapid termination. These characters render FRP many disadvantages. The main disadvantage of FRP is the ill-controlled termination reactions between radicals. Thus, it is difficult to control molecular weight and polydispersity. The fast propagation rate is another key factor. The lifetime of a propagating chain is very short, typically in the range of 1.0 second and thousands of monomers units could be able to add to the newly generated active center before termination during that time.

Furthermore, when the growing chain is terminated, it can hardly be initiated again and becomes a 'dead' chain. Thus, it is difficult to control the chain growth or add a new monomer to form special block copolymer chain and end functionalities. Two methods were used to provide polymers with lower or controlled molecular weights. The first method is the application of a large amount of initiator to supply more propagating opportunities, while the other approach is based on irreversible transfer agents to provide polymer with controlled molecular weight and functionalities. However, the polydispersity cannot be well-controlled and the polymer chains cannot maintain the living character in these ways.

1.1.2 Controlled/living Radical Polymerization

According to the IUPAC definition, living polymerization is a form of chain growth polymerization from which chain transfer and chain termination are absent[5]. Living polymerization is desirable because it offers control in macromolecular synthesis, which could result in novel and useful properties. Also, since the chain termination and chain transfer reactions are absent and the rate of initiation is usually much larger than the rate of chain propagation, the polymer chains grow at a more constant rate than that seen in conventional chain polymerization and their lengths remain very similar (low polydispersity). Furthermore, living polymerization is a popular method for synthesizing block copolymers since the polymer can be synthesized in stages, each stage containing a different monomer. Additional advantages are predetermined molar mass and control over end-groups.

Until now, only the anionic and cationic polymerization (including some ring-opening polymerizations) can be strictly considered as living polymerization. In the situation of FRP, the chain transfer and chain termination always existed. To overcome the limitations of conventional FRP[6, 7, 8] and to take the advantage of its universality for vinyl monomers, scientists have successfully developed new and universal polymerization techniques to minimized the chain transfer and chain termination for the characteristics of living polymerization. That's why this type of

polymerization is called ‘controlled/living radical polymerization’ (CRP). While living polymerization and CRP are very similar, there is a distinct difference in the definitions of these two reactions. While living polymerizations are defined as polymerization reactions where termination or chain transfer is eliminated, CRP reactions are reactions where termination is suppressed, but not eliminated, through the introduction of a dormant state of the polymer. Although CRP has some limitations in that termination cannot be totally eliminated, this technique also has many advantages, including relative insensitivity to transfer and protic impurities and a very large range of (co)polymerizable monomers.

Similar to living polymerization, a CRP process usually displays the features below:

First, a CRP reaction should manifest the first-order kinetics behavior, that is, the polymerization rate (R) which with respect to the log of the monomer concentration ([M]) is a linear function of time (Eq. 1.5 and 1.6). This is because the concentration of the active propagating species ([P$^{\bullet}$]) is constant when the non-reversible termination is negligible.

$$R_p = -\frac{d[M]}{dt} = k_p[P^{\bullet}][M] \qquad \text{Eq. 1.5}$$

$$\ln\frac{[M]_0}{[M]} = k_p[P^{\bullet}]t = k_p^{app}[P^{\bullet}]t \text{ (if } [P^{\bullet}] \text{ is constant)} \qquad \text{Eq. 1.6}$$

Figure 1.2 shows the dependence of ln([M]$_0$/[M]) on time. The slope of semi-logarithmic plot is highly dependent on the concentration of the active propagating species. Instead of balancing the rates of initiation and termination as in a conventional FRP, CRP establishes a steady [P$^{\bullet}$] by balancing the rates of activation and deactivation and the constant [P$^{\bullet}$] is revealed by a straight line. This line could be curved upward in the case of slow initiation due to an increased [P$^{\bullet}$] and downward in the case of termination which reduces [P$^{\bullet}$]. It should be noted that the slope of the plot is not sensitive to the chain transfer processes, since they do not affect the concentration of the active propagating species [P$^{\bullet}$]. However, the molecular

weight will be affected by the chain transfer processes.

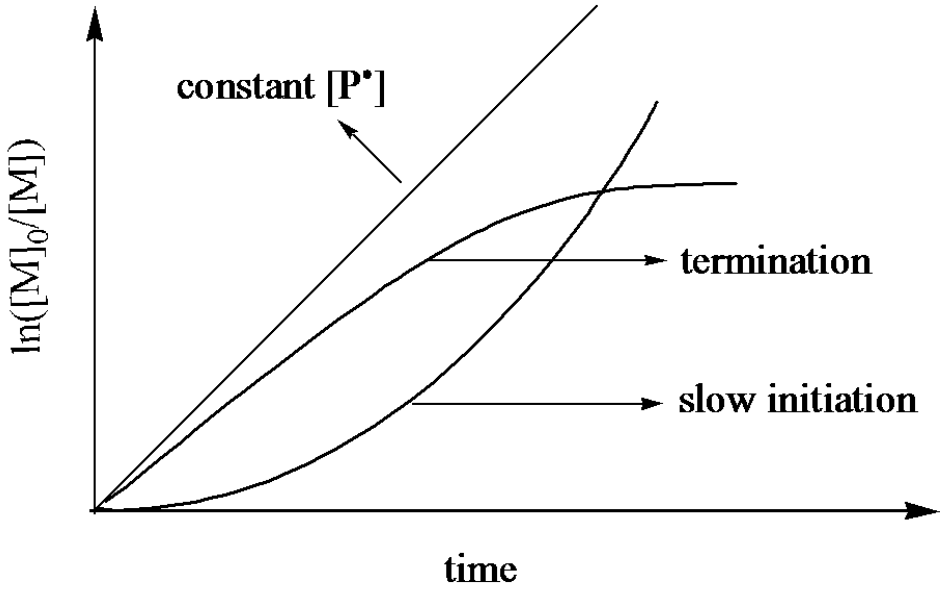

Figure 1.2 The kinetic plots of ln($[M]_0$/M]) versus time in a normal controlled/living radical polymerization and other situations. The scheme is redrawn from the original picture in the reference paper.[8] Copyright 2001, American Chemical Society.

Second, a CRP reaction should have a predetermined degree of polymerization (DP), which means the number average molecular weight (M_n) is a linear function of monomer conversion (Eq. 1.7). This requires a constant number of propagating chains throughout the polymerization. Fast initiation and avoidance of chain transfer are needed to meet this requirement. The plot of ideal growth of molecular weights with conversion as well as the situation of slow initiation, coupling and chain transfer is shown in Figure 1.3. It should be noted that the Eq. 1.7 is not applicable to the RAFT polymerization. In RAFT, the equation should be demonstrated as DP= $[M]_0/[RAFT]_0$ * conversion.

$$DP=\frac{\Delta[M]}{[I]_0}=\frac{[M]_0}{[I]_0}\times \text{conversion} \qquad \text{Eq. 1.7}$$

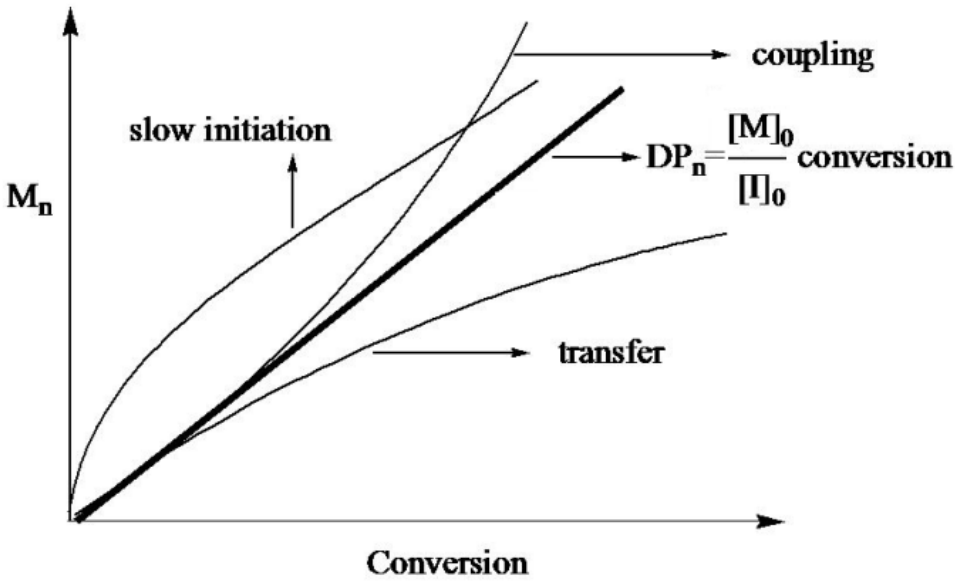

Figure 1.3 Plots of molecular weights versus conversion in an ideal controlled/living radical polymerization, as well as the effects of slow initiation, coupling and chain transfer on the molecular weight evolution. The scheme is redrawn from the original picture in the original paper.[8] Copyright 2001, American Chemical Society.

Third, a CRP reaction should have a narrow molecular weight distribution or low polydispersity. To achieve this, the rate of initiation must be competitive with the rate of propagation, which allows that all propagating centers are activated at the beginning of the polymerization. Also, the exchange rate of dynamic equilibrium must be faster than propagation rate, which ensures that all the active propagating center equally react with monomers. Furthermore, there must be a negligible chain termination or other side reactions. Additionally, the system should be homogeneous and interaction between molecules should be sufficiently fast.[9, 10]

$$\frac{X_w}{X_n} = \frac{M_w}{M_n} = 1 + \frac{X_n}{(X_n+1)^2} \cong 1 + \frac{1}{X_n} \qquad \text{Eq. 1.8}$$

A polymerization that satisfies all of the above requirements should yield a Poisson distribution, as quantified in Eq. 1.8,[8] where X_w is the weight average degree of polymerization, X_n is the number average degree of polymerization. It can be indicated from the equation that the polydispersity (M_w/M_n) will decrease with an increasing molecular weight. The

approximation in the equation is made when the X_n is larger than 10.

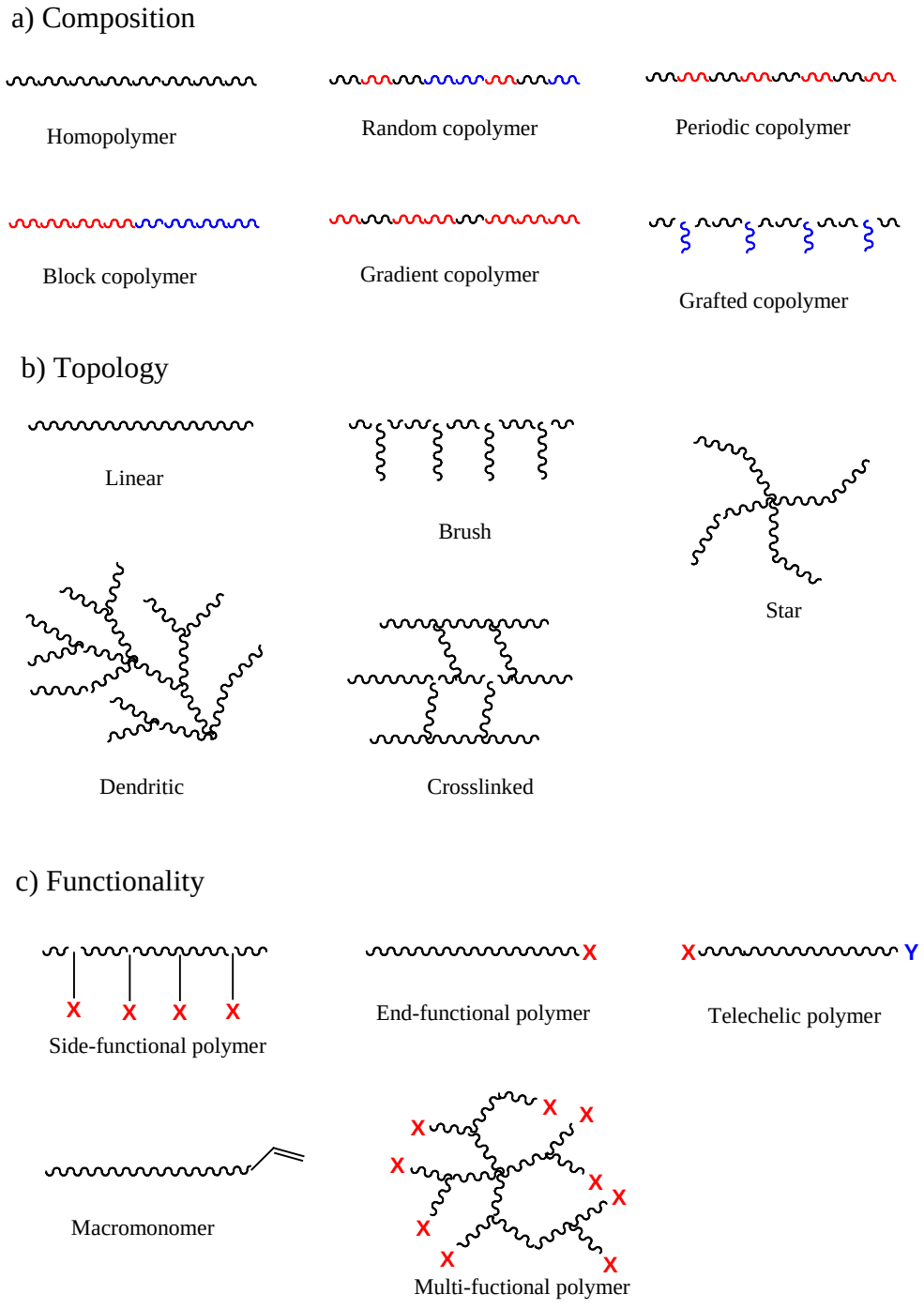

Figure 1.4 Main precision controls provided by controlled/living radical polymerizations, including (a) composition, (b) architecture or (c) functionality.

Fourth, a CRP reaction should create polymer chains with preserved end-functionality. Since the radical termination is minimized, all the chains

retain their active centers even after the consumption of the monomers. This provides the opportunity of the subsequent propagation of additional monomer. This unique feature enables the preparation of macroinitiators and block copolymers with different architectures. Various examples of gradient,[11] block[12] and graft[13] copolymers have been created, as well as polymers with more complex architectures, including stars,[14] comb shaped brushes,[13] and hyperbranched polymers.[15]

The CRP provides a good opportunity to control and manipulate the polymers in composition, topology and functionality at molecular level (Figure 1.4). It also gives us a chance to explore the differences in polymer structures when the propagation is slowed down. Thus, the CRP is recognized as a powerful synthetic tool since it allows manufacturers to improve the properties of materials existing in the current market and create new markets for materials uniquely meeting the targeted properties.

The development of CRP is based on the establishment a dynamic equilibrium between a low concentration of active propagating chains and a large number of dormant chains, which are not terminated but can be re-activated for propagation. The concentration of propagating chains is maintained at a low level by shifting the equilibrium towards dormant species. Thus, the termination becomes less significant compared to propagation. Otsu[16, 17] is a pioneer for CRP exploration and published his research in 1982, using an 'iniferter' agent, containing C-S bonds for chain transfer. Since then, the CRP began to attract many scientists' attention due to the desire of synthesis of novel materials from a wide range of vinyl monomers. There are several CRP processes based on this fundamental concept, including atom transfer radical polymerization (ATRP),[8, 18, 19, 20] which is based on the fundamental work on ATRA,[21, 22, 23] the reversible addition fragmentation chain transfer (RAFT),[24, 25] and nitroxide mediated polymerization (NMP).[7] Dynamic equilibria were established in different ways between the propagating radicals and dormant species for the above CRP processes (Figure 1.5).

(a) Atom transfer radical polymerization (ATRP).

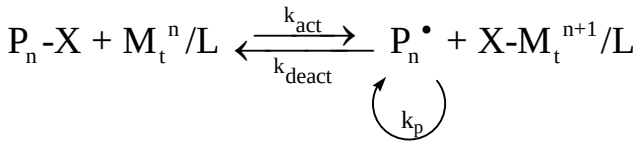

(b) Reversible addition fragmentation chain transfer (RAFT).

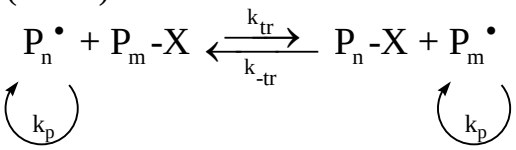

(c) Nitroxide-mediated polymerization (NMP).

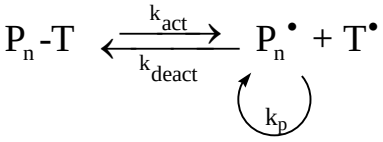

Figure 1.5 Dynamic equilibriums existed in (a) ATRP, (b) RAFT and (c) NMP systems.

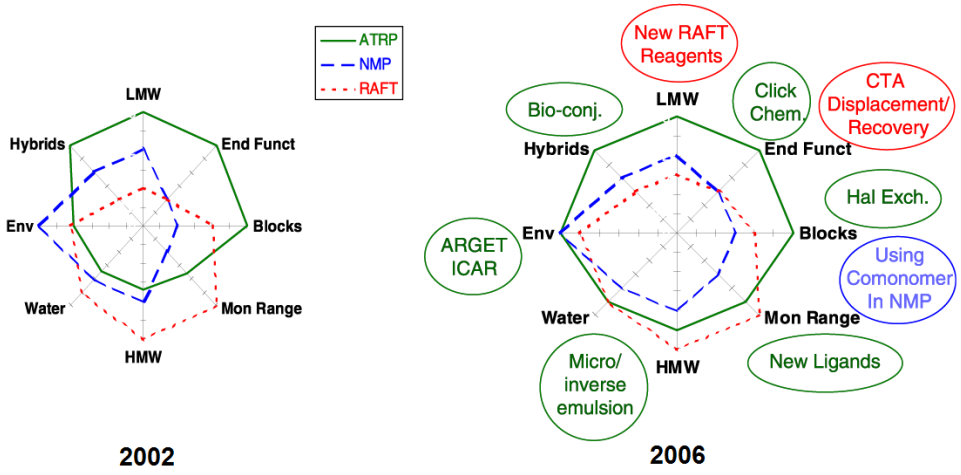

Figure 1.6 Evaluation and comparison of ATRP, RAFT and NMP in different areas in the year 2002 and 2006,[27] showing the evolution and development of CRP techniques. Copyright 2007, Elsevier.

Each of the three major systems have some relative advantages and limitations, depending on the monomers used, the particular synthetic targets, and additional requirements concerning functionality, purity, process such as bulk, solution or biphasic, and perhaps the cost of the final

product. Thus it is not possible to provide an absolute evaluation of these three techniques and state which one is overall most efficient. However, one may compare the three systems from the point of view of targeted structures and particular processes. Such a comparison was attempted by Matyjaszewski in 2002[26] and updated in 2006[27] (Figure 1.6) in the areas including the synthesis of high molecular weight polymers (HMW), low molecular weight polymers (LMW), end functional polymers (End Funct), block copolymers (Blocks), range of polymerizable monomers (Mon Range), synthesis of various hybrid materials (Hybrids), environmental issues (Env) and polymerization in aqueous media (Water). It has also been recognized that this qualitative chart always changes with developments of new chemical agents and improvement in polymerization catalysts and reaction conditions.

1.2 Atom Transfer Radical Polymerization

Since the mid-1950s, many chemists attempted to develop a "living" or controlled radical polymerization process that would create well-defined polymers in a simple and inexpensive manner. Several laboratories across the world surmounted this vexing problem by developing different CRP methods.[16, 28] In 1995, one of the most robust CRP methods, copper-mediated ATRP was discovered by Matyjaszewski in Carnegie Mellon University[19]. The original paper published in the *Journal of the American Chemical Society* has been cited over 3,400 times and the initial patent over 250 times.

ATRP is among the most effective and most widely used methods of CRP. Scientists are allowed to synthesize polymers by putting together monomers in a controlled, piece-by-piece fashion with ATRP. Assembling polymers in such a manner helps to create a wide range of polymers with specific tailored functionalities targeting specific properties for high value applications and are currently under investigation for use in the medical and environmental fields.

1.2.1 From ATRA to ATRP

In the 1940s, methods were developed for radical addition reactions in organic synthesis.[21, 22] One of these reactions was promoted by a transition metal complex, named atom transfer radical addition (ATRA).[29, 30, 31, 32] It is the addition of halogenated compounds to alkenes or alkynes through a radical process. The basic idea of using a transition metal complex was to increase chain transfer constant by recognizing that transition metal complexes are more effective halogen transfer agents than alkyl halides. A transition metal complex was used as the halogen atom (X) carrier by way of a redox reaction of itself. This reaction is widely used for addition and cyclisation reactions in organic synthesis.[29, 30] Chemical substrates for transition metal-catalyzed ATRA are chosen such that if addition occurs, the newly formed radical is much less stabilized than the initial radical and will essentially react irreversibly with the transition metal complex to form an inactive monoadduct. Therefore, usually only one addition step occurs in transition metal-mediated ATRA. However, the radical-radical coupling reaction is ignored due to the low concentration of free radicals. And this is one of the features of the living polymerization.

In 1995, the concept of atom transfer radical polymerization (ATRP) was firstly and independently proposed by Matyjaszewski[18, 19, 20] (copper catalyst) and Sawamoto[33, 34] (ruthenium catalyst). They demonstrated that the ATRA reaction could be vastly extended to a polymerization reaction. Based on the principles of ATRA reaction, ATRP comes from the atom transfer step. The key to transfer ATRA into ATRP is to modify the reaction condition to afford more stable radical species. Thus, the addition cycles will repeat many times until all the monomers are consumed. Specific catalysts based on transition metal compounds with various ligands were developed for ATRP.[8]

1.2.2 Mechanism of ATRP

Figure 1.7 presents the general mechanism of ATRP. The reaction starts off from the transfer of halogen atom from initiator (R-X) to a transition metal

complex in a lower oxidation state (M^z/L_n). And this results in the formation of a propagating radical (R·) and a metal complex in its higher oxidation state with a coordinated halide ligand. This step is called the activation step, with a rate constant of activation (k_{act}). Subsequently, the active radical either attacks vinyl monomers around it and form a new radical with a rate constant (k_p) or reversibly be deactivated by the metal complex of higher oxidation ($M^{z+1}X/L_n$) with a rate constant of deactivation (k_{deact}). The above processes repeat until all the vinyl monomers are consumed or the equilibrium is forced towards deactivation. Termination reactions (k_t) can also occur in ATRP by radical coupling and disproportionation. However, the termination step is suppressed to a minimum in a well-controlled ATRP. As the termination progresses, the $M^{z+1}X/L_n$ are accumulated and radical concentration is decreased, known as the persistent radical effect (PRE), thus the termination could be suppressed by itself in ATRP. The concentration of radicals in ATRP remains low also because the rate constant of deactivation is usually larger than that of activation ($k_{act} << k_{deact}$) and the equilibrium is shifted towards the dormant species.

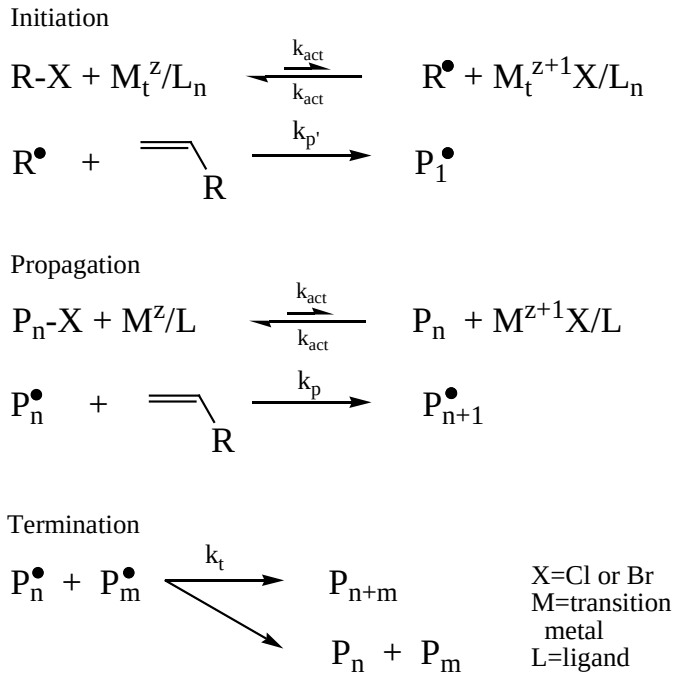

Figure 1.7 General steps happened in atom transfer radical polymerization (ATRP).

1.2.3 ISET vs OSET

Since ATRP is the derivative of ATRA, the mechanism of ATRP firstly was demonstrated by Wang[18, 19, 20] in 1995 following the principles of ATRA and was widely accepted in the field of polymer science. Meanwhile, it is found that olefins such as vinyl chloride cannot be polymerized in ATRP because it is unable to be activated by Cu^{I}/ligand. However, the CRP of vinyl chloride was successfully conducted in a water/THF medium at room temperature in the presence of initial Cu^{0} and ligand.[35] And the method has become popular in controlled polymer synthesis since 2006, when Percec and coworkers published a paper on efficient CRP in the presence of Cu^{0}.[36] The mechanism was postulated to be single electron transfer (SET).[37, 38, 39, 40, 41]

The major difference between ATRP and SET mechanisms lies in the initiation step, as shown in Figure 1.8.[41] The ATRP follows the inner sphere electron transfer (ISET) process, in which the metal approaches the halogen atom and forms an intermedium transition state ($R\text{-}X\text{-}M^{z}$), from which the halogen atom is transferred with one electron, leaving an alkyl radical behind. On the other hand, the SET was suggested to follow the outer sphere electron transfer (OSET) mechanism. The electron is transferred from the metal to the alkyl halide to produce a radical anion, and then the radical anion split into a radical and halogen anion. These two mechanisms are usually judged depending on the nature of solvent, monomer and initiator. Percec suggested that the ISET mechanism dominates in the polymerization of styrene, methacrylate, and acrylates, and is activated by Cu^{I} compounds, whereas the OSET mechanism operates in the systems with electron-rich donors (Cu^{0}) and electron-poor acceptors *(e.g.* CHI_3 used as initiator). However, Matyjaszewski believes that OSET has an energy barrier ~15 kcal/mol higher than what is experimentally measured, i.e., OSET is $\sim 10^{10}$ times slower than ISET,[42] and consequently, it must be concluded that a copper-catalyzed ATRP occurs via concerted hemolytic dissociation of the alkyl halide via ISET, i.e., an atom transfer process. The debate about ATRP or SET mechanism is still continuing and there is no absolute proof for or against any of these possibilities. In this thesis, ISET or atom transfer was

considered as the main mechanism and the following kinetics studies are all based on the ISET or atom transfer mechanism.

Inner sphere electron transfer

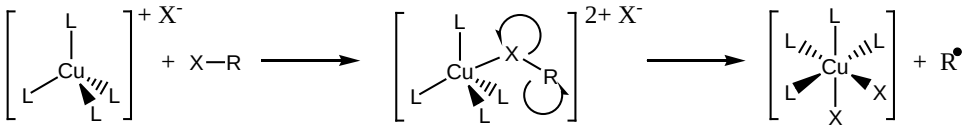

Outer sphere electron transfer

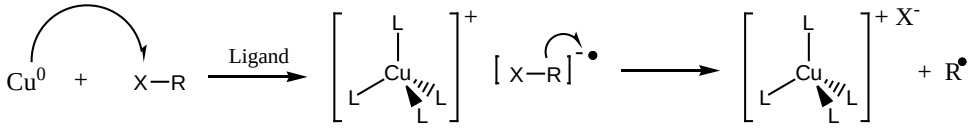

Figure 1.8 Comparison of ISET and OSET mechanism in the reaction of copper complex with alkyl halides.[43]

1.2.4 Components and Kinetics

The main components of ATRP include an initiator with a weak C-X bond, a transition metal complex and a monomer. Other components such as solvent, regenerative activators (e.g. AIBN or reducing agents) and deactivators (e.g. $Cu^{II}X_2$) are sometimes introduced for special purposes.

The rate of an ATRP depends on the rate constant of propagation, the concentrations of monomer and the concentrations of growing radicals. The ATRP equilibrium constant and the concentration of dormant species, activators, and deactivators determine the radical concentration. Thus the rate of an ATRP is illustrated as Eq. 1.9, where k_p is the rate constant of propagation, K_{ATRP} is the equilibrium constant in ATRP ($K_{ATRP} = k_{act}/k_{deact}$), [M] is the monomer concentration, $[P_nX]$ is the concentration of dormant initiators.

$$R_p = k_p[M][P_n^*] = k_p K_{ATRP}\left(\frac{[P_nX][Cu^I/L][M]}{[X\text{-}Cu^{II}/L]}\right) \qquad \text{Eq. 1.9}$$

The values of the rate constants, k_{act}[44] and k_{deact},[45] and their ratio, K_{ATRP}[46, 47] are strongly influenced by the coordination property of the ligand and monomer/dormant species as well as reaction conditions (solvent, temperature, and pressure). The rate of ATRP increase with catalysts' activity (K_{ATRP}) but may decrease as a result of low $[Cu^{I}/L]/[X\text{-}Cu^{II}/L]$ ratio caused by radical termination and a resulting buildup in the $[X\text{-}Cu^{II}/L]$ via the persistent radical effect.[6]

The number average degree of polymerization DP_n and molecular weights of the polymers in an ideal ATRP follow the ratio of the mass of the consumed monomer to the effective initiator concentration (Eq. 1.10).

$$DP_n = \frac{[M]_0}{[I]_0} \times \text{conversion} \qquad \text{Eq. 1.10}$$

The molecular weight distribution or polydispersity index (PDI) refers to the polymer chain length distribution. Eq. 1.11 shows that in the ideal case for fast initiation and no chain termination or chain transfer, the PDI (M_w/M_n) of polymers prepared by ATRP is affected by the concentration of dormant species (P_nX) and deactivator ($X\text{-}Cu^{II}$), the rate constants of propagation (k_p) and deactivation (k_{deact}), and monomer conversion (p).[48]

$$\frac{M_w}{M_n} = 1 + \frac{1}{DP_n} = \left(\frac{k_p[P_nX]}{k_{deact}[X\text{-}Cu^{II}/L]}\right)\left(\frac{2}{p} - 1\right) \qquad \text{Eq. 1.11}$$

It can be seen from Eq. 1.11 that for the same monomer, a catalyst that deactivates the growing chains faster will result in a lower M_w/M_n value and a narrower molecular weight distribution. This value can be decreased by increasing the concentration of deactivator, reducing the concentration of the dormant species, and reaching higher conversion.

Chain growth in ATRP occurs via radical intermediates that exchange with dormant species. These radicals are not only intermittently formed and propagate but also continuously temporally terminate. In ATRP, the life time of propagating chains is expanded from about 1 second in conventional FRP to more than 1 day, by inserting dormant periods of ~1 minute after each ~1 ms activity. Thus, the 1 second of radical activity is expanded to

several hours with hundreds of intermediate dormancy periods.

Two key factors are needed for a good kinetic control in ATRP. Firstly, because the rate constant of radical termination (k_t) is usually high, the radical concentration must be much lower than that in conventional FRP in order to eliminate the chain termination. This requires the equilibrium shift towards the deactivation reaction. Therefore, k_{deact} must be significantly higher than k_{act} in order to ensure a sufficiently low concentration of polymer radicals and minimize termination reactions. Secondly, the rates of both activation and deactivation (R_{act} and R_{deact}) should be much higher than propagation rate (R_p) so that addition of monomer units in each cycle controlled. As a result, the polymer chains will grow concurrently and the polydispersity index will be kept low (e.g. PDI < 1.5). Furthermore, low temperatures are not required for ATRP compared to anionic living polymerization and this mild reaction condition could attract more industrial interest.

Although ATRP is one of the most promising CRP systems, it still bears some drawbacks which significantly limit its commercial scale application: 1) High molecular weights are often difficult to achieve due to outer sphere electron transfer processes, involving oxidation or reduction of radicals, as well as β-H elimination reactions; 2) ATRP typically requires a relatively high concentration of transition metal catalyst to ensure a rapid shift between activation and deactivation. These catalysts are normally toxic to organism and not friendly to the environment; 3) There are limitations in the range of polymerizable monomers. For instance, the controlled polymerizations of vinyl chloride, vinyl acetate, acrylamide and some acidic monomers are still challenging. To overcome these drawbacks, different approaches and processes have been developed.

1.2.5 ATRP Initiation Systems

There is a huge evolution of ATRP processes during the past 20 years. These ATRP processes were conducted by the different conditions for initiation step. The mechanisms of these ATRP processes are shown in Figure 1.9.

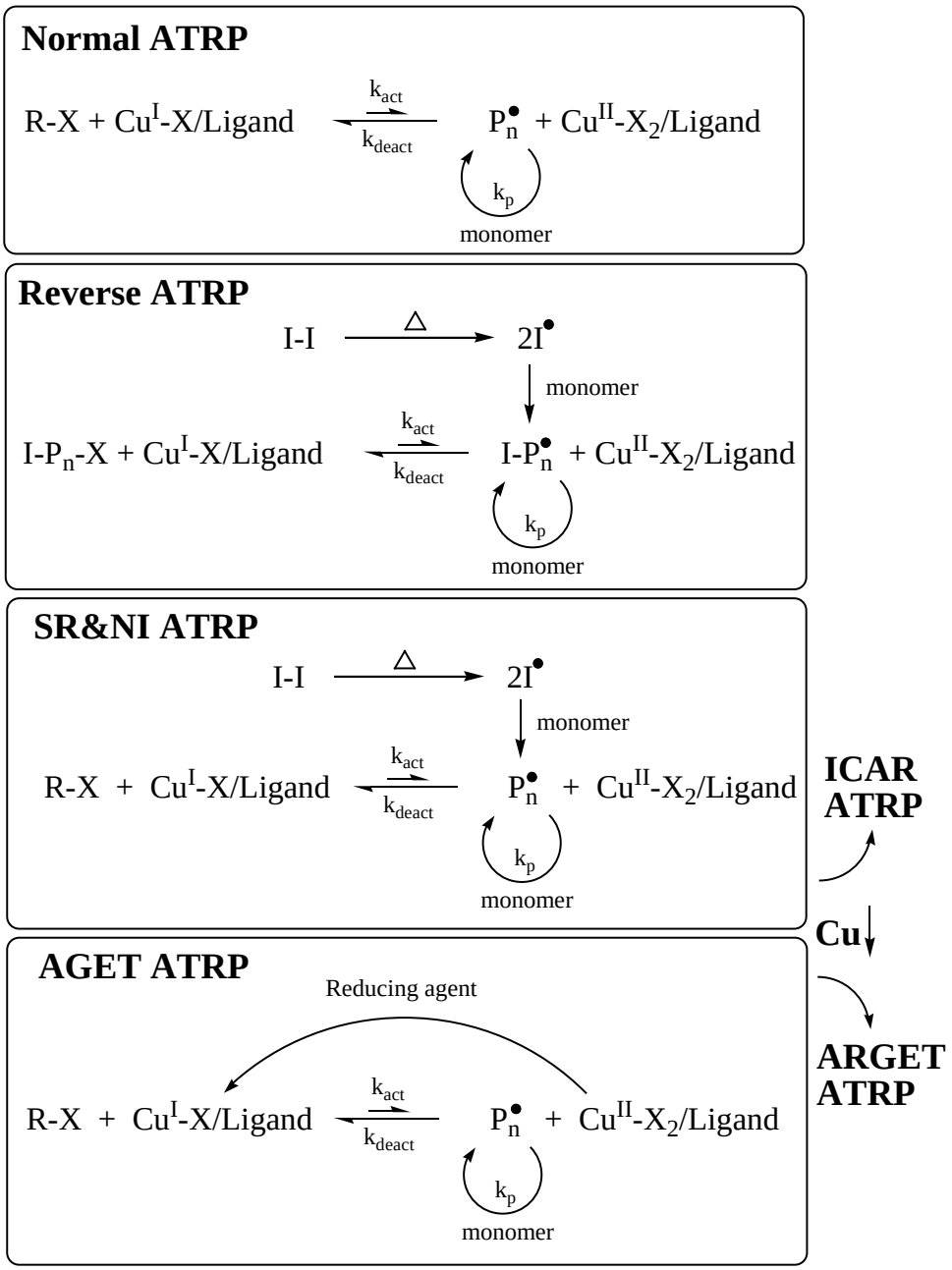

Figure 1.9 General initiation mechanisms of normal ATRP, reverse ATRP, SR&NI ATRP reaction, ICAR ATRP, AGET ATRP and ARGET ATRP.

The normal ATRP procedure is firstly developed in 1995.[18, 19] The polymerization starts by an alkyl halide (R-X, initiator), transition metal catalyst in a lower oxidation (Cu^I/Ligand) and monomers (Figure 1.9). A relatively high concentration of metal and ligands is introduced. Meanwhile, the metal catalyst at a lower oxidation (e.g. Cu^I) is sensitive to the air.

Furthermore, due to the lack of deactivator (Cu^{II}) at the initial stage, the initial polymerization suffers from bad control.

The reverse ATRP was also developed in 1995.[20, 49] In the reverse ATRP, the transition metal complexes in its higher oxidation state (e.g. Cu^{II}) were added initially to the reaction and the alkyl halide initiator was substituted with conventional thermal initiator (e.g. AIBN) to generate free radicals (Figure 1.9). The ATRP initiator and lower oxidation state transition metal activator (e.g. Cu^{I}) are generated from the deactivation of the radicals and the higher oxidation state deactivator (Cu^{II}). The degree of polymerization is calculated by Eq. 1.12, where [M] is concentration of monomer, [I-I] is the concentration of thermal initiator, f is the initiation efficiency. The initial components in reverse ATRP is not sensitive to oxygen and can be easily prepared, stored, and shipped for commercial use. However, because the radicals are generated by thermal decomposition which is not efficient enough, the concurrent growth of polymer chains is affected and thus the polydispersity is relative higher than normal ATRP. Moreover, the initiator end group (I) remains in the polymer chain (I-P-X). Additionally, this process could only be used for the preparation of linear homopolymers rather than block copolymers or polymers with a more complex architecture.

$$DP_n = \frac{[M]_0}{2 \times f \times [I\text{-}I]_0} \times \text{conversion} \qquad \text{Eq. 1.12}$$

Normal ATRP and reverse ATRP was merged into a new procedure named simultaneous reverse and normal initiation ATRP (SR&NI) which was reported in 2001.[50] SR&NI ATRP takes advantage of using more active catalyst complexes in higher oxidation state (Cu^{II}) with addition of a dual initiation system comprised of a relatively high ratio of alkyl halide initiator (R-X) concurrently with a low ratio of thermal initiator (e.g. AIBN) (Figure 1.9). Firstly, the thermal initiator (I-I) decomposes into radicals which can transfer the metal in higher oxidation state (Cu^{II}) into the lower oxidation state (Cu^{I}) as the activator. Once the Cu^{I} is generated, the alkyl halides will be initiated as the main initiator for polymer growth via normal ATRP initiation mechanism. The degree of polymerization can be calculated by Eq.

1.13, where [M] is the concentration of monomer, [R-X] is the concentration of alkyl halide, [I-I] is the concentration of conventional initiator, f is the initiation efficiency of the thermal initiator. SR&NI ATRP takes the advantage of normal ATRP and reverse ATRP by using stable oxidized metal complex and alkyl halide initiator. This procedure has also been applied in mini-emulsion systems.[51, 52] A limitation of SR&NI was the formation of a small fraction of polymer chains initiated by the added free radical initiator. This also happens in systems based on degenerative transfer, such as RAFT, as new chains are always continuously generated.

$$DP_n = \frac{[M]_0}{[R\text{-}X]_0 + 2 \times f \times [I\text{-}I]_0} \times \text{conversion} \qquad \text{Eq. 1.13}$$

SR&NI evolved into activators generated by electron transfer (AGET) in 2005 to overcome the disadvantage in SR&NI procedure.[53, 54] In AGET ATRP, the higher oxidation state transition metal complex (Cu^{II}) is initially added and reduced into the activator (Cu^{I}) by reducing agent (Figure 1.9). Then, the radicals can be generated by the activation of alkyl halide initiators with Cu^{I}. In this way, thermal initiator can be left out with no end group (I) remains in the polymer chain (I-P-X). The molecular weight of polymer chain can be calculated as the same as normal ATRP (Eq. 1.10). Various reducing agents could be used in AGET, such as tin(II) 2-ethylhexanoate, glucose and ascorbic acid which are all approved by food and drug administration (FDA). Thus, the AGET ATRP shows many advantages, including stable catalyzing system, thermal initiator end-group free product and controlled molecular weight and polydispersity. The technique has proven particularly useful in aqueous and miniemulsion systems.

Due to the industrial requirements of acceptable polymerization rate and low metal/ligand concentration, the activator regenerated by electron transfer (ARGET) ATRP and the initiators for continuous activator regeneration (ICAR) ATRP was developed in 2006,[55, 56] as extensions of the concept of AGET ATRP and SR&NI ATRP to reduce the amount of metal complex catalyst in the polymerization. In ARGET ATRP, small amount of

catalyst is continuously regenerated by a reducing agent to account for unavoidable levels of radical termination. ARGET is a 'green' procedure that uses ppm of the catalyst in the presence of appropriate reducing agents. Since the reducing agents allow starting an ATRP with the stable Cu^{II} species, the reducing/reactivating cycle can be also employed to eliminate air, or other radical traps, in the system. An additional advantage of ARGET ATRP is that catalyst induced side reactions are diminished. Therefore, it is possible to prepare copolymers with higher molecular weight while retaining chain end functionality.[57, 58, 59] In ICAR ATRP, a source of organic free radicals is employed to continuously regenerate the Cu^{I} activator, which would otherwise be consumed in termination reactions, when catalysts are used at very low concentrations. With ICAR ATRP, controlled synthesis of polystyrene and poly(methacrylates) ($M_w/M_n < 1.2$) can be conducted with catalyst concentrations between 5 and 50 ppm, levels at which removal or recycling of the catalyst complex could be avoided for some applications. The reaction is driven to completion with addition of low concentrations of standard free radical initiators.[60] The rate of ICAR ATRP is governed by the rate of decomposition of the added free radical initiator, while the degree of control, the rate of deactivation, and PDI are controlled by K_{ATRP}, as in ATRP[60]. The key point to reduce the amount of metal complex catalyst in both ARGET ATRP and ICAR ATRP lies in the high activity of the metal complex catalyst (K_{ATRP}, k_{act}, k_{deact} are high, *e.g.* Cu/Me_6TREN) so that it can support both an acceptable polymerization rate and a kinetic control.

1.2.6 Deactivation Enhanced ATRP

When a radical is generated in the ATRP system, it mainly has three options: 1) to propagate with monomer; 2) to terminate and 3) to be deactivated into a dormant species. These three reactions form a dynamic competition which depends on their reaction rates. It can be noticed that as long as the deactivation rate is fast enough, the termination will be neglected and chain growth will be slowed down so that the initiation will become fast enough compared to chain growth. Most importantly, the kinetic chain length (ν) is strongly dependent on deactivation rate as shown in Eq. 1.14.

$$\nu = \frac{R_p}{R_{deact} + R_t} \approx \frac{R_p}{R_{deact}} = \frac{k_p[M][P^\bullet]}{k_{deact}[P^\bullet][Cu^{II}]} = \frac{k_p[M]}{k_{deact}[Cu^{II}]} \qquad \text{Eq. 1.14}$$

Based on this consideration, deactivation enhanced ATRP (DE-ATRP) was developed with initial deactivator added.[61, 62] In copper-mediated ATRP, the added Cu^{II} will significantly increase the deactivation rate ($R_{deact}=k_{deact}[Cu^{II}][P^\bullet]$) and thus push the equilibrium towards deactivation. Furthermore, added Cu^{II} can stabilize the ratio of Cu^{I} and Cu^{II} and keep it similar to their initial ratio after the equilibrium gets balanced. The normal ATRP and DE-ATRP has been modelled by Matyjaszewski[61, 63] and Fischer.[6] As shown in Figure 1.10, in the presence of initial Cu^{II}, the concentrations of almost all species, including the dormant species [P-X], $[Cu^{I}]$, $[Cu^{II}]$ and the radical concentration $[P^\bullet]$, are constant during the whole polymerization, because the Cu^{II} do not need to be accumulated to a sufficient concentration. $[Cu^{II}]$ starts to accumulate and radical concentration starts to decrease only after the reaction reaches a high conversion. The ATRP equilibrium ($R_{act}=R_{deact}$) is set up immediately from the beginning of the reaction, due to the initial presence of Cu^{II}. This is beneficial for the control of polymerization, since no sacrificial loss of growing chains is needed to produce a sufficient Cu^{II} amount.

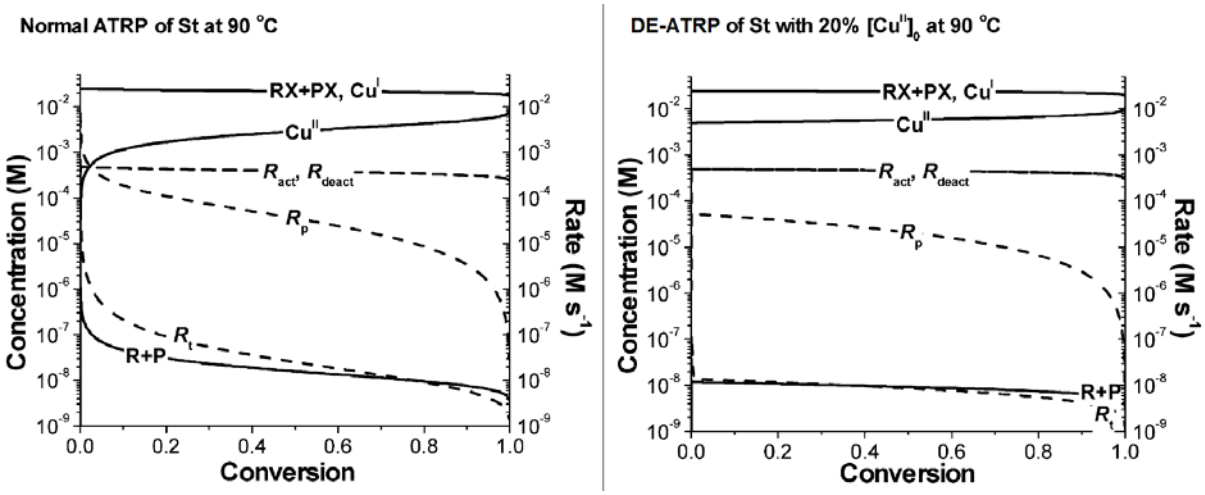

Figure 1.10 Simulated concentrations of all species (solid lines) and all rates (broken lines) for normal ATRP and DE-ATRP of styrene at 90°C,[63] showing the concentrations of all species in DE-ATRP are almost constant during the whole polymerization. Copyright 2008, Wiley.

With the help of the kinetics calculations, it is much easier to understand the effect of all species in the reactions. Here, kinetic calculations were implemented to reveal the difference between the normal ATRP and DE-ATRP. The concentration of radicals ($[P^{\bullet}]$), instantaneous kinetic chain length (ν), average life-time of the radicals (τ) and the time span of activation (τ_{act}) and deactivation (τ_{deact}) periods are investigated under the same conditions (*e.g.* $[M]_0$, $[I]_0$, $[Cu^I]$/Ligand, solvent and temperature) with the same rate constant (*e.g.* k_p, k_{act}, k_{deact}, k_t) in ATRP and DE-ATRP reactions. The chain transfer and other side reactions are excluded in this part.

Kinetics study of normal ATRP

In normal ATRP, the Cu^I firstly activate the initiators into free radicals ($P^{\bullet}$) and convert itself into Cu^{II} species. The $[P^{\bullet}]$ increases concurrently with the $[Cu^{II}]$ when the reaction starts. When R_{deact} ($R_{deact}=[Cu^{II}][P^{\bullet}]k_{deact}$) reaches the value of R_{act} ($R_{act}=[Cu^{I}][I]k_{act}$), the reaction enters the quasi-equilibrium stage. During this stage, the deactivation becomes the major process of the radical consumption ($R_{deact}>>R_t$). In this calculation, the quasi-equilibrium is the only stage considered for comparison purpose. The polymerization of styrene was analyzed by the parameters listed in Table 1.1.

Table 1.1 Rate constant values of normal ATRP and DE-ATRP of styrene. $[M]_0/[I]_0/[Cu^I]_0/[Cu^{II}]_0/[L]_0=100/1/1/x/1$, I=PEBr (l-phenylethyl bromide), L=PMDETA (N,N,N'N'N"-pentamethyldiethylenetriamine, $[M]_0=2.5$ M; $[I]_0=0.025$ M, T=90 °C. The rate constants values were taken from references.[43, 44, 46, 64, 65]

Rate constant	activation rate (k_{act})	deactivation rate (k_{deact})	propagation rate (k_p)	termination rate (k_t)
Value ($M^{-1}s^{-1}$)	0.79	$8.4*10^6$	665	$1.1*10^8$

The reaction time of the equilibrium can be calculated by the Eq. 1.15,[6, 63] showing that the quasi-equilibrium was reached 0.14 s after the reaction started.

$$t_{equilibrium} = \frac{\sqrt{6k_t}K_{ATRP}}{k_{act}^{3/2}[I]_0} = \frac{\sqrt{6\times1.1\times10^8}\times\frac{0.79}{8.4\times10^6}}{0.79^{3/2}\times0.025} = 0.14s \quad \text{Eq. 1.15}$$

During the quasi-equilibrium stage, the R_{act} is equal to R_{deact}. Thus, the $[Cu^{II}]$ and $[P^{\bullet}]$ were calculated assuming the equilibrium was established. The values are calculated by the Eq. 1.16 and Eq. 1.17.[63]

$$[Cu^{II}]_{equilibrium} = k_{act}[Cu^{I}]_0[I]_0 t$$
$$= 0.79M^{-1}s^{-1}\times0.025M\times0.025M\times0.14s = 6.9\times10^{-5}M \quad \text{Eq. 1.16}$$

$$R_{act} = R_{deact}$$
$$k_{act}[I][Cu^{I}] = k_{deact}[P^{\bullet}][Cu^{II}]$$

$$[P^{\bullet}]_{ATRP} = \frac{k_{act}}{k_{deact}}[I]\frac{[Cu^{I}]}{[Cu^{II}]}$$
$$= \frac{0.79}{8.4\times10^6}\times0.025\times\frac{0.025-6.9\times10^{-5}}{6.9\times10^{-5}} = 8.5\times10^{-7}M \quad \text{Eq. 1.17}$$

The instantaneous kinetic chain length of ATRP is defined as the average number of monomer units added to the propagating radical during each activation-deactivation cycle. The Eq. 1.18 calculates that an average number of 2.87 of monomer units were inserted to the propagating center during each activation-deactivation cycle.

$$\nu_{ATRP} = \frac{R_p}{R_{deact}} = \frac{k_p[M][P^{\bullet}]}{k_{deact}[P^{\bullet}][Cu^{II}]}$$
$$= \frac{665M^{-1}s^{-1}\times2.5M}{8.4\times10^6M^{-1}s^{-1}\times6.9\times10^{-5}M} = 2.87 \quad \text{Eq. 1.18}$$

The radical life-time (τ_{ATRP}) was calculated by Eq. 1.19. The life-time of radical is extended to 0.005 s due to the relative lower radical concentration.

$$\tau_{ATRP} = \frac{[P^{\bullet}]}{R_t} = \frac{[P^{\bullet}]}{2k_t[P^{\bullet}]^2}$$
$$= \frac{1}{2\times1.1\times10^8M^{-1}s^{-1}\times8.5\times10^{-7}M} = 0.005s \quad \text{Eq. 1.19}$$

Moreover, the time span of deactivation ($\tau_{deact(ATRP)}$) and activation ($\tau_{act(ATRP)}$) periods were calculated to be $1.7*10^{-3}$ s (Eq. 1.20) and 50.6 s (Eq. 1.21), respectively. This indicates that the dormant species is activated every 50.6 s and then deactivated after $1.7*10^{-3}$ s.

$$\tau_{deact(ATRP)} = \frac{[P^\bullet]}{R_{deact}} = \frac{[P^\bullet]}{k_{deact}[P^\bullet][Cu^{II}]}$$
$$= \frac{1}{8.4\times10^{6} M^{-1}s^{-1} \times 6.9\times10^{-5} M} = 1.7\times10^{-3} s \qquad \text{Eq. 1.20}$$

$$\tau_{act(ATRP)} = \frac{[P^\bullet]}{R_{act}} = \frac{[P^\bullet]}{k_{act}[P^\bullet][Cu^{I}]}$$
$$= \frac{1}{0.79 M^{-1}s^{-1} \times (0.025 - 6.9\times10^{-5}) M} = 50.6 s \qquad \text{Eq. 1.21}$$

The actual life-time of the radicals in normal ATRP is 148 seconds which include the activation-deactivation cycles from the Eq. 1.22.

$$\tau'_{ATRP} = \frac{\tau_{ATRP}}{\tau_{deact}}\tau_{act} = \frac{0.005 s}{1.7\times10^{-3} s} \times 50.6 s = 148 s \qquad \text{Eq. 1.22}$$

Kinetics study of DE-ATRP

With initially added Cu^{II} (30% of Cu^{I}), the kinetics of DE-ATRP is quite different from normal ATRP. The polymerization reached the quasi-steady-state at the very beginning of reaction because the PRE effect is ignored in this process. The concentrations of almost all species were constant during the polymerization.[62, 63] In this comparison, 30% Cu^{II} (of Cu^{I}) was initially added to the system. The polymerization of styrene was calculated by the parameters listed in Table 1.1.

The concentration of radicals can be calculated as Eq. 1.23. The result ($7.84*10^{-9}$ M) is much lower than previous calculation in normal ATRP.

$$[P^\bullet]_{DE-ATRP} = \frac{k_{act}}{k_{deact}}[I]\frac{[Cu^{I}]}{[Cu^{II}]}$$
$$= \frac{0.79}{8.4\times10^{6}} \times 0.025 \times \frac{0.025}{0.0075} = 7.84\times10^{-9} M \qquad \text{Eq. 1.23}$$

For DE-ATRP, the instantaneous kinetic chain length is calculated to be 0.026 from Eq. 1.24. This value was much smaller than in a normal ATRP (ν_{ATRP}=2.87). This means one monomer unit is added to an active radical after 37 cycles of activation and deactivation in DE-ATRP. This also ensures that all the radicals are activated and propagate at the same time.

$$\nu_{DE-ATRP} = \frac{R_p}{R_{deact}} = \frac{k_p[M][P^\bullet]}{k_{deact}[P^\bullet][Cu^{II}]} = \frac{665 M^{-1}s^{-1} \times 2.5M}{8.4\times10^6 M^{-1}s^{-1} \times 0.0075M} = 0.026 \quad \text{Eq. 1.24}$$

The radical life-time ($\tau_{DE\text{-}ATRP}$) is calculated to be 0.58s from Eq. 1.25 which is 116 times longer than the normal ATRP (0.005s), due to the quite lower radical concentration.

$$\tau_{DE-ATRP} = \frac{[P^\bullet]}{R_t} = \frac{[P^\bullet]}{2k_t[P^\bullet]^2} = \frac{1}{2\times1.1\times10^8 M^{-1}s^{-1} \times 7.84\times10^{-9}M} = 0.58s \quad \text{Eq. 1.25}$$

In addition, the time span of deactivation ($\tau_{deact(ATRP)}$) and activation ($\tau_{act(ATRP)}$) periods were calculated to be 1.59*10^{-5} s (Eq. 1.26) and 50.6 s (Eq. 1.27), respectively. This means the active species will only exist for 1.59*10^{-5} seconds and then be deactivated for 50.6 seconds until another activation occurs.

$$\tau_{deact(DE-ATRP)} = \frac{[P^\bullet]}{R_{deact}} = \frac{[P^\bullet]}{k_{deact}[P^\bullet][Cu^{II}]} = \frac{1}{8.4\times10^6 M^{-1}s^{-1} \times 0.0075M} = 1.59\times10^{-5}s \quad \text{Eq. 1.26}$$

$$\tau_{act(DE-ATRP)} = \frac{[P^\bullet]}{R_{act}} = \frac{[P^\bullet]}{k_{act}[P^\bullet][Cu^{I}]} = \frac{1}{0.79 M^{-1}s^{-1} \times (0.025 - 6.9\times10^{-5})M} = 50.6s \quad \text{Eq. 1.27}$$

As a result, the actual life-time of the radicals was extended to 1.8*10^6 seconds (21 days) in DE-ATRP reaction which includes numerous

activation-deactivation cycles (Eq. 1.28).

$$\tau'_{DE-ATRP} = \frac{\tau_{DE-ATRP}}{\tau_{deact}}\tau_{act}$$
$$= \frac{0.58s}{1.59\times10^{-5}s}\times 50.6s = 1.8\times10^{6}s \approx 21days \qquad \text{Eq. 1.28}$$

The above results are all summarized in Table 1.2, from which we can see that: 1) the concentration of radicals ([P$^{\bullet}$]) in DE-ATRP is much lower than normal ATRP. Therefore, the chance of radical termination is tremendously suppressed. The life time of radical (τ) in DE-ATRP is also extended longer than normal ATRP. 2) The instantaneous kinetic chain length (ν) of DE-ATRP is much lower than normal ATRP, since the time span of deactivation (τ_{deact}) is much shorter in DE-ATRP. Therefore, the propagating radical is only allowed add very few monomer units (ν_{ATRP}) during each activation-deactivation cycle. 3) The actual life-time of the radicals (τ') is increased from 148 seconds to $1.8*10^6$ seconds (21 days) in DE-ATRP, so that more polymer chains remain their living characters in DE-ATRP.

Table 1.2 The Summary results of kinetics calculation in the polymerization of styrene by normal ATRP and DE-ATRP reaction (Eq.1.16 - Eq.1.28). ATRP reaction conditions: T=90 °C, $[M]_0/[I]_0/[Cu^I]_0/[L]_0$=100/1/1/1, I=PEBr, L=PMDETA, $[M]_0$=2.5 M; $[I]_0$=0.025 M; DE-ATRP reaction conditions: T=90 °C, $[M]_0/[I]_0/[Cu^I]_0/[Cu^{II}]_0/[L]_0$= 100/1/1/0.3/1.3, I=PEBr, L=PMDETA, $[M]_0$=2.5 M; $[I]_0$=0.025 M.

	Normal ATRP	DE-ATRP
Concentration of radicals ($[P^{\bullet}]$) /M	$8.5*10^{-7}$	$7.84*10^{-9}$
Kinetic chain length (ν) [a]	2.87	0.026
Life-time of radicals (τ) /s	0.005	0.58
Time span of deactivation (τ_{deact}) /s	$1.7*10^{-3}$	$1.59*10^{-5}$
Time span of activation (τ_{act}) /s	50.6	50.6
Actual life-time of the radicals (τ') /s	148	$1.8*10^{6}$

[a] The instantaneous kinetic chain length is defined as the average number of monomer units added to the propagating free radical during each activation-deactivation cycle.

1.3 Hyperbranched Polymers

1.3.1 Concept and History

Hyperbranched polymers (HBPs) are defined as random branched dendritic macromolecules prepared in a single-step polymerization. They belong to a subclass of dendritic polymers which mainly include dendrimers with perfect globular structures and hyperbranched polymers with random branches.[66] Although the term and definition of HBPs were coined by the DuPont researchers, Kim and Webster, in the late 1980s,[67, 68] the history of HBP can be dated back to the end of the 19th century, when Berzelius

synthesized a HB resin from tartaric acid (A_2B_2-type monomer) and glycerol (B_3-type monomer).[69] In 1901, the reaction of phthalic anhydride or phthalic acid and glycerol was attempted by Watson Smith and further investigated by Kienle who showed that the specific viscosities of HBPs were lower than those of linear polymers (e.g., polystyrene).[69] In 1909, using formaldehyde (latent A_2 monomer) and phenol (latent B_3 monomer), Baekeland produced synthetic plastic and phenolic HBPs in his Bakelite Company and further commercialized this product.

In the 1940s, Flory *et al*. introduced the concepts of 'degree of branching' and 'highly branched species' when they calculated the molecular weight (MW) distribution of three-dimensional polymers in the state of gelation.[70, 71, 72] In 1952, Flory pointed out theoretically that highly branched polymers can be synthesized without the risk of gelation by polycondensation of AB_2 monomer.[73] This work primarily lays the theoretical foundation of highly branched polymers. The subsequent three decades had witnessed the fast and incredible development of linear, cross-linked and chain branched polymers.

The real flourish of HBPs began after the discovery of dendrimers with the focus shifting from strength to functionality in the field of polymer science and technology. The focus was firstly concentrated on the preparation and studies of perfect monodisperse dendrimers. Step-by-step synthesis, purification, protection and deprotection are needed for accessing these well-defined macromolecules. Although the employment of 'click' chemistry, especially the Cu^I-catalyzed azide-alkyne click chemistry[74, 75] and thiol-ene click chemistry which possesses the merits of specificity, fast reaction, tolerance to common functional groups and water, greatly furthers the progress of dendrimer synthesis because tedious protection/deprotection and chromatography-based purification steps are not required any more,[76, 77] the accessible varieties and structures through click chemistry are still limited at present. For use as engineering materials, dendrimers are still far too complicated and costly to produce.

This limitation was soon realized by Kim and Webster at DuPont Experimental Station, from which several publications emerged in the early

1990s.[68, 78] The requirement of rapid synthesis and large quantities forced them to develop a route for a one-step synthesis of dendritic polyphenylenes.[67, 68, 79] These polymer products were polydispersed with defects of linear segments but they were still highly branched dendritic molecules. Kim and Webster named them *Hyperbranched Polymers*. Since then, a variety of HBPs have been synthesized and presented in the literature.

Since the mid-1990s, the field of polymer chemistry has witnessed the explosive development of a number of procedures of controlled/living radical polymerization (CRP).[27, 43] CRP allows the synthesis of various types of functional polymeric materials and provides the capability of designing branched polymers with controlled site-specific functionality and predeterminable topology. The development of the Self-Condensing Vinyl Polymerization (SCVP) broke the conventional opinions that preparation of HBPs has been restricted to the polycondensation and provided a route to prepare HBP by addition polymerization of vinyl monomers which remains one of the most heavily used raw materials in polymer industry.

In 2000, Sherrington[80, 81] and co-workers developed a facile synthetic methodology (the ‘Strathclyde synthesis') for the high yielding synthesis of branched vinyl polymer using conventional free radical copolymerization of a vinyl monomer with a divinyl monomer with appropriate levels of a stoichiometric free radical chain transfer agent. In 2003, a similar radical copolymerization was reported by Sato[82, 83, 84] who incorporated an initiator fragment and termed the method as initiator-fragment incorporation radical polymerization (IFIRP). This radical copolymerization is further enriched by using different CRP techniques, known as controlled radical crosslinking copolymerization (CRCC). The main history of development of HBPs was summarized in Table 1.3.

Table 1.3 History of hyperbranched polymers[66]

Year	Case	Lead Authors	Reference
Before 1900	Tartaric acid + glycerol	Berzelius	69
1901	Glycerol + phthalic anhydride	Smith	69
1929-1939	Glycerol + phthalic anhydride	Kienle	77, 78, 79
1941	Molecular size distribution in theory	Flory	70, 71, 72
1952	AB_n polymerization in theory	Flory	73
1982	AB_2 + AB copolymerization	Kricheldorf	85
1987-1991	AB_2 homopolymerization	Kim/Webster	68
		Odian/Tomalia	86
		Fréchet/Hawker	87
1995	SCVP	Fréchet	88
		Matyjaszewski	15, 89, 90
2000	Strathclyde synthesis	Sherrington	80, 81
2003	IFIRP	Sato	82, 83, 84
Since 1997	CRCC	Fukuda	91, 92
		Armes	93
		Perrier	94, 95

1.3.2 Degree of Branching

Degree of branching (DB) is an important parameter to characterize a hyperbranched polymer. Generally, there are linear (L), dendritic (D) and terminal (T) repeating units in a hyperbranched macromolecule prepared from an AB_2-type monomer. The degree of branching is defined as the ratio of branched, terminal, and linear units in the polymer (Eq. 1.29) by Fréchet.

According to this definition, the DB equals to 1 for an ideal dendrimer. The DB of hyperbranched polymer varies between 0 and 1. However, for a linear polymer, the DB value is higher than 0 by this way of calculation (Figure 1.11).

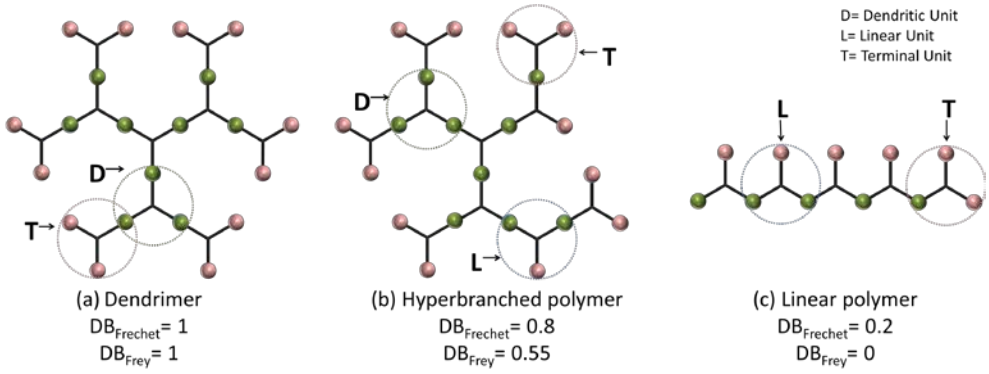

Figure 1.11 Scheme of different units in dendrimer, hyperbranched polymer and linear polymer. The different degree of branching values were given according to two different definitions ($DB_{Frechet}$ and DB_{Frey}).

$$DB_{Frechet} = \frac{\sum \text{dendritic units} + \sum \text{terminal units}}{\sum \text{dendritic units} + \sum \text{terminal units} + \sum \text{linear units}} = \frac{D+T}{D+T+L}$$

Eq. 1.29

$$DB_{Frey} = \frac{r}{r_m} = \frac{2 \times \sum \text{dendritic units}}{2 \times \sum \text{dendritic units} + \sum \text{linear units}} = \frac{2D}{2D+T}$$

Eq. 1.30

Therefore, Frey, Müller and Yan introduced a modified equation for the calculation of DB.[96, 97] The DB_{Frey} is defined as the ratio of the number of growth directions (r) to the maximum possible number of growth directions (r_m) (Eq. 1.30). As a result, the DB_{Frey} of dendrimer remains as 1 (Figure 1.11), but this value decreases to 0 for the linear polymer. The degree of branching in this thesis will follow the definition of DB_{Frey}.

DB is one of the most important parameters for HBP because it has a close relationship with polymer properties such as chain entanglement, mean-square radius of gyration (R_g), free volume, glass-transition temperature (T_g), degree of crystallization (DC), mechanical strength,

melting/solution viscosity (η), self-assembly behaviors, capability of encapsulation and biocompatibility. For instance, Frey revealed that hyperbranched polyglycerol (HPG) showed much higher capacity in supramolecular encapsulation of guest dyes than its linear analog;[98] Haag demonstrated that hyperbranched poly(ethyleneimine) (PEI) with a moderate DB (0.5-0.7), rather than too high or too low, is beneficial to gene transfection in the gene delivery.[99] So the research on this aspect would be a promising direction, which will discover the essential difference and intrinsic similarity among linear polymers and HBPs. The knowledge can then help scientists to design materials with desirable properties.

1.3.3 Synthesis Methodology of HBP

Up to now, the synthetic techniques used to prepare HBPs could be divided into two major categories according to the reaction mechanism: (1) Step growth polymerization (or polycondensation)[67, 68, 86, 100, 101, 102, 103] and (2) Chain growth polymerization (or additional polymerization), including self-condensing vinyl polymerization (SCVP)[15, 88, 89, 90, 104] and controlled radical polymerization (CRP) of multi-vinyl monomers (MVMs).[80, 82, 93, 95, 105, 106, 107]

1.3.3.1 Polycondensation towards HBP

Polycondensation or step-growth polymerization is a traditional and widely used method to prepare HBPs. There are mainly two types of polycondensations towards HBPs. The first type is the technique of polymerization of a single AB_n monomer (Figure 1.12). The other type uses two types of monomers (such as A_2 and B_3) or a monomer pair as raw materials to generate HBPs (Figure 1.13).

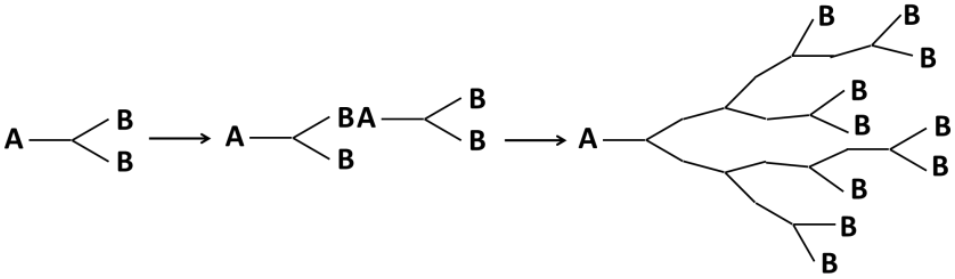

Figure 1.12 Hyperbranched polymer prepared by AB_2 type monomer.

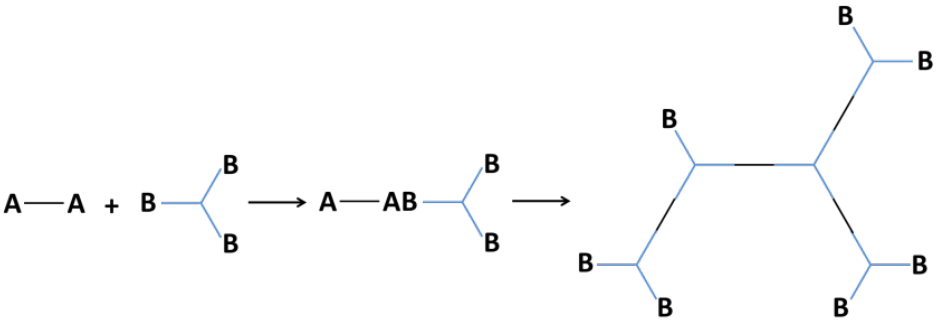

Figure 1.13 Hyperbranched polymer prepared by A_2+B_3 methodology.

The step-growth polymerization of AB_n monomers became the first and most intensively studied route to HBPs.[108, 109] A typical procedure involves a one-step reaction in which the monomer, initiator and catalyst are firstly mixed and then heated to the required reaction temperature. The one-pot polymerization of AB_n monomers provides polymer products with a distribution in molar mass and branching. Oligomers are formed throughout the reaction and are often removed by blowing an inert gas or by reducing the pressure of the reaction for the purpose of reaching a high conversion. The polymer product is generally precipitated against anti-solvent and dried without any other special purification process.

A number of commercial AB_2 monomers were chosen for step-growth polymerizations. A broad range of HBPs, including hyperbranched polyphenylenes, polyethers, polyesters, polyamides, polycarbonates, and poly(ether ketone)s, are prepared via one-step polycondensation of AB_n type monomers. AB_3, AB_4, AB_5, and even AB_6 monomers are also used to

synthesize HBPs while controlling the branching pattern. Typically, the DB of these polymers ranges between 0.5~0.6.[87, 110, 111]

Furthermore, a 'core' molecule B_n (n > 2) was added to the AB_n polycondensation (Figure 1.14) for achieving a better control over the molecular weight and the polymer shape.[112, 113, 114] Moreover, polymerization of AB_n monomers with core molecules (B_n) can also increase the DB of HBPs. For instance, in the reaction of 2,2 -bis(methylol)propionic acid (bis-MPA) and tris(methylol) propane (TMP), the DB is increased to 0.8.[108, 109]

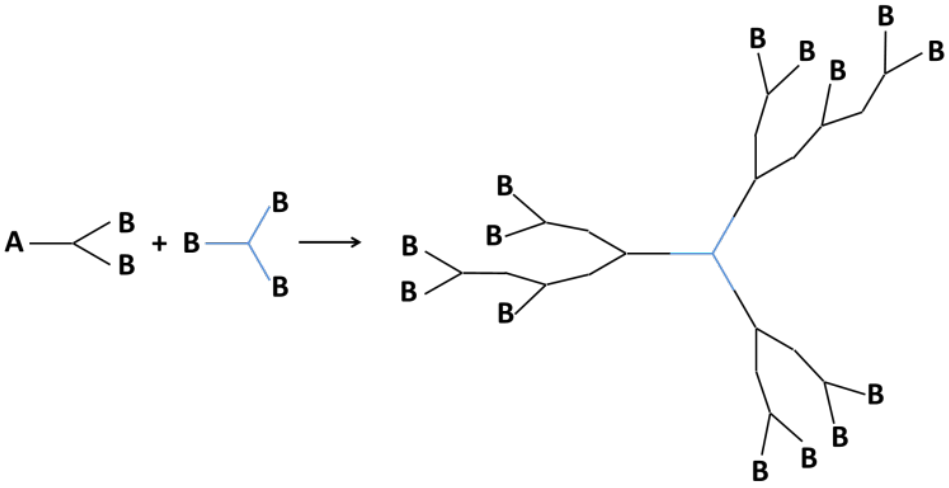

Figure 1.14 Hyperbranched polymer prepared by AB_2 and B_3 type monomer.

The polymerization of A_2 and B_3 (or B_n, n>2) or the 'A_2+B_3' methodology was first adopted by Kakimoto[103] and Fréchet[115] to prepare soluble HBPs. Although the 'A_2+B_3' approach to HBPs holds some merits over the traditional AB_2 polycondensation approach, such as adjustable polymer composition and commercial availability of monomers, it still bears the major problem of uncontrollable gelation, especially under conditions of high reaction temperature and high monomer concentration. To avoid gelation, the monomer concentration must be reduced or the monomers must be slowly added to the reaction. Also, the polymerization must be stopped prior to the critical gelling point. This strongly limits the industrial application of the 'A_2+B_3' approach in large-scale manufacture of HBPs.

One strategy based on the non-equal reactivity of functional groups and *in situ* formation of AB_n intermediates from specific monomer pairs was invented[116, 117, 118]. Because the two sorts of raw monomers would preferentially generate one type of AB_n intermediate *in situ* in the initial stage of polymerization, to produce hyperbranched macromolecules without gelation, the strategy was coined as couple-monomer methodology (CMM).

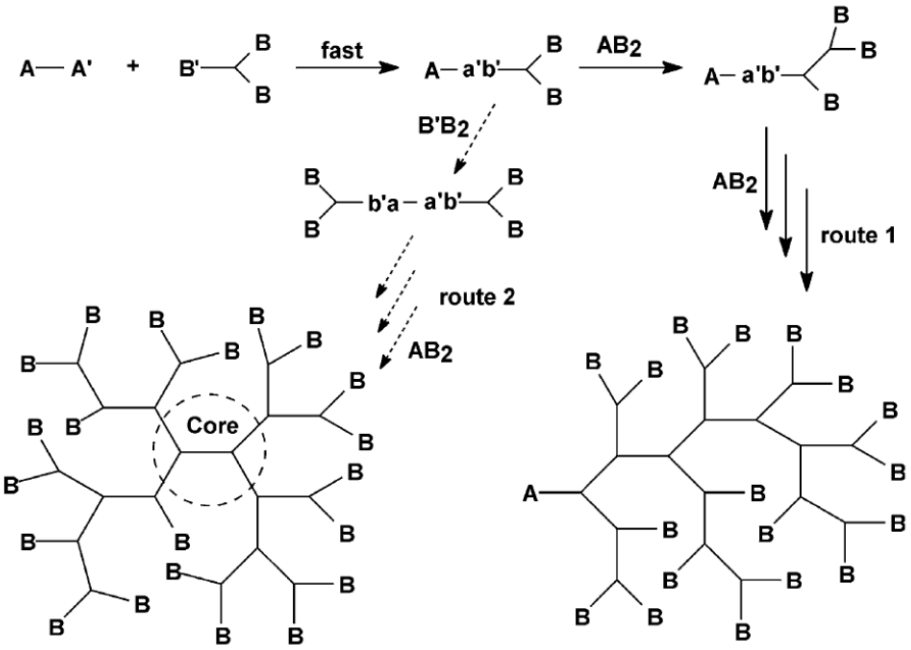

Figure 1.15 Hyperbranched polymer prepared by AA' + B'B_2 approach or couple-monomer methodology (CMM).[66] Copyright 2004, Elsevier.

A suitable monomer pair is essential for the molecular design of a HBP using CMM. The basic principle is shown in Figure 1.15. In a typical CMM system, AB_2 intermediates will be firstly generated due to the higher reactivity of A' and B' groups, and further self-polycondensation of the formed AB_2 species will result in HBPs without gelation, as shown in route 1 of Figure 1.15. On the other hand, B_4 groups will be generated if the formed AB_2 further reacts with a B'B_2 molecule due to the higher reactivity of B' group. The species B_4 can act as a core molecule in the preparation of HBPs and thus leads to the narrower molecular weight distribution. Further polymerization of AB_2 and B_4 generates a hyperbranched macromolecule with a core, as shown in route 1 of Figure 1.15.

The disadvantage of polycondensation is that it is unable to provide a

kinetic control over the polymer growth. Also, the HBP products usually have large molecular weight distributions. Furthermore, the HBPs prepared by polycondensation usually suffer from their sensitivity to hydrolysis. This feature sometimes hinders their application. More hydrolytically stable polymers can be prepared by ring opening or substitution reactions.

1.3.3.2 Self-condensing Vinyl Polymerization towards HBP

Vinyl monomers remain one of the most heavily used raw materials to produce millions of tons of polymers every year. And scientists have always been attempting to alter the 'linear' propagation manner of vinyl monomers in order to prepare novel polymer architectures such as hyperbranched ones from vinyl monomers. SCVP was invented by Fréchet and coworkers in 1995.[88] As shown in Figure 1.16, a special vinyl monomer which is called inimer presents a second B functional group capable of initiating the polymerization of other vinyl groups. The B groups are activated to generate an initiating B* sites. B* initiates the propagation of the vinyl group of another monomer, forming a dimer with a vinyl group, a growth site, and an initiating site. The dimer can function as an AB_2 monomer. Each addition of an inimer is equal to the addition of an AB_2 monomer in the polycondensation reaction. This process continues to yield a HBP. Although Fréchet's method used cationic living polymerization, The inimer can be designed and activated by different CRP methods. This polymerization method is versatile as HBPs can be approached via polymerization of vinyl monomers. In SCVP, the activities of chain propagation of the growth sites and the initiating sites differ, resulting in a lower DB when compared to the DB of the HBP prepared via polycondensation of AB_2 monomers. The theoretical maximum DB of SCVP is 46.5%.[97] On the other hand, SCVP does exhibit some disadvantages. For example, side reactions may lead to gelation, the molecular weight distribution is still broad, and it is difficult to determine DB directly via an NMR analysis. Soon after the development of SCVP, the method has been expanded for use with radical polymerization, in particular with CRP to control the molecular weight distribution and prevent gelation.

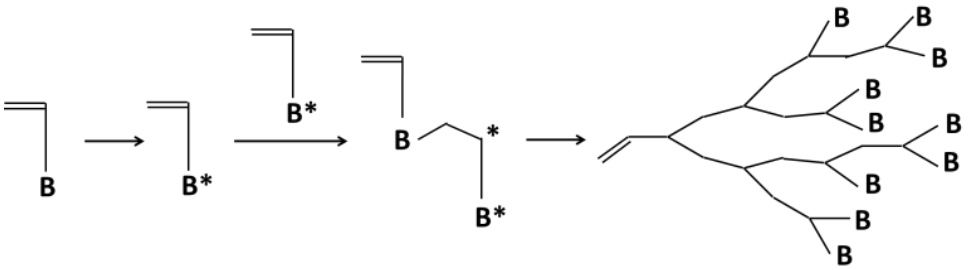

Figure 1.16 Schematic representation of the self-condensing vinyl polymerization (SCVP) of an AB* monomer to give a hyperbranched vinyl polymer.

Nitroxide SCVP

SCVP with nitroxide mediated polymerization (NMP) was investigated by Hawker *et al*., using a styryl group and an initiating/propagating moiety consisting of a nitroxide linked to a substituted benzylic carbon atom, **1**,[119] as shown in Figure 1.17. HBP were prepared with weight average molecular weights ranging from 65,000 to 300,000 g·mol^{-1} and with polydispersities from 1.6 to 4.4 showing that the living nature of the reaction enhanced control over the molecular weight distribution. Tao *et al*. prepared 'weak-linked' HBP by using two nitroxides, **2** and **3** (Figure 1.17).[120] When polymerized, the presence of the nitroxides at the branch points rather than at the chain ends resulted in 'weak-links' in the material. The thermal homolysis/recombination of the nitroxide allows for branches to be severed from the main chain. The branches can be irreversibly cleaved by using the reducing agent phenylhydrazine to terminate the nitroxyl and carbon-centered radicals or by adding other quenching agents such as ascorbic acid and heating the polymer in solution.[121] These cleavable branches can act as branched macroinitiators giving the opportunity of further propagation of other monomers close to the branching points.

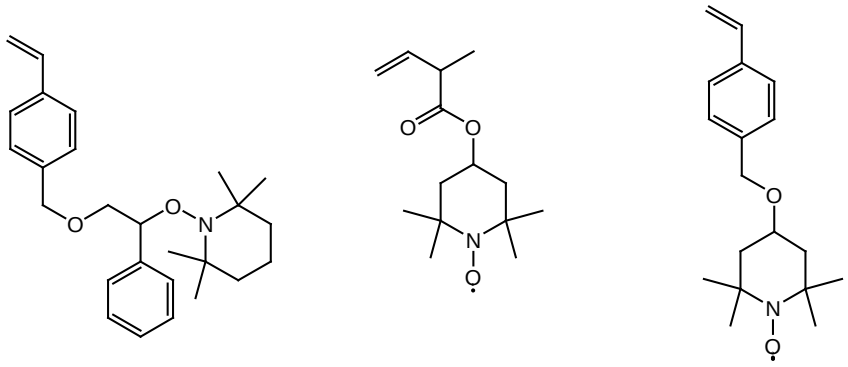

1 2 3

Figure 1.17 Monomers of nitroxide SCVP to create HBP.

ATRP SCVP

ATRP SCVP was firstly investigated in 1996 by Matyjaszewski *et al*,[107] who polymerized the monomer, 4-(chloromethyl) styrene with normal ATRP conditions (Cu^{I} and 2,2'-bipyridyl). The resulting primary chain was a chain with a double bond at one end and a chlorine atom at the other. The double bond could be incorporated into the growing polymer chain and therefore acted as a branch point. However, due to an unequal reactivity of initiating and propagating species the reaction did not follow an ideal SCVP. Low catalyst to monomer ratio led to largely linear polymer formation and little in the way of HBP. For SCVP using ATRP conditions, there has to be a high initiator concentration which favors a shift in equilibrium towards the active radicals. This usually results in an initial large concentration of radicals which terminate efficiently, leaving an excess of $X\text{-}Cu^{II}$. This process consumes large proportions of the Cu^{I} and prevents the activation or reactivation of alkyl halides. In order to produce HBPs to high conversion using SCVP with inimers such as those shown in Figure 1.18, there is a need for a sufficient concentration of Cu^{I} to be maintained throughout the reaction. Matyjaszewski's group later accomplished this by using copper in its zero valence state as it reduces the $X\text{-}Cu^{II}$ complex to generate two equivalents of Cu^{I}.[122] Monomers **4, 5**, **6** and **7** in Figure 1.18 were successfully polymerized with this method.

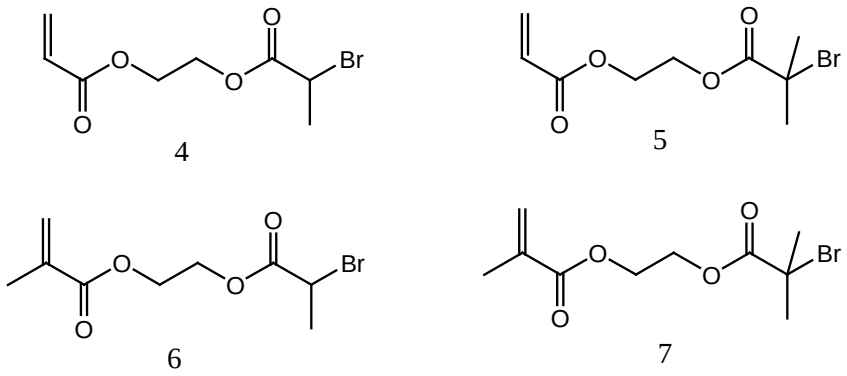

Figure 1.18 Monomers used for ATRP SCVP to create HBP.

ATRP SCVP can create fluorinated branched polymers which can provide low surface energy surfaces. For this purpose, ATRP has been applied to copolymerization of either 4-chloromethyl styrene, 4-bromomethyl styrene or a PEG containing inimer with 2,3,4,5,6-penta-fluorostyrene.[123, 124] Highly fluorinated HBPs were produced with approximately 30% of the repeat units containing a branch point. Extra initiator with higher initiation efficiency can also be introduced into the ATRP SCVP system. For instance, Wooley *et al*. used a trifunctional initiator to copolymerise chloromethyl styrene and lauryl acrylate.[125] Similar procedures have been used to prepare HB polyelectyrolytes[126] and HBPs with sugar functionality.[127, 128]

The molecular weight distribution is difficult to control with SCVP. However, if a multi-step approach is adopted in which segments are synthesized then modified using protection-deprotection ways, much narrower distributions will become possible. Such approach was reported by Percec *et al.*[129] who conducted a sequential synthesis of HB poly(methyl methacrylate) (HB-PMMA) by first capping PMMA with a halide end group derived from ATRP with a silylenol ether containing also two dialkyl thiocarbamate groups, which act as latent initiating groups. Then the dialkyl thiocarbamate groups were converted to aryl sulfonyl chloride groups that can reinitiate ATRP. Iteration of these steps resulted in successive branching.

RAFT SCVP

In 2003, the pioneer work of RAFT SCVP was done by Yang *et al.*[130] who

produced an inimer by incorporating a dithioester into a styrene monomer. Although this work showed the possibility of using RAFT polymerization to produce branched polymers, the branching agent (8, Figure 1.19) placed a weak link in the form of the dithioester in the resulting polymers, similar to Tao's design for NMP SCVP. This method was modified later by Carter *et al*. to place the dithioester at the chain ends such as 9 or 10 in Figure 1.19.[131, 132] This route to HBP appears to be extremely promising and copolymerization based on this route was used to produce HB poly(N-isopropyl acrylamide-block-glycerol monomethacrylate).[133]

There are also some drawbacks for RAFT SCVP. The branched copolymers produced by RAFT SCVP are generally of high molecular weight whereas the homopolymers tend to be of much lower molecular weight. Photoinitiation via homolytic cleavage of the dithiocarbamate group has also been combined with RAFT SCVP. Ishizu *et al*. used the photolysis of dithiocarbamate chain ends to generate radicals and produce block HB copolymers by using the inimers 11 and 12 in Figure 1.19.[134, 135]

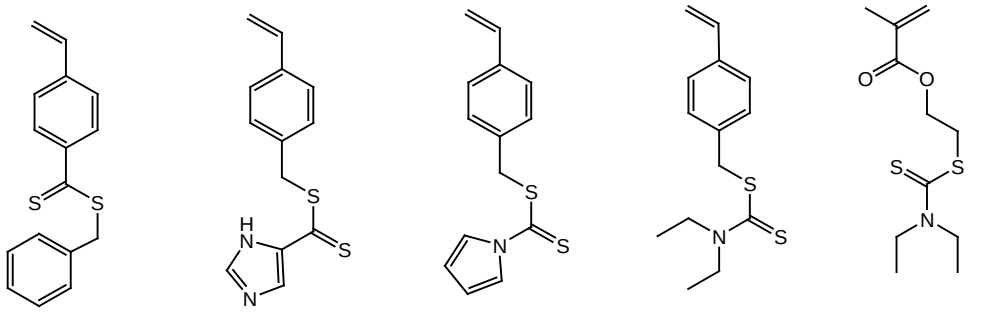

8 9 10 11 12

Figure 1.19 Monomers used for RAFT SCVP to create HBP.

For RAFT SCVP, large amount of dithiocarbonyl end groups will exist in the final products. The dithiocarbonyl end groups can be removed by the reaction of the polymer with an excess of a radical initiator.[136] The initiator decomposes to form radicals. When the initiator radicals concentrations are in excess of the polymer chain end radicals, terminations will happen between the polymer chain end radicals and the initiator radicals. The chain end group structures depend on the radical initiator used and this can be

utilised to provide terminal chain end functionality. The benefits are: 1) all of the thiocarbonyl-thio end groups are completely removed; 2) a wide range of chain-end functionalities are introduced, and 3) the chain transfer agent (CTA) is recovered. With this method, pyrrole dithioate chain end groups were converted into carboxylic acids using the azo-initiator, 4,4'-azobis(4-cyanopentanoic acid) and the modified material was proved to be a key precursor for attaching peptide sequences, e.g. arginine-glycine-aspartic acid, that bind to cell surface receptors.

The mechanism of SCVP method has the limitation that it needs specific tailored monomers, since only a few inimers with specific structures can be used in this method. Furthermore, the strict conditions and requirements of SCVP hinder the promotion of this method to the industry.

1.3.3.3 Controlled Radical Polymerization of Multi-vinyl Monomers

Multi-vinyl monomers (MVMs) have long been regarded as chemicals to make crosslinked materials. In free-radical polymerization the inclusion of only small amounts of MVMs will lead to a crosslinked network. Clearly, for a given conversion of monomer to polymer the number of chains increase with decreasing DP_n and gelation occurs at lower conversion as the DP_n increases. It has been reported that even in very dilute solution polymerization (~10% monomer), the gel point is limited at substantially less than 20% conversion of monomer to polymer.[137] Not surprisingly, the synthesis of soluble branched polymers to high conversion without crosslinking had seemed impossible in the free radical copolymerization of MVMs. However, in 2000, Sherrington and co-workers developed an approach based on the suppression of gel formation by extensive chain transfer for synthesizing a new class of HBP.[80, 81] This method has become known as the 'Strathclyde synthesis', as it was developed at the University of Strathclyde in the UK. The process is a facile, one step and cost-effective way to produce branched vinyl polymers, employing conventional free radical polymerization (Figure 1.20).

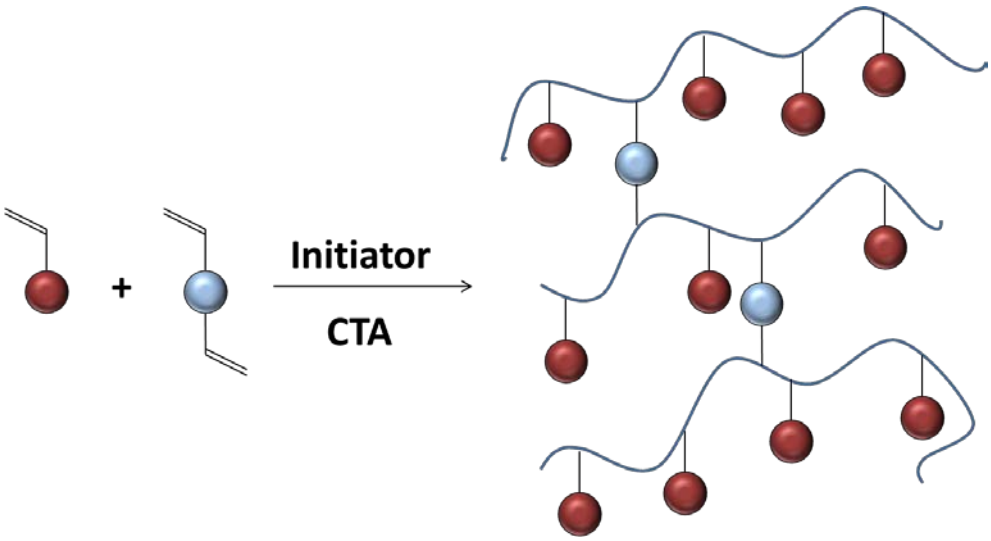

Figure 1.20 Synthesis of branched vinyl polymers using a combination of multi-vinyl monomer and radical transfer agent (Strathclyde synthesis).

The 'Strathclyde synthesis' can delay the gelation because chain transfer decreases the DP_n of the primary kinetic chain so that the average number of branch points per chain is reduced and the intermolecular reaction is suppressed when compared to the analogous process in the absence of chain transfer. The 'Strathclyde synthesis' used sufficiently concentrated solutions of mono-vinyl monomers but with a low concentration of multi-vinyl monomer and equimolar concentrations of a chain transfer agent (CTA). It becomes possible to rapidly obtain HBP at high yields with this method. By changing the functionality of the mono-vinyl monomer[138, 139] and choice of CTA,[140] the molecular weights, architectures and yields of the polymers can be tailored. Whilst thiol based CTA are suitable for the polymerization of methacrylates and acrylamides, they quench the polymerizations of other monomers, such as vinyl acetate and N-vinyl pyrrolidinone, which grow by non-resonance stabilized radicals.[141] Also, the 'Strathclyde synthesis' requires use of an organic solvent which dilutes the whole reaction medium and contributes to the inhibition of cross-linking. It was reported that a low concentration of MVM and a limited molar ratio of MVM to initiator (≤ 1) were required to ensure the formation of soluble HBPs. When this ratio of MVM to initiator exceeds 1, it will lead to an insoluble crosslinked material or a microgel. Therefore, the resulted copolymers can only reach a limited DB.

With the development of CRP, the 'Strathclyde synthesis' was tremendously improved. As one of the most robust CRP techniques, ATRP was used to regulate chain length and prevent gelation.[142] Even homopolymerization of MVMs using ATRP has been reported to produce soluble polymer with limited conversions.[143] The ATRP can also potentially provide better control of end group functionality. Isaure *et al*. were able to produce soluble HB PMMA in a one pot ATRP reaction and the later work from the same group further expanded this approach by polymerizing hydroxypropyl methacrylate by ATRP in the presence of ethylene glycol dimethacrylate[144] or a cleavable disulfide dimethacrylate.[93] Monte Carlo model was applied to simulate the statistics of branching in the ATRP systems. With a simpler simulation than that of non-controlled polymerizations, Bannister *et al*. predicted that the proportions of small loops in the system was low at critical fractions of MVM so that HBPs could be prepared.[145]

Perrier *et al*. were the first to copolymerize MVM with mono-vinyl monomer in a RAFT polymerization.[94, 95] They further investigated the RAFT homopolymerization of divinylbenzene and prepared soluble HBPs without gelation.[146] Asymmetric divinyl monomers were also introduced in RAFT polymerization.[147] Such example was reported by Dong *et al*. who synthesized HB polystyrene with many pendant vinyl groups by using an asymmetric divinyl monomer containing a more reactive styryl group and a less reactive butenyl group. The pendant butenyl vinyl groups allowed for further modification of the polymers, which include epoxidation, amination and hydroxylation. Because only small quantities of the butenyl vinyl groups were consumed, the crosslinking density could be reduced and the gelation could be avoided. The low reactivity of the butenyl group in RAFT polymerization would undoubtedly allow for the synthesis of butenyl-functionalized polymers. However, recent work on polymerization in the presence of MVMs using the RAFT technique has pointed out that a high monomer concentration (above c* (the critical entanglement concentration) for an equivalent linear polymer) can prevent the production of intramolecular cyclic structures without the need to use MVMs with alkenes of different reactivity.[148, 149] Recently, the NMP process has also

been used in the controlled/living polymerization of MVMs.[150]

Until recently, attentions have been paid more on the homopolymerization of MVMs via CRP to produce vinyl polymers with linear[151], branched[143, 152, 153] or cyclic structures.[154, 155, 156] The homopolymerization were not widely explored previously because it is widely accepted that critical gelation happens when the average number of crosslinkages (crosslinker in which both vinyl groups have reacted) per primary chain exceeds unity if the primary chains are uniform,[157] according to Flory-Stockmayor's mean-field theory. However, it has been shown by many experiments that if the monomer conversion is kept incomplete and a portion of the divinyl cross-linker does not fully react, or is consumed by intramolecular cyclization, gelation could be avoided. Homopolymerization of EGDMA was studied in bulk at 70˚C by ATRP. Less than 10% of monomer conversion is reached before gelation occurred.[158] By manipulating the deactivation equilibrium and varying Cu^{I}:Cu^{II}, Wang and coworkers[143] applied a deactivation enhanced ATRP to the homopolymerization of DVB and EGDMA and achieved 60% polymer conversion in a dense system that had not been achieved by other approaches. Wang also found that even at the early stage of reaction (10% of yield), the portion of reacted divinyl monomers reached to a high level (26%) in the product. Perrier and coworkers[146] homo-polymerized DVB also in a dense system via RAFT polymerization and achieved conversions as high as 68% before gelation, instead of 15% for conventional FRP. In a dilute conditions, Mori and coworker[156] explored the RAFT homopolymerization of poly(ethylene glycol) diacrylates (PEGDA) with different lengths of PEG spacers and obtained product yield between 40%~63%. Most interestingly, the vinyl content of their final product is much lower (0%~10%) than expected for homopolymerization product. In other words, >90% vinyl groups were consumed in the product. These results provide us with two classical alternatives: either highly branched structure (no cyclization) with low conversion or cyclized products with high conversion can be obtained. Most importantly, it has been realized by an increasing number of researchers that intramolecular cyclization cannot be neglected in the CRP of MVMs, including the homopolymerization and copolymerization.[159, 160]

The intramolecular cyclization could help to create some novel macromolecular structures, such as knots[154, 155] or ladders.[161, 162] However, it consumes the pendent vinyl groups on the polymer chains and reduces the vinyl content of the product. Furthermore, due to the significant competition between the intramolecular cyclization and intermolecular branching, synthesis of pure hyperbranched structures is still challenging.

1.3.4 Biomedical Application of HBP

1.3.4.1 HBPs for Tissue Engineering

HBPs with a three-dimensional architecture exhibit good functionality, high reactivity due to the presence of a large number of exposed chain end functional groups, and they may alter the absorption profile of biomolecules/proteins on a polymeric biomaterial. One can introduce structural variations to tailor degradation kinetics as well as incorporation of appropriate functional groups for improved cell attachment. Besides, HBPs are capable of forming porous hydrogels or films as scaffolds, and are promising to promote adhesion and proliferation of cells. Thus, HBPs, due to their special topological structures, have found various applications in tissue engineering fields.[163]

The potential for cell and tissue adhesives from multivalent HBP scaffolds is enormous. Taking advantage of the multiple functionalization of HBPs, Brooks, Kizhakkedathu and colleagues synthesized hyperbranched polyglycerols (HPGs) decorated with multiple choline phosphate (CP) groups, which possessed the inverse orientation of phosphatidyl choline (PC), the end group of the major lipid presented in eukaryotic cell membranes (Figure 1.21).[164] These functionalized HPGs displayed a strong affinity for biological membranes. The researchers observed that these multivalent dendritic structures strongly bound to human red blood cells.

The highly hydrophilic nature of HPGs in combination with its hydroxyl functionalities makes them suitable for the design of hydrogels. Frey and coworkers were pioneers in the synthesis of structured HPG hydrogels based on PEG multi-arm stars with a hyperbranched dendritic core.[165] The hydrogel products showed excellent stability with a high compression

module. Substantial suitability of these hydrogels as substrates for cell growth has been demonstrated. The biocompatibility of HPGs was presented by Brooks *et al*. in 2006.[166] The *in vitro* assays showed remarkably low cytotoxicity of HPG against fibroblast and endothelial cells. Hennink and coworkers functionalized the end hydroxyl group of HPG into the photo-crosslinkable acrylate with different degrees of substitution (DS) and fabricated hydrogels with both chemical and photo initiation methods.[167] The obtained hydrogels had a limited swelling capacity indicating that rather dimensionally stable networks were obtained. Alblas and coworkers encapsulated bone marrow derived multi-potent stromal cells (MSCs) in the same photo-polymerized hydrogel for the development of printed bone grafts.[168] They demonstrated the adverse effects of photo-polymerization on the viability and cell cycle progression of exposed MSC monolayers, but their differentiation potential remained intact. The hydrogel with incorporated MSC supported survival and osteogenic differentiation of the embedded cells to a variable degree.

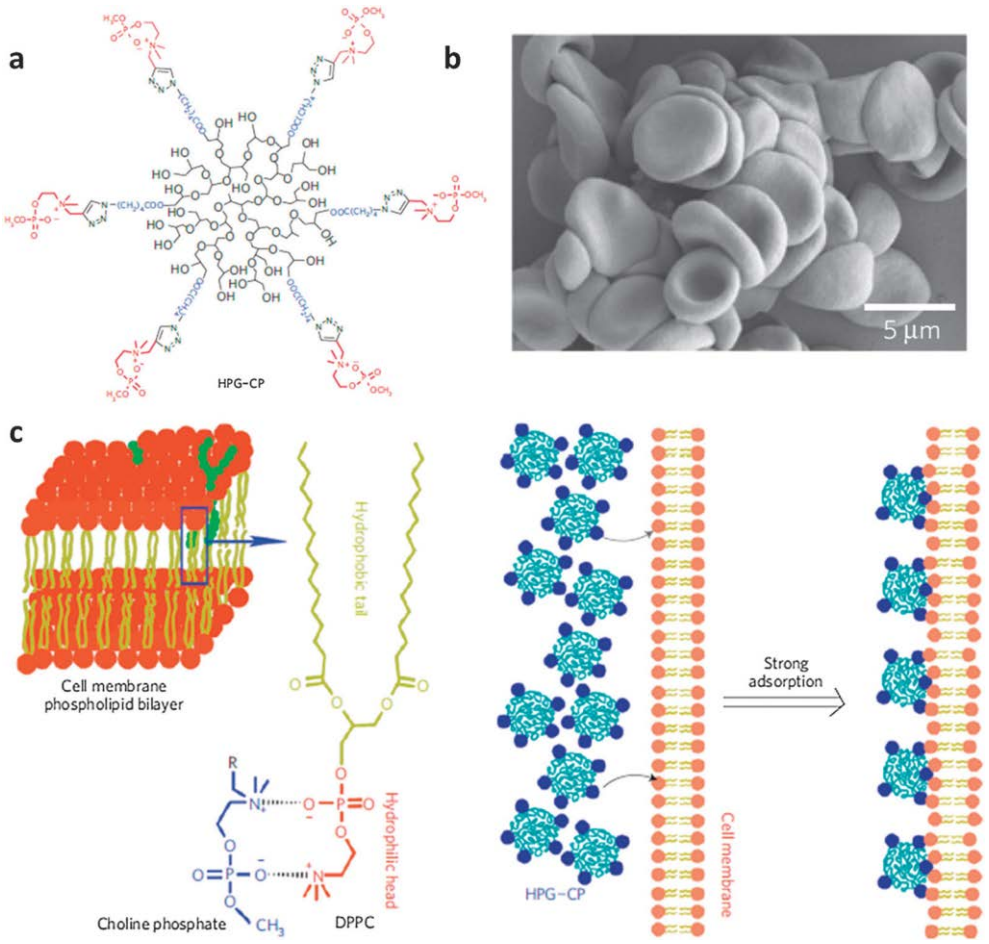

Figure 1.21 Example of HPG-CP for tissue adhesive: (a) multivalent HPG structures with CP end groups linked by 1,2,3-triazol units; (b) SEM images (5,000) of red blood cells forming aggregates in saline solution as a result of cell adhesion; (c) the mechanism of the biomembrane adhesion interaction.[164] Copyright 2012, Nature Publishing Group.

Hyperbranched PEG-based polymers are another example of a synthetic material that has been investigated to form hydrogel scaffolds for the encapsulation and culture of stem cells. The techniques of controlled/living radical polymerization (CRP) have given birth to a number of hyperbranched PEG-based copolymers with controlled molecular weights, well-defined chain ends, and different degrees of branching. Poly(MEO_2MA-co-OEGMA) was firstly reported by Lutz and his colleagues.[169] This linear copolymer with LCST around 37 °C was prepared via ATRP. The same group also attempted to introduce the multifunctional vinyl monomer of ethylene glycol dimethacrylate (EGDMA) to achieve HB

structures. However, only one percent of EGDMA caused macro gelation.[170] In contrast, a higher degree of EGDMA (up to 30% molar ratio of total feed monomers) was introduced as a multifunctional vinyl monomer by Tai's group.[171, 172] Instead of causing macro gelation, they successfully achieved hyperbranched PEGMEMA-PPGMA-EGDMA copolymers via a one-step deactivation enhanced ATRP approach. The introduction of the multi-vinyl crosslinker EGDMA endows the copolymer with the capability of easy tailoring and photo-crosslinkable properties. Meanwhile, by adjusting the hydrophilic PEGMEMA and hydrophobic PPGMA composition, they can sensitively alter the polymer hydrophilicity and control the LCST value of the copolymers around body temperature. The combination of physical interaction (*in situ* thermal gelation) and covalent crosslinking (*in situ* photopolymerization) endows the gels with significantly enhanced mechanical properties compared to non-photocrosslinked thermoresponsive hydrogels. Furthermore, due to the thermoresponsive property, the gels release the carmoisine red dye at a faster rate in warm water (37 °C) compared to a slow release in cold water (25 °C). Similar thermoresponsive polymers were synthesized by Wang's group.[173] The 3T3 mouse fibroblast cell line was encapsulated in the hydrogel and no significant difference of cell viability was found between the control (cells alone) and polymer samples after four days of incubation.

Although PEG-based hydrogels provide tissue engineers with large flexibility in material design, they do not have an intrinsic mechanism for interacting with cells, and cell adhesion is typically mediated by non-specific cell adhesion.[174] Thus, PEG hydrogels are often modified with tethered groups, such as adhesion peptides[175, 176] or phosphates[177] to alter cellular interactions. PEG-based hydrogels have been used for the culture and differentiation of stem cells toward the engineering of numerous tissues.

Cooper-White *et al*. have generated hydroxy phenol functionalized hyperbranched PEG hydrogels, cross-linked via an enzyme mediated, oxidative process.[178] Göepferich *et al*. modified hyperbranched PEG-amines with collagenase sensitive peptides and cross-linked with hyperbranched PEG-succinimidyl propionates without the use of free-radical initiators

(enzymatically degradable hydrogels).[179] Enzyme mediated gel degradation occurred within 10, 16, and 19 days. The hydrogels were functionalized with the laminin-derived adhesion peptide YIGSR, and seeded with 3T3-L1 preadipocytes. Compared to a standard two-dimensional cell culture model, the developed hydrogels significantly enhanced the intracellular triglyceride accumulation of encapsulated adipocytes.

1.3.4.2 HBPs for Gene Delivery

Gene therapy represents a promising approach for the treatment of various human diseases by delivery of exogenous nucleic acids into the nucleus of the specific cells of the patient. Considering the fact that genetic materials (free oligonucleotides, DNA and RNA) are easily degraded by serum nucleases in the blood when injected intravenously, it is of great significance to develop effective gene vectors to protect genetic materials from degradation. Compared to the viruses and cationic liposomes, cationic polymers show several favorable characteristics such as enhanced bio-safety and biocompatibility, favorable biodegradability, high flexibility of trans-gene size, high stability and applicable scale-up to production. Therefore, non-viral polycationic vectors are receiving considerable attention as gene delivery systems. Among various cationic polymers, cationic HBPs that integrate a high density of amino groups with a three dimensional branched structure and high molecular design flexibility, which greatly facilitates the therapeutic genes to arrive at the target tissues with high efficiency and specificity, would be very attractive for successful gene transfection.

In a hyperbranched molecule, the modular arrangement of branches confers a two-fold structural parameter which is beneficial for gene delivery. With increasing numbers of generations, the molecule takes on a 3D spherical shape due to congestion of the branching units, thereby yielding supramolecular void spaces and, furthermore, multiple surface functional groups which render the molecule amenable to a wide range of chemical modifications.[180] These two features have particularly made HBPs suitable for delivering genetic drugs either by supramolecular interaction within the structural voids or by direct chemical conjugation to peripheral

functionalities. In both cases, it is possible to generate gene vehicles, where the genetic compounds are homogeneously distributed within the defined nanosystem, and the complex/conjugate is stable enough to withstand the fluctuating *in-vivo* milieu. The presence of multiple, terminally active groups also endows the molecule with a 'multivalent' capacity to interact with different cellular components, for instance, HBPs with pharmacologically active end groups such as sulfates and phosphates have been designed to electrostatically interact with negatively charged cellular components in order to interfere with a particular biochemical event.[181, 182]

In the field of cationic HBP vectors, hyperbranched polyamines including hyperbranched polyethylenimine (HPEI) and hyperbranched polypropylenimine (HPPI) are very promising for effective gene transfection because of their high positive charge density. Especially, HPEI displays superior transfection efficiency in various cell lines and tissues and has been known as the gold standard among nonviral polymeric gene delivery systems.[99] HPEI-based gene vectors have several attractive characteristics that are beneficial to gene delivery. Firstly, due to the existence of numerous terminal primary amines, they can condense nucleic acids sufficiently into nanosized compactable particles through electrostatic interaction at physiological pH, which facilitates cellular uptake. Furthermore, the plenty of tertiary amine groups present in the HPEI structure endow them with a strong proton buffer capacity, which can prevent polyplexes from lysosomal degradation and enable them to escape into the cytoplasm. This process is called the 'proton-sponge effect'. While HPEI offers these advantages, there are still several obstacles associated with gene delivery, especially high cytotoxicity and non-degradation property, all of which seriously limit its further application.

To overcome the limitations of HPEI, the biodegradable linkages such as reducible disulfide bonds or ester conjugation are incorporated into the backbone of hyperbranched polyamine.[183] The introduction of biodegradable linkages in the backbone of hyperbranched polyamines not only facilitates the controlled release of DNA in the cytoplasm, but also helps to reduce cytotoxicity by avoiding accumulation of high molecular

weight cationic polymers inside the cells. Take the reduction type for an example, biodegradable HPEIs containing the disulfide bond can be polymerized by monomers containing disulfide bonds or by crosslinking low molecular weight HPEI segments with reducible disulfide crosslinkers. It has been reported that connection of low molecular weight HPEI (e.g., 800 and 1800 Da) with different disulfide-containing cross-linking agents resulted in considerably enhanced *in vitro* transfection efficiency as compared with the parent low molecular weight HPEI, with transfection activity approaching or in some cases over that of 25 kDa HPEI control.[184, 185, 186, 187, 188] As an example, Wang and coworkers prepared bioreducible disulfide bond-containing HPEI (SS-HPEI) by chemical coupling of the 3'-dithiobispropanoic acid (DTPA) and the low molecular weight HPEI (800 Da) via an EDC/NHS activation reaction (Figure 1.22), which was employed as a siRNA carrier for intracellular delivery of the human telomerase reverse transcriptase (hTERT) siRNA in vitro and in vivo.[188] *In vitro* transfection experiments demonstrated that the complexes of SS-PEI/siRNA were able to transfect HepG2 cells efficiently and revealed relatively low cytotoxicity, due to the fact that the SS-HPEI was cleaved in an intracellular reducing environment, which further facilitated intracellular siRNA release (Figure 1.22). Importantly, *in vivo* results showed that the complexes of SS-PEI/siRNA could inhibit HepG2 tumor growth in a xenograft mouse model and exhibited almost no adverse effect on liver and kidney functions.

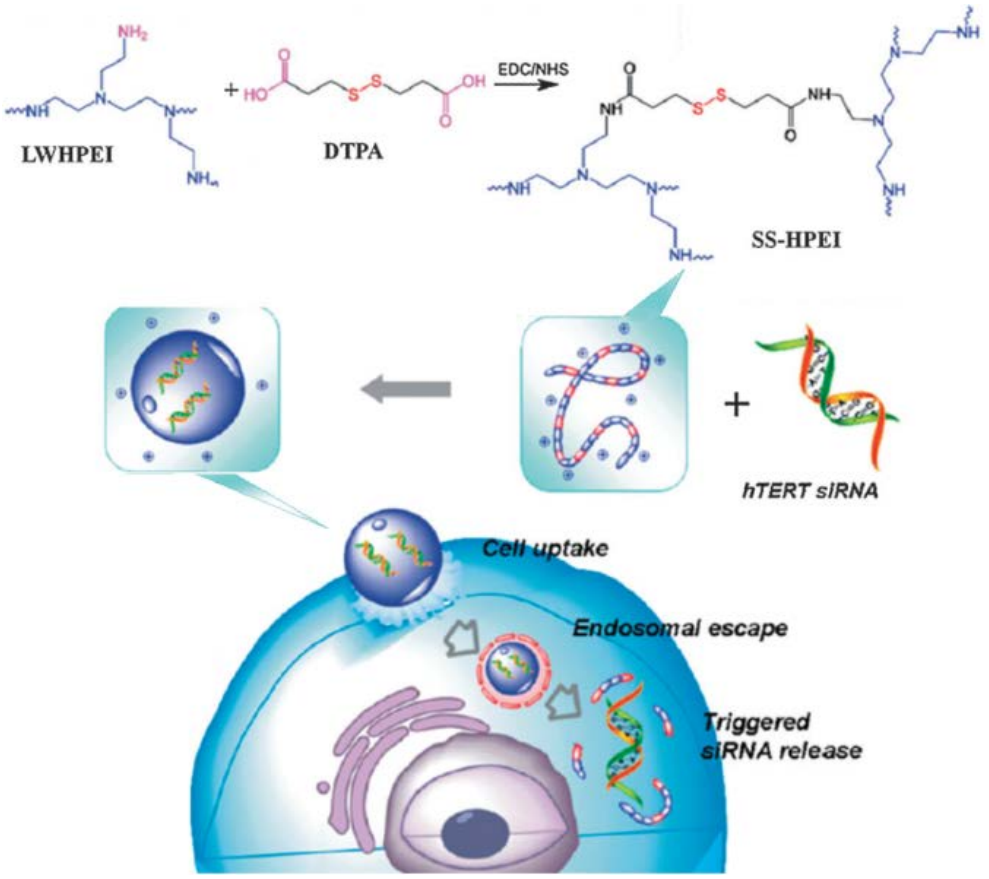

Figure 1.22 Schematic representation of bioreducible SS-HPEI-mediated intracellular siRNA delivery.[188, 189] Copyright 2012, Elsevier.

A number of hyperbranched poly(ester-amine)s (HPEAs) have been developed as hyperbranched polyamine analogues which are readily biodegradable. Similar to HPEI, HPEAs possess high density of primary amines for DNA condensation and tertiary amine for the proton-sponge effect. Meanwhile, they exhibit excellent biodegradability due to the hydrolytically degradable ester groups. Thus, HPEAs are promising for effective gene delivery because of their reduced cytotoxicity, their ability for controlled DNA release within the cells and great potential for structural diversity. Park and coworkers reported a cationic HPEA with a biodegradable ester backbone, primary amine at the periphery, and tertiary amine groups in the interior.[190] This biodegradable cationic polymer was minimally toxic and could condense negatively charged DNA. Subsequently, Liu and coworkers prepared a biodegradable HPEA polymer containing primary, secondary and tertiary amines simultaneously through the Michael

addition polymerization of trifunctional amine monomers with diacrylate.[191] The different types of amine groups may play various roles such as the condensation of DNA and improve the pH-buffering ability to facilitate escape of vectors from lysosomes. This HPEA polymer displayed low cytotoxicity and high transfection efficiency at a polymer/DNA weight ratio of 30:1 comparable to those of HPEI. Feijen and coworkers also reported a series of water-soluble and degradable gene carriers based on HPEAs containing primary, secondary and tertiary amino groups, which exhibited high buffering capacities between pH 5.1 and 7.4 and effectively condensed plasmid DNA into positively charged complexes with the diameters of 94-135 nm.[192] More importantly, these HPEAs revealed no or low cytotoxicity, demonstrating that HPEAs could be applied as safe and efficient gene delivery carriers.

Poly(dimethylaminoethyl methacrylate) (PDMAEMA) is another important poly(ester-amine) containing protonated tertiary amine groups at physiological pH. PDMAEMA exhibited excellent transfection efficiency because of its endosomal destabilizing property and ability to release DNA into cytosol.[193, 194] Nevertheless, the high cytotoxicity of the linear PDMAEMAs had hindered their further application. To date, several hyperbranched PDMAEMAs have been reported to reduce their cytotoxicity while trying to retain their high gene transfer efficiency. Davis and coworkers prepared biodegradable disulfide-based hyperbranched PDMAEMA through reverse addition-fragmentation chain transfer (RAFT) polymerization.[195] The hyperbranched PDMAEMA could package DNA efficiently to yield DNA polyplexes via multivalent electrostatic interactions. Under cellular reducing conditions, inherently biodegradable polyplexes could be cleaved, thus enhancing gene release and subsequently generating small molecular weight oligomer chains with low cytotoxicity. Freitag and coworkers studied PDMAEMAs with three different structures (linear, highly branched, and star-shaped) for gene delivery, and linear and branched PEI were used as the control.[196] They found that highly branched PDMAEMA only had a slight increase in transfection efficiency in comparison with its linear counterpart but efficiency was considerably lower than the branched PEI standard. PEGylation of hyperbranched PDMAEMA

makes the polymer less effective for cell uptake and DNA condensation, presumably owing to the 'stealth' effect from PEG.[197] However, when the polycation was functionalized with folic acid, the DNA-polycation complex showed enhanced cell uptake at the higher N/P ratios due to the interaction between folic acid ligands and overexpressed folic acid receptors on the cell surface of tumor cells.

Hyperbranched PDMAEMA is a promising material for gene transfection because the design and precise synthesis of well-defined architectures and functionalities is possible via CRP from vinyl monomer of DMAEMA.

The development of CRP techniques has provided important tools for the design and synthesis of biomedical used macromolecules with well-defined and precise structures. The further research on precisely control over the macromolecule structures, components and functionalities is still a necessary part, which will discover the different and similar effect of macromolecules on their biomedical properties.

1.4 Aims and Objectives of This Thesis

Recently, hyperbranched materials obtained from chain growth polymerization have gained attention. However, they are still confined to only a low level of branching (e.g. CRCC) and their production is limited by low yield. Moreover, complex procedures of synthesis (e.g. SCVP) allows only for the use of a few specialised monomers. It is highly desirable to develop new synthetic routes to hyperbranched polymeric materials with controlled architectures utilizing commercially available monomers. The work presented in this thesis focuses primarily on the design and preparation of HBPs from divinyl monomers via CRPs. The overall aim is to develop a universal approach for the preparation of new, highly branched macromolecules that address the requirements of different biomedical applications.

This thesis includes three specific objectives: 1. to establish the optimal, well-controlled reaction system for ATRP of vinyl monomers; 2. to design a strategy towards HBPs with a high degree of branching and a high

conversion from commercial multi-vinyl monomers; 3. to synthesize specific polymers through the newly developed approach and to evaluate biomedical properties of the polymers.

In Chapter 2, different copper-catalyzed ATRA reactions were initially evaluated with two mono-vinyl monomers (styrene and methyl methacrylate) to obtain a good kinetic control over the chain growth of vinyl monomers. The system with the highest monoadduct yield and monomer conversion was regarded the best ATRP system which provides the best kinetic control for further synthesis of HBP.

In Chapter 3, homopolymerization of MVMs were implemented as a universal approach to produce HBPs via CRP by combining the optimal, kinetically controlled system with a molecular interspace and overlap concept. It was found that by adjusting the ratio of initiator to divinyl monomer, primary chain length and chain concentration are varied and thus the polymers obtained can be either a 'single cyclized' structure or a hyperbranched structure. A series of HBPs were synthesized from different commercial MVMs, proving that this method towards HBPs can be applied to a variety of MVMs.

Chapters 4 and 5 focused on two specific bioapplications including a PEG-based HBP for a photo-crosslinkable hydrogel and a degradable cationic HBP as a gene delivery vector. Both HBPs were synthesized by the aforementioned method and their biomedical properties were investigated.

1.5 References

1. Flory, P. J. The Mechanism of vinyl polymerizations. *Journal of the American Chemical Society* **1937,** *59* (2), 241-253.
2. Burnett, G. M. Rate constants in radical polymerization reactions. *Quarterly Reviews* **1950,** *4* (3), 292-326.
3. Engel, P. S. Mechanism of the thermal and photochemical decomposition of azoalkanes. *Chemical Reviews* **1980,** *80* (2), 99-150.
4. Matyjaszewski, K.; Wang, J. L.; Grimaud, T.; Shipp, D. A. Controlled/"living" atom transfer radical polymerization of methyl methacrylate using various initiation systems. *Macromolecules* **1998,** *31* (5), 1527-1534.

5. Jenkins, A. D.; Kratochvil, P.; Stepto, R. F. T.; Suter, U. W. Glossary of basic terms in polymer science. *Pure and Applied Chemistry* **1996,** *68* (12), 2287-2311.
6. Fischer, H. The persistent radical effect: A principle for selective radical reactions and living radical polymerizations. *Chemical Reviews* **2001,** *101* (12), 3581-3610.
7. Hawker, C. J.; Bosman, A. W.; Harth, E. New polymer synthesis by nitroxide mediated living radical polymerizations. *Chemical Reviews* **2001,** *101* (12), 3661-3688.
8. Matyjaszewski, K.; Xia, J. H. Atom transfer radical polymerization. *Chemical Reviews* **2001,** *101* (9), 2921-2990.
9. Coleman, B. D.; Fox, T. G. A multistate mechanism for homogeneous ionic polymerization. II. The molecular weight distribution. *Journal of the American Chemical Society* **1963,** *85* (9), 1241-1244.
10. Patten, T. E.; Xia, J. H.; Abernathy, T.; Matyjaszewski, K. Polymers with very low polydispersities from atom transfer radical polymerization. *Science* **1996,** *272* (5263), 866-868.
11. Matyjaszewski, K.; Ziegler, M. J.; Arehart, S. V.; Greszta, D.; Pakula, T. Gradient copolymers by atom transfer radical copolymerization. *Journal of Physical Organic Chemistry* **2000,** *13* (12), 775-786.
12. Davis, K. A.; Matyjaszewski, K. Statistical, gradient, block, and graft copolymers by controlled/living radical polymerizations. *Advances in Polymer Science* **2002,** *159*, 1-169.
13. Beers, K. L.; Gaynor, S. G.; Matyjaszewski, K.; Sheiko, S. S.; Moller, M. The synthesis of densely grafted copolymers by atom transfer radical polymerization. *Macromolecules* **1998,** *31* (26), 9413-9415.
14. Matyjaszewski, K. The synthesis of functional star copolymers as an illustration of the importance of controlling polymer structures in the design of new materials. *Polymer International* **2003,** *52* (10), 1559-1565.
15. Matyjaszewski, K.; Gaynor, S. G.; Kulfan, A.; Podwika, M. Preparation of hyperbranched polyacrylates by atom transfer radical polymerization. 1. Acrylic AB* monomers in 'living' radical polymerizations. *Macromolecules* **1997,** *30* (17), 5192-5194.
16. Otsu, T.; Yoshida, M. Role of initiator-transfer agent-terminator (iniferter) in radical polymerizations: Polymer design by organic disulfides as iniferters. *Makromolekulare Chemie-Rapid Communications* **1982,** *3* (2), 127-132.
17. Otsu, T. Iniferter concept and living radical polymerization. *Journal of Polymer Science Part A-Polymer Chemistry* **2000,** *38* (12), 2121-2136.
18. Wang, J. S.; Matyjaszewski, K. Controlled/"living" radical polymerization. Halogen atom transfer radical polymerization promoted by a Cu(I)/Cu(II) redox process. *Macromolecules* **1995,** *28* (23), 7901-7910.
19. Wang, J. S.; Matyjaszewski, K. Controlled/"living" radical

polymerization. Atom transfer radical polymerization in the presence of transition-metal complexes. *Journal of the American Chemical Society* **1995,** *117* (20), 5614-5615.
20. Wang, J. S.; Matyjaszewski, K. "Living"/controlled radical polymerization. Transition-metal-catalyzed atom transfer radical polymerization in the presence of a conventional radical initiator. *Macromolecules* **1995,** *28* (22), 7572-7573.
21. Curran, D. P. The design and application of free radical chain reactions in organic synthesis. Part 1. *Synthesis-Stuttgart* **1988,** (6), 417-439.
22. Curran, D. P. The design and application of free radical chain reactions in organic synthesis. Part 2. *Synthesis-Stuttgart* **1988,** (7), 489-513.
23. Kharasch, M. S.; Jensen, E. V.; Urry, W. H. Addition of carbon tetrachloride and chloroform to olefins. *Science* **1945,** *102* (2640), 128-128.
24. Chiefari, J.; Chong, Y. K.; Ercole, F.; Krstina, J.; Jeffery, J.; Le, T. P. T.; Mayadunne, R. T. A.; Meijs, G. F.; Moad, C. L.; Moad, G.; Rizzardo, E.; Thang, S. H. Living free-radical polymerization by reversible addition-fragmentation chain transfer: The RAFT process. *Macromolecules* **1998,** *31* (16), 5559-5562.
25. Moad, G.; Chiefari, J.; Chong, Y. K.; Krstina, J.; Mayadunne, R. T. A.; Postma, A.; Rizzardo, E.; Thang, S. H. Living free radical polymerization with reversible addition-fragmentation chain transfer (The life of RAFT). *Polymer International* **2000,** *49* (9), 993-1001.
26. Matyjaszewski, K. Controlled/living radical polymerization: State of the art in 2002. In *Advances in Controlled/Living Radical Polymerization*, Matyjaszewski, K., Ed., **2003**; Vol. 854, pp 2-9.
27. Braunecker, W. A.; Matyjaszewski, K. Controlled/living radical polymerization: Features, developments, and perspectives. *Progress in Polymer Science* **2007,** *32* (1), 93-146.
28. Georges, M. K.; Veregin, R. P. N.; Kazmaier, P. M.; Hamer, G. K. Narrow molecular weight resins by a free-radical polymerization process. *Macromolecules* **1993,** *26* (11), 2987-2988.
29. Nagashima, H.; Ozaki, N.; Ishii, M.; Seki, K.; Washiyama, M.; Itoh, K. Transition metal-catalyzed radical cyclizations: A low-temperature process for the cyclization of N-protected N-allyltrichloroacetamides to trichlorinated γ-lactams and application to the stereoselective preparation of β,γ-disubstituted γ-lactams. *Journal of Organic Chemistry* **1993,** *58* (2), 464-470.
30. Nagashima, H.; Wakamatsu, H.; Ozaki, N.; Ishii, T.; Watanabe, M.; Tajima, T.; Itoh, K. Transition metal catalyzed radical cyclization: New preparative route to .gamma.-lactams from allylic alcohols via the [3.3]-sigmatropic tearrangement of allylic trichloroacetimidates and the subsequent ruthenium-catalyzed cyclization of N-allyltrichloroacetamides. *Journal of Organic Chemistry* **1992,** *57* (6), 1682-1689.

31. Seijas, J. A.; Vazqueztato, M. P.; Castedo, L.; Estevez, R. J.; Onega, M. G.; Ruiz, M. Synthesis of pyrrolizidines via copper(I) catalyzed radical atom transfer cyclization. *Tetrahedron* **1992,** *48* (9), 1637-1642.
32. Udding, J. H.; Tuijp, C. J. M.; Hiemstra, H.; Speckamp, W. N. Transition metal-catalyzed chlorine transfer cyclizations of carbon-centered glycine radicals; A novel synthetic route to cyclic α-amino acids. *Tetrahedron* **1994,** *50* (6), 1907-1918.
33. Kotani, Y.; Kato, M.; Kamigaito, M.; Sawamoto, M. Living radical polymerization of alkyl methacrylates with ruthenium complex and synthesis of their block copolymers. *Macromolecules* **1996,** *29* (22), 6979-6982.
34. Kamigaito, M.; Sawamoto, M.; Higashimura, T. Polymerization of methyl methacrylate with the carbon tetrachloride/dichlorotris-(triphenylphosphine)ruthenium(II)/methylaluminum
bis(2,6-di-tert-butylphenoxide) initiating system: Possibility of living radical polymerization. *Macromolecules* **1995,** *28* (5), 1721-1723.
35. Percec, V.; Popov, A. V.; Ramirez-Castillo, E.; Monteiro, M.; Barboiu, B.; Weichold, O.; Asandei, A. D.; Mitchell, C. M. Aqueous room temperature metal-catalyzed living radical polymerization of vinyl chloride. *Journal of the American Chemical Society* **2002,** *124* (18), 4940-4941.
36. Percec, V.; Guliashvili, T.; Ladislaw, J. S.; Wistrand, A.; Stjerndahl, A.; Sienkowska, M. J.; Monteiro, M. J.; Sahoo, S. Ultrafast synthesis of ultrahigh molar mass polymers by metal-catalyzed living radical polymerization of acrylates, methacrylates, and vinyl chloride mediated by SET at 25 degrees C. *Journal of the American Chemical Society* **2006,** *128* (43), 14156-14165.
37. Rosen, B. M.; Percec, V. Implications of monomer and initiator structure on the dissociative electron-transfer step of SET-LRP. *Journal of Polymer Science Part A-Polymer Chemistry* **2008,** *46* (16), 5663-5697.
38. Lligadas, G.; Rosen, B. M.; Monteiro, M. J.; Percec, V. Solvent choice differentiates SET-LRP and Cu-mediated radical polymerization with non-first-order kinetics. *Macromolecules* **2008,** *41* (22), 8360-8364.
39. Lligadas, G.; Rosen, B. M.; Bell, C. A.; Monteiro, M. J.; Percec, V. Effect of Cu(0) particle size on the kinetics of SET-LRP in DMSO and Cu-mediated radical polymerization in MeCN at 25 °C. *Macromolecules* **2008,** *41* (22), 8365-8371.
40. Percec, V.; Guliashvili, T.; Ladislaw, J. S.; Wistrand, A.; Stjerndahl, A.; Sienkowska, M. J.; Monteiro, M. J.; Sahoo, S. Ultrafast synthesis of ultrahigh molar mass polymers by metal-catalyzed living rRadical polymerization of acrylates, methacrylates, and vinyl chloride mediated by SET at 25 °C. *Journal of the American Chemical Society* **2006,** *128* (43), 14156-14165.
41. Percec, V.; Popov, A. V.; Ramirez-Castillo, E.; Weichold, O. Living

radical polymerization of vinyl chloride initiated with iodoform and catalyzed by nascent Cu0/tris(2-aminoethyl)amine or polyethyleneimine in water at 25 °C proceeds by a new competing pathways mechanism. *Journal of Polymer Science Part A-Polymer Chemistry* **2003,** *41* (21), 3283-3299.
42. Lin, C. Y.; Coote, M. L.; Gennaro, A.; Matyjaszewski, K. Ab initio evaluation of the thermodynamic and electrochemical properties of alkyl halides and radicals and their mechanistic implications for atom transfer radical polymerization. *Journal of the American Chemical Society* **2008,** *130* (38), 12762-12774.
43. Matyjaszewski, K. Atom transfer radical polymerization (ATRP): current status and future perspectives. *Macromolecules* **2012,** *45* (10), 4015-4039.
44. Tang, W.; Matyjaszewski, K. Effect of ligand structure on activation rate constants in ATRP. *Macromolecules* **2006,** *39* (15), 4953-4959.
45. Tang, W.; Kwak, Y.; Braunecker, W.; Tsarevsky, N. V.; Coote, M. L.; Matyjaszewski, K. Understanding atom transfer radical polymerization: Effect of ligand and initiator structures on the equilibrium constants. *Journal of the American Chemical Society* **2008,** *130* (32), 10702-10713.
46. Tang, W.; Tsarevsky, N. V.; Matyjaszewski, K. Determination of equilibrium constants for atom transfer radical polymerization. *Journal of the American Chemical Society* **2006,** *128* (5), 1598-1604.
47. Matyjaszewski, K.; Paik, H. J.; Zhou, P.; Diamanti, S. J. Determination of activation and deactivation rate constants of model compounds in atom transfer radical polymerization. *Macromolecules* **2001,** *34* (15), 5125-5131.
48. Matyjaszewski, K. The importance of exchange reactions in controlled/living radical polymerization in the presence of alkoxyamines and transition metals. *Macromolecular Symposia* **1996,** *111*, 47-61.
49. Xia, J. H.; Matyjaszewski, K. Controlled/"living" radical polymerization. Homogeneous reverse atom transfer radical polymerization using AIBN as the initiator. *Macromolecules* **1997,** *30* (25), 7692-7696.
50. Gromada, J.; Matyjaszewski, K. Simultaneous reverse and normal initiation in atom transfer radical polymerization. *Macromolecules* **2001,** *34* (22), 7664-7671.
51. Li, M.; Min, K.; Matyjaszewski, K. ATRP in waterborne miniemulsion via a simultaneous reverse and normal initiation process. *Macromolecules* **2004,** *37* (6), 2106-2112.
52. Li, M.; Jahed, N. M.; Min, K.; Matyjaszewski, K. Preparation of linear and star-shaped block copolymers by ATRP using simultaneous reverse and normal initiation process in bulk and miniemulsion. *Macromolecules* **2004,** *37* (7), 2434-2441.
53. Min, K.; Gao, H. F.; Matyjaszewski, K. Preparation of homopolymers and block copolymers in miniemulsion by ATRP using activators generated by electron transfer (AGET). *Journal of the American Chemical Society*

2005, *127* (11), 3825-3830.
54. Jakubowski, W.; Matyjaszewski, K. Activator generated by electron transfer for atom transfer radical polymerization. *Macromolecules* **2005,** *38* (10), 4139-4146.
55. Jakubowski, W.; Min, K.; Matyjaszewski, K. Activators regenerated by electron transfer for atom transfer radical polymerization of styrene. *Macromolecules* **2006,** *39* (1), 39-45.
56. Jakubowski, W.; Matyjaszewski, K. Activators regenerated by electron transfer for atom-transfer radical polymerization of (meth)acrylates and related block copolymers. *Angewandte Chemie-International Edition* **2006,** *45* (27), 4482-4486.
57. Pietrasik, J.; Dong, H.; Matyjaszewski, K. Synthesis of high molecular weight poly(styrene-co-acrylonitrile) copolymers with controlled architecture. *Macromolecules* **2006,** *39* (19), 6384-6390.
58. Dong, H.; Tang, W.; Matyjaszewski, K. Well-defined high-molecular-weight polyacrylonitrile via activators regenerated by electron transfer ATRP. *Macromolecules* **2007,** *40* (9), 2974-2977.
59. Mueller, L.; Jakubowski, W.; Tang, W.; Matyjaszewski, K. Successful chain extension of polyacrylate and polystyrene macroinitiators with methacrylates in an ARGET and ICAR ATRP. *Macromolecules* **2007,** *40* (18), 6464-6472.
60. Matyjaszewski, K.; Jakubowski, W.; Min, K.; Tang, W.; Huang, J.; Braunecker, W. A.; Tsarevsky, N. V. Diminishing catalyst concentration in atom transfer radical polymerization with reducing agents. *Proceedings of the National Academy of Sciences of the United States of America* **2006,** *103* (42), 15309-15314.
61. Matyjaszewski, K.; Nanda, A. K.; Tang, W. Effect of [CuII] on the rate of activation in ATRP. *Macromolecules* **2005,** *38* (5), 2015-2018.
62. Zhang, H. Q.; Klumperman, B.; Ming, W. H.; Fischer, H.; van der Linde, R. Effect of Cu(II) on the kinetics of the homogeneous atom transfer radical polymerization of methyl methacrylate. *Macromolecules* **2001,** *34* (18), 6169-6173.
63. Tang, W.; Matyjaszewski, K. Kinetic modeling of normal ATRP, normal ATRP with [CuII]0, reverse ATRP and SR&NI ATRP. *Macromolecular Theory and Simulations* **2008,** *17* (7-8), 359-375.
64. Tang, W.; Matyjaszewski, K. Effects of initiator structure on activation rate constants in ATRP. *Macromolecules* **2007,** *40* (6), 1858-1863.
65. Barner-Kowollik, C.; Buback, M.; Egorov, M.; Fukuda, T.; Goto, A.; Olaj, O. F.; Russell, G. T.; Vana, P.; Yamada, B.; Zetterlund, P. B. Critically evaluated termination rate coefficients for free-radical polymerization: Experimental methods. *Progress in Polymer Science* **2005,** *30* (6), 605-643.
66. Gao, C.; Yan, D. Hyperbranched polymers: from synthesis to

applications. *Progress in Polymer Science* **2004,** *29* (3), 183-275.
67. Kim, Y. H.; Webster, O. W. Hyperbranched polyphenylenes. *Macromolecules* **1992,** *25* (21), 5561-5572.
68. Kim, Y. H.; Webster, O. W. Water soluble hyperbranched polyphenylene - a unimolecular micelle. *Journal of the American Chemical Society* **1990,** *112* (11), 4592-4593.
69. Kienle, R. H.; Hovey, A. G. The polyhydric alcohol–polybasic acid reactions. I. Glycerol–phthalic anhydride. *Journal of the American Chemical Society* **1929,** *51* (2), 509-519.
70. Flory, P. J. Molecular size distribution in three dimensional polymers. III. Tetrafunctional branching units. *Journal of the American Chemical Society* **1941,** *63*, 3096-3100.
71. Flory, P. J. Molecular size distribution in three dimensional polymers. II. Trifunctional branching units. *Journal of the American Chemical Society* **1941,** *63*, 3091-3096.
72. Flory, P. J. Molecular size distribution in three dimensional polymers. I. Gelation. *Journal of the American Chemical Society* **1941,** *63*, 3083-3090.
73. Flory, P. J. Molecular size distribution in three dimensional polymers. IV. Branched polymers containing A-R-Bf-1 type units. *Journal of the American Chemical Society* **1952,** *74* (11), 2718-2723.
74. Kolb, H. C.; Finn, M. G.; Sharpless, K. B. Click chemistry: diverse chemical function from a few good reactions. *Angewandte Chemie-International Edition* **2001,** *40* (11), 2004-2021.
75. Lutz, J.-F. 1,3-Dipolar cycloadditions of azides and alkynes: A universal ligation tool in polymer and materials science. *Angewandte Chemie-International Edition* **2007,** *46* (7), 1018-1025.
76. Killops, K. L.; Campos, L. M.; Hawker, C. J. Robust, efficient, and orthogonal synthesis of dendrimers via thiol-ene "click" chemistry. *Journal of the American Chemical Society* **2008,** *130* (15), 5062-+.
77. Ma, X.; Tang, J.; Shen, Y.; Fan, M.; Tang, H.; Radosz, M. Facile synthesis of polyester dendrimers from sequential click coupling of asymmetrical monomers. *Journal of the American Chemical Society* **2009,** *131* (41), 14795-14803.
78. Kim, Y. H. Lyotropic liquid crystalline hyperbranched aromatic polyamides. *Journal of the American Chemical Society* **1992,** *114* (12), 4947-4948.
79. Kim, Y. H.; Beckerbauer, R. Role of end groups on the glass transition of hyperbranched polyphenylene and triphenylbenzene derivatives. *Macromolecules* **1994,** *27* (7), 1968-1971.
80. O'Brien, N.; McKee, A.; Sherrington, D. C.; Slark, A. T.; Titterton, A. Facile, versatile and cost effective route to branched vinyl polymers. *Polymer* **2000,** *41* (15), 6027-6031.
81. Costello, P. A.; Martin, I. K.; Slark, A. T.; Sherrington, D. C.; Titterton,

A. Branched methacrylate copolymers from multifunctional monomers: chemical composition and physical architecture distributions. *Polymer* **2002,** *43* (2), 245-254.
82. Sato, T.; Sato, N.; Seno, M.; Hirano, T. Initiator-fragment incorporation radical polymerization of divinylbenzene in the presence of glyoxylic oxime ether: Formation of soluble hyperbranched polymer. *Journal of Polymer Science Part A-Polymer Chemistry* **2003,** *41* (19), 3038-3047.
83. Sato, T.; Arima, Y.; Seno, M.; Hirano, T. Initiator-fragment incorporation radical polymerization of divinyl adipate with dimethyl 2,2 '-azobis(isobutyrate): Kinetics and formation of soluble hyperbranched polymer. *Macromolecules* **2005,** *38* (5), 1627-1632.
84. Sato, T.; Nakamura, T.; Seno, M.; Hirano, T. Soluble hyperbranched copolymer via initiator-fragment incorporation radical copolymerization using a trivinyl monomer. *Polymer* **2006,** *47* (13), 4630-4637.
85. Kricheldorf, H. R.; Zang, Q. Z.; Schwarz, G. New polymer syntheses. 6. Linear and branched poly(3-hydroxy-benzoates). *Polymer* **1982,** *23* (12), 1821-1829.
86. Gunatillake, P. A.; Odian, G.; Tomalia, D. A. Thermal polymerization of a 2-(carboxyalkyl)-2-oxazoline. *Macromolecules* **1988,** *21* (6), 1556-1562.
87. Hawker, C. J.; Lee, R.; Frechet, J. M. J. One-step synthesis of hyperbranched dendritic polyesters. *Journal of the American Chemical Society* **1991,** *113* (12), 4583-4588.
88. Frechét, J. M. J.; Henmi, M.; Gitsov, I.; Aoshima, S.; Leduc, M. R.; Grubbs, R. B. Self-condensing vinyl polymerization - an approach to dendritic materials. *Science* **1995,** *269* (5227), 1080-1083.
89. Matyjaszewski, K.; Gaynor, S. G. Preparation of hyperbranched polyacrylates by atom transfer radical polymerization .3. Effect of reaction conditions on the self-condensing vinyl polymerization of 2-((2-bromopropionyl)oxy) ethyl acrylate. *Macromolecules* **1997,** *30* (23), 7042-7049.
90. Matyjaszewski, K.; Gaynor, S. G.; Müller, A. H. E. Preparation of hyperbranched polyacrylates by atom transfer radical polymerization .2. Kinetics and mechanism of chain growth for the self-condensing vinyl polymerization of 2-((2-bromopropionyl)oxy) ethyl acrylate. *Macromolecules* **1997,** *30* (23), 7034-7041.
91. Ide, N.; Fukuda, T. Nitroxide-controlled free-radical copolymerization of vinyl and divinyl monomers. Evaluation of pendant-vinyl reactivity. *Macromolecules* **1997,** *30* (15), 4268-4271.
92. Ide, N.; Fukuda, T. Nitroxide-controlled free-radical copolymerization of vinyl and divinyl monomers. 2. Gelation. *Macromolecules* **1999,** *32* (1), 95-99.
93. Li, Y. T.; Armes, S. P. Synthesis and chemical degradation of branched

vinyl polymers prepared via ATRP: Use of a cleavable disulfide-based branching agent. *Macromolecules* **2005,** *38* (20), 8155-8162.
94. Liu, B. L.; Kazlauciunas, A.; Guthrie, J. T.; Perrier, S. Influence of reaction parameters on the synthesis of hyperbranched polymers via reversible addition fragmentation chain transfer (RAFT) polymerization. *Polymer* **2005,** *46* (17), 6293-6299.
95. Liu, B. L.; Kazlauciunas, A.; Guthrie, J. T.; Perrier, S. One-pot hyperbranched polymer synthesis mediated by reversible addition fragmentation chain transfer (RAFT) polymerization. *Macromolecules* **2005,** *38* (6), 2131-2136.
96. Holter, D.; Burgath, A.; Frey, H. Degree of Bbanching in hyperbranched polymers. *Acta Polymerica* **1997,** *48* (1-2), 30-35.
97. Yan, D. Y.; Muller, A. H. E.; Matyjaszewski, K. Molecular parameters of hyperbranched polymers made by self-condensing vinyl polymerization .2. Degree of branching. *Macromolecules* **1997,** *30* (23), 7024-7033.
98. Stiriba, S. E.; Kautz, H.; Frey, H. Hyperbranched molecular nanocapsules: Comparison of the hyperbranched architecture with the perfect linear analogue. *Journal of the American Chemical Society* **2002,** *124* (33), 9698-9699.
99. Kramer, M.; Stumbe, J. F.; Grimm, G.; Kaufmann, B.; Kruger, U.; Weber, M.; Haag, R. Dendritic polyamines: Simple access to new materials with defined treelike structures for application in nonviral gene delivery. *Chembiochem* **2004,** *5* (8), 1081-1087.
100. Newkome, G. R.; Baker, G. R.; Saunders, M. J.; Russo, P. S.; Gupta, V. K.; Yao, Z. Q.; Miller, J. E.; Bouillion, K. Two-directional cascade molecules: synthesis and characterization of [9]-n-[9] arborols. *Journal of the Chemical Society-Chemical Communications* **1986,** (10), 752-753.
101. Newkome, G. R.; Yao, Z. Q.; Baker, G. R.; Gupta, V. K. Micelles. Part 1. Cascade molecules: a new approach to micelles. A [27]-arborol. *Journal of Organic Chemistry* **1985,** *50* (11), 2003-2004.
102. Newkome, G. R.; Yao, Z. Q.; Baker, G. R.; Gupta, V. K.; Russo, P. S.; Saunders, M. J. Chemistry of micelles series. Part 2. Cascade molecules. Synthesis and characterization of a benzene [9] 3-arborol. *Journal of the American Chemical Society* **1986,** *108* (4), 849-850.
103. Jikei, M.; Chon, S. H.; Kakimoto, M.; Kawauchi, S.; Imase, T.; Watanebe, J. Synthesis of hyperbranched aromatic polyamide from aromatic diamines and trimesic acid. *Macromolecules* **1999,** *32* (6), 2061-2064.
104. Muller, A. H. E.; Yan, D. Y.; Wulkow, M. Molecular parameters of hyperbranched polymers made by self-condensing vinyl polymerization .1. Molecular weight distribution. *Macromolecules* **1997,** *30* (23), 7015-7023.
105. Guan, Z. Control of polymer topology through transition-metal

catalysis: Synthesis of hyperbranched polymers by cobalt-mediated free radical polymerization. *Journal of the American Chemical Society* **2002,** *124* (20), 5616-5617.
106. Li, Y. T.; Armes, S. P. Synthesis of branched water-soluble vinyl polymers via oxyanionic polymerization. *Macromolecules* **2005,** *38* (12), 5002-5009.
107. Gaynor, S. G.; Edelman, S.; Matyjaszewski, K. Synthesis of branched and hyperbranched polystyrenes. *Macromolecules* **1996,** *29* (3), 1079-1081.
108. Malmstrom, E.; Hult, A. Kinetics of formation of hyperbranched polyesters based on 2,2-bis(methylol)propionic acid. *Macromolecules* **1996,** *29* (4), 1222-1228.
109. Malmstrom, E.; Johansson, M.; Hult, A. Hyperbranched aliphatic polyesters. *Macromolecules* **1995,** *28* (5), 1698-1703.
110. Turner, S. R.; Voit, B. I.; Mourey, T. H. All-aromatic hyperbranched polyesters with phenol and acetate end-groups - synthesis and characterization. *Macromolecules* **1993,** *26* (17), 4617-4623.
111. Voit, B. New developments in hyperbranched polymers. *Journal of Polymer Science Part A-Polymer Chemistry* **2000,** *38* (14), 2505-2525.
112. Frey, H.; Lach, C.; Lorenz, K. Heteroatom-based dendrimers. *Advanced Materials* **1998,** *10* (4), 279-293.
113. Kricheldorf, H. R.; Bolender, O.; Wollheim, T. New polymer syntheses. 103. In situ end group modification of hyperbranched poly(3,5-dihydroxybenzoate). *Macromolecules* **1999,** *32* (12), 3878-3882.
114. Kricheldorf, H. R.; Zang, Q. Z.; Schwarz, G. New polymer syntheses: 6. Linear and branched poly (3-hydroxy-benzoates). *Polymer* **1982,** *23* (12), 1821-1829.
115. Emrick, T.; Chang, H. T.; Frechet, J. M. J. An A2 + B3 approach to hyperbranched aliphatic polyethers containing chain end epoxy substituents. *Macromolecules* **1999,** *32* (19), 6380-6382.
116. Yan, D. Y.; Gao, C. Hyperbranched polymers made from A(2) and BB '(2) type monomers. 1. Polyaddition of 1-(2-aminoethyl)piperazine to divinyl sulfone. *Macromolecules* **2000,** *33* (21), 7693-7699.
117. Froehling, P.; Brackman, J. Properties and applications of poly(propylene imine) dendrimers and poly(esteramide) hyperbranched polymers. *Macromolecular Symposia* **2000,** *151*, 581-589.
118. van Benthem, R.; Meijerink, N.; Gelade, E.; de Koster, C. G.; Muscat, D.; Froehling, P. E.; Hendriks, P. H. M.; Vermeulen, C.; Zwartkruis, T. J. G. Synthesis and characterization of bis(2-hydroxypropyl)amide-based hyperbranched polyesteramides. *Macromolecules* **2001,** *34* (11), 3559-3566.
119. Hawker, C. J.; Frechet, J. M. J.; Grubbs, R. B.; Dao, J. Preparation of hyperbranched and star polymers by a" living", self-condensing free radical polymerization. *Journal of the American Chemical Society* **1995,**

117 (43), 10763-10764.
120. Tao, Y. F.; He, J. P.; Wang, Z. M.; Pan, J. Y.; Jiang, H. J.; Chen, S. M.; Yang, Y. L. Synthesis of branched polystyrene and poly(styrene-b-4-methoxystyrene) by nitroxyl stable radical controlled polymerization. *Macromolecules* **2001,** *34* (14), 4742-4748.
121. Li, C. M.; He, J. P.; Li, L.; Cao, J. Z.; Yang, Y. L. Controlled radical polymerization of styrene in the presence of a polymerizable nitroxide compound. *Macromolecules* **1999,** *32* (21), 7012-7014.
122. Matyjaszewski, K.; Pyun, J.; Gaynor, S. G. Preparation of hyperbranched polyacrylates by atom transfer radical polymerization, 4 - The use of zero-valent copper. *Macromolecular Rapid Communications* **1998,** *19* (12), 665-670.
123. Cheng, C.; Wooley, K. L.; Khoshdel, E. Hyperbranched fluorocopolymers by atom transfer radical self-condensing vinyl copolymerization. *Journal of Polymer Science Part A-Polymer Chemistry* **2005,** *43* (20), 4754-4770.
124. Powell, K. T.; Cheng, C.; Wooley, K. L. Complex amphiphilic hyperbranched fluoropolymers by atom transfer radical self-condensing vinyl (co)polymerization. *Macromolecules* **2007,** *40* (13), 4509-4515.
125. Du, W.; Nystrom, A. M.; Zhang, L.; Powell, K. T.; Li, Y.; Cheng, C.; Wickline, S. A.; Wooley, K. L. Amphiphilic hyperbranched fluoropolymers as nanoscopic (19)F magnetic resonance imaging agent assemblies. *Biomacromolecules* **2008,** *9* (10), 2826-2833.
126. Mori, H.; Walther, A.; Andre, X.; Lanzendorfer, M. G.; Muller, A. H. E. Synthesis of highly branched cationic polyelectrolytes via self-condensing atom transfer radical copolymerization with 2-(diethylamino)ethyl methacrylate. *Macromolecules* **2004,** *37* (6), 2054-2066.
127. Muthukrishnan, S.; Jutz, G.; Andre, X.; Mori, H.; Muller, A. H. E. Synthesis of hyperbranched glycopolymers via self-condensing atom transfer radical copolymerization of a sugar-carrying acrylate. *Macromolecules* **2005,** *38* (1), 9-18.
128. Muthukrishnan, S.; Mori, H.; Muller, A. H. E. Synthesis and characterization of methacrylate-type hyperbranched glycopolymers via self-condensing atom transfer radical copolymerization. *Macromolecules* **2005,** *38* (8), 3108-3119.
129. Percec, V.; Barboiu, B.; Grigoras, C.; Bera, T. K. Universal iterative strategy for the divergent synthesis of dendritic macromolecules from conventional monomers by a combination of living radical polymerization and irreversible TERminator Multifunctional INItiator (TERMINI). *Journal of the American Chemical Society* **2003,** *125* (21), 6503-6516.
130. Wang, Z. M.; He, J. P.; Tao, Y. F.; Yang, L.; Jiang, H. J.; Yang, Y.

L. Controlled chain branching by RAFT-based radical polymerization. *Macromolecules* **2003,** *36* (20), 7446-7452.
131. Carter, S.; Hunt, B.; Rimmer, S. Highly branched poly(N-isopropylacrylamide)s with imidazole end groups prepared by radical polymerization in the presence of a styryl monomer containing a dithioester group. *Macromolecules* **2005,** *38* (11), 4595-4603.
132. Rimmer, S.; Carter, S.; Rutkaite, R.; Haycock, J. W.; Swanson, L. Highly branched poly-(N-isopropylacrylamide)s with arginine-glycine-aspartic acid (RGD)- or COOH-chain ends that form sub-micron stimulus-responsive particles above the critical solution temperature. *Soft Matter* **2007,** *3* (8), 971-973.
133. Carter, S.; Rimmer, S.; Sturdy, A.; Webb, M. Highly branched stimuli responsive poly (N-isopropyl acrylamide)-co-(1,2-propandiol-3-methacrylate)s with protein binding functionality. *Macromolecular Bioscience* **2005,** *5* (5), 373-378.
134. Ishizu, K.; Kojima, T.; Ohta, Y.; Shibuya, T. Nanopattern formation on polymer substrate using star-hyperbranched nanospheres. *Journal of Colloid and Interface Science* **2004,** *272* (1), 76-81.
135. Ishizu, K.; Khan, R. A.; Furukawa, T.; Furo, M. Controlled radical polymerization of N-isopropylacrylamide initiated by photofunctional 2-(N,N-diethyldithiocarbamyl)isobutyric acid sodium salt in aqueous medium. *Journal of Applied Polymer Science* **2004,** *91* (5), 3233-3238.
136. Perrier, S.; Takolpuckdee, P.; Mars, C. A. Reversible addition-fragmentation chain transfer polymerization: End group modification for functionalized polymers and chain transfer agent recovery. *Macromolecules* **2005,** *38* (6), 2033-2036.
137. Matsumoto, A. Free-radical crosslinking polymerization and copolymerization of multivinyl compounds. *Synthesis and Photosynthesis* **1995,** *123*, 41-80.
138. Slark, A. T.; Sherrington, D. C.; Titterton, A.; Martin, I. K. Branched methacrylate copolymers from multifunctional comonomers: the effect of multifunctional monomer functionality on polymer architecture and properties. *Journal of Materials Chemistry* **2003,** *13* (11), 2711-2720.
139. Isaure, F.; Cormack, P. A. G.; Sherrington, D. C. Synthesis of branched poly(methyl methacrylate)s: Effect of the branching comonomer structure. *Macromolecules* **2004,** *37* (6), 2096-2105.
140. Baudry, R.; Sherrington, D. C. Synthesis of highly branched poly(methyl methacrylate)s using the "strathclyde methodology" in aqueous emulsion. *Macromolecules* **2006,** *39* (4), 1455-1460.
141. Baudry, R.; Sherrington, D. C. Facile synthesis of branched poly(vinyl alcohol)s. *Macromolecules* **2006,** *39* (16), 5230-5237.
142. Isaure, F.; Cormack, P. A. G.; Graham, S.; Sherrington, D. C.; Armes, S. P.; Butun, V. Synthesis of branched poly(methyl methacrylate)s

via controlled/living polymerizations exploiting ethylene glycol dimethacrylate as branching agent. *Chemical Communications* **2004,** (9), 1138-1139.
143. Wang, W.; Zheng, Y.; Roberts, E.; Duxbury, C. J.; Ding, L.; Irvine, D. J.; Howdle, S. M. Controlling chain growth: A new strategy to hyperbranched materials. *Macromolecules* **2007,** *40* (20), 7184-7194.
144. Bannister, I.; Billingham, N. C.; Armes, S. P.; Rannard, S. P.; Findlay, P. Development of branching in living radical copolymerization of vinyl and divinyl monomers. *Macromolecules* **2006,** *39* (22), 7483-7492.
145. Bannister, I.; Billingham, N. C.; Armes, S. P. Monte Carlo modelling of living branching copolymerisation of monovinyl and divinyl monomers: comparison of simulated and experimental data for ATRP copolymerisation of methacrylic monomers. *Soft Matter* **2009,** *5* (18), 3495-3504.
146. Koh, M. L.; Konkolewicz, D.; Perrier, S. A simple route to functional highly branched structures: RAFT homopolymerization of divinylbenzene. *Macromolecules* **2011,** *44* (8), 2715-2724.
147. Dong, Z.-M.; Liu, X.-H.; Lin, Y.; Li, Y.-S. Branched polystyrene with abundant pendant vinyl functional groups from asymmetric divinyl monomer. *Journal of Polymer Science Part A-Polymer Chemistry* **2008,** *46* (18), 6023-6034.
148. Rosselgong, J.; Armes, S. P.; Barton, W.; Price, D. Synthesis of highly branched methacrylic copolymers: Observation of near-ideal behavior using RAFT polymerization. *Macromolecules* **2009,** *42* (16), 5919-5924.
149. Rosselgong, J.; Armes, S. P.; Barton, W. R. S.; Price, D. Synthesis of branched methacrylic copolymers: Comparison between RAFT and ATRP and effect of varying the monomer concentration. *Macromolecules* **2010,** *43* (5), 2145-2156.
150. Khan, A.; Malkoch, M.; Montague, M. F.; Hawker, C. J. Synthesis and characterization of hyperbranched polymers with increased chemical versatility for imprint lithographic resists. *Journal of Polymer Science Part A-Polymer Chemistry* **2008,** *46* (18), 6238-6254.
151. Akiyama, M.; Yoshida, K.; Mori, H. Controlled synthesis of vinyl-functionalized homopolymers and block copolymers by RAFT polymerization of vinyl methacrylate. *Polymer* **2014,** *55* (3), 813-823.
152. Lin, Y.; Liu, X.; Li, X.; Zhan, J.; Li, Y. Reversible addition-fragmentation chain transfer mediated radical polymerization of asymmetrical divinyl monomers targeting hyperbranched vinyl polymers. *Journal of Polymer Science Part A-Polymer Chemistry* **2007,** *45* (1), 26-40.
153. Zhao, T.; Zheng, Y.; Poly, J.; Wang, W. Controlled multi-vinyl monomer homopolymerization through vinyl oligomer combination as a universal approach to hyperbranched architectures. *Nature Communications*

2013, *4*, Article number: 1873.
154. Zheng, Y.; Cao, H.; Newland, B.; Dong, Y.; Pandit, A.; Wang, W. 3D single cyclized polymer chain structure from controlled polymerization of multi-vinyl monomers: Beyond Flory-Stockmayer theory. *Journal of the American Chemical Society* **2011,** *133* (33), 13130-13137.
155. Zheng, Y.; Newland, B.; Tai, H.; Pandit, A.; Wang, W. Single cyclized molecule structures from RAFT homopolymerization of multi-vinyl monomers. *Chemical Communications* **2012,** *48* (25), 3085-3087.
156. Mori, H.; Tsukamoto, M. RAFT polymerization of diacrylate derivatives having different spacers in dilute conditions. *Polymer* **2011,** *52* (3), 635-645.
157. Gao, H.; Matyjaszewski, K. Synthesis of functional polymers with controlled architecture by CRP of monomers in the presence of cross-linkers: From stars to gels. *Progress in Polymer Science* **2009,** *34* (4), 317-350.
158. Yu, Q.; Zeng, F. Q.; Zhu, S. P. Atom transfer radical polymerization of poly(ethylene glycol) dimethacrylate. *Macromolecules* **2001,** *34* (6), 1612-1618.
159. Landin, D. T.; Macosko, C. W. Cyclization and reduced reactivity of pendant vinyls during the copolymerization of methyl-methacrylate and ethylene-glycol dimethacrylate. *Macromolecules* **1988,** *21* (3), 846-851.
160. Wang, R.; Luo, Y.; Li, B.-G.; Zhu, S. Modeling of branching and gelation in RAFT copolymerization of vinyl/divinyl systems. *Macromolecules* **2009,** *42* (1), 85-94.
161. Saito, R.; Iijima, Y.; Yokoi, K. Atom transfer radical polymerization of poly(2-methacryloyloxyethyl methacrylate). *Macromolecules* **2006,** *39* (20), 6838-6844.
162. Saito, R. Combination of template polymerization and atom transfer radical polymerization: Strategy for synthesis of specifically structural polymers. *Polymer* **2008,** *49* (11), 2625-2631.
163. Wang, D.; Zhao, T.; Zhu, X.; Yan, D.; Wang, W. Bioapplications of hyperbranched polymers. *Chemical Society Reviews* **2015**.
164. Yu, X.; Liu, Z.; Janzen, J.; Chafeeva, I.; Horte, S.; Chen, W.; Kainthan, R. K.; Kizhakkedathu, J. N.; Brooks, D. E. Polyvalent choline phosphate as a universal biomembrane adhesive. *Nature Materials* **2012,** *11* (5), 468-476.
165. Frey, H.; Haag, R. Dendritic polyglycerol: a new versatile biocompatible-material. *Journal of biotechnology* **2002,** *90* (3-4), 257-67.
166. Kainthan, R. K.; Janzen, J.; Levin, E.; Devine, D. V.; Brooks, D. E. Biocompatibility testing of branched and linear polyglycidol. *Biomacromolecules* **2006,** *7* (3), 703-709.
167. Oudshoorn, M. H. M.; Rissmann, R.; Bouwstra, J. A.; Hennink, W. E. Synthesis and characterization of hyperbranched polyglycerol hydrogels.

Biomaterials **2006,** *27* (32), 5471-5479.
168. Fedorovich, N. E.; Oudshoorn, M. H.; van Geemen, D.; Hennink, W. E.; Alblas, J.; Dhert, W. J. A. The effect of photopolymerization on stem cells embedded in hydrogels. *Biomaterials* **2009,** *30* (3), 344-353.
169. Lutz, J.-F.; Akdemir, O.; Hoth, A. Point by point comparison of two thermosensitive polymers exhibiting a similar LCST: Is the age of poly(NIPAM) over? *Journal of the American Chemical Society* **2006,** *128* (40), 13046-13047.
170. Lutz, J.-F.; Weichenhan, K.; Akdemir, O.; Hoth, A. About the phase transitions in aqueous solutions of thermoresponsive copolymers and hydrogels based on 2-(2-methoxyethoxy)ethyl methacrylate and oligo(ethylene glycol) methacrylate. *Macromolecules* **2007,** *40* (7), 2503-2508.
171. Tai, H.; Wang, W.; Alexander, C.; Shakesheff, K. M.; Howdle, S. M. Thermal-responsive and photocrosslinkable hyperbranched polymers synthesised by deactivation enhanced ATRP and RAFT polymerisations. *Journal of Controlled Release* **2008,** *132* (3), E48-E50.
172. Tai, H.; Howard, D.; Takae, S.; Wang, W.; Vermonden, T.; Hennink, W. E.; Stayton, P. S.; Hoffman, A. S.; Endruweit, A.; Alexander, C.; Howdle, S. M.; Shakesheff, K. M. Photo-cross-linked hydrogels from thermoresponsive PEGMEMA-PPGMA-EGDMA copolymers containing multiple methacrylate groups: mechanical property, swelling, protein release, and cytotoxicity. *Biomacromolecules* **2009,** *10* (10), 2895-2903.
173. Dong, Y.; Gunning, P.; Cao, H.; Mathew, A.; Newland, B.; Saeed, A. O.; Magnusson, J. P.; Alexander, C.; Tai, H.; Pandit, A.; Wang, W. Dual stimuli responsive PEG based hyperbranched polymers. *Polymer Chemistry* **2010,** *1* (6), 827-830.
174. Nikolovski, J.; Mooney, D. J. Smooth muscle cell adhesion to tissue engineering scaffolds. *Biomaterials* **2000,** *21* (20), 2025-2032.
175. Burdick, J. A.; Anseth, K. S. Photoencapsulation of osteoblasts in injectable RGD-modified PEG hydrogels for bone tissue engineering. *Biomaterials* **2002,** *23* (22), 4315-4323.
176. Yang, F.; Williams, C. G.; Wang, D. A.; Lee, H.; Manson, P. N.; Elisseeff, J. The effect of incorporating RGD adhesive peptide in polyethylene glycol diacrylate hydrogel on osteogenesis of bone marrow stromal cells. *Biomaterials* **2005,** *26* (30), 5991-5998.
177. Nuttelman, C. R.; Tripodi, M. C.; Anseth, K. S. In vitro osteogenic differentiation of human mesenchymal stem cells photoencapsulated in PEG hydrogels. *Journal of Biomedical Materials Research Part A* **2004,** *68A* (4), 773-782.
178. Menzies, D. J.; Cameron, A.; Maisonneuve, B. G. C.; GrOndahl, L.; Wolvetang, E.; Cooper-White, J. Enzyme mediated, oxidative crosslinking of multifunctional, branched PEG: Characterization, particle formation and

stem cell encapsulation. *Journal of Tissue Engineering and Regenerative Medicine* **2012,** *6*, 208-208.
179. Brandl, F. P.; Seitz, A. K.; Tessmar, J. K. V.; Blunk, T.; Goepferich, A. M. Enzymatically degradable poly(ethylene glycol) based hydrogels for adipose tissue engineering. *Biomaterials* **2010,** *31* (14), 3957-3966.
180. Menjoge, A. R.; Kannan, R. M.; Tomalia, D. A. Dendrimer-based drug and imaging conjugates: design considerations for nanomedical applications. *Drug Discovery Today* **2010,** *15* (5-6), 171-185.
181. Mintzer, M. A.; Grinstaff, M. W. Biomedical applications of dendrimers: a tutorial. *Chemical Society Reviews* **2011,** *40* (1), 173-190.
182. Malik, N.; Wiwattanapatapee, R.; Klopsch, R.; Lorenz, K.; Frey, H.; Weener, J. W.; Meijer, E. W.; Paulus, W.; Duncan, R. Dendrimers: Relationship between structure and biocompatibility in vitro, and preliminary studies on the biodistribution of I-125-labelled polyamidoamine dendrimers in vivo. *Journal of Controlled Release* **2000,** *65* (1-2), 133-148.
183. Jiang, H.-L.; Kim, Y.-K.; Arote, R.; Nah, J.-W.; Cho, M.-H.; Choi, Y.-J.; Akaike, T.; Cho, C.-S. Chitosan-graft-polyethylenimine as a gene carrier. *Journal of Controlled Release* **2007,** *117* (2), 273-280.
184. Gosselin, M. A.; Guo, W. J.; Lee, R. J. Efficient gene transfer using reversibly cross-linked low molecular weight polyethylenimine. *Bioconjugate Chemistry* **2001,** *12* (6), 989-994.
185. Choi, S.; Lee, K.-D. Enhanced gene delivery using disulfide-crosslinked low molecular weight polyethylenimine with listeriolysin o-polyethylenimine disulfide conjugate. *Journal of Controlled Release* **2008,** *131* (1), 70-76.
186. Wang, Y.; Chen, P.; Shen, J. The development and characterization of a glutathione-sensitive cross-linked polyethylenimine gene vector. *Biomaterials* **2006,** *27* (30), 5292-5298.
187. Liu, J.; Jiang, X.; Xu, L.; Wang, X.; Hennink, W. E.; Zhuo, R. Novel reduction-responsive cross-linked polyethylenimine derivatives by click chemistry for nonviral gene delivery. *Bioconjugate Chemistry* **2010,** *21* (10), 1827-1835.
188. Xia, W.; Wang, P.; Lin, C.; Li, Z.; Gao, X.; Wang, G.; Zhao, X. Bioreducible polyethylenimine-delivered siRNA targeting human telomerase reverse transcriptase inhibits HepG2 cell growth in vitro and in vivo. *Journal of Controlled Release* **2012,** *157* (3), 427-436.
189. Dey, D.; Inayathullah, M.; Lee, A. S.; LeMieux, M. C.; Zhang, X.; Wu, Y.; Nag, D.; De Almeida, P. E.; Han, L.; Rajadas, J.; Wu, J. C. Efficient gene delivery of primary human cells using peptide linked polyethylenimine polymer hybrid. *Biomaterials* **2011,** *32* (20), 4647-4658.
190. Lim, Y. B.; Kim, S. M.; Lee, Y.; Lee, W. K.; Yang, T. G.; Lee, M. J.; Suh, H.; Park, J. S. Cationic hyperbranched poly(amino ester): A novel class of DNA condensing molecule with cationic surface, biodegradable

three-dimensional structure, and tertiary amine groups in the interior. *Journal of the American Chemical Society* **2001,** *123* (10), 2460-2461.
191. Liu, Y.; Wu, D. C.; Ma, Y. X.; Tang, G. P.; Wang, S.; He, C. B.; Chung, T. S.; Goh, S. Novel poly(amino ester)s obtained from Michael addition polymerizations of trifunctional amine monomers with diacrylates: safe and efficient DNA carriers. *Chemical Communications* **2003,** (20), 2630-2631.
192. Zhong, Z. Y.; Song, Y.; Engbersen, J. F. J.; Lok, M. C.; Hennink, W. E.; Feijen, J. A versatile family of degradable non-viral gene carriers based on hyperbranched poly(ester amine)s. *Journal of Controlled Release* **2005,** *109* (1-3), 317-329.
193. Cherng, J. Y.; vandeWetering, P.; Talsma, H.; Crommelin, D. J. A.; Hennink, W. E. Effect of size and serum proteins on transfection efficiency of poly((2-dimethylamino)ethyl methacrylate)-plasmid nanoparticles. *Pharmaceutical Research* **1996,** *13* (7), 1038-1042.
194. vandeWetering, P.; Cherng, J. Y.; Talsma, H.; Hennink, W. E. Relation between transfection efficiency and cytotoxicity of poly(2-(dimethylamino)ethyl methacrylate)/plasmid complexes. *Journal of Controlled Release* **1997,** *49* (1), 59-69.
195. Tao, L.; Liu, J.; Tan, B. H.; Davis, T. P. RAFT synthesis and DNA binding of biodegradable, hyperbranched poly(2-(dimethylamino)ethyl methacrylate. *Macromolecules* **2009,** *42* (14), 4960-4962.
196. Schallon, A.; Jerome, V.; Walther, A.; Synatschke, C. V.; Mueller, A. H. E.; Freitag, R. Performance of three PDMAEMA-based polycation architectures as gene delivery agents in comparison to linear and branched PEI. *Reactive & Functional Polymers* **2010,** *70* (1), 1-10.
197. Tan, J. H.; McMillan, N. A. J.; Payne, E.; Alexander, C.; Heath, F.; Whittaker, A. K.; Thurecht, K. J. Hyperbranched polymers as delivery vectors for oligonucleotides. *Journal of Polymer Science Part A-Polymer Chemistry* **2012,** *50* (13), 2585-2595.

Chapter Two

Optimizing Atom Transfer Radical Addition towards Good Kinetical Control of Homopolymerization of Multi-vinyl Monomers

Parts of this chapter have been published in:

Zheng, Y., **Zhao, T.**, Newland, B., Poly, J., Wang, W. 'Controlled homopolymerization of multi-vinyl monomers: dendritic polymers synthesized via an optimized ATRA reaction' *CHEMCAL COMMUNICATIONS*, **2013**, 49, 10124-10126. **(First co-author)**

2.1 Introduction

2.1.1 Atom Transfer Radical Addition

It is known that the widely used ATRP method was extended and developed from the organic synthetic process called atom transfer radical addition (ATRA). Many reactions involving free radicals exhibit high chemoselectivities[1, 2]. When stable radicals, such as nitroxides, or metalloradicals (e.g. X-Cu^{II} species) are generated together with reactive alkyl radicals, the cross-coupling is much faster than the homocoupling of alkyl radicals. Therefore, above 90% yields of 1:1 monoadducts of alkyl halide (RX) and alkenes are often observed in ATRA. These reactions may be initiated by light or radical initiators like in Kharasch addition[3] or may be catalyzed by transition metals[4]. The former reaction is shown in Figure 2.1. Alkyl halide, **1**, in the presence of some radical source generates radical **2**. In the presence of large excess of alkene **3**, addition occurs resulting in product radical **4**. In the halogen transfer step with 1, it yields the product **5** and regenerates radical **2**. If trapping with **1** is not efficient, some oligomerization may happen. The escaped radicals **4n** may then be trapped by **1** to form products **5n**.

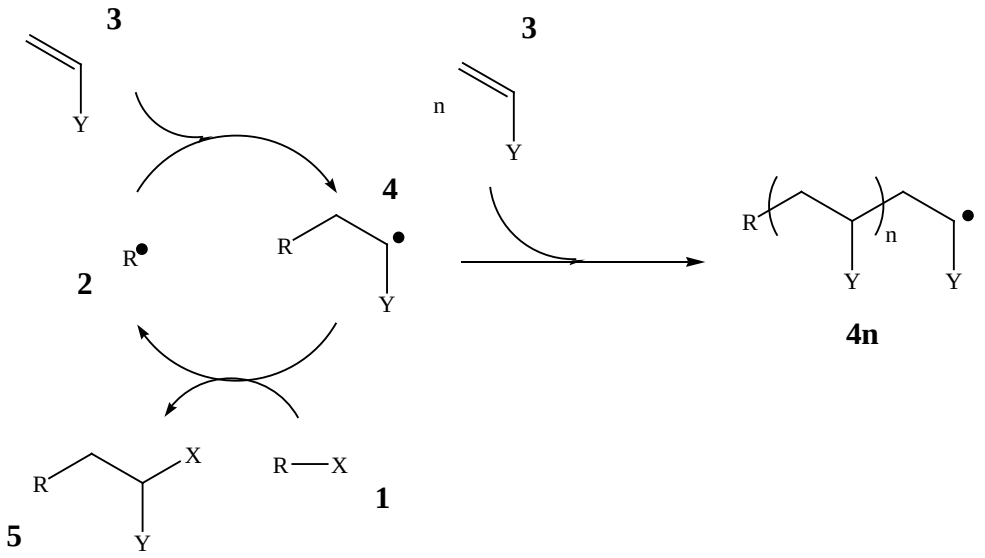

Figure 2.1 Basic steps in Kharasch addition.

The transition metal catalyzed ATRA is shown in Figure 2.2. It has a similar sequence of reactions but the radicals **4** are trapped not by RX but by much

more efficient transition metal halides in higher oxidation state **7**. This may lead to different selectivities than in Kharasch addition. e.g. in the reaction with chloroform the alkene will "insert" across the H-CCl_3 bond under Kharasch conditions but across the Cl-$CHCl_2$ bond in ATRA, because the C-Cl bond is more rapidly activated by the Fe^{II} or Cu^{I} complexes[5]. Also the deactivation step does not involve RX but proceeds by the abstraction of X from complex **7**, which may be much bulkier than RX (different regioselctivity and stereoselectivity). Moreover, deactivation step may be much faster (different chemoselectivities). Figure 2.2 is simplified because in reality, both activation and deactivation steps are reversible. In ATRA a metal catalyst, such as a copper(I) halide complexed by suitable ligands (Ni, Pd, Ru, Fe, and other metals have been used as well)[6] undergoes an inner sphere oxidation via abstraction of a halogen atom from a substrate.

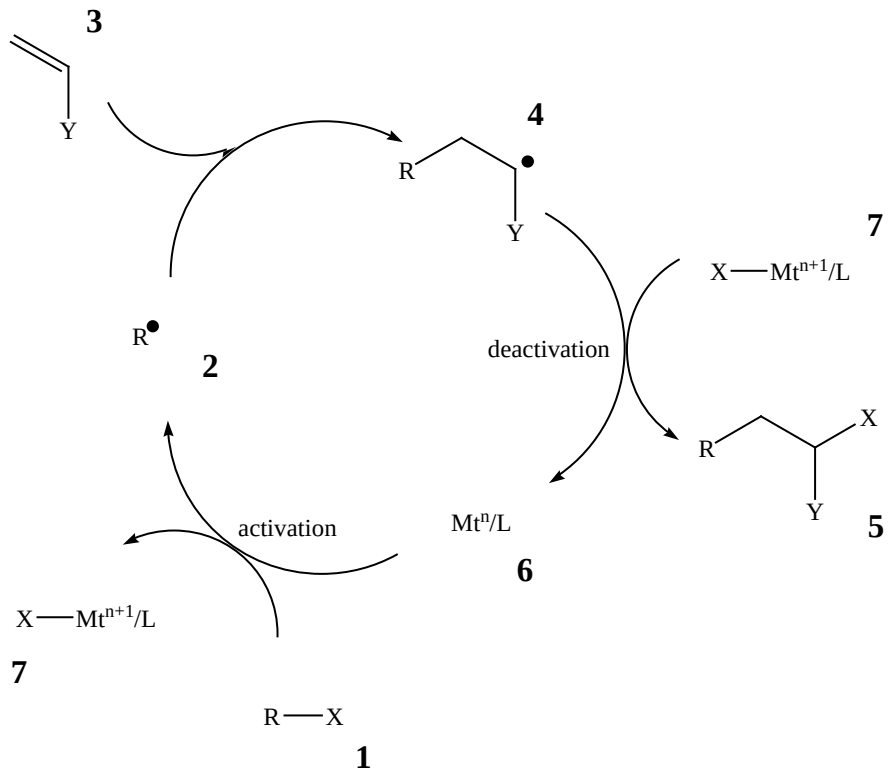

Figure 2.2 Basic steps in transition metal catalyzed ATRA.

The correct choice of alkene and RX leads to high yield of **5**, which should be much more difficult to activate than **1**. Very little coupling products between radicals **2-2**, **2-4** and **4-4** are formed and the radicals react nearly exclusively with **7** to form **5**. The unusual selectivity in these systems have been explained by persistent radical effect (PRE)[7]. Its essence is that the “preference” for cross-coupling over homo-coupling is not due to different rate constants of the coupling reactions but is due to different rates. Reactive

radicals **2** and **4** are present at very low concentrations, e.g. ~10^{-8} M but persistent radicals at concentration ~10^{-3}M, i.e. thousands time higher. With every act of termination of radicals **2** or **4**, a persistent radical (PR) is accumulated. Though at the very beginning of the reaction, the **2** and **7** are present at the equal molar concentrations, very soon concentrations of **2** (and **4**) drops whereas concentration of **7** continuously increases. The amount of PR present equals the amount of homo-coupling products and can be as low as 1%, meaning that reactions are unusually selective.

PRE is a very important concept which is at the very essence of ATRA. One could argue that without termination and PRE, radical addition could not be controlled. It is possible to enhance PRE by additional amounts of stable radicals at the beginning of the reaction. This eliminates needs for spontaneous formation of PRE and termination of some chains. This process is also used when deactivators act relatively slowly or propagation is fast.

ATRA can be extended to ATRP if the conditions can be modified such that more than one addition step occurs[8, 9]. Thus, if the radical species in Figure 2.3 before and after addition of the unsaturated substrate (monomer) possess comparable reactivity, then the activation-addition-deactivation cycle will repeat until all of monomer present is consumed. This process results in a chain-growth polymerization. However, not only one but several monomer molecules may be added during one activation step. The precise number depends on the relative rates of propagation (k_p) and deactivation (k_{deact}) and affects polydispersity of the obtained polymers. In a well-controlled ATRP system, contribution of termination (k_t) can be essentially neglected. Therefore, an ideal ATRP reaction should be totally made up of multiple steps of ATRA. Whether an ATRP reaction is successful largely depends on whether there are good ATRA processes occurring in the reaction.

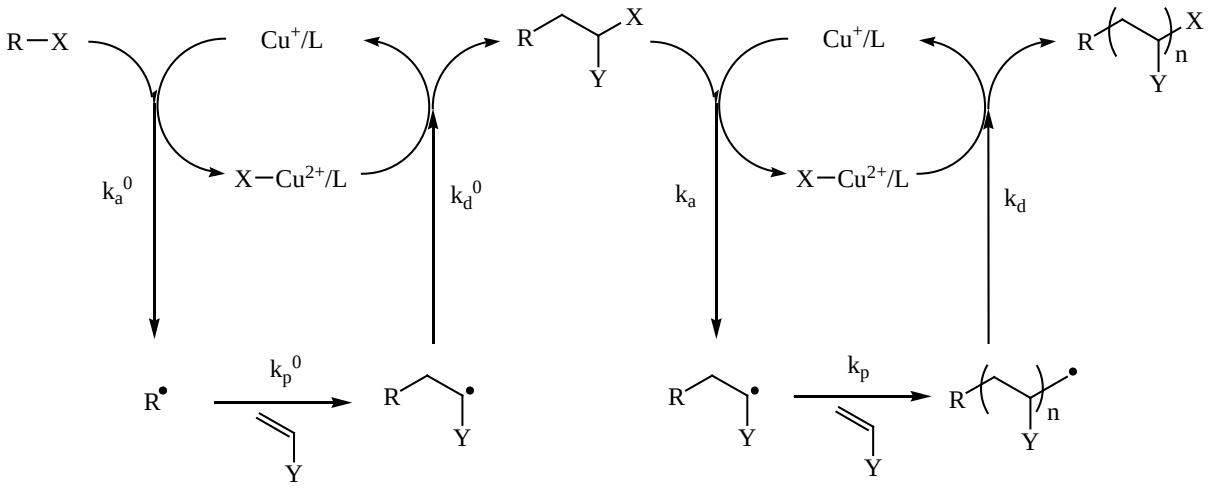

Figure 2.3 Schematic representation of multi-steps of propagation accompanied by reversible activation/deactivation in ATRP.

2.1.2 Effect of Kinetical Control on Polymer Architecture

The kinetical control of ATRP could affect not only the polydispersity of the propagating chains but also the architecture of the polymers. In the homopolymerization of divinyl monomer, the different mechanisms via conventional free radical polymerization (FRP), normal ATRP and a well-controlled ATRA are shown in the Figure 2.4. In the FRP reaction, the propagating free radical grows quickly without control, since large numbers of vinyl groups will react with the propagating center. Thus, high MW polymers were produced at the beginning of reaction (Upper, Figure 2.4). Consequently, these large molecules can easily form molecules with long primary chains and low degree of branching. Intermolecular crosslinking of these large molecules will lead to fast gelation due to their size and pendant vinyl groups. Once the intermolecular cross-links were formed, the whole reaction turned to gel quickly.

In a normal ATRP, the propagation process was controlled by activation-deactivation equilibrium, and only several vinyl groups were reacted with the propagating center during each active cycle. However, this level of control is not good enough to accomplish a hyperbranched structure and suppress the gelation. Under normal condition, gelation normally occurs at below 10-15% conversion in the homopolymerization of divinyl monomers via normal ATRP.[10, 11]

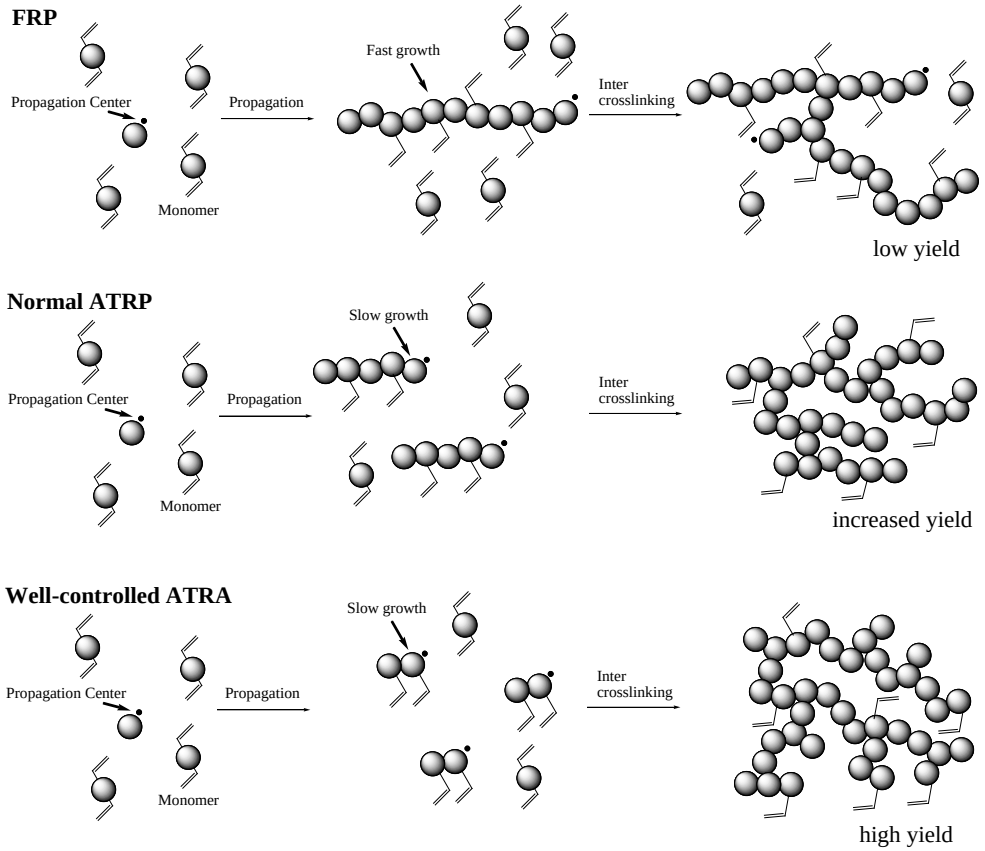

Figure 2.4 Mechanism of a well-controlled ATRA for achieving highly branched polymer in the homopolymerization of divinyl monomer. In contrast, the free radical polymerization (FRP) or the normal ATRP reaction will lead to less branched polymers and low conversion before gelation.

In a well-controlled ATRA reaction, there are two key factors to facilitate the formation of highly branched structure from the homopolymerization of divinyl monomer. Firstly, the well-contolled ATRA provides much better control over the size and polydispersity of the propagating chain and thus leads to shorter and more uniform primary chains before intermolecular crosslinking. So the chain length between each branching points is kept small. And that is a typical feature for a highly branched structure. Secondly, the equilibrium between the dormant chains and the active propagating chains ensures that only one vinyl groups are incorporated into the polymer chains during each activation-deactivation cycle. Thereafter, the propagating center becomes a dormant species quickly and stays for a longer time in the dormant state. This ensures that the chain propagation stays in the same rate level as the intermolecular crosslinking. And this two form of chain growth work synergistically in the favor of a highly branched structure.

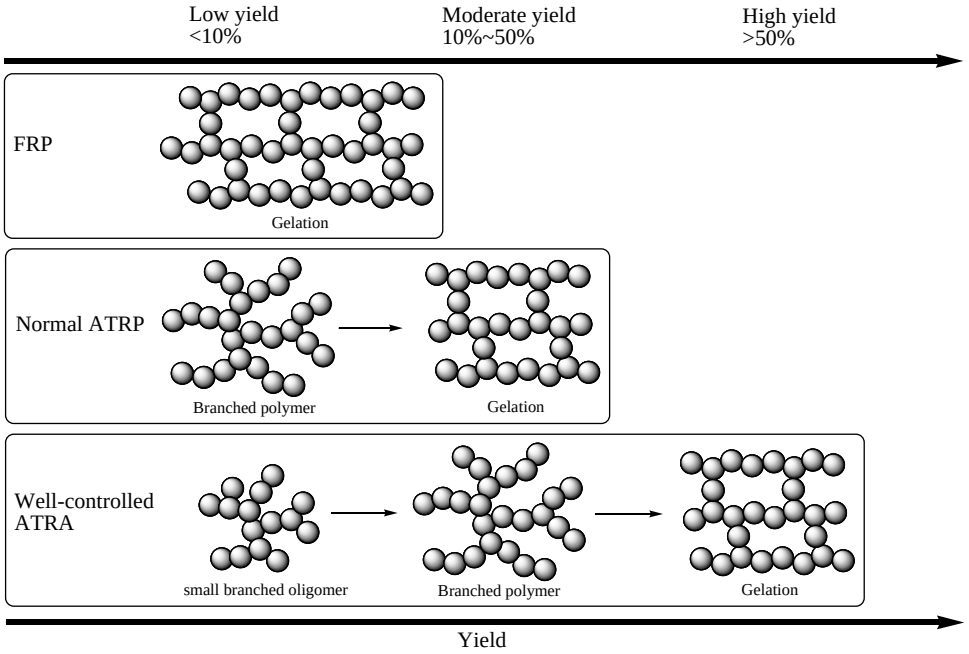

Figure 2.5 Different gelation processes of the homopolymerization of divinyl monomer between FRP, normal ATRP and well-controlled ATRA. In the well-controlled ATRA, gelation can be postponed until high yield. Whereas the FRP and normal ATRP will lead to gelation at low or moderate yield due to the lack of kinetical control and the high polydispersity of the primary chains.

Furthermore, the different gelation processes between FRP, normal ATRP and well-controlled ATRA in the concentrated system are shown in Figure 2.5. In the FRP and normal ATRP, the reaction gels at a relatively low conversion due to fast propagation. On the other hand, the polymers prepared by a well-controlled ATRA indicate the remarkable differences from the gel produced via FRP or normal ATRP (Figure 2.5). At low conversion, short polymer chains or oligomers are formed due to the relatively high monomer concentration at the beginning of the reaction. At moderate conversion, the branched polymers are formed by the intermolecular reaction between the linear chains together with linear propagation. Thus, the number of branching points increases significantly during the reaction. Finally, the large macromolecules will form a gel via intermolecular crosslinking at high yield, since the concentration of polymer chains is relatively high and the contribution of intermolecular crosslinking becomes significant at the high yield (Figure 2.5).

In a copper catalyzed ATRA, the mechanism is listed in Figure 2.6. The key to increasing the chemoselectivity of the monoadduct lies in the radical-generating step. In order to achieve high selectivity, the following

guidelines need to be met: (a) the radical concentration must be low in order to suppress radical termination reactions (rate constant of activation (k_{a1} and k_{a2}) << rate constant of deactivation (k_{d1} and k_{d2})), (b) further activation of the monoadduct should be avoided ($k_{a1}>>k_{a2}$), and (c) the formation of oligomers/polymers should be suppressed [rate of transfer ($k_{d2}\cdot[X\text{-}Cu^{II}X/L]$) >> rate of propagation ($k_p\cdot[alkene]$)]. The guideline (a) is highly dependent on the reaction system and the metal/ligand complex, whilst the guideline (b) is mainly related to the chemical structure of the halide R-X. The guideline (c) is the most important prerequisite for a well-controlled ATRA, since it confines that the number of alkene added on the radical during an activation-deactivation circle should be smaller than 1. It means the reversible activation-deactivation process should happen much more frequently than the chain propagation and one alkene can be inserted after several times of activation-deactivation transfer. In ATRP, this concept is defined as the kinetic chain length (v), which is proportional to the constant of propagation (k_p) and concentration of monomer ([M]), and inversely proportional to constant of deactivation (k_{deact}) and concentration of Cu^{II} ($[Cu^{II}]$) (Eq. 2.1).

$$\nu_{ATRP} = \frac{R_p}{R_{deact}} = \frac{k_p[M][P^{\bullet}]}{k_{deact}[P^{\bullet}][Cu^{II}]} = \frac{k_p[M]}{k_{deact}[Cu^{II}]} \qquad \text{Eq. 2.1}$$

Luckily this kinetic chain length value can be manipulated through many factors. Wang *et al*. realized that by controlling the competition between chain growth and reversible chain termination via a deactivation enhanced method, the kinetic chain length can be effectively reduced. By the addition of Cu^{II} species to the ATRP system the equilibrium was manipulated to increase the deactivation rate and slow down the polymerization rate. This ATRP procedure, termed deactivation-enhanced ATRP (DE-ATRP) retains a large proportion of deactivated species (via Cu^{II}) and thus significantly decreases the kinetics chain length. Using this strategy, it is possible to make the propagation rate of a polymer chain much slower than the deactivation rate, and thus minimize kinetics chain length to an extremely low level.

The DE-ATRP shows better control over the polymerization of vinyl monomer than the normal ATRP. This technique has recently been utilized with great success in postponing the gelation of homopolymerization of MVMs (e.g. DVB and EGDMA) to high monomer conversion[12].

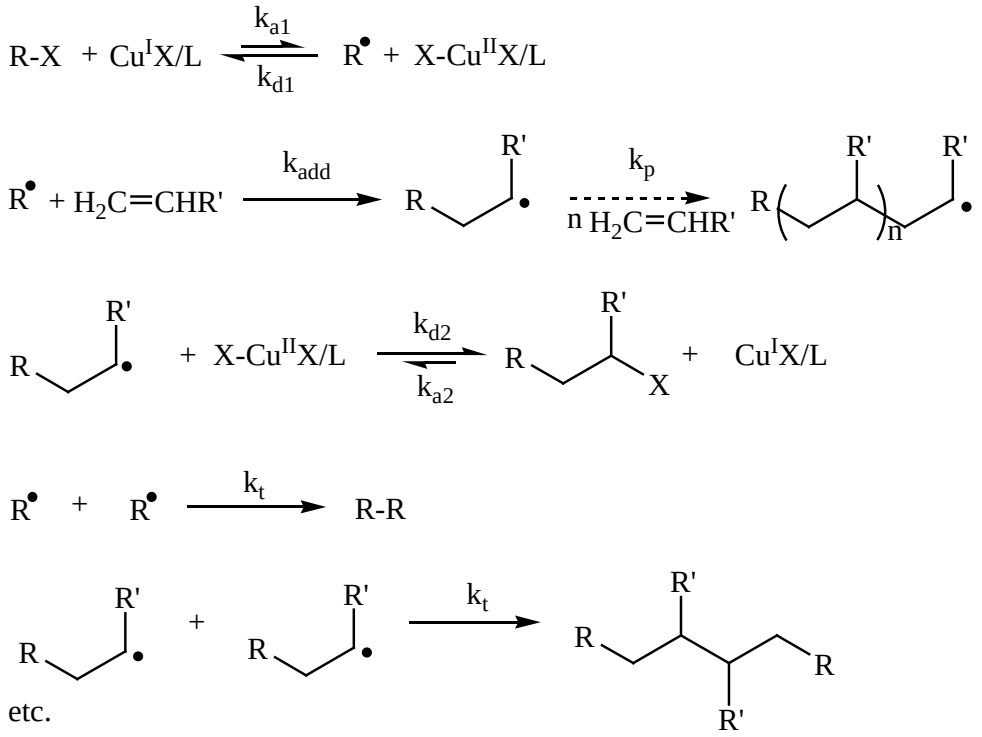

L=complexing ligand
X=halide or pseudo halide

Figure 2.6 Proposed mechanism for copper-catalyzed ATRA.

The DE-ATRP was further improved to *in situ* DE-ATRP.[13] Similar to the activators generated by electron transfer (AGET) process, *in situ* DE-ATRP uses a reducing agent (e.g., ascorbic acid, AA) to reduce the catalyst from the higher oxidation state (Cu^{II}) to the active state (Cu^{I}) for the activation of alkyl halide initiators, hence leading to free radical formation and chain propagation. However, the important difference is that low proportion of reducing agent is used for *in situ* DE-ATRP, compared to the high amount used for AGET-ATRP.[14, 15]

In this chapter, deactivation enhanced ATRA reaction of chloroform and mono-vinyl monomers was firstly determined and optimized. To the best of our knowledge, the deactivation enhanced strategy has never been determined using ATRA reaction. It is hypothesized that if a strategy could be used to form a high yield of the monoadduct, this method could then be applied to the polymerization of MVMs to produce HBPs that approach an ideal dendritic structure, with a short primary chain length and large amounts of functional end groups. To verify this hypothesis, different reaction systems based on copper catalyzed mechanism were evaluated and optimized towards a high monoadduct yield and a high conversion. Then,

through the optimized ATRA system, divinyl monomers were used to synthesize highly branched dendritic polymers which were carefully characterized. This reaction has unique features that have never been achieved before: (1) good kinetic control via ATRA allows the formation of extremely short primary chains, which is not easily obtained using any of the previous methods; (2) homopolymerization of a divinyl monomer and a high initiator to monomer ratio (1:2) provide an extremely high branch ratio and functionality.

2.2 Experimental

2.2.1 Materials

Styrene (≥95%), methyl methacrylate (MMA, 99%), divinylbenzene (DVB, 80%), ethylene glycol dimethacrylate (EGDMA, 98%) was purchased from Sigma-Aldrich. Monomers were passed through a column to remove inhibitors. The chloroform ($CHCl_3$, ≥99%, Aldrich) and 1,1′-azobis (cyclohexanecarbonitrile) (ACCN, 98%, Aldrich) were used as the initiator. Pentamethyldiethylenetriamine (PMDETA, 99%, Aldrich), copper (I) chloride (CuCl, 99%, Aldrich), copper (II) chloride ($CuCl_2$, 99%, Aldrich), L-ascorbic acid (AA, 99%, Aldrich), d-chloroform (99.8%, Aldrich), 2-butanone (HPLC grade, Aldrich), toluene (HPLC grade, Aldrich), tetrahydrofuran (THF, HPLC grade, Aldrich), dimethylformamide (DMF, HPLC grade, Aldrich) n-hexane (ACS reagent grade, Aldrich) and diethyl ether (ACS reagent grade, Aldrich) were used as received.

2.2.2 Characterization Method

Gel permeation chromatography (GPC) characterizations: Weight average molecular weight (M_w), number average molecular weight (M_n) and polydispersity (M_w/M_n) were obtained by GPC (Varian 920-LC) equipped with triple detectors including an RI detector, viscometer and an LS detector. The columns (30 cm PLgel Mixed-C, two in series) were eluted using dimethylformamide (DMF) and calibrated using a series of 12 near-monodisperse PMMA standards (M_p from 690 to 1,944,000 $gmol^{-1}$). The polymers were analyzed in DMF at a concentration of 5.0 mg/ml. All calibrations and analysis were performed at 60 ^oC and a flow rate of 1 ml/min.

^{1}H NMR characterizations: ^{1}H NMR analysis was carried out on a S4 300 MHz Bruker NMR with JEOL Delta v5.0.1 processing software. The

chemical shifts were referenced to the lock chloroform (7.26 ppm).

2.2.3 Reaction Procedure

FRP of styrene: Styrene (25 mmol, 1 equiv), $CHCl_3$ (100 mmol, 4 equiv) and toluene (5.2 ml) were added into the flask and oxygen was removed by bubbling argon through the solutions for 20 min at room temperature. ACCN (0.1 mmol, 0.004 equiv) was carefully transferred into the flask under an argon blanket. The solution was stirred at 800 rpm and the polymerization was conducted at 60 °C in an oil bath for the desired reaction time.

ARGET-ATRA1 of styrene: Styrene (25 mmol, 1 equiv), $CHCl_3$ (100 mmol, 4 equiv), $CuBr_2$ (0.025 mmol, 0.001 equiv), PMDETA (0.025 mmol, 0.001 equiv) and toluene (5.2 ml) were added into the flask and oxygen was removed by bubbling argon through the solutions for 20 min at room temperature. AA (0.25 mmol, 0.01 equiv, 1000% of $CuCl_2$) was carefully transferred into the flask under an argon blanket. The solution was stirred at 800 rpm and the polymerization was conducted at 60 °C in an oil bath for the desired reaction time.

ARGET-ATRA2 of styrene: Styrene (25 mmol, 1 equiv), $CHCl_3$ (100 mmol, 4 equiv), $CuBr_2$ (0.1 mmol, 0.004 equiv), PMDETA (0.1 mmol, 0.004 equiv) and toluene (5.2 ml) were added into the flask and oxygen was removed by bubbling argon through the solutions for 20 min at room temperature. AA (0.1 mmol, 0.004 equiv, 100% of $CuCl_2$) was carefully transferred into the flask under an argon blanket. The solution was stirred at 800 rpm and the polymerization was conducted at 60 °C in an oil bath for the desired reaction time.

ATRA1 of styrene: Styrene (25 mmol, 1 equiv), $CHCl_3$ (100 mmol, 4 equiv) and toluene (5.2 ml) were added into the flask and oxygen was removed by bubbling argon through the solutions for 20 min at room temperature. CuCl (0.1 mmol, 0.004 equiv) was carefully transferred into the flask under an argon blanket. The solution was stirred at 800 rpm and the polymerization was conducted at 60 °C in an oil bath for the desired reaction time.

***In situ* DE-ATRA1 of styrene:** Styrene (25 mmol, 1 equiv), $CHCl_3$ (100 mmol, 4 equiv), $CuCl_2$ (0.15 mmol, 0.006 equiv), PMDETA (0.15 mmol, 0.006 equiv) and toluene (5.2 ml) were added into the flask and oxygen was removed by bubbling argon through the solutions for 20 min at room temperature. AA (0.03 mmol, 0.0012 equiv, 20% of $CuCl_2$) was carefully

transferred into the flask under an argon blanket. The solution was stirred at 800 rpm and the polymerization was conducted at 60 °C in an oil bath for the desired reaction time.

***In situ* DE-ATRA2 of styrene:** Styrene (25 mmol, 1 equiv), $CHCl_3$ (100 mmol, 4 equiv), $CuCl_2$ (0.25 mmol, 0.01 equiv), PMDETA (0.25 mmol, 0.01 equiv) and toluene (5.2 ml) were added into the flask and oxygen was removed by bubbling argon through the solutions for 20 min at room temperature. AA (0.05 mmol, 0.002 equiv, 20% of $CuCl_2$) was carefully transferred into the flask under an argon blanket. The solution was stirred at 800 rpm and the polymerization was conducted at 60 °C in an oil bath for the desired reaction time.

FRP of methyl methacrylate (MMA): MMA (25 mmol, 1 equiv), $CHCl_3$ (100 mmol, 4 equiv) and 2-butanone (5.4 ml) were added into the flask and oxygen was removed by bubbling argon through the solutions for 20 min at room temperature. ACCN (0.1 mmol, 0.004 equiv) was carefully transferred into the flask under an argon blanket. The solution was stirred at 800 rpm and the polymerization was conducted at 60 °C in an oil bath for the desired reaction time.

ATRA1 of MMA: MMA (25 mmol, 1 equiv), $CHCl_3$ (100 mmol, 4 equiv), PMDETA (0.1 mmol, 0.004 equiv) and 2-butanone (5.4 ml) were added into the flask and oxygen was removed by bubbling argon through the solutions for 20 min at room temperature. CuCl (0.1 mmol, 0.004 equiv) was carefully transferred into the flask under an argon blanket. The solution was stirred at 800 rpm and the polymerization was conducted at 60 °C in an oil bath for the desired reaction time.

ATRA2 of MMA: MMA (25 mmol, 1 equiv), $CHCl_3$ (100 mmol, 4 equiv), PMDETA (0.2 mmol, 0.008 equiv) and 2-butanone (5.4 ml) were added into the flask and oxygen was removed by bubbling argon through the solutions for 20 min at room temperature. CuCl (0.2 mmol, 0.008 equiv) was carefully transferred into the flask under an argon blanket. The solution was stirred at 800 rpm and the polymerization was conducted at 60 °C in an oil bath for the desired reaction time.

***In situ* DE-ATRA of MMA:** MMA (25 mmol, 1 equiv), $CHCl_3$ (100 mmol, 4 equiv), $CuCl_2$ (0.625 mmol, 0.025 equiv), PMDETA (0.625 mmol, 0.025 equiv) and 2-butanone (5.4 ml) were added into the flask and oxygen was removed by bubbling argon through the solutions for 20 min at room temperature. AA (0.047 mmol, 0.00188 equiv, 7.5% of $CuCl_2$) was carefully transferred into the flask under an argon blanket. The solution was stirred at

800 rpm and the polymerization was conducted at 60 °C in an oil bath for the desired reaction time.

Preparation of hyperbranched polyDVB: DVB (25 mmol, 1 equiv), $CHCl_3$ (12.5 mmol, 0.5 equiv), $CuCl_2$ (0.25 mmol, 0.01 equiv), PMDETA (0.25 mmol, 0.01 equiv) and toluene (4.7 ml) were added into the flask and oxygen was removed by bubbling argon through the solutions for 20 min at room temperature. AA (0.05 mmol, 0.002 equiv, 20% of $CuCl_2$) was carefully transferred into the flask under an argon blanket. The solution was stirred at 800 rpm and the polymerization was conducted at 60 °C in an oil bath for the desired reaction time.

Preparation of hyperbranched polyEGDMA: Ethylene glycol dimethacrylate (EGDMA, 20 mmol, 1 equiv), 2-butanone (4.9 ml), $CHCl_3$ (10 mmol, 0.5 equiv), $CuCl_2$ (0.5 mmol, 0.025 equiv) and PMDETA (0.5 mmol, 0.025 equiv) were added into the flask and oxygen was removed by bubbling argon through the solutions for 20 min at room temperature. AA (0.0375 mmol, 0.00188 equiv, 7.5% of $CuCl_2$) was carefully transferred into the flask under an argon blanket. The solution was stirred at 800 rpm and the polymerization was conducted at 60 °C in an oil bath for the desired reaction time

2.3 Results and Discussions

2.3.1 Evaluation of Different ATRA Systems

In this section, the first target was to examine the different reaction conditions for ATRA of monovinyl monomers, especially the ratio of Cu^{I} to Cu^{II}, in order to probe the effect on the monoadduct yield and identify the kinetic control ability of different systems.

Recently, the concept of initiators for continuous activator regeneration (ICAR)-ATRP and activators regenerated by electron transfer (ARGET)-ATRP are introduced, whereby a constant source of organic free radicals or various organic reducing agents work to regenerate the Cu^{I} activator. With this technique, controlled synthesis of polystyrene and poly(methyl methacrylate) (M_w/M_n < 1.2) can be implemented with diminished catalyst concentrations between 10 and 50 ppm[16], which is quite promising and could have important industrial implications. The ICAR-ATRA has also been successfully applied to ATRA reaction and manifest good reaction rate and monoadduct yield[17, 18, 19]. However, as far as

our knowledge, the ARGET strategy has never been reported for ATRA reaction. Therefore, in this section, the ARGET ATRA is also included for the exploration of a fine ATRA system.

Four reaction systems were tested:

1. Free radical polymerization (FRP) - no copper catalyst was used;

2. Normal ATRA - with initial Cu^{I};

3. ARGET ATRA - excess AA was used that reduces not only the added Cu^{II} but also Cu^{II} formed via the initiator, back to Cu^{I};

4. *In situ* DE-ATRA - the Cu^{II} added is only partially reduced thus leaving higher amounts of the deactivating Cu^{II} present (Figure 2.8).

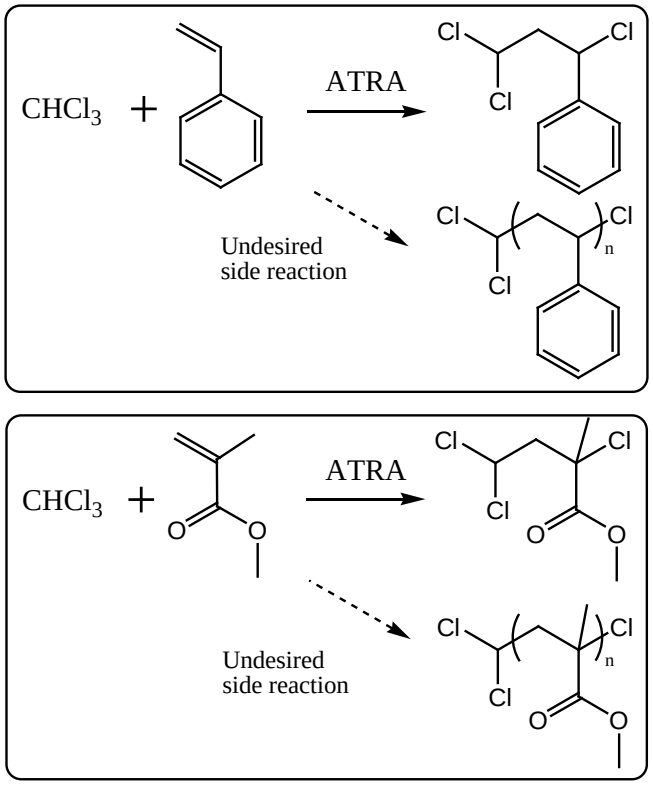

Figure 2.7 ATRA reactions of chloroform with two mono-vinyl monomers (styrene and methyl methacrylate). The kinetic chain length (v) can be indirectly reflected by the monoadduct yield of products at a certain chloroform/ mono-vinyl monomer ratio.

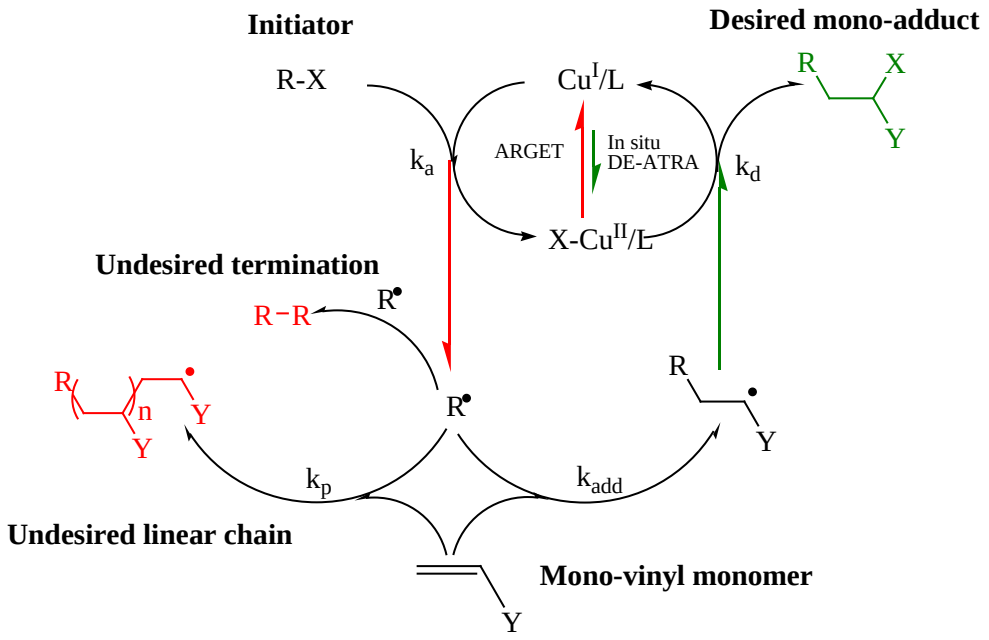

Figure 2.8 The difference between ARGET ATRP and *in situ* DE-ATRA. For ARGET ATRA, excess AA was used that reduces not only the initial Cu^{II} but also the newly formed Cu^{II}, while for *in situ* DE-ATRA, the Cu^{II} is partially reduced, leaving higher amounts of the deactivating Cu^{II}. The scheme shows that monoadduct formation is largely dependent on the Cu^{I} to Cu^{II} ratio.

Two monovinyl monomers (styrene and methyl methacrylate) were chosen for ATRA reaction as shown in Figure 2.7. Chloroform was used as halide for copper-catalysed initiation. Styrene was first evaluated by the non-metal catalyzed Kharasch addition which is actually the FRP condition (entry 1, table 2.1). It can be clearly seen from the GPC trace shown in Figure 2.9 that only polymer with high molecular weight was produced and the molecular weight did not significantly change from 1 hour to 4 hour. The result is similar to the feature of a normal FRP reaction, indicating that the non-metal catalyzed Kharasch addition of chloroform to styrene is not successful with FRP condition, which was initiated by the decomposition of ACCN. The desired monoadduct was not obtained in the presence of chloroform compound (entry 1 in 4 hour Table 2.1 and Figure 2.9), suggesting that chloroform cannot provide control during the propagation process.

Table 2.1 Reaction results for ATRA of styrene.

	Reaction[a]	[M]:[I]:[Cu^{II}]:[AA] Feed ratio	Time (hrs)	M_w (KDa)[b]	PDI[b]	Conv[c] (%)	Mono yield[c]
1	FRP	1000:4000:-:-	4	63.2	1.7	10	0
2	ARGET-ATRA1	1000:4000:1:10	24	19	2.0	14	0
3	ARGET-ATRA2	1000:4000:4:4	5	1.4	1.8	26	7
4	ATRA1	1000:4000:4([Cu^{I}])	24	0.4	1.2	15.7	85
5	*In situ* DE-ATRA1	1000:4000:6:1.2	24	0.2	1.1	50.2	90
6	*In situ* DE-ATRA2	1000:4000:10:2	24	0.2	1.1	65.0	92

[a] FRP [I]:[M]:[ACCN]= 4: 1: 0.004 no copper catalyst, [I]=2.5 M; ARGET-ATRA1 [I]:[M]:[$CuCl_2$]:[AA]= 4: 1: 0.001: 0.01, [I]= 2.5 M; ARGET-ATRA2 [I]:[M]:[$CuCl_2$]:[AA]= 4: 1: 0.004: 0.004, [I]= 2.5 M; ATRA1 [I]:[M]:[CuCl]= 4: 1: 0.004, [I]=2.5 M; *in situ* DE-ATRA1 [I]:[M]:[$CuCl_2$]:[AA]= 4: 1: 0.006: 0.0012, [I]=2.5 M; *in situ* DE-ATRA1 [I]:[M]:[$CuCl_2$]:[AA]= 4: 1: 0.01: 0.002, [I]=2.5 M; In all reaction I= $CHCl_3$, T=60^{o}C, [CuCl] or [$CuCl_2$] :[PMDETA]=1:1, toluene was used as the solvent for styrene; [b] Mw and PDI was characterized by SEC equipped with RI detector, it should be noted that M_w below 690kDa are outside the calibration range; [c] monomer conversion and monoadduct yield were confirmed by ^{1}H NMR (see Figure 2.13 and 2.8, Eq. 2.2 and 2.3).

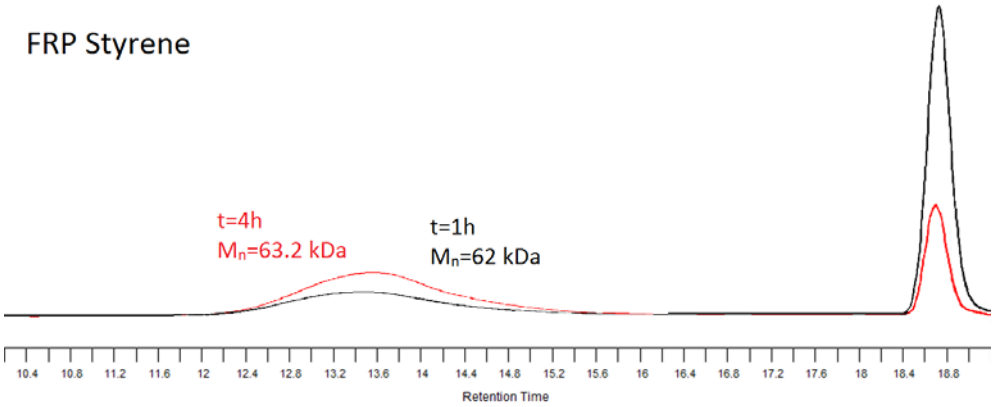

Figure 2.9 GPC traces for FRP of styrene (entry 1, Table 2.1). Only polymers with high molecular weight were produced and the molecular weight did not significantly change from 1 hour to 4 hour.

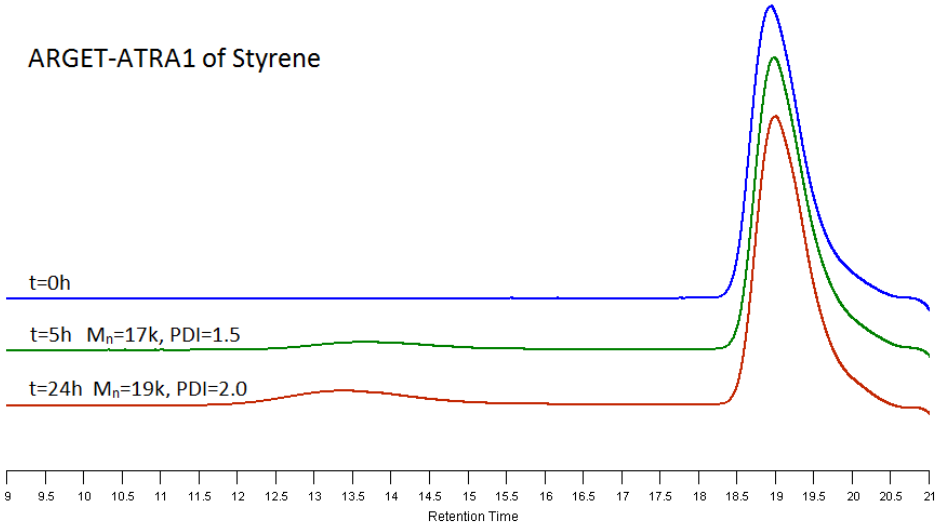

Figure 2.10 GPC traces for ARGET-ATRA1 of styrene with molar ratio of [Styrene]:[$CHCl_3$]:[Cu^{II}]:[AA]=1000:4000:1:10 (entry 2 in Table 2.1). Polymer rather than monoadduct was produced after 24 hours reaction time.

For ARGET-ATRA, the styrene/Cu/AA feed ratio was firstly set at 1000/1/10 (ARGET-ATRA1), which is a typical ratio for an ARGET-ATRP reaction. The GPC trace in Figure 2.10 shows that only polymer with M_n of 19kDa was produced after 24 hours reaction time. No monoadduct formed in this reaction condition. This result indicates that excess ascorbic acid over reduced the Cu^{II} into Cu^{I} (Figure 2.8), providing poor control in the reaction. The conversion of styrene is also low (14%). This could be attributed to the small amount of catalyst which is very easy to be transferred into its higher valence (Cu^{II}) due to the PRE. The large amount of $CHCl_3$ and lack of Cu^{II} are both the reason for a stronger PRE. Thus, even though the amount of

ascorbic acid is 10 times of that of Cu^{II}, it still cannot compensate the significant PRE.

When the copper amount is increased with a decreased reducing agent (styrene/Cu/AA = 1000/4/4, ARGET-ATRA2), a 1.4 kDa polymer with low monoadduct yield was obtained, which again showed a poor reaction control (entry 3 in Table 2.1 and Figure 2.11). Because theoretically one ascorbic acid molecule can reduce two Cu^{II} molecules into Cu^{I}, the ascorbic acid was still at an excessive level. However, the result for ARGET-ATRA2 system shows improvements in both kinetic control and vinyl monomer conversion, since multiple peaks of monoadducts and oligomers appeared. However, there is also a conspicuous peak for high molecular polymers. The two ARGET-ATRA reactions showed that the system of low copper concentration with excessive reducing agent cannot provide a good kinetic control for the formation of monoadduct at a high yield.

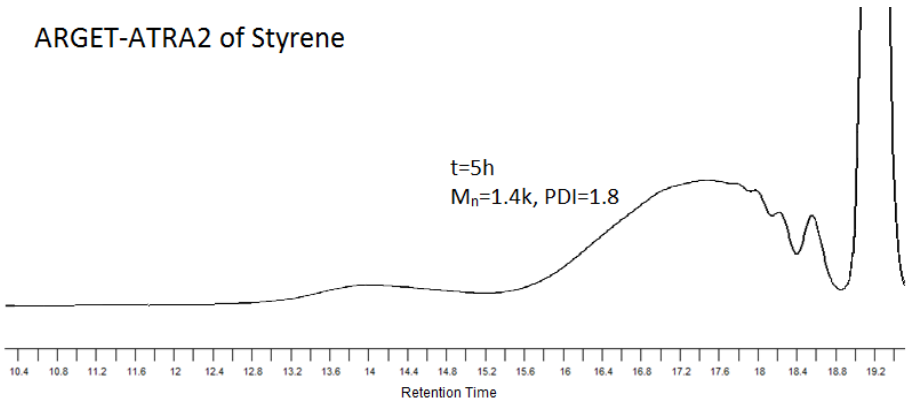

Figure 2.11 GPC traces for ARGET-ATRA2 of styrene with molar ratio of [Styrene]:[$CHCl_3$]:[Cu^{II}]:[PMDETA]:[AA]=1000:4000:4:4:4 (entry 3, Table 2.1). Multimodal peaks of oligomer and polymer were observed. The result shows the monoadduct yield was increased compared to the ARGET-ATRA1.

ATRA was then implemented in the presence of Cu^{I}/PMDETA catalysts (entries 4 in Table 2.1 and Figure 2.12). The $CHCl_3$-styrene monoadduct was successfully formed with ATRA system using 0.4 mol% of Cu^{I}/PMDETA species. Analysis from The ^{1}H NMR spectrum for samples of different time points were analysed as shown in Figure 2.13. Calculation by eq. 2.2 and eq. 2.3 manifested that the monoadduct yield was 55% at the beginning of reaction (1h) and increased to 85% after 24 hours. However, due to the low amount of copper catalyst and strong PRE, the conversion of styrene is not high (15.7%) after 24 hours' reaction.

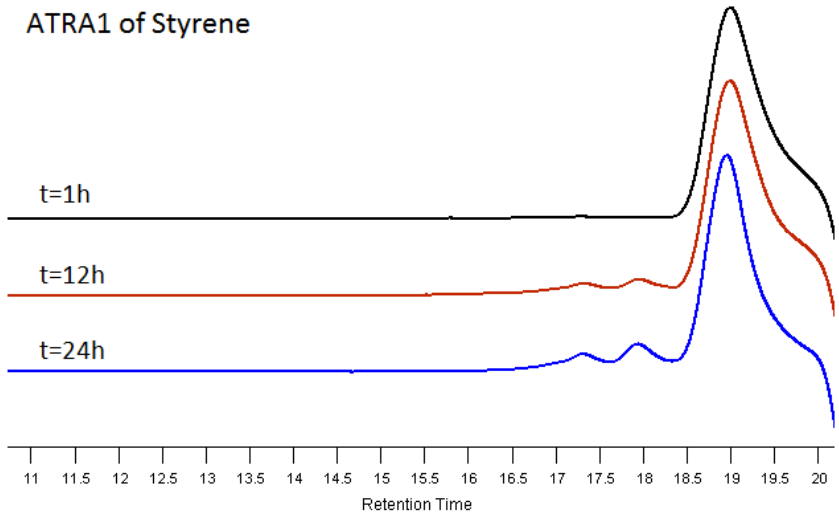

Figure 2.12 GPC traces for ATRA1 of styrene with molar ratio of [Styrene]:[$CHCl_3$]:[Cu^I] =1000:4000:4 (entry 4, Table 2.1). Only peaks of monoadduct and oligomer were observed.

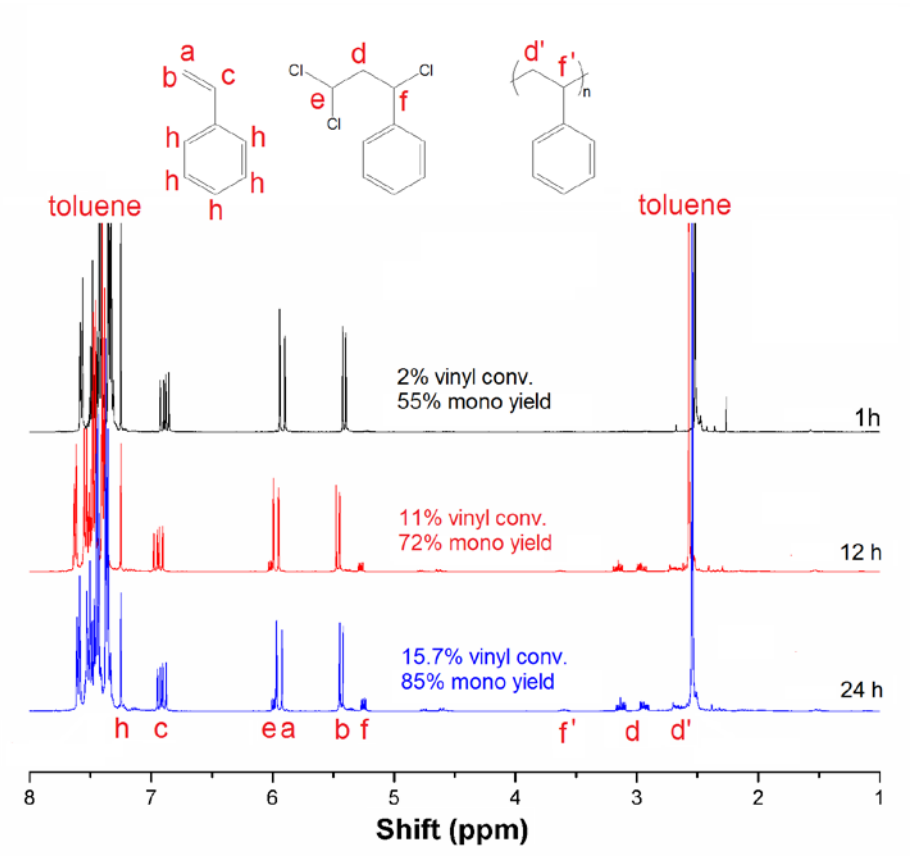

Figure 2.13 ^{1}H NMR spectrum of ATRA1 reaction of styrene (entry 4, Table 2.1), indicating low vinyl conversions and increased monoadduct yields with time.

$$Monomer\ conversion = \frac{Integral\ of\ (f + f')}{Integral\ of\ (c + f + f')} \qquad \text{Eq. 2.2}$$

$$Monoadduct\ yield = \frac{Integral\ of\ f}{Integral\ of\ (f + f')} \qquad \text{Eq. 2.3}$$

The *in situ* DE-ATRA was implemented with initial Cu^{II} /PMDETA species. Ascorbic acid was added to partially reduced 40% of Cu^{II}, thus leaving higher amounts of the deactivating Cu^{II} present. It was hypothesized that 1) by additional amounts of Cu^{II} species at the beginning of the reaction, spontaneous formation of Cu^{II} by PRE and termination of some chains will be eliminated, and the reaction rate will then be maintained at a constant level to accomplish a higher conversion; 2) the high amount of Cu^{II} species will enhance the deactivation process and thus will increase the monoadduct yield. The difference between *in situ* DE-ATRA1 and *in situ* DE-ATRA2 is the initial copper amount (0.6 mol% of styrene for *in situ* DE-ATRA1 and 1 mol% of styrene for *in situ* DE-ATRA2). The amount of ascorbic acid is set at 20 mol% of Cu^{II}. The GPC trace in Figure 2.14 showed that a notable peak of the monoadduct appeared after 24 hours of *in situ* DE-ATRA1 reaction. No polymer formed during the reaction, indicating a good kinetic control.

When the initial amount of Cu^{II} /PMDETA was increased to 1 mol% of styrene, the peak of monoadduct became stronger, as shown in Figure 2.15. Calculation from ^{1}H NMR spectrum provided the monomer conversion and monoadduct yield (Figure 2.16 and Table 2.1). The *in situ* DE-ATRA reactions obtained both higher conversions and higher monoadduct yield compared to the ATRA1 reaction. The results were in accordance with our hypotheses. The increased Cu^{II} amount ensured a limited PRE and an enhanced deactivation process, and thus facilitated the ATRA reaction with a high conversion and a high monoadduct yield.

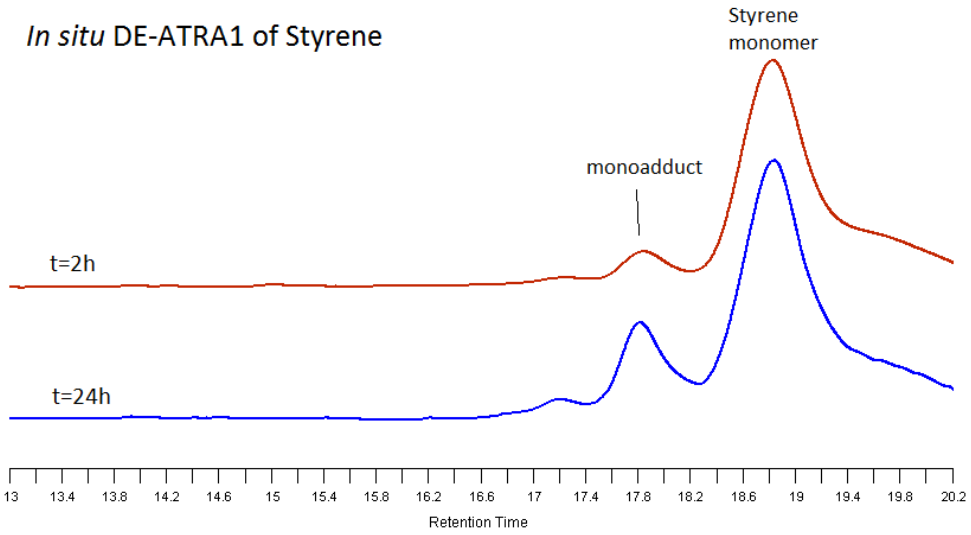

Figure 2.14 GPC traces for *in situ* DE-ATRA1 of styrene with molar ratio of [Styrene]:[$CHCl_3$]:[Cu^{II}]:[AA] = 1000:4000:6:1.2. (entry 5 in Table 2.1). A notable peak of the monoadduct appeared after 24 hours.

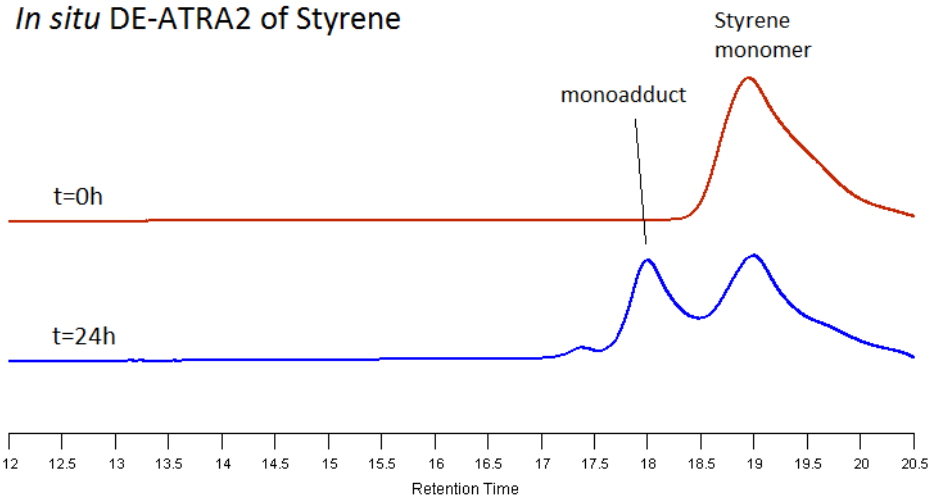

Figure 2.15 GPC traces for *in situ* DE-ATRA2 of styrene with molar ratio of [Styrene]:[$CHCl_3$]:[Cu^{II}]:[AA] = 1000:4000:10:2. (entry 6 in Table 2.1). The peak of the monoadduct is more significant compared to in situ DE-ATRA1.

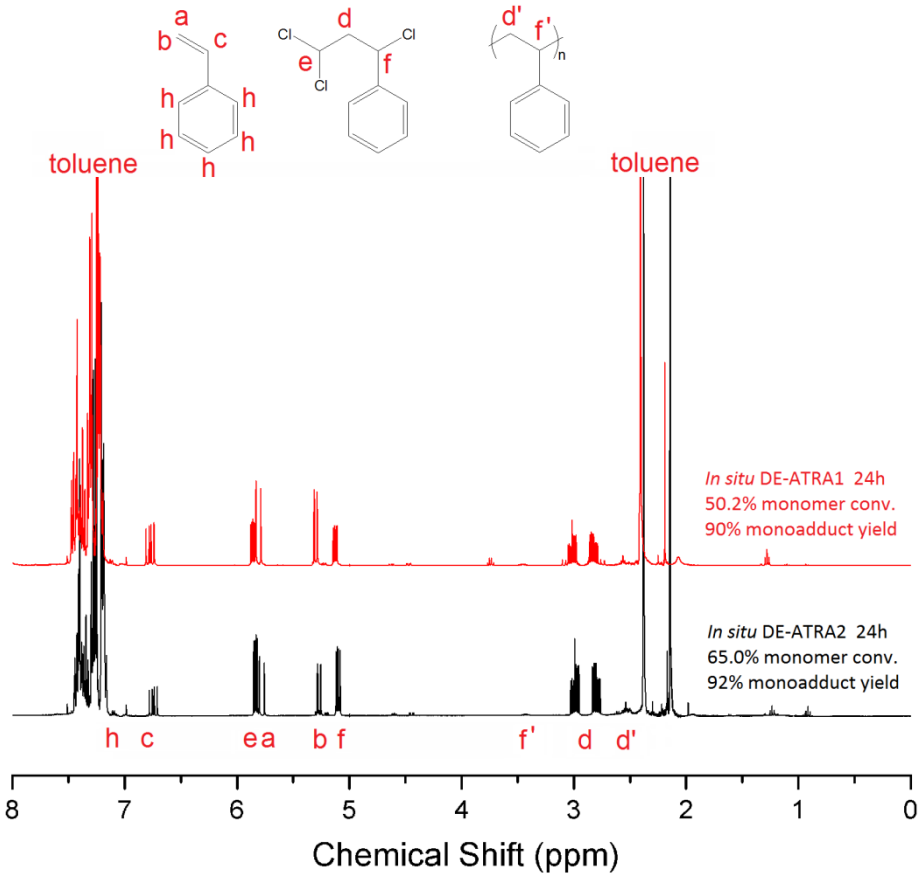

Figure 2.16 ^{1}H NMR spectrum of in situ DE-ATRA1 and in situ DE-ATRA2 of styrene (entry 5 and 6 in Table 2.1), indicating high vinyl conversions and high monoadduct yields.

It can be seen that both high conversion and high monoadduct yield were obtained in the *in situ* DE-ATRA of styrene and chloroform. The ATRA reaction in the presence of Cu^{I} catalyst at 100 ppm proceeded less efficiently but can still have good control for the formation of monoadduct. In contrast, FRP and ARGET-ATRA could not achieve the preparation of monoadduct in either the absence of Cu^{I} or in the Cu^{II} with excess AA condition. High initial Cu^{II} concentration and low proportion of reducing agent are essential for a well-controlled ATRA reaction.

Table 2.2 Reaction results for ATRA of MMA.

	Reaction[a]	[M]:[I]:[Cu^{II}]:[AA] Feed ratio	Time (hrs)	M_w (KDa)[b]	PDI[b]	Conv[c] (%)	Mono yield[c]
1	FRP	1000:4000:-:-	12	60	2.0	47	0
2	ATRA1	1000:4000:4([Cu^{I}])	24	0.9	1.4	58	6.5
3	ATRA2	1000:4000:8([Cu^{I}])	24	0.7	1.3	63	34
4	*In situ* DE-ATRA	1000:4000:25:1.88	24	0.6	1.3	58	69

[a] FRP [I]:[M]:[ACCN]= 4: 1: 0.004 no copper catalyst, [I]=2.5 M; ATRA1 [I]:[M]:[CuCl]= 4: 1: 0.004, [I]=2.5 M; ATRA2 [I]:[M]:[CuCl]= 4: 1: 0.008, [I]=2.5 M; *in situ* DE-ATRA [I]:[M]:[$CuCl_2$]:[AA]= 4: 1: 0.025: 0.00188, [I]=2.5 M; In all reaction I= $CHCl_3$, T=60^oC, [CuCl] or [$CuCl_2$] :[PMDETA]=1:1, 2-butanone was used as the solvent for the reaction; [b] Mw and PDI was characterized by GPC equipped with RI detector, it should be noted that M_w below 690kDa are outside the calibration range; [c] monomer conversion and monoadduct yield were confirmed by ^1H NMR (see Figure 2.18, Eq. 2.4 and 2.5).

Kharasch addition of halogenated compound to another highly active alkene - methyl methacrylate - was also evaluated. FRP was firstly conducted without a copper catalyst (entries 1 in Table 2.2 and Figure 2.17 (a)). Similar to the result of styrene, no MMA monoadducts were obtained in the presence of only chloroform. The results indicate that the chloroform compounds are also ineffective chain transfer agents in Kharasch addition for the highly active methyl methacrylate monomer.

Certain control could be achieved by adding Cu^I into the system. For example, at Cu^I loadings as high as 0.4 mol% (relative to MMA), the overall molecular weight decreased to approximately 0.9 kDa (entries 2 in Table 2.2 and Figure 2.17 (b)). However, in contrast to styrene, the monoaddition control for MMA was not as good, even at the Cu^I 100 ppm level, affording only 6.5% monoadduct yield.

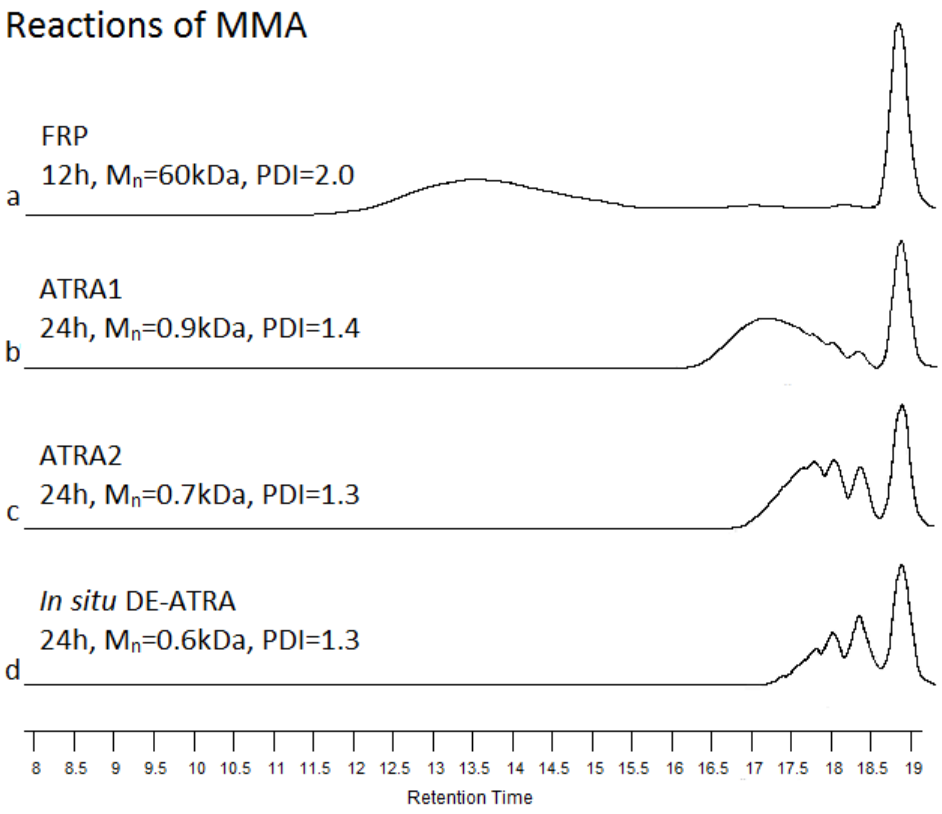

Figure 2.17 GPC traces for the reactions of MMA. (a) FRP [I]:[M]:[ACCN]= 4: 1: 0.004 no copper catalyst, [I]=2.5 M; (b) ATRA1 [I]:[M]:[CuCl]= 4: 1: 0.004, [I]=2.5 M; (c) ATRA2 [I]:[M]:[CuCl]= 4: 1: 0.008, [I]=2.5 M; (d) *in situ* DE-ATRA [I]:[M]:[$CuCl_2$]:[AA]= 4: 1: 0.025: 0.00188, [I]=2.5 M; In all reaction I= $CHCl_3$, T=60^oC, [CuCl] or [$CuCl_2$]: [PMDETA]=1:1, 2-butanone was used as the solvent for the reaction. Molecular weight and PDI were characterized by GPC equipped with RI detector. No monoadducts were obtained in FRP, whilst oligomer and monoadduct were obtained in ATRA and *in situ* DE-ATRA. The *in situ* DE-ATRA showed highest monoadduct yield among all the reaction systems.

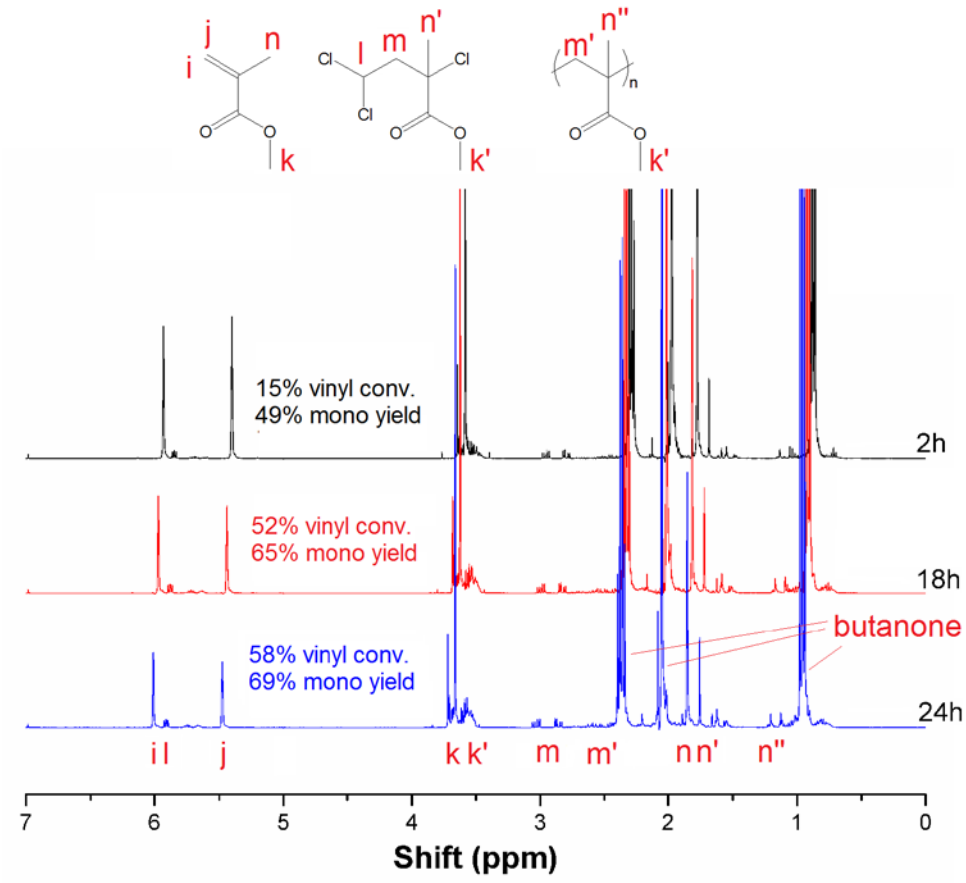

Figure 2.18 ^{1}H NMR spectrum of *in situ* DE-ATRA reaction of MMA. (entry 4 in Table 2.2), indicating high vinyl conversions and high monoadduct yields.

$$Monomer\ conversion = \frac{Integral\ of\ k'}{Integral\ of\ (k + k')} \qquad \text{Eq. 2.4}$$

$$Monoadduct\ yield = \frac{Integral\ of\ m}{Integral\ of\ (m + m')} \qquad \text{Eq. 2.5}$$

The results for ATRA of MMA could be further improved by adding a higher concentration of Cu^{I}. The significant increase in monoadduct can clearly be attributed to the higher Cu^{I} (entries 3 in Table 2.2 and Figure 2.17 (c)). Higher initial Cu^{I} concentration leads to both higher Cu^{I} and Cu^{II} concentration on both sides of equilibrium of activation and deactivation. This dynamic equilibrium is therefore accelerated and obtains a greater chance to have the priority over the chain growth reaction or other side

reactions of the free radicals (Figure 2.8). Encouraged by the results obtained in the addition of high Cu^{I} level, *in situ* DE-ATRA (a reaction that starts with a high ratio Cu^{II} species with a low ratio of AA compound) was also tested to achieve monoaddition. The best result in terms of highest percentage of monoadduct formed for MMA was achieved by *in situ* DE-ATRA. As Figure 2.8 depicts, *in situ* DE-ATRA contains a large presence of Cu^{II} which serves to increase the deactivation/activation equilibrium assisting in monoadduct formation. The analysis by ^{1}H NMR showed 69% monoadduct yield (entries 4 in Table 2.2 and Figure 2.17 (d)).

2.3.2 Synthesis and Characterization of HBPs through the *in situ* DE-ATRA System

The results in Table 2.1 and Table 2.2 indicate that the *in situ* DE-ATRA can provide a relatively high yield of monoadduct and is thus attractive from the point of view of further synthesis of the ideal dendritic polymer. Divinyl monomers - including DVB and EGDMA - were then chosen to react with chloroform in the *in situ* DE-ATRA reaction system. Monitoring the homopolymerization of EGDMA via *in situ* DE-ATRA by GPC at regular time intervals during the reaction provides us with data that strongly supports our proposed mechanism (Figure 2.19). It can be clearly seen that after the first 15 minutes, the polymerization mixture consists mainly of small oligomers. The broadening of peaks at 1h (PDI=1.8) (Figure 2.19) suggests that the combination of lower molecular weight oligomers appears to be the major reaction pathway at the later stage. It is likely that at later stages of the reaction, with most of the monomer being already consumed, the reaction conditions are more favourable for statistical branching rather than for linear growth.

The data in Table 2.3 shows that the measured LS molecular weight is always higher than the RI results, strongly supporting the formation of a hyperbranched architecture[20]. It is clear from comparison of the RI and LS data that there is a significant difference in the measured Mw and PDIs for the same sample from these differing detector systems[21, 22, 23]. This is very likely to be due to the highly branched nature of the structures being produced. It is believed that the LS data are the more trustworthy and representative of the true Mw of these systems and that the RI system is underestimating the true molecular weights very significantly as a result of three dimensional shapes of the polymers synthesized.

Table 2.3 Detailed information of polyDVB and polyEGDMA via *in situ* DE-ATRA reaction.

Reaction [a]	Time (hrs)	RI		LS		Vinyl conv[c] (%)	Branch ratio[c] (%)
		M_w[b] (KDa)	PDI[b]	M_w[b] (KDa)	PDI[b]		
In situ DE-ATRA EGDMA	0.25	0.8	1.1	0.9	1.1	3.3	-
	0.5	1.2	1.3	1.7	1.2	14	-
	1	3.6	1.8	4.3	1.6	42	-
	2	22.2	5.4	30	3.3	72[d]	-
	purified	34	1.7	41	1.5	-	28%
In situ DE-ATRA DVB	1	0.7	1.2	0.9	1.1	4	-
	10	3.3	1.6	4.7	1.4	37	-
	24	4.8	1.8	6.2	2.0	63[d]	-
	purified	10.1	1.8	12.1	1.6	-	23%

[a] *In situ* DE-ATRA of DVB [I]:[M]:[$CuCl_2$]:[AA]= 0.5: 1: 0.01: 0.002, [I]=1.25 M; *in situ* DE-ATRA of EGDMA [I]:[M]:[$CuCl_2$]: [AA]= 0.5: 1: 0.025: 0.00188, [I]=1.25 M; In all reaction I= $CHCl_3$, T=60°C, [CuCl] or [$CuCl_2$] :[PMDETA]=1:1, DVB reaction was conducted in toluene, EGDMA reaction was conducted in 2-butanone; [b] M_w and PDI was characterized by GPC equipped with RI detector and LS detector; [c] vinyl conversion and branch ratio were confirmed by ^{1}H NMR. [d] Beyond this conversion gelation occurred.

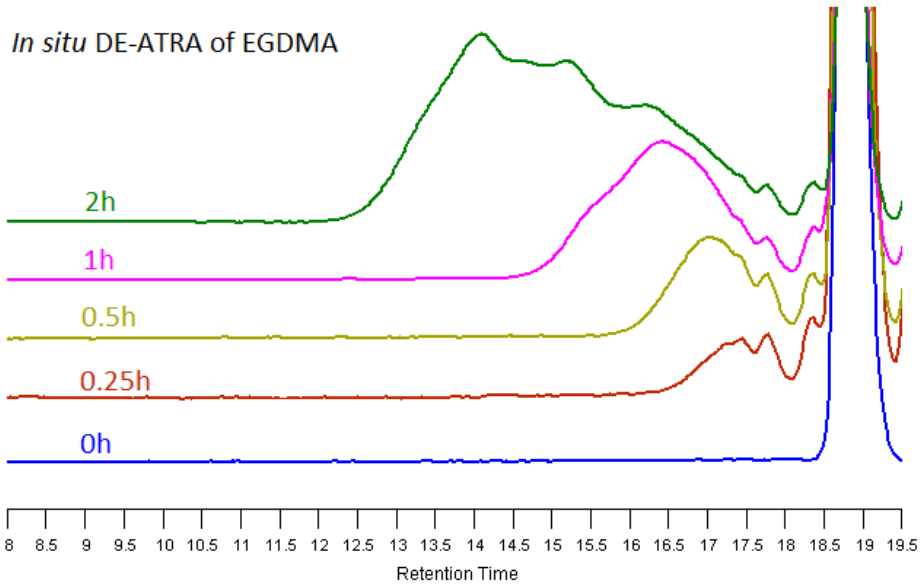

Figure 2.19 GPC traces for *in situ* DE-ATRA of EGDMA. (Table 2.3), showing that the EGDMA firstly undergo a linear propagation (<0.5h) followed by oligomer combination. (>0.5h)

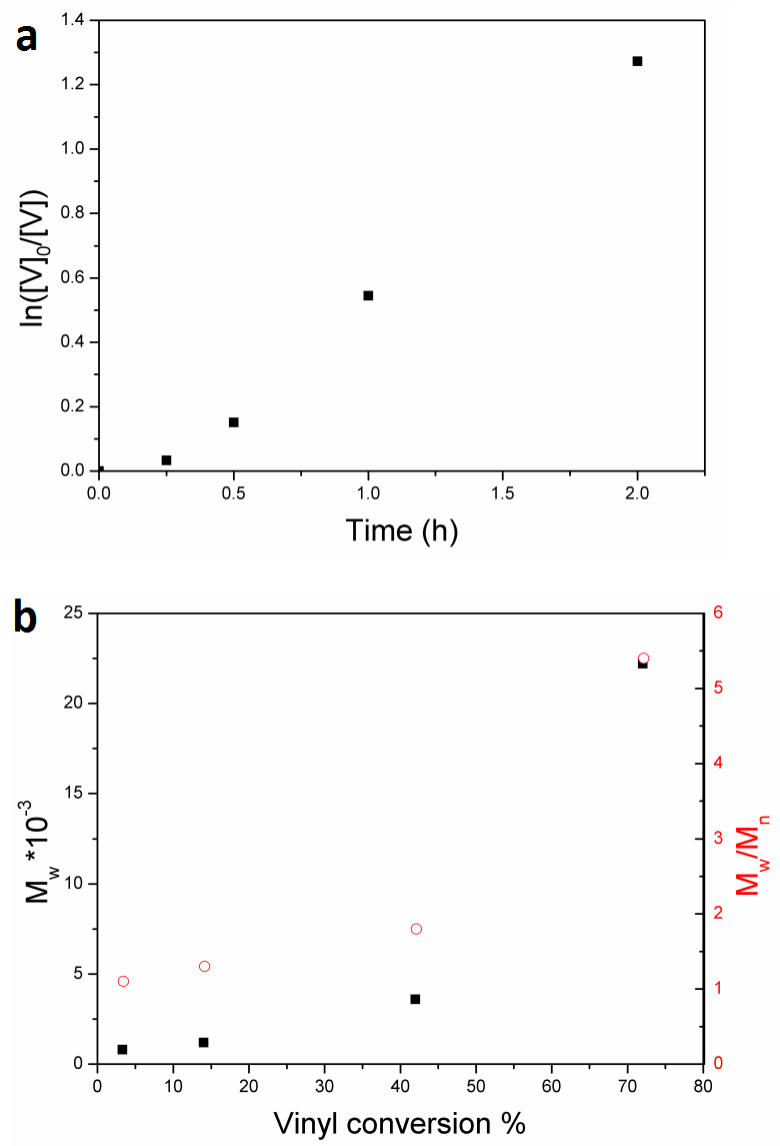

Figure 2.20 Kinetic studies for *in situ* DE-ATRA of EGDMA (Table 2.3), include (a) plots of ln($[V]_0/[V]$) versus time ([V] is the mole concentration of the vinyl group in the system) and (b) M_w and PDI versus vinyl conversion.

A kinetic plot (Figure 2.20) shows the evolution of the reaction of *in situ* DE-ATRA of EGDMA. The plot of ln($[V]_0/[V]$)~time (Figure 2.20 (a)) showed a linear relationship, indicating a constant reaction rate even at a high conversion. This also implied that the radical concentration is stable during the most period of the reaction. It also showed that there is a period of induction at the beginning of the reaction. This may be attributed to the large amount of $CHCl_3$ which will take a period of time to be activated and reach the dynamic balance of the copper-catalyzed ATRA system. The plot of MW (and PDI) versus vinyl conversion (Figure 2.20 (b)) demonstrates that the reaction can be pushed to a conversion higher than 72%.

'H NMR spectroscopy analysis (Figure 2.21) of the precipitated polymer can confirm the formation of hyperbranched structure for poly(EGDMA). The presence of potentially useful vinyl functionalities (resonance of protons d and e from vinyl group at 5.5-6.5 ppm, Figure 2.21) is clearly revealed in the 'H NMR spectra.

Here, an example of the calculation for the different unit ratio in the polyEGDMA (Table 2.3 and Figure 2.21) is given as below. The degrees of branching were calculated by Eq. 2.6 and Eq. 2.7, respectively.

$$Branch\ ratio = \frac{Branched\ EGDMA}{Linear\ EGDMA + Branched\ EGDMA} = \frac{Integral\ of\ (\frac{c}{4} - d)}{Integral\ of\ \frac{c}{4}} \qquad \text{Eq. 2.6}$$

$$DB_{Frey} = \frac{2 \times \sum dendritic\ units}{2 \times \sum dendritic\ units + \sum linear\ units} = \frac{2 \times Integral\ of\ (\frac{c}{4} - d)}{2 \times Integral\ of\ (\frac{c}{4} - d) + Integral\ of\ d} \qquad \text{Eq. 2.7}$$

The precipitated polymer possessed a branch ratio of 28% and a DB_{Frey} of 43.8% as determined by ^{1}H NMR spectroscopy. It should be noticed that characterization of the topological structure of hyperbranched polymer by NMR spectroscopy analysis is essentially statistical. The results only represent the macroscopic topology of the overall polymer chains.

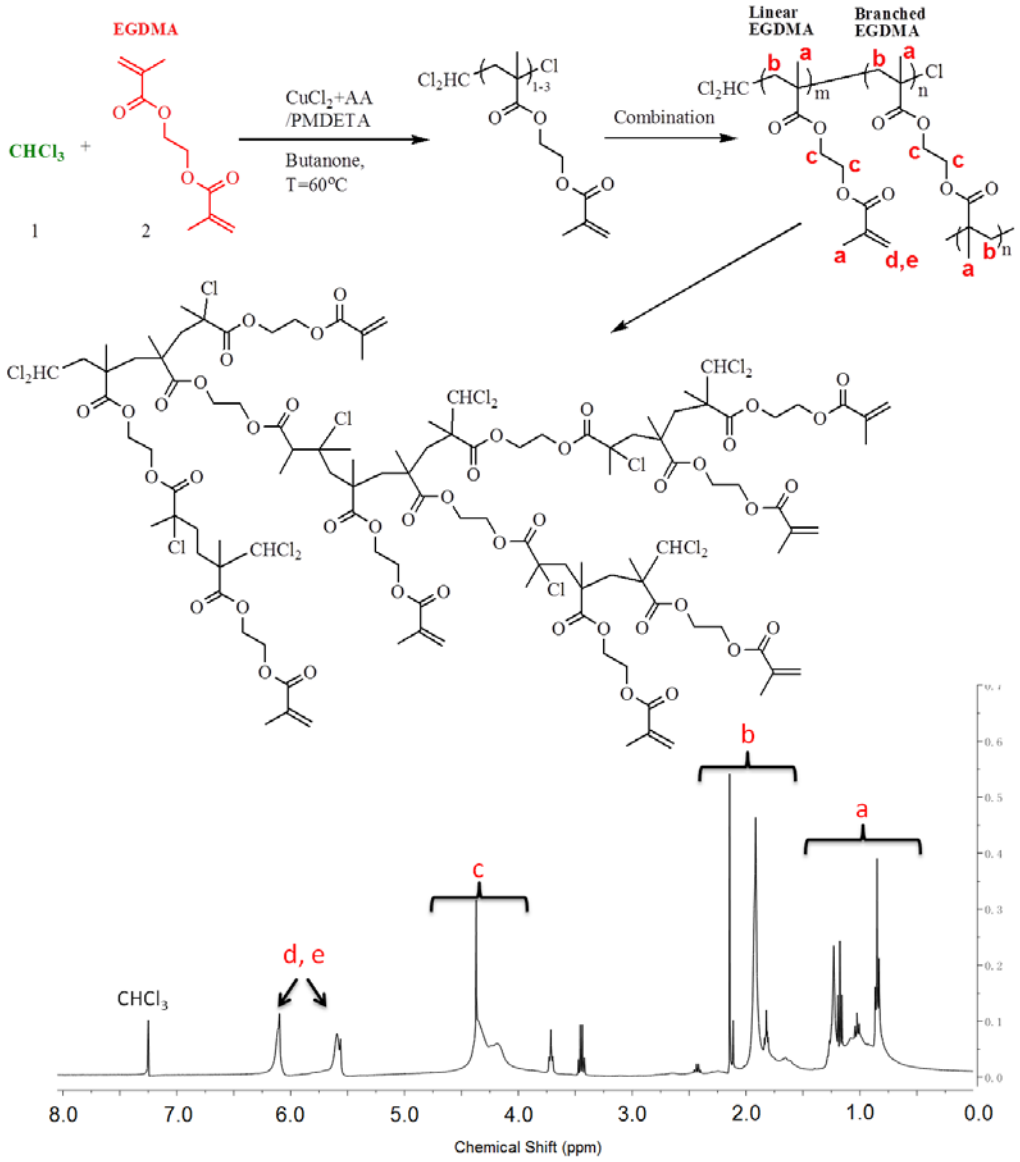

Figure 2.21 Scheme of *in situ* DE-ATRA of EGDMA and ^{1}H NMR results for the final product, the results indicate the purified polyEGDMA contains 28% branched EGDMA unit.

The structural characterization of hyperbranched polyEGDMA by NMR spectroscopy is insufficient to define the polymer topology. A complete characterization requires the use of particular properties of polymers, for example, dynamic radius and viscosity in solution. GPC with triple detectors (RI, VS and LS) can determine the molar mass and root mean square (RMS) radius for the polymer fractions eluting from the GPC separation. Then information about the polymer chain structure can be gained from the relationship between the molar mass and size. This study of the GPC elution behavior of the branched macromolecules was carried out

as part of an extensive study of the application of GPC-triple for the characterization of branched polymers. In the following part, the role of architecture and branched density on the solution properties and rheology of linear and hyperbranched polymers will be investigated. Specifically, the size of the molecular structures and their topology will be characterized by using a combination of GPC, viscometer, and two-angle light scattering (LS).

HBPs exhibited interesting solution properties. To further support the formation of the highly branched structure of the polyEGDMA, the viscosity behaviour of the polymers was studied. The relationship between intrinsic viscosity and the molecular weight allows to judge the topology of the polymers in solution by Mark-Houwink-Sakurada (MHS) equation (Eq.2.8)[24, 25], where [η] is intrinsic viscosity, K is a constant for different polymers, M is the experiment average molecular weight (viscosity) and α is a constant which relates to the stiffness of the polymer chain. For example, if α<0.5, the polymers are hard spheres; if α=0.5-0.8, the polymers are random coils in good solvent; if α=2, the polymers are rigid rods. The increasing in the degree of branching is accompanied by the decrease of the exponent α in the dependence of the intrinsic viscosity on molar mass. Mark-Houwink-Sakurada equation:

$$[\eta] = KM^{\alpha},\ \log[\eta] = \log K + \alpha \log M \qquad \text{Eq. 2.8}$$

A classic Mark-Houwink-Sakurada (MHS) plot (Figure 2.22) shows that the intrinsic viscosity [η] of polyEGDMA is much lower than that of linear polyPMMA having an equivalent molecular weight. In addition, the slope of log [η] *versus* log M_r is much lower (MHS exponent α = 0.70 for linear PMMA *versus* 0.25 for the hyperbranched polyEGDMA (Table 2.3), demonstrating a significantly decreased level of interaction between solvent and polymer as is typically encountered in densely branched macromolecules[26, 27].

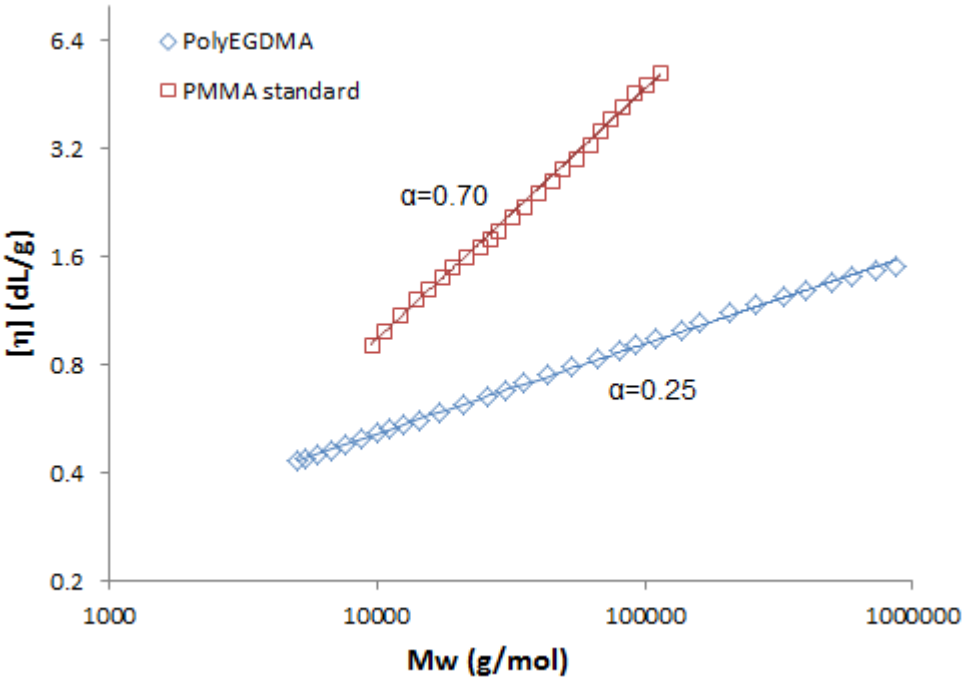

Figure 2.22 Plot of intrinsic viscosity *versus* molecular weight for hyperbranched polyEGDMA and linear PMMA standards. The intrinsic viscosities [η] of the hyperbranched polyEGDMA are much lower than those of linear PMMA. MHS exponent *α*= 0.70 for PMMA versus 0.25 for the hyperbranched polyEGDMA. (Table 2.3)

Similar results were achieved with the homopolymerization of divinylbenzene via *in situ* DE-ATRA reaction (Table 2.3, Figure 2.23). Beyond this conversion, the system will eventually form an insoluble gel as the large-scale intermolecular combination occurs at a later reaction stage when a certain concentration of oligomer chains is reached.

The difference in intrinsic viscosity [η] between polyDVB and linear PS further supports the hyperbranched structure within these polymers. A classical Mark-Houwink-Sakurada (MHS) plot (Figure 2.24) shows that the intrinsic viscosity of polyDVB is much lower than that of PMMA of similar molecular weight. In addition, the lower slope of log [η] *versus* log Mw indicates less interaction between the solvent and the highly branched polymer[24, 26, 27].

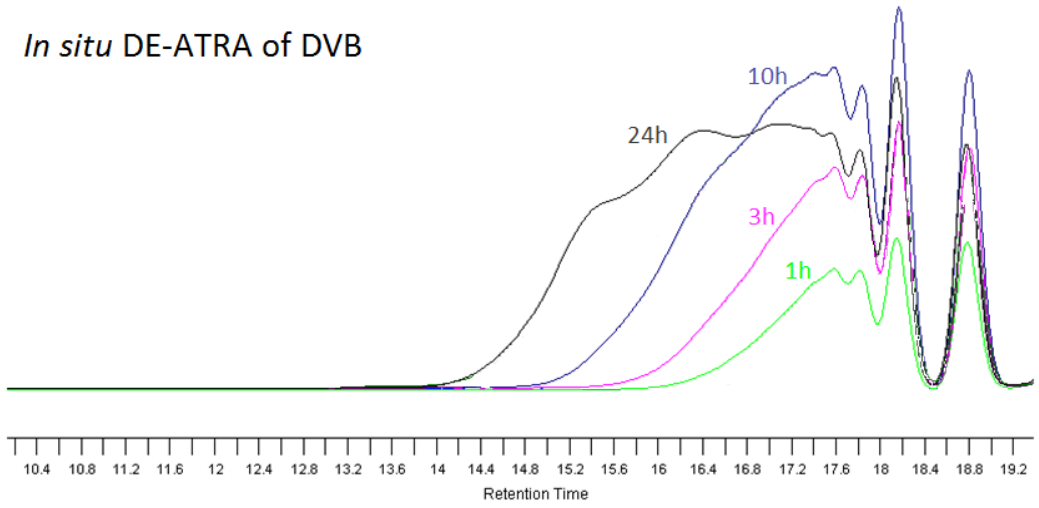

Figure 2.23 GPC traces for *in situ* DE-ATRA of DVB, showing that the DVB monomers firstly undergo a linear propagation (<1h) followed by oligomer combination. (>1h)

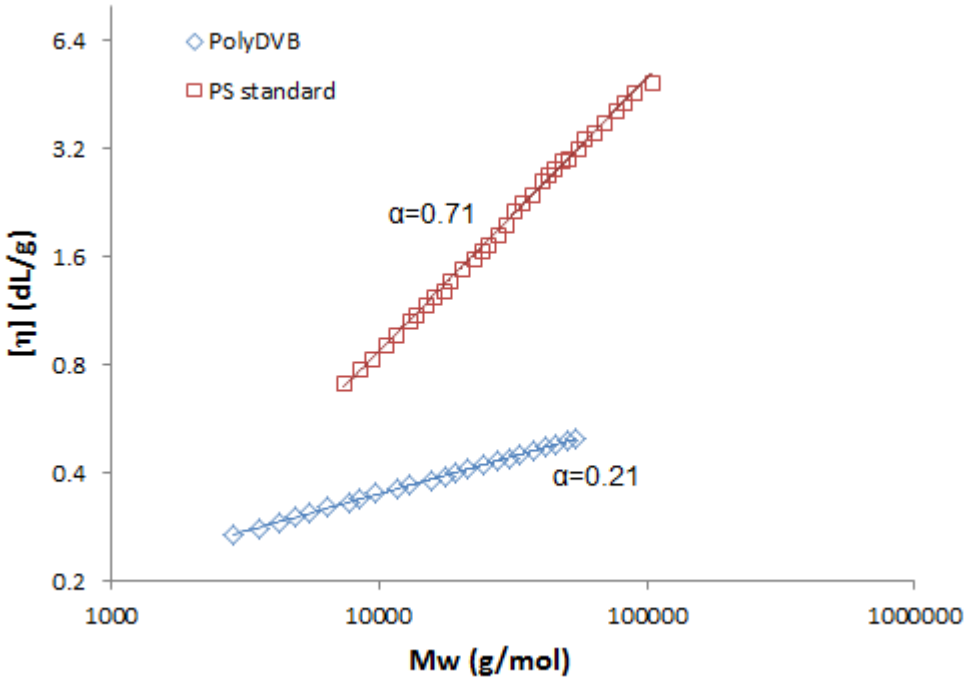

Figure 2.24 Plot of intrinsic viscosity *versus* molecular weight for hyperbranched polyDVB and linear poly(styrene) standards. The intrinsic viscosities [η] of the hyperbranched polyDVB are much lower than those of linear poly(styrene). MHS exponent *α*= 0.71 for poly(styrene) versus 0.21 for the hyperbranched polyDVB (Table 2.3).

The root mean square (RMS) radius $(r_g^2)^{1/2}$ (also called the radius of

gyration) describes the size of a macromolecular particle in a solution, regardless of its shape or structure. It is important to note that RMS radius is not identical to the geometrical radius for the species. Figure 2.25 presents the plot of gyration radius versus Log MW for linear PS and polyDVB species obtained from GPC-triple analysis. The $(r_g^2)^{1/2}$ values were obtained directly from the GPC-triple data. The results clearly showed the radius of gyration from polyDVB is quite different from that of the linear PS (Figure 2.25). Thus indicating that the species synthesized in this study possessed a highly branched structure.

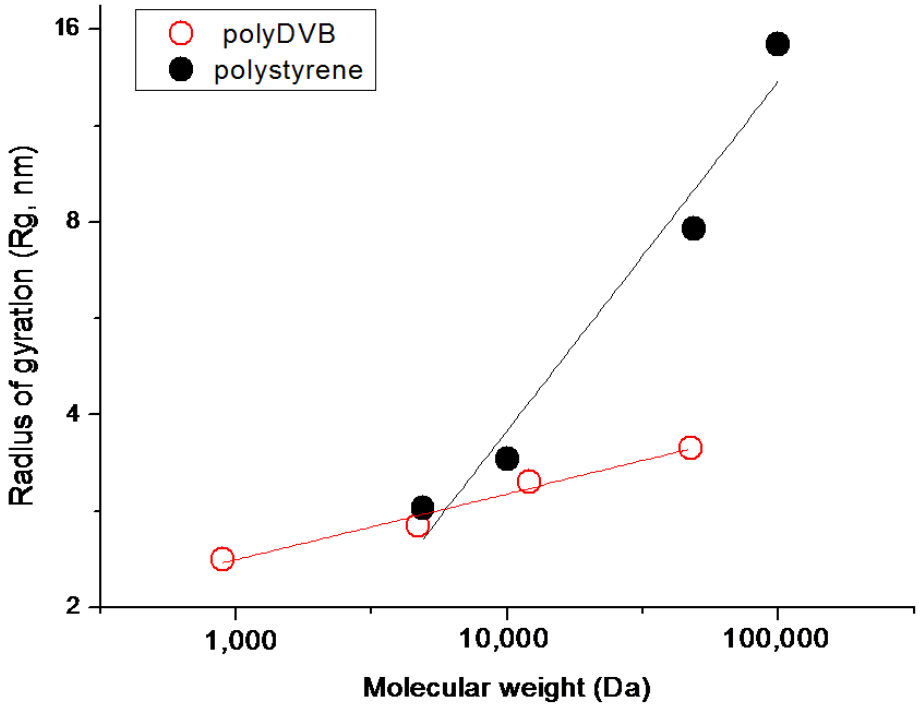

Figure 2.25 The plot of the gyration radius versus Log MW of *in situ* DE-ATRA of DVB (Figure 2.21) using GPC equipped with light scattering detector.

2.4 Conclusions

In this chapter, different copper-catalyzed ATRA systems were firstly evaluated with two monovinyl monomers and chloroform. Both high conversion and high monoadduct yield were obtained in the *in situ* DE-ATRA system in the presence of initial Cu^{II} and a low portion of reducing agent. The ATRA reaction in the presence of Cu^{I} catalyst at 100 ppm proceeded less efficiently but can still have good control for the

formation of monoadduct. In contrast, FRP and ARGET-ATRA could not achieve the preparation of monoadduct in either the absence of Cu^{I} or in the Cu^{II} with excess AA condition. High initial Cu^{II} concentration and low proportion of reducing agent are benefit for a high and constant reaction rate and are essential for a well-controlled ATRA reaction.

With the optimized ATRA reaction system (*in situ* DE-ATRA), we can minimize the chain growth of divinyl monomers and drive the chains towards branching. In this way, a veritable HBP was prepared with a high branch ratio and a large amount of vinyl functional groups. It can be foreseen that this new strategy for preparation of HBPs could open up the field to the polymerization of a very wide range of multivinyl monomers or combinations of comonomers in any proportion, bringing about similar properties to dendrimers.

2.5 References

1. Curran, D. P. The design and application of free-radical chain reactions in organic-synthesis. 1. *Synthesis-Stuttgart* **1988,** (6), 417-439.
2. Curran, D. P. The design and application of free-radical chain reactions in organic-synthesis. 2. *Synthesis-Stuttgart* **1988,** (7), 489-513.
3. Kharasch, M. S.; Jensen, E. V.; Urry, W. H. Addition of carbon tetrachloride and chloroform to olefins. *Science* **1945,** *102* (2640), 128-128.
4. Minisci, F. Free-radical additions to olefins in presence of redox systems. *Accounts of Chemical Research* **1975,** *8* (5), 165-171.
5. Asscher, M.; Vofsi, D. Chlorine-activation by redox-transfer. 3. Abnormal addition of chloroform to olefins. *Journal of the Chemical Society* **1963,** 3921-3927.
6. Iqbal, J.; Bhatia, B.; Nayyar, N. K. Transition metal-promoted free-radical reactions in organic-synthesis - the formation of carbon-carbon bonds. *Chemical Reviews* **1994,** *94* (2), 519-564.
7. Fischer, H. Unusual selectivities of radical reactions by internal suppression of fast modes. *Journal of the American Chemical Society* **1986,** *108* (14), 3925-3927.
8. Kato, M.; Kamigaito, M.; Sawamoto, M.; Higashimura, T. Polymerization of methyl-methacrylate with the carbon-tetrachloride dichlorotris(triphenylphosphine)ruthenium(II) methyl aluminum bis(2,6-di-tert-butylphenoxide) initiating system - possiblility of living radical polymerization. *Macromolecules* **1995,** *28* (5), 1721-1723.
9. Matyjaszewski, K.; Xia, J. H. Atom transfer radical polymerization. *Chemical Reviews* **2001,** *101* (9), 2921-2990.
10. Gao, H.; Li, W.; Matyjaszewski, K. Synthesis of polyacrylate networks

by ATRP: Parameters influencing experimental gel points. *Macromolecules* **2008,** *41* (7), 2335-2340.
11. Yu, Q.; Zeng, F. Q.; Zhu, S. P. Atom transfer radical polymerization of poly(ethylene glycol) dimethacrylate. *Macromolecules* **2001,** *34* (6), 1612-1618.
12. Wang, W.; Zheng, Y.; Roberts, E.; Duxbury, C. J.; Ding, L.; Irvine, D. J.; Howdle, S. M. Controlling chain growth: A new strategy to hyperbranched materials. *Macromolecules* **2007,** *40* (20), 7184-7194.
13. Zheng, Y.; Cao, H.; Newland, B.; Dong, Y.; Pandit, A.; Wang, W. 3D single cyclized polymer chain structure from controlled polymerization of multi-vinyl monomers: beyond Flory-Stockmayer theory. *Journal of the American Chemical Society* **2011,** *133* (33), 13130-13137.
14. Jakubowski, W.; Matyjaszewski, K. Activator generated by electron transfer for atom transfer radical polymerization. *Macromolecules* **2005,** *38* (10), 4139-4146.
15. Min, K.; Gao, H. F.; Matyjaszewski, K. Preparation of homopolymers and block copolymers in miniemulsion by ATRP using activators generated by electron transfer (AGET). *Journal of the American Chemical Society* **2005,** *127* (11), 3825-3830.
16. Pintauer, T.; Matyjaszewski, K. Atom transfer radical addition and polymerization reactions catalyzed by ppm amounts of copper complexes. *Chemical Society Reviews* **2008,** *37* (6), 1087-1097.
17. Eckenhoff, W. T.; Garrity, S. T.; Pintauer, T. Highly efficient copper-mediated atom-transfer radical addition (ATRA) in the presence of reducing agent. *European Journal of Inorganic Chemistry* **2008,** (4), 563-571.
18. Eckenhoff, W. T.; Pintauer, T. Copper catalyzed atom transfer radical addition (ATRA) and cyclization (ATRC) reactions in the presence of reducing agents. *Catalysis Reviews-Science and Engineering* **2010,** *52* (1), 1-59.
19. Matyjaszewski, K.; Jakubowski, W.; Min, K.; Tang, W.; Huang, J.; Braunecker, W. A.; Tsarevsky, N. V. Diminishing catalyst concentration in atom transfer radical polymerization with reducing agents. *Proceedings of the National Academy of Sciences of the United States of America* **2006,** *103* (42), 15309-15314.
20. Podzimek, S. The use of GPC coupled with a multiangle laser-light scattering photometer for the characterization of polymers - on the determination of molecular-weight, size, and branching. *Journal of Applied Polymer Science* **1994,** *54* (1), 91-103.
21. Baudry, R.; Sherrington, D. C. Facile synthesis of branched poly(vinyl alcohol)s. *Macromolecules* **2006,** *39* (16), 5230-5237.
22. Podzimek, S.; Vlcek, T.; Johann, C. Characterization of branched polymers by size exclusion chromatography coupled with multiangle light

scattering detector. I. Size exclusion chromatography elution behavior of branched polymers. *Journal of Applied Polymer Science* **2001,** *81* (7), 1588-1594.
23. Podzimek, S.; Vlcek, T. Characterization of branched polymers by SEC coupled with a multiangle light scattering detector. II. Data processing and interpretation. *Journal of Applied Polymer Science* **2001,** *82* (2), 454-460.
24. Mourey, T. H.; Turner, S. R.; Rubinstein, M.; Frechet, J. M. J.; Hawker, C. J.; Wooley, K. L. Unique behavior of dendritic macromolecules - intrinsic-viscosity of polyether dendrmers. *Macromolecules* **1992,** *25* (9), 2401-2406.
25. Zimm, B. H.; Stockmayer, W. H. The dimensions of chain molecules containing branches and rings. *Journal of Chemical Physics* **1949,** *17* (12), 1301-1314.
26. Guan, Z. Control of polymer topology through transition-metal catalysis: Synthesis of hyperbranched polymers by cobalt-mediated free radical polymerization. *Journal of the American Chemical Society* **2002,** *124* (20), 5616-5617.
27. Frechet, J. M. J.; Henmi, M.; Gitsov, I.; Aoshima, S.; Leduc, M. R.; Grubbs, R. B. Self-condensing vinyl polymerization - an approach to dendritic materials. *Science* **1995,** *269* (5227), 1080-1083.

Chapter Three

Controlled Homopolymerization of Multi-vinyl Monomer through Vinyl Oligomer Combination as a Universal Approach to Hyperbranched Architectures

Parts of this chapter have been published in:

Zhao, T., Zheng, Y., Poly, J., Wang, W., 'Controlled multi-vinyl monomer homopolymerization through vinyl oligomer combination as a universal approach to hyperbranched architectures' *NATURE COMMUNICATIONS*, **2013**, 4, article number: 1874.

3.1 Introduction

Hyperbranched polymers have received much attention in different scientific fields far beyond polymer science. They offer superior features such as low viscosity, good solubility, and a high range of functionality. Moreover, their much simpler and more cost-effective synthesis mechanism[1, 2] have allowed hyperbranched polymers to be considered as alternatives to dendrimers for emerging applications in a variety of fields, ranging from nano building blocks, microelectronics, sensors to applications in drug delivery[3, 4, 5].

3.1.1 Previous Methods to Synthesize HBPs

To date, polycondensation of AB_n-type monomers still predominate in synthetic approaches to hyperbranched polymers[6, 7], but this approach suffers from poor control over the polymer structure. With the introduction of controlled/living polymerization, one of the most successful approaches is the self-condensing vinyl polymerization (SCVP) introduced by Fréchet[8, 9, 10, 11, 12, 13].

Another approach is the copolymerization of a mono-vinyl monomer with a multi-vinyl monomer (MVM). It has been long recognised that without any particular precaution, such as low MVM concentration or dilute solution condition, this copolymerization leads to the formation of insoluble networks (Figure 3.1 (a)), as predicted by the Flory-Stockmayer (F-S) theory. The introduction of a chain transfer agent in this polymerization allowed the synthesis of various soluble highly branched polymers, thanks to the increase of primary chains concentration. This strategy, coined 'Strathclyde synthesis'[14], was then enriched thanks to living/controlled radical polymerization mechanisms. The so-called controlled radical cross-linking copolymerization (CRCC) methodology has enabled the synthesis of various branched polymers with well-defined primary chain lengths (Figure 3.1 (b))[15, 16, 17, 18, 19, 20, 21, 22, 23]. However, only low proportions of MVM could be used to avoid gelation, which limits the formed polymers to a low branching degree.

Hence, there is a dilemma in the case of preparation of hyperbranched polymer via CRCC. Hyperbranched polymers are expected to be prepared with high branching degrees. However, the high ratio of divinyl monomer

easily leads the polymer to a cross-linked gel. Consequently, the ratio of MVM has to be kept low to a percentage of up to approximately 15% in order to prevent crosslink. The soluble products cannot be hyperbranched polymers but only “highly” branched ones.

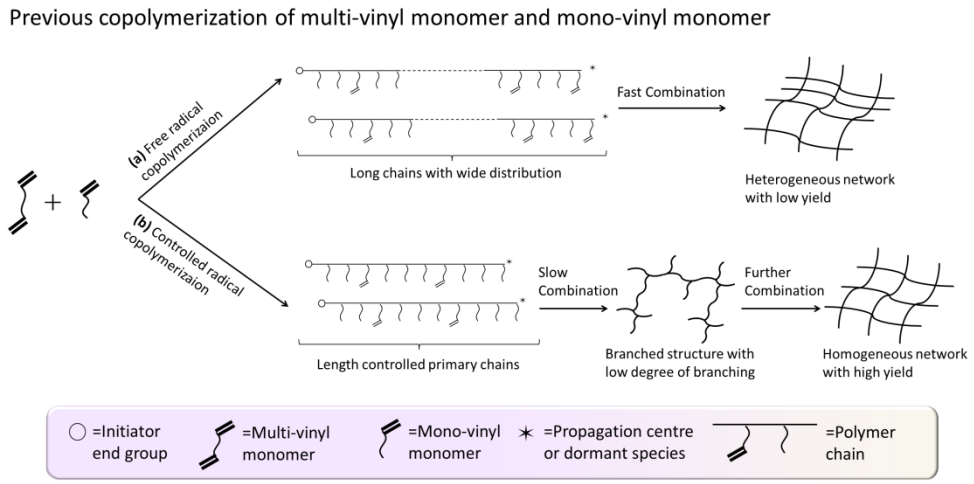

Figure 3.1 Previous copolymerization of multi-vinyl monomer and mono-vinyl monomer: (a) Cross-linked structure formed by combination of long linear polymer chain through FRP; (b) Branched structure consisting of a large proportion of mono-vinyl monomer and a small amount of multi-vinyl monomer (MVM) as crosslinkers through controlled/living radical copolymerization. The polymers usually have a low density of branching.

Hyperbranched (HB) polymers can be defined as structures in which each monomer unit is either a branching unit or a potential branching unit. Resorting to controlled radical polymerization mechanisms, the only access up to now to such HB structures has been the aforementioned SCVP approach. However, this approach suffers from its lack of versatility as it implies tailor-synthesized inimers. Developing new synthetic routes to hyperbranched polymeric materials is of great interest. Also, a method that can directly polymerize existing commercial monomers to form dendritic materials with controlled architecture will be highly desirable.

3.1.2 Polymerization Mechanism

In the homopolymerization of divinyl monomers, there are four possible growth processes in the reaction (Figure 3.2). Firstly, the monomers are added onto the propagating center by linear growth (Figure 3.2 (a)). The free radical was reacted with the vinyl groups in the monomers during this

process. Secondly, the propagating center could react with the vinyl groups in another polymer chain to form a branching point (Figure 3.2 (b)). Thirdly, the free radical can react with the pendant vinyl groups belonging to the same polymer chain to form a cyclic or intramolecular crosslinking (Figure 3.2 (c)). Finally, the gel network is formed between the high molecular weight polymer chains by intermolecular and intramolecular crosslinking (Figure 3.2 (d)). A small fraction of the units might form an 'infinite' network, while the other polymer units yield comparatively dissolvable molecules. Gelation is due to the infinite network with plenty of loops formed by the intramolecular crosslinking. Thus, 'high MW' and ' intramolecular crosslinking' are the two key reasons for the macroscopic gelation (macrogel). Typically, the gelation reaction will be formed via conventional FRP under 10-15% yield.

The control over the polymerization of MVMs has been long considered as an impossible task, since the Flory-Stockmayer mean field theory predicted that the polymerization of multi-vinyl monomers (MVM) only lead to insoluble cross-linked materials even at low conversion[24, 25, 26, 27, 28, 29]. Indeed, the inclusion of only small amounts of MVMs, if carried out in addition polymerizations e.g. FRP, will result in the formation of a macroscopic cross-linked network of MVMs.

However, a deactivation enhanced strategy can efficiently delay the gel point of the MVM homopolymerization up to 60% monomer conversion in a concentrated polymerization system[30, 31, 32, 33]. By this approach, a novel 3D ‘single cyclized’ architecture was formed attributable to the suppressed intermolecular reactions (Figure 3.3 (a)). This discovery prompted us to develop a new model which gives a significant supplementation to the classical Flory-Stockmayer theory based on the space and instantaneous growth boundary concept[31]. Most importantly, this study subverted the traditional impression of MVMs reactions - “uncontrolled and challenging”. Doors have now been opened for the design and manipulation of various polymer architectures from the homopolymerization of MVMs.

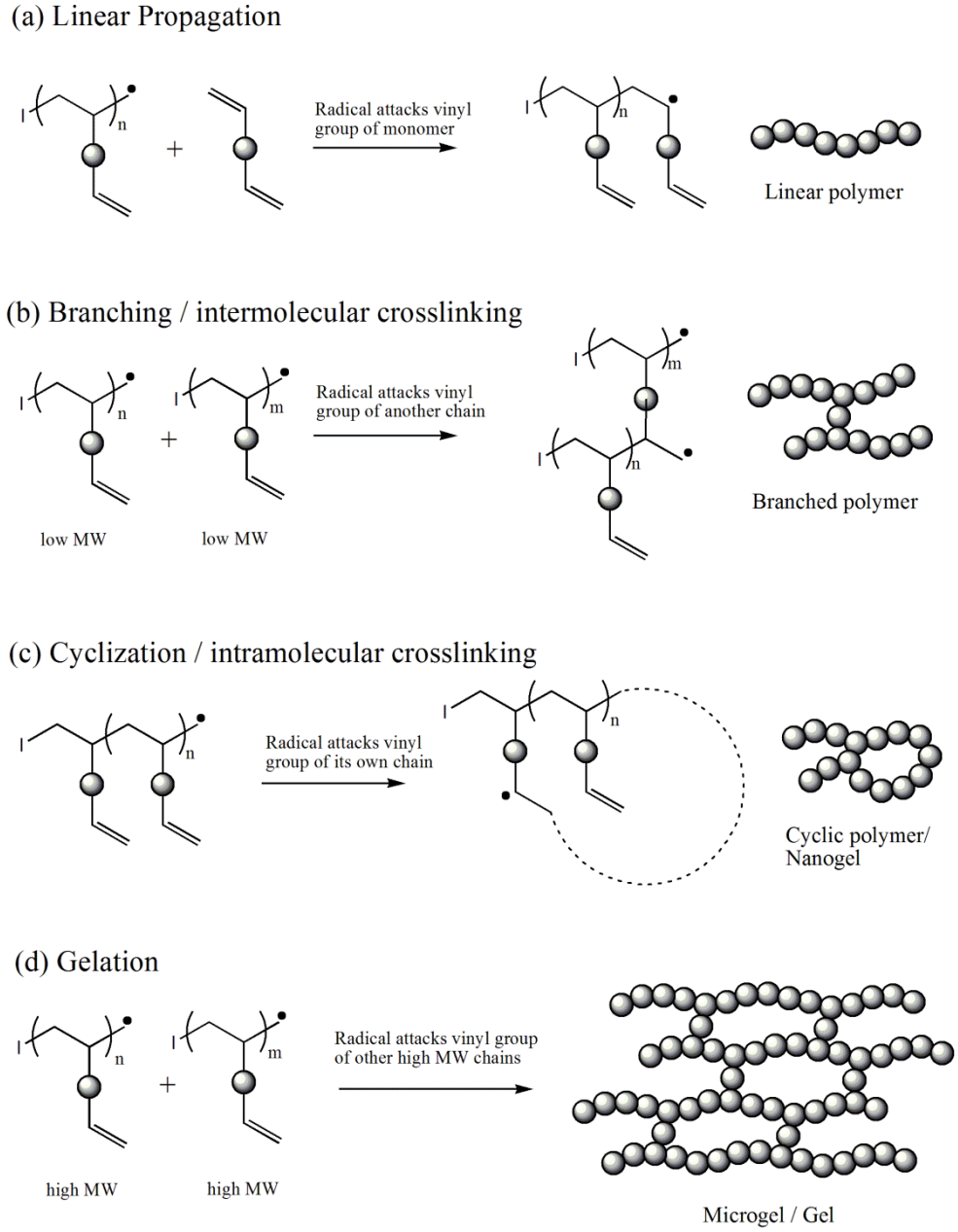

Figure 3.2 The scheme of the four different processes which involved in the homopolymerization of divinyl monomers.

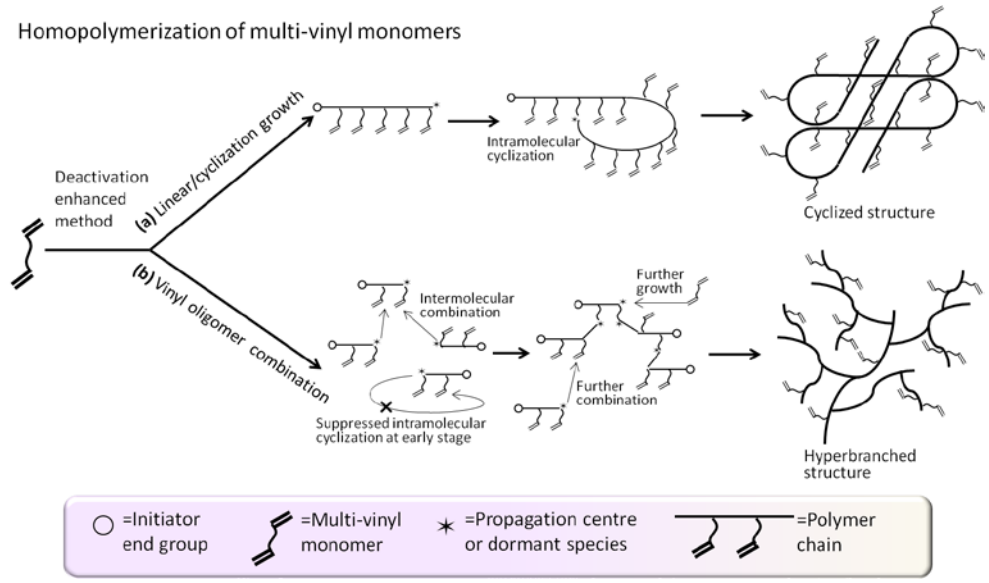

Figure 3.3 Homopolymerization of multi-vinyl monomer (MVM) via deactivation enhanced atom transfer radical polymerization (DE-ATRP) with different strategies leading to either cyclized or hyperbranched structures. (a) Under the condition of a restricted growth boundary (short kinetic chain length), cyclized structures are formed through the strategy of intra-enhanced propagation. The intramolecular cyclization is enhanced due to the high local/spatial vinyl concentration within the growth boundary. (b) Hyperbranched structures are formed under the strategy of vinyl oligomer combination. The intermolecular reaction is facilitated from early reaction stages when numerous oligomers are formed and become the predominant species in the reaction system. In this situation, the intramolecular cyclization is suppressed due to the short chain length during the linear growth period.

It is well known that two types of reactions lead to the formation of cross-links during crosslinking copolymerization or MVM homopolymerization: intramolecular crosslinking (cyclization), leading to the formation of “loops” in the structure, and intermolecular crosslinking, leading to the increase of molecular weights through the formation of cross-links between chains. As aforementionned, the case of favored intramolecular events during MVMs homopolymerization that leads to single cyclized polymers was already investigated[30, 31]. This led us to ask a further question: if the intramolecular reaction can be enhanced by the suppression of intermolecular reactions (leading to a cyclized polymer structure), how can the intermolecular reaction be facilitated with the suppression of intramolecular reactions? Theoretically in this situation a maximally hyperbranched structure should be possible (Figure 3.3 (b)).

3.1.3 Preparation of Hyperbranched Polymers via *in situ* DE-ATRP Method

In chapter 2, we have evaluated different copper-catalyzed ATRA systems to obtain the optimum kinetic control for two types of vinyl monomers. It was found that the *in situ* DE-ATRA with high concentration of copper catalyst can provide high monomer conversion and high monoadduct yield. With this reaction system, tentative polymerizations of two divinyl monomers were studied using chloroform as initiator.

In this chapter, we switched to a more efficient initiator to enhance activation of alkyl halide for concurrent vinyl addition and chain propagation. We propose this strategy as a universal approach to the synthesis of HBPs by CRP of MVMs. This approach which mixes kinetical and statistical control has allowed the successful fabrication of hyperbranched polymer architectures with extremely high branching density as well as numerous vinyl functional groups. The hyperbranched architecture consists purely of extremely short primary chains, which is fundamentally distinct from the architecture produced by any previous method (*e.g.* 'Strathclyde synthesis', CRCC and even SCVP). We provide solid evidence to demonstrate that it is possible to kinetically and statistically control and manipulate the hyperbranched structure in the homopolymerization of MVMs in a concentrated polymerization system. This approach, which we name it 'vinyl oligomer combination', demonstrates great advantages for the synthesis of hyperbranched polymers for industrial applications, through its sheer simplicity, monomer possibilities (broad range of commercially available MVMs) and high yield.

To achieve the hyperbranched structure, two critical parameters must be adhered to. The first is the short kinetic chain length which is the length that a growing chain reaches in a single active cycle. As evaluated in Chapter 2, an *in situ* DE-ATRP system with a high initial concentration of Cu^{II} and a small portion of reducing agent could achieve a high yield of monoadduct in the ATRA reaction because it retains a large proportion of deactivated species (via Cu^{II}) and thus significantly decreases the kinetics chain length ($\nu=k_p[M]/k_{de}[Cu^{II}]$). Using this strategy, it is possible to make the propagation rate of a polymer chain much slower than the deactivation rate, and thus minimize kinetics chain length to an extremely low level. The second crucial premise is the high ratio of initiator to MVM. This will not only lead to extremely short primary chains but also will decrease the chance of intramolecular cyclization at the early reaction stage. In this study,

we introduced a high initiator to divinyl monomer ratio at 1:2. We hypothesize that short linear chains or oligomers will form at the early stages of the reaction according to statistical prediction, and then large-scale intermolecular combination occurs at a later reaction stage when a certain concentration of oligomer chains is reached (Figure 3.3 (b)).

3.2 Experimental

3.2.1 Materials

1,3-butanediol diacrylate (BDA 98%), acryloyl chloride (≥97%) and 2-hydroxyethyl disulfide (90%) were purchased from Sigma-Aldrich. Bis(2-acryloyl)oxyethyl disulfide (disulfide-based diacrylate, DSDA, ≥95%) was synthesized according to literature[34]. Di(ethylene glycol) diacrylate (DEGDA 75%), ethylene glycol dimethacrylate (EGDMA 98%), divinylbenzene (DVB 80%) were purchased from Sigma-Aldrich. The ethyl 2-bromoisobutyrate (EBriB, 98%, Aldrich) was used as the initiator. Pentamethyldiethylenetriamine (PMDETA, 99%, Aldrich), triethylamine (TEA, 99%, Aldrich), copper (II) bromide ($CuBr_2$, 97%, Aldrich), L-ascorbic acid (AA, 99%, Aldrich), tributylphosphine (Bu_3P 97% Aldrich), d-Chloroform (99.8%, Aldrich), 2-butanone (HPLC grade, Aldrich), toluene (HPLC grade, Aldrich), tetrahydrofuran (THF, HPLC grade, Aldrich), n-hexane (ACS reagent grade, Aldrich), diethyl ether (ACS reagent grade, Aldrich) and dichloromethane (DCM, ACS reagent grade, Aldrich) were used as received.

3.2.2 Characterization method

Gel permeation chromatography (GPC) characterizations of hyperbranched and cyclized polymer: Weight average molecular weight (M_w), number average molecular weight (M_n) and polydispersity (M_w/M_n) were obtained by GPC (Varian 920-LC) equipped with a RI detector. The columns (30 cm PL gel Mixed-C, two in series) were eluted using THF and calibrated using a series of 12 near-monodisperse PMMA standards (M_p from 690 to 1,944,000 $g \cdot mol^{-1}$). The polymers were analyzed in THF at a concentration of 5.0 mg/ml. All calibrations and analysis were performed at 40°C and a flow rate of 1 ml/min. All of the products must be easily dissolved in THF, and pass through 0.2μm filter before injection with little or no backpressure observed - demonstrating the absence of gelation.

^{1}H NMR characterizations of hyperbranched and cyclized polymer: ^{1}H NMR analysis was carried out on a S4 300 MHz Bruker NMR with JEOL Delta v5.0.1 processing software. The chemical shifts were referenced to the lock chloroform (7.26 ppm).

Gas chromatography (GC) characterization: Gas chromatography analysis was carried out with a Varien 3900 chromatograph using an RTx-5 crossbound 5% diphenyl/95% dimethyl polysiloxane (15m × 0.25mm × 0.25μm) column. The oven temperature is set to 200°C with the heating rate of 30.0°C/Min.

Mass spectrometry (MS) characterization: ESI mass spectra were acquired using a Waters LCT Premier XE time-of-flight mass spectrometer equipped with electrospray ionization source (Water Corp., Milford, MA). Samples were dissolved in (specify solvent) and introduced into the instrument via a Water Alliance 2795 separations module at a rate of 20uL/min using a syringe pump and a polyetheretherketone capillary line. The heated capillary temperature was 250°C and the spray voltage was 5kV.

3.2.3 Reaction Procedure

Preparation and purification of the bis(2-acryloyl)oxyethyl disulfide monomer: 2-hydroxyethyl disulfide (9.79 ml) and TEA (22.25 ml) were added in a two-necked round bottom flask, with THF (200 ml) as solvent. Acryloyl chloride (25.8 ml) was then added dropwise under the argon protection. The flask was sealed and the mixture was stirred in an ice bath for 24hrs. The by-produced salt was removed by filtering under reduced pressure. The reaction mixture was redissolved in DCM and extracted with sodium carbonate aqueous solution (Na_2CO_3, 0.1M), then purified by basic alumina column with DCM as eluents. The obtained product of bis(2-acryloyl)oxyethyl disulfide was determined by ^{1}H NMR in $CDCl_3$: 2.84 ppm t (4H), 4.45 ppm t (4H), 5.80 ppm d (2H), 6.05 ppm q (2H), 6.43 ppm d (2H).

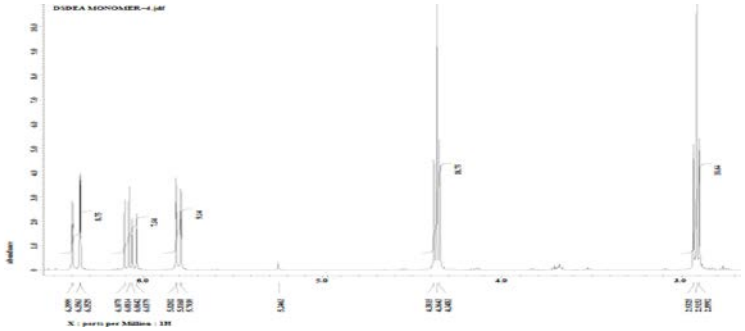

Polymerization of methyl acrylate (MA): MA (40 mmol, 4 equiv), 2-butanone (8.5 ml), EBriB (10 mmol, 1 equiv), $CuBr_2$ (0.5 mmol, 0.05 equiv) and PMDETA (0.5 mmol, 0.05 equiv) was added into the flask and oxygen was removed by bubbling argon through the solutions for 20 min at room temperature. AA (0.15 mmol, 0.015 equiv) was carefully transferred into the flask under an argon blanket. The solution was stirred at 800 rpm and the polymerization was conducted at 60 °C in an oil bath for the desired reaction time.

Preparation of hyperbranched polyBDA: 1,3-butanediol diacrylate (BDA, 20 mmol, 2 equiv), 2-butanone (8.5 ml), EBriB (10 mmol, 1 equiv), $CuBr_2$ (0.5 mmol, 0.05 equiv) and PMDETA (0.5 mmol, 0.05 equiv) was added into the flask and oxygen was removed by bubbling argon through the solutions for 20 min at room temperature. AA (0.15 mmol, 0.015 equiv) was carefully transferred into the flask under an argon blanket. The solution was stirred at 800 rpm and the polymerization was conducted at 60 °C in an oil bath for the desired reaction time.

Preparation of hyperbranched polyDEGDA: Di(ethylene glycol) diacrylate (DEGDA, 20 mmol, 2 equiv), 2-butanone (8.5 ml), EBriB (10 mmol, 1 equiv), $CuBr_2$ (0.5 mmol, 0.05 equiv) and PMDETA (0.5 mmol, 0.05 equiv) was added into the flask and oxygen was removed by bubbling argon through the solutions for 20 min at room temperature. AA (0.15 mmol, 0.015 equiv) was carefully transferred into the flask under an argon blanket. The solution was stirred at 800 rpm and the polymerization was conducted at 60 °C in an oil bath for the desired reaction time.

Preparation of hyperbranched polyEGDMA: Ethylene glycol dimethacrylate (EGDMA, 20 mmol, 2 equiv), 2-butanone (8.5 ml), EBriB (10 mmol, 1 equiv), $CuBr_2$ (0.5 mmol, 0.05 equiv) and PMDETA (0.5 mmol, 0.05 equiv) was added into the flask and oxygen was removed by bubbling argon through the solutions for 20 min at room temperature. AA (0.0375 mmol, 0.00375 equiv) was carefully transferred into the flask under an argon blanket. The solution was stirred at 800 rpm and the polymerization was conducted at 60 °C in an oil bath for the desired reaction time.

Preparation of hyperbranched polyDVB: Divinylbenzene (DVB, 20 mmol, 2 equiv), toluene (8.5 ml), EBriB (10 mmol, 1 equiv), $CuBr_2$ (0.5 mmol, 0.05 equiv) and PMDETA (0.5 mmol, 0.05 equiv) was added into the flask and oxygen was removed by bubbling argon through the solutions for 20 min at room temperature. AA (0.25 mmol, 0.025 equiv) was carefully transferred into the flask under an argon blanket. The solution was stirred at 800 rpm and the polymerization was conducted at 90 °C in an oil bath for

the desired reaction time.

Preparation of hyperbranched polyDSDA: Bis(2-acryloyl)oxyethyl disulfide (disulfide-based diacrylate, DSDA, 20 mmol, 2 equiv), 2-Butanone (8.5 ml), EBriB (10 mmol, 1 equiv), $CuBr_2$ (0.5 mmol, 0.05 equiv) and PMDETA (0.5 mmol, 0.05 equiv) was added into the flask and oxygen was removed by bubbling argon through the solutions for 20 min at room temperature. AA (0.15 mmol, 0.015 equiv) was carefully transferred into the flask under an argon blanket. The solution was stirred at 800 rpm and the polymerization was conducted at 60 °C in an oil bath for the desired reaction time.

Preparation of cyclized polyBDA: 1,3-butanediol diacrylate (BDA, 20 mmol, 100 equiv), 2-butanone (8.5 ml), EBriB (0.2 mmol, 1 equiv), $CuBr_2$ (0.5 mmol, 2.5 equiv) and PMDETA (0.5 mmol, 2.5 equiv) was added into the flask and oxygen was removed by bubbling argon through the solutions for 20 min at room temperature. AA (0.15 mmol, 0.015 equiv) was carefully transferred into the flask under an argon blanket. The solution was stirred at 800 rpm and the polymerization was conducted at 60 °C in an oil bath for the desired reaction time.

Purification of hyperbranched and cyclized polymer: The experiment was stopped by opening the flask and exposing the catalyst to air. Samples taken from reaction at different reaction time points were diluted with butanone and precipitate into a large excess of mixed solvent of hexane and diethyl ether (1:1) to remove monomer. The precipitated mixture was redissolved in tetrahydrofuran followed by passing through a silica column to remove the residual copper. The product solution was evaporated in vacuum at room temperature for 2 hrs and collected for further analysis.

The procedure for the cleavage of polyDSDA: 0.05 g of purified polyDSDA was dissolved in 2 ml of THF followed by adding 30 µl of Bu_3P. The mixture was stirred at room temperature for 2 h and collected for further analysis.

3.3 Results and Discussions

3.3.1 Evaluation of *in situ* DE-ATRP of Methyl Acrylate

Acrylate divinyl monomers were firstly used to implement the reaction. Before the diacrylate monomer polymerization, *in situ* DE-ATRP reaction

system was firstly evaluated to see whether it can provide good kinetic control for the acrylate monomers. Methyl acrylate (MA), which is regarded as the most active acrylate was used for the evaluation. Ethyl 2-bromoisobutyrate (EBriB) was used as the initiator for its high initiation efficiency. The feed ratio of EBriB to MA was set as 1:4. High Cu^{II} concentration (1.25mol% of MA) was used for a good kinetic control according to the conclusion of Chapter 2. High Cu^{II} concentration was also used to diminish the PRE because in the condition of a high initiator concentration, a shift is favored towards the active radicals in equilibrium. This usually results in an initial large concentration of radicals which terminate efficiently, leaving an excess of X-Cu^{II}. This process consumes large proportions of the Cu^{I} and prevents the activation or reactivation of alkyl halides. The high concentration of Cu^{II} can not only pull the shift back to a lower radical concentration but also enhance the deactivation reaction, thus prevent the radical termination.

The GPC traces shown in Figure 3.4 manifested the reaction components at different time periods of reaction. It shows that only oligomers, e.g. monoadduct, dimer, trimer and tetramer, were produced during the reaction and there were no peaks for high MW molecules. Moreover, it can be seen that the MA monomer were gradually added onto the oligomers so that the main peak shifted slowly to bigger molecules. The peaks for the monoadduct and dimer decreased while the peaks for the trimer and tetramer increased. Finally, the tetramer peak became the main peak as the MA was exhausted. This is quite in accordance with the characterization of a controlled polymerization since when the feed ratio of EBriB to MA was set at 1 to 4, the theoretical DP_n was 4 if the conversion is 100%. The result indicated that the kinetic chain length was reduced to an extremely low level, the molecular weight distribution is kept narrow and the reaction is in a good kinetic control.

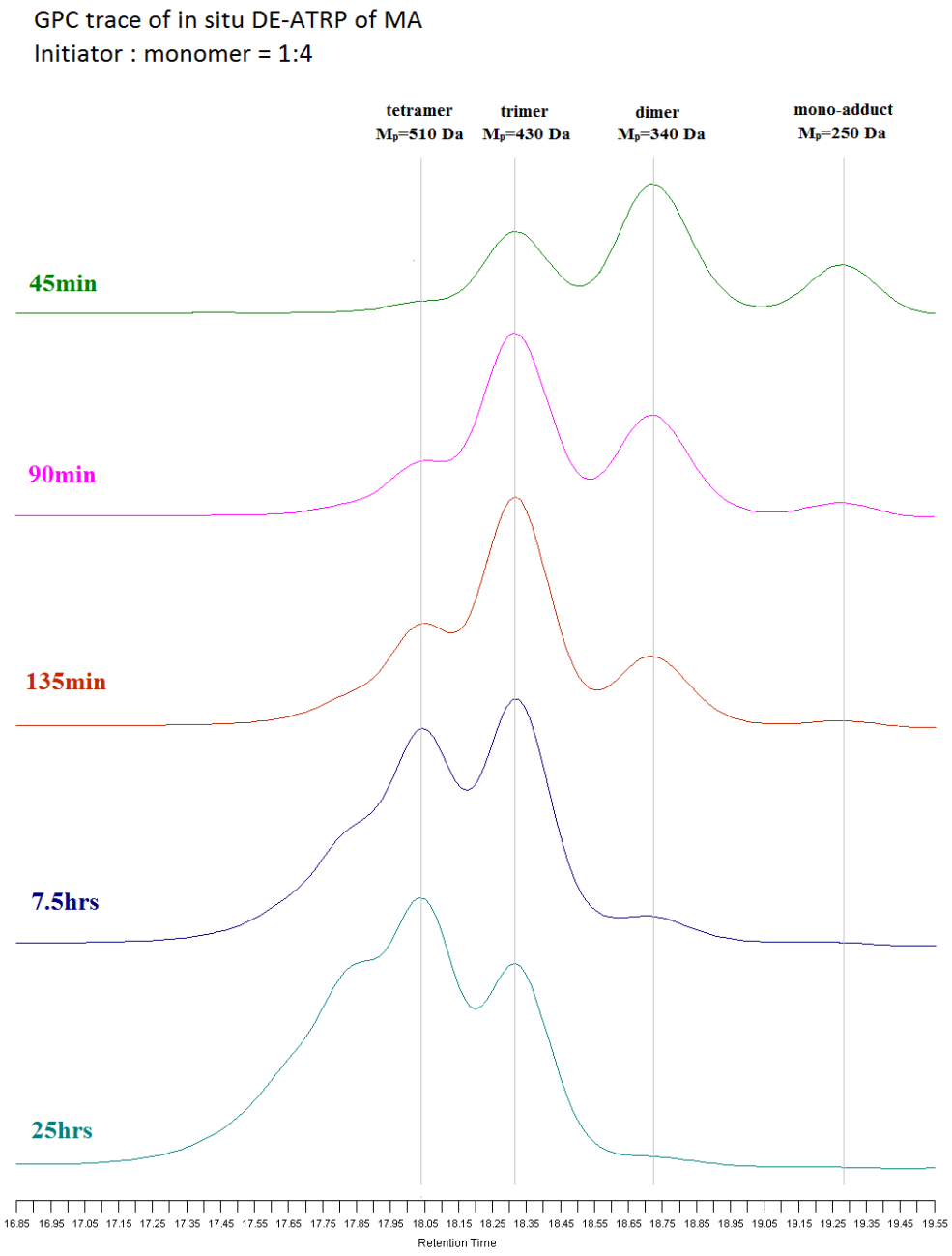

Figure 3.4 GPC traces of polymerization of methyl acrylate (MA) with a high initiator to monomer ratio (1:4) via *in situ* DE-ATRP (30mol% AA of Cu^{II}). The result shows a characteristic of living polymerization, which indicates that the kinetics chain length of *in situ* DE-ATRP can be diminished to an extremely low level.

3.3.2 Homopolymerization of BDA via *in situ* DE-ATRP

After confirming that the *in situ* DE-ATRP provides a good control over the

polymerization of acrylate monomers, diacrylate monomers were used in the homopolymerization towards a hyperbranched structure. The polymerization conditions and characterization were collected in Table 3.1. Monitoring the homopolymerization of 1,3-butanediol diacrylate (BDA) via *in situ* DE-ATRP by GPC at regular time intervals during the reaction provides us with data that strongly supports our proposed mechanism (Figure 3.5). It can be clearly seen that at first (within one hour) the polymerization mixture consists mainly of monoadducts of monomer and initiator as well as a certain portion of oligomers. The more broadening of peaks at 2 hours (PDI=1.6) and 3.5 hours (PDI=3.7) suggests that the combination of lower molecular weight oligomers appears to be the major reaction pathway at the later stage. It is likely that at later stages of the reaction, with most of the monomer already consumed, the reaction conditions are more favorable for statistical branching rather than for linear growth.

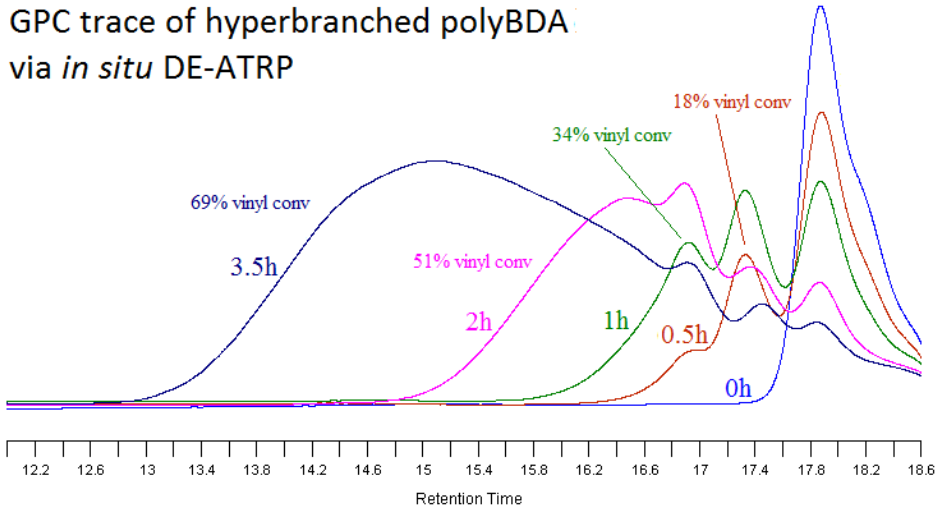

Figure 3.5 Time dependence of the composition of the polymerization mixtures monitored by GPC equipped with a refractive index (RI) detector, showing the reaction pathway that the divinyl monomer firstly underwent a large-scale linear oligomerization (<1h) followed by oligomer combination. (>1h)

Table 3.1 Polymerization conditions and molecular weight characteristics of the hyperbranched polyBDA

	Time (hrs)	M_n[c] (Da)	M_w[c] (Da)	PDI[c]	Vinyl[d] conv.	Branch[e] ratio
Hyperbranched[a] polyBDA (I:M=1:2)	0.5	450	490	1.1	18%	~0%
	1.0	580	700	1.2	34%	4%
	2.0	840	1400	1.6	51%	35%
	3.5	1800	6800	3.7	69%	66%
FRP[b] (I:M=1:2)	0.08	Gel				

[a] I/BDA/$CuBr_2$/PMDETA/AA = 1 : 2 : 0.05 : 0.05 : 0.015, I: ethyl 2-bromoisobutyrate (EBriB), PMDETA: 1,1,4,7,7-pentamethyldiethylenetriamine, AA: L-Ascorbic Acid, Solvent: 2-butanone, [BDA]= 1.44 mol/L, T = 60 °C; [b] I/BDA = 1 : 2, I: 1,1'-azobis-cyclohexane carbonitrile (ACCN), Solvent: 2-butanone, [BDA]= 1.44 mol/L, T = 70 °C; [c] M_n, M_w and PDI are determined by GPC equipped with a refractive index (RI) detector; [d] Vinyl conversion was calculated by ^{1}H NMR, as seen in Figure 3.8 and eq. 3.1; [e] Branch ratios were calculated by ^{1}H NMR, as seen in Figure 3.11 and eq. 3.6.

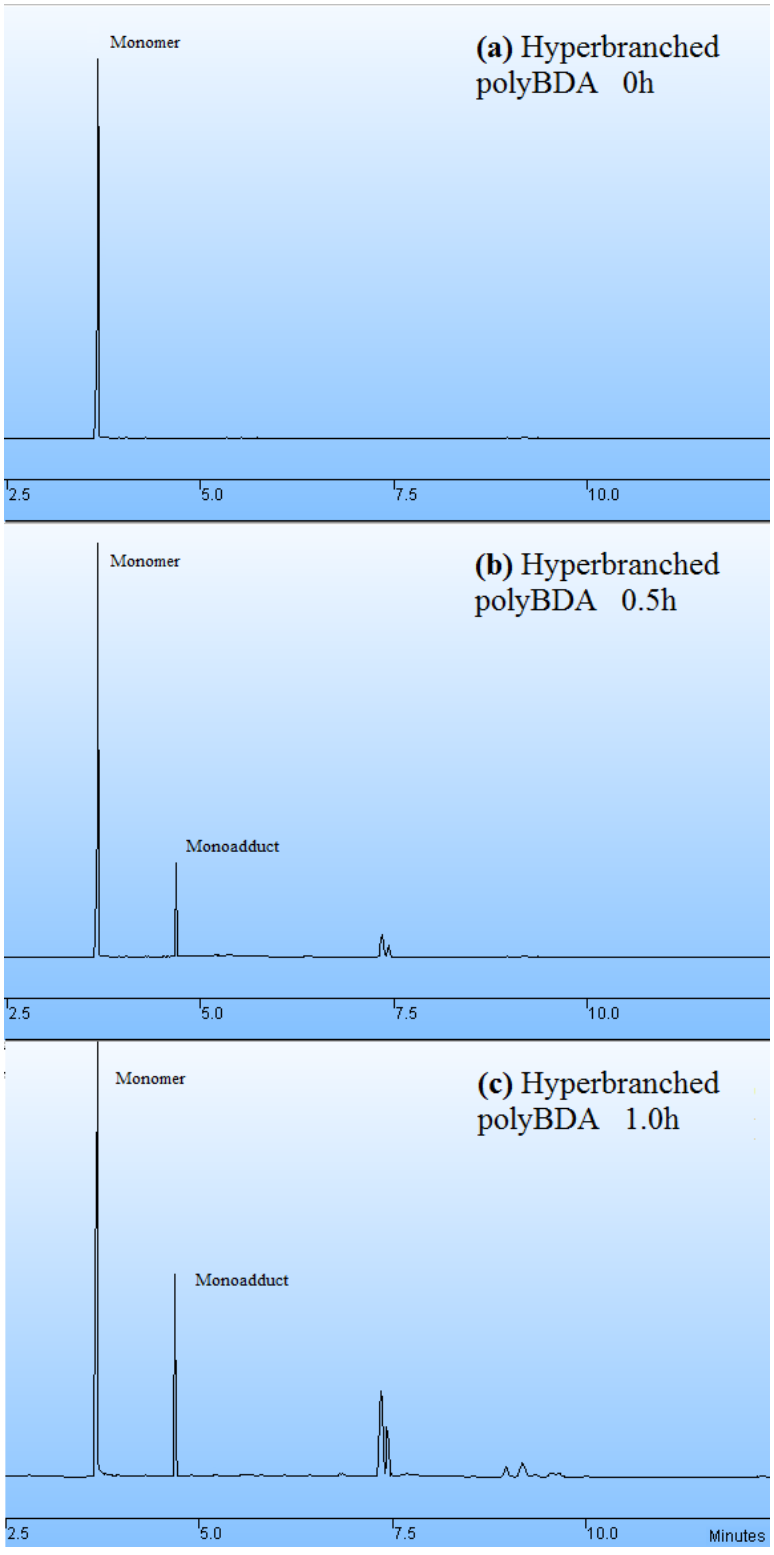

Figure 3.6 GC for the samples from the early period of polymerization of hyperbranched polyBDA, showing the composition evolution within the polymerization system: (a) GC of 0h sample in Figure 3.5; (b) GC of 0.5h sample in Figure 3.5; (c) GC of 1h sample in in Figure 3.5.

Gas chromatography (GC) was also performed to monitor composition evolution during the early period of polymerization[35] (Figure 3.6). Monomer conversion at 0.5h (32%) and 1h (60%), calculated from GC, are approximately twice as high as the vinyl conversion (18% for 0.5h, 34% for 1h), which is in accordance with the assumption that the divinyl monomer are mainly consumed on one side instead of on both sides and very few of branched units are formed at the early period of the reaction.

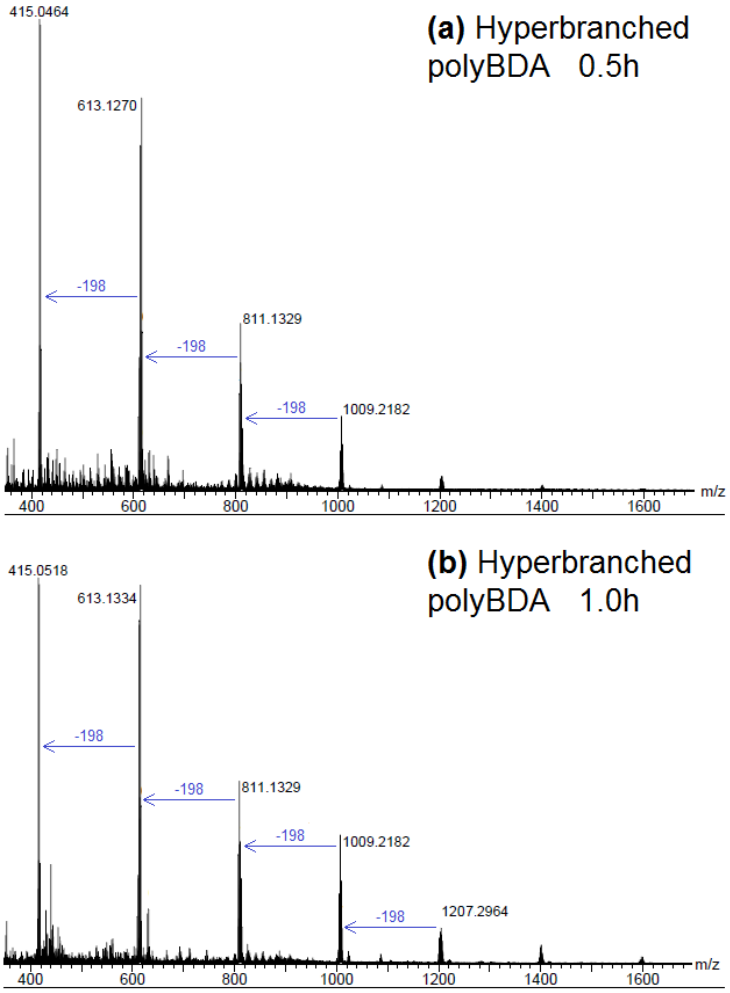

Figure 3.7 Mass spectrum for the samples from early period of polymerization of hyperbranched polyBDA, showing the chemical composition within the polymerization system: (a) Mass spectrum of 0.5h sample in Figure 3.5; (b) Mass spectrum of 1h's sample in Figure 3.5. The number gap between each major peak is exactly the molecular weight of BDA, which indicates that the molecular weight increases by 1 monomer unit and the vinyl groups of the divinyl monomer are mainly consumed on one side instead of on both sides at the beginning period.

Mass spectroscopy was also performed for the 0.5h and 1h samples to investigate the composition at the early period of reaction (Figure 3.7). It can be clearly seen that the polymerization mixture within one hour consists mainly of monoadduct as well as a certain portion of oligomers, matching with the GPC results. The number gap between each major peak is exactly the molecular weight of BDA, which indicates that the molecular weight increases by 1 unit and the vinyl groups of the divinyl monomer are mainly consumed on one side instead of on both sides at the beginning period.

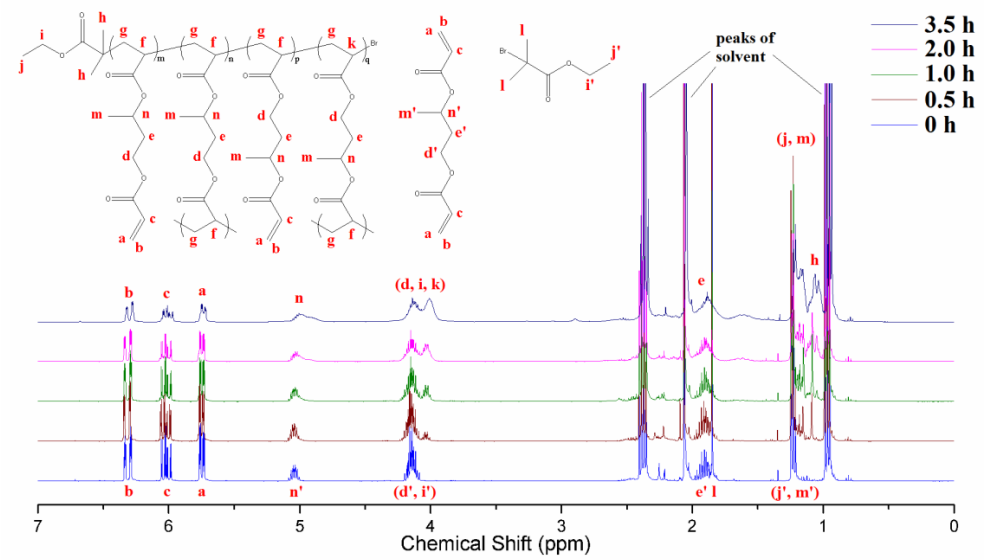

Figure 3.8 ^{1}H NMR spectrum of different periods of polymerization of 1,3-butanediol diacrylate (BDA) towards hyperbranched structure via *in situ* DE-ATRP (30% AA of Cu^{II}). The vinyl conversion is defined as the ratio of consumed vinyl groups to all the original vinyl groups, as shown in Eq. 3.1.

$$Vinyl\ conversion = \frac{consumed\ vinyl\ groups}{initial\ vinyl\ groups}$$

$$= 1 - \frac{retained\ vinyl\ groups}{initial\ vinyl\ groups} = 1 - \frac{Integral\ of\ a}{2 \times Integral\ of\ n} \qquad \text{Eq. 3.1}$$

^{1}H NMR analysis of samples from different time interval (Figure 3.8) gives us the information of vinyl conversion, which was recorded in Table 3.1. The result showed that the vinyl conversion at 3.5 hours reached 69% without occurring of gelation. The kinetic plot $\ln(V_0/V)$~time (Figure 3.9) manifested a generally linear relationship, indicating that the reaction rate was kept at a constant level. It is worth noted that the reaction rate before and after 1.0h shows a slight difference. According to the GPC trace in

Figure 3.5, the combination between the oligomer also happened after 1.0h. Therefore, it is possible that the reaction rates of the two stages (monomer addition and oligomer combination) are different because of the different reactivity between the vinyl groups in the monomer and in the oligomer. The initiator conversion was also available from the ^{1}H NMR analysis. It showed that 74% of initiator was consumed at 1.0 hour and 95% of the initiator converted at 2.0 hour. This fact indicated that the majority of oligomer combinations occur when the primary initiator is nearly exhausted.

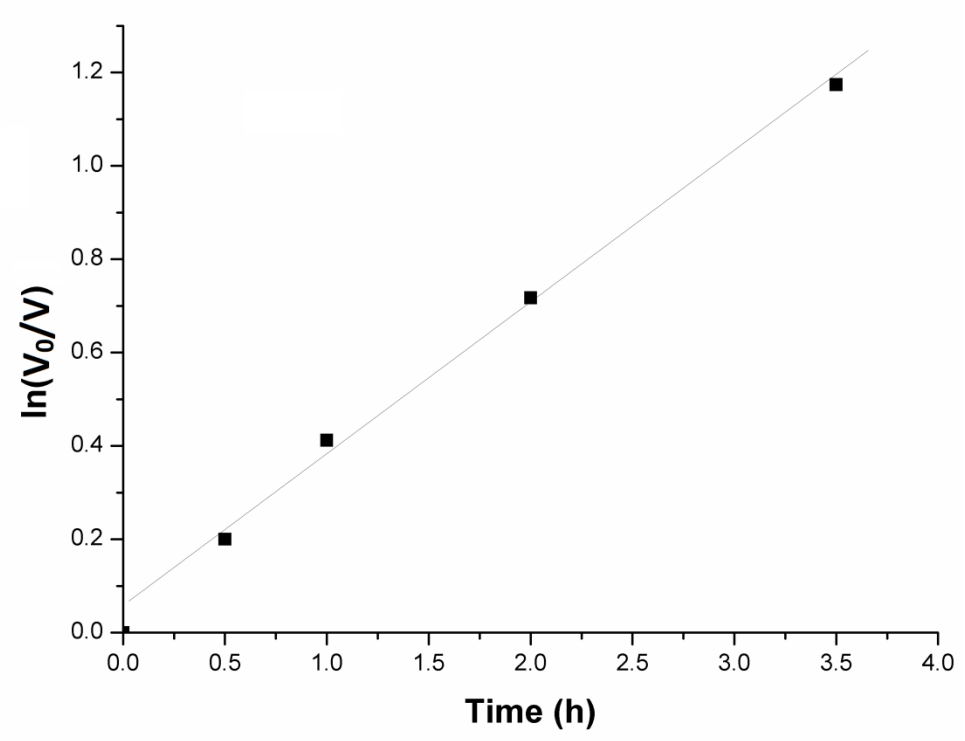

Figure 3.9 Kinetic plot of ln([V]$_0$/[V]) versus time for the *in situ* DE-ATRP of BDA ([V] is the concentration of vinyl groups in the reaction).

We managed to calculate the theoretical branch ratio as follow, and compared our reaction data with the theoretical curve as shown in Figure 3.10. It can be seen that the trend for branch ratio versus time is in accordance with the theoretical curve. However, there is a certain degree of deviation, which could be due to either inconstant reaction rate through the two stages of reaction or the substance loss during the purification process.

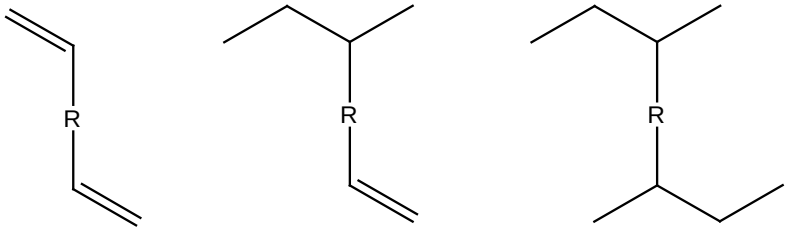

Concentration: [M] [M_1] [M_2]

$[M]+[M_1]+[M_2]=[M]_0$

$[Vinyl]=2[M]+[M_1]$

Assuming that all vinyl groups have the same reactivity and radical concentration is constant, so

$$-\frac{d[Vinyl]}{dt}=k[Vinyl] \qquad (k=k_{app}=k_p[R^{\bullet}])$$

$$\text{So, } \begin{cases} -\dfrac{d[M]}{dt}=2k[M] \\ \dfrac{d[M_1]}{dt}=-\dfrac{d[M]}{dt}-\dfrac{d[M_2]}{dt}=2k[M]-k[M_1] \\ \dfrac{d[M_2]}{dt}=k[M_1] \end{cases}$$

$$[M]=[M_0]e^{-2kt}$$
$$\Rightarrow [M_1]=[M_0](2e^{-kt}-2e^{-2kt})$$
$$[M_2]=[M_0](1-e^{-kt})^2$$

$$\Rightarrow \text{Branch ratio}=\frac{[M_2]}{[M_1]+[M_2]}=\frac{(1-e^{-kt})^2}{1-e^{-2kt}} \qquad \text{Eq. 3.2}$$

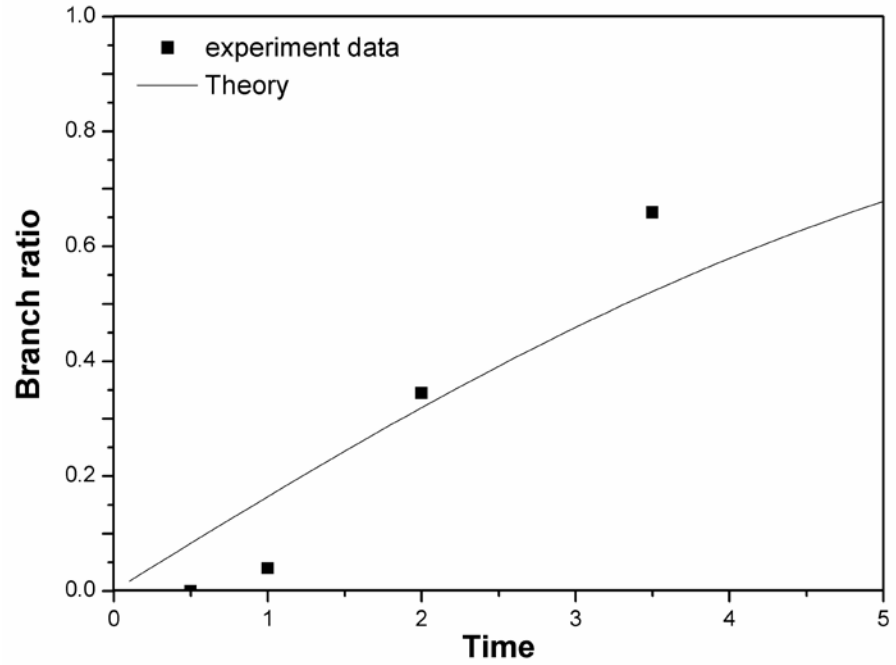

Figure 3.10 Comparison of theoretical and experimental results of branch ratio versus time. Theoretical curve was described according to eq. 3.2. Constant k is calculated based on the line slope in Figure 3.9.

The 3.5 hour's sample was precipitated against hexane and diethyl ether mixture to remove all of the BDA monomer and analyzed by ^{1}H NMR, as shown in Figure 3.11. The precipitated polymer possessed a branch ratio of 66% (the percentage of divinyl-consumed units in all of the constructive units), which is much higher than the previously reported MVM-derived polymers[30, 31, 32, 33]. This high branch ratio indicates a highly branched structure formed from the enhanced intermolecular coupling rather than the traditional chain growth.

By integration of the initiator end group (proton j and h) and that of the BDA units (proton of m), we were able to calculate the ratio of initiator units to BDA units. This ratio was calculated to be 1:1.5, which means that each primary chain consists of only ~1.5 BDA units. This result proves that the hyperbranched polymer consisted of extremely short primary chains.

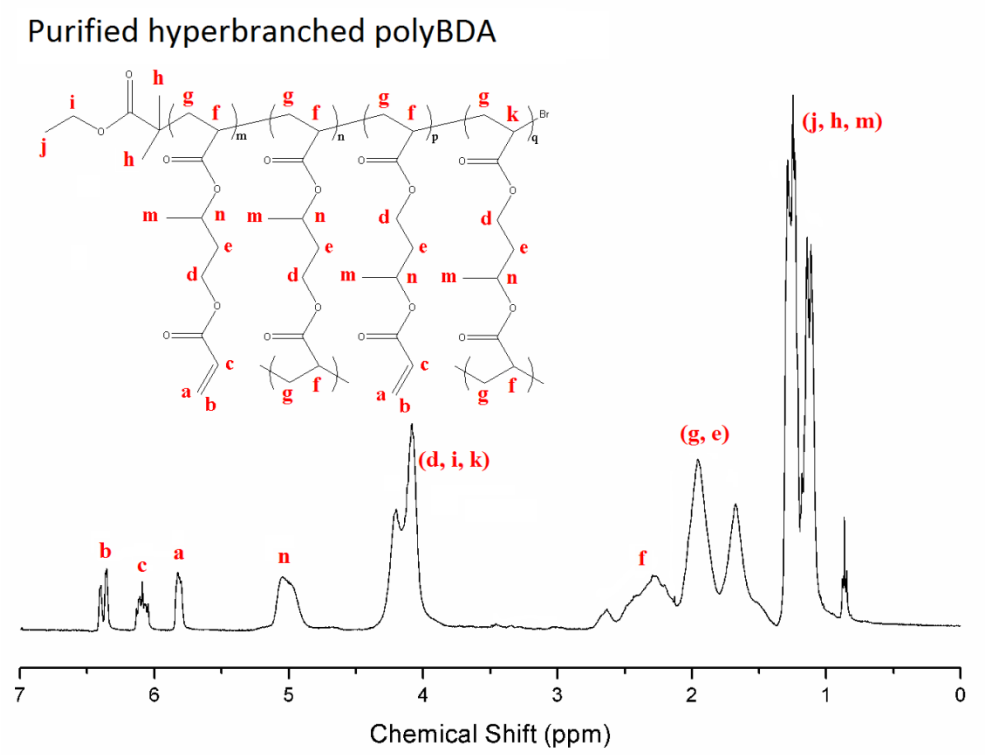

Figure 3.11 ^{1}H NMR spectra of purified polymer hyperbranched polyBDA (3.5h product in Figure 3.5). The component ratio of the different units was calculated by eq. 3.3-eq. 3.5 and summarized in Table 3.2. The branched ratio is defined as the ratio of branched BDA units to all the BDA units, as shown in eq. 3.6.

$$\text{Initiator} = \frac{j+h+m-3n}{9} \qquad \text{Eq. 3.3}$$

$$\text{Linear BDA} = a \qquad \text{Eq. 3.4}$$

$$\text{Branched BDA} = n-a \qquad \text{Eq. 3.5}$$

$$\text{Branch ratio} = \frac{\text{Branched BDA units}}{\text{All BDA units}} = 1-\frac{\text{Linear BDA units}}{\text{All BDA units}} = 1-\frac{a}{n} \qquad \text{Eq. 3.6}$$

$$DB_{Frey} = \frac{2\times\sum\text{dendritic units}}{2\times\sum\text{dendritic units}+\sum\text{linear units}} = \frac{2\times\text{branched units}}{2\times\text{branched units}+\text{linear units}+\text{initiator}} = \frac{2\times(n-a)}{2\times(n-a)+a+\frac{(j+h+m-3n)}{9}} \qquad \text{Eq. 3.7}$$

Table 3.2 The component ratio of the different units in the purified 3.5h's sample polyBDA by ^{1}H NMR spectroscopy analysis

Initiator[a]	Linear BDA[a]	Branched BDA[a]	Degree of Branching[b]
39.4%	20.6%	40.0%	57.1%

[a]The ratio of different units in the polymer is calculated from the Eq. 3.3-Eq. 3.5. [b]Degree of branching is calculated from the Eq. 3.7.

The structure of hyperbranched polymer prepared via the homopolymerization DE-ATRP of divinyl monomers is shown as below (Figure 3.12). A crosslinker (also referred as branched unit) is formed in the polymer chains via reaction of a pendent vinyl group with a propagating center. One crosslinker (or branched unit) consists of two branch points (Figure 3.12). In ATRP, all of the polymer chains should be initiated by the halide alkyl initiator. Thus, there is an initiator fragment at the end of each polymer chain (Figure 3.12). The number of initiator fragments is equal to the number of primary linear chains ($N_{Primary\ chains}=N_{Initiators}$). Statistically, the ratio of the branching units ($N_{Branched\ units}$) to the initiators ($N_{Initiators}$) can generally indicate the structure of the polymer.

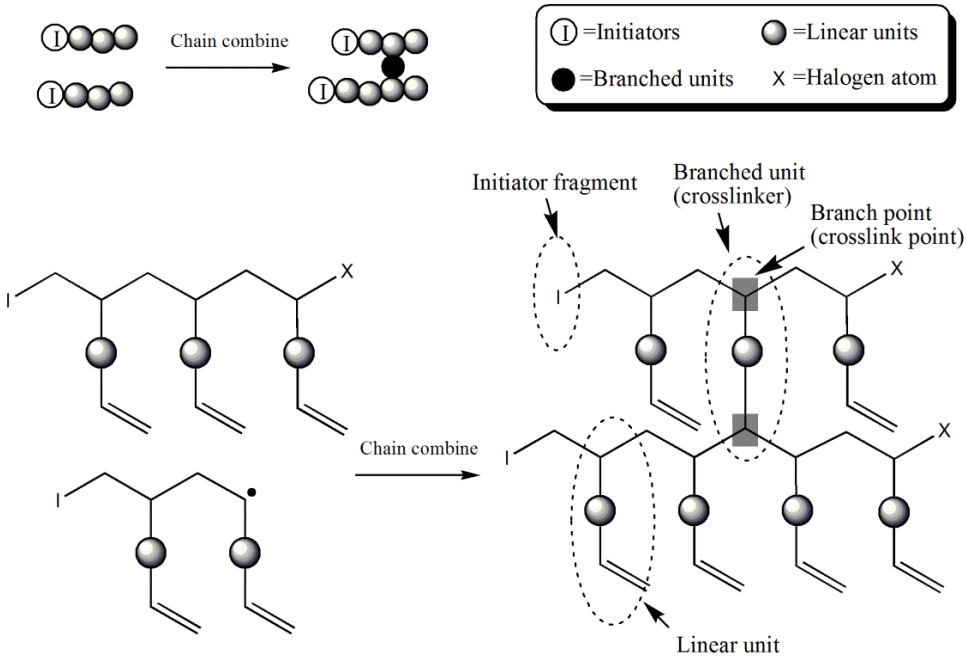

Figure 3.12 The molecular structure in polyBDA. The ratio of branched units to initiators should below 1 in the ideal hyperbranched polymer. Also, this ratio will be higher than 1 for the cyclic or intramolecular crosslinked polymers.

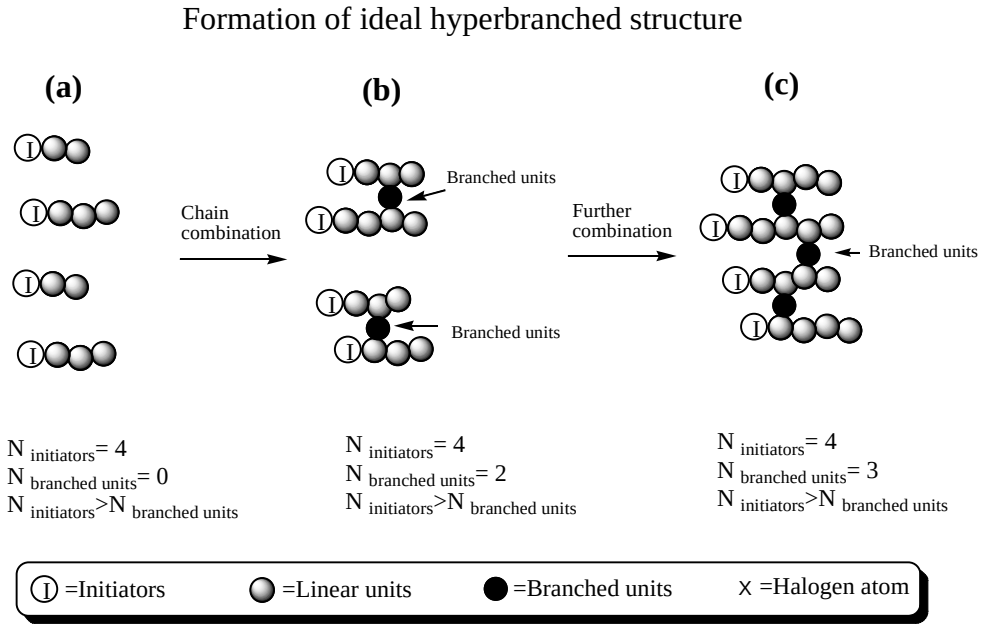

Figure 3.13 Mechanism of an ideal hyperbranched polymer formation and the relationship between branched units and initiators. The ratio of branched units to initiators is lower than 1 in an ideal hyperbranched polymer ($N_{branched\ units} < N_{initiators}$).

In ATRP, the branched polymers were formed by the combination of linear polymer chains. From Flory-Stockmayer theory[24, 26], the critical gelation is one branch point per primary chain[17]. Consequently, Sherrington and Armes have shown that it requires at least (N-l) branched units to form a hyperbranched or crosslinked molecule from N primary chains by divinyl crosslinker[14, 15, 23] (Figure 3. 12). For the ideal hyperbranched polymer, there is a branched unit between each two linear chains (Figure 3. 12 (b)). Therefore, the number of branching units should be lower than the number of initiators in the ideal hyperbranched polymer (Eq. 3.8).

In an ideal hyperbranched polymer:

$N_{branched\ units} = N_{primary\ units} - 1$

$N_{primary\ units} = N_{initiators} \rightarrow N_{branched\ units} = N_{initiators} - 1$

If $N_{initiators} >> 1$, $N_{branched\ units} \approx N_{initiators}$

$\rightarrow N_{branched\ units} / N_{initiators} \leq 1$ Eq. 3.8

For example in Figure 3.13 (c)

$N_{branched\ units} = 3$, $N_{initiators} = 4$,

$N_{branched\ units} / N_{initiators} = 0.75 < 1$

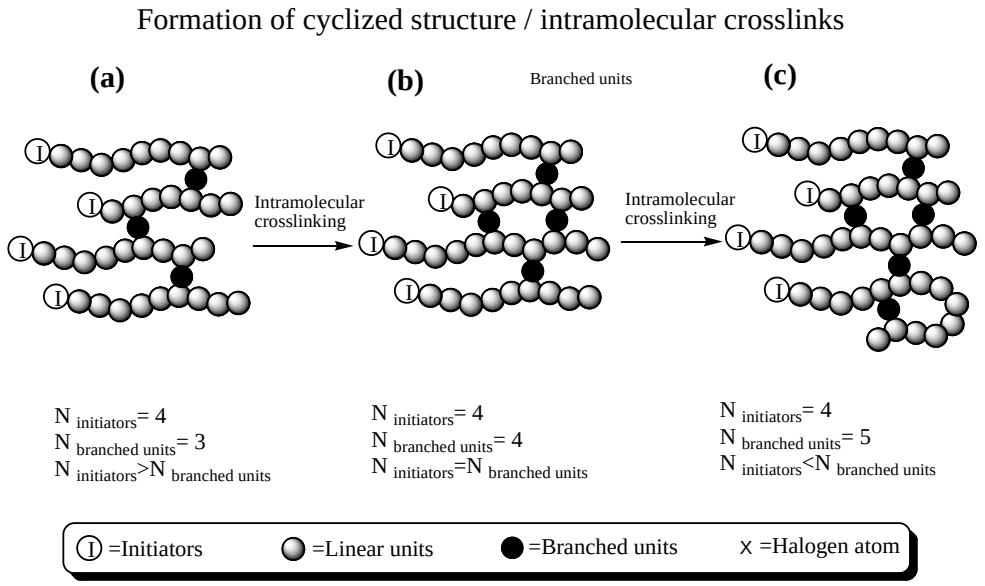

Figure 3.14 Mechanism of the cyclic polymer/intramolecular crosslinks formation and the relationship between branched units and initiators. The ratio of branched units to initiator is higher than 1 in cyclic polymer due to the unavoidable intramolecular crosslinks ($N_{branched\ units} \geq N_{initiators}$).

In the cyclic polymer, the branched units between each two linear chains are increased due to the unavoidable intramolecular crosslinks (Figure 3.14). Therefore, the number of branched units should be higher than the number of primary linear chains. Apparently, the ratio of branching units to initiators should be higher than 1 ($N_{branched\ units} / N_{initiators} > 1$) in the cyclic/ intramolecular crosslinked polymer (Eq. 3.9). Finally, the cyclization points can be calculated by Eq. 3.10.

In a cyclized / intramolecular crosslinked polymer:

All $N_{branched\ units} = N_{intramolecular\ crosslinker} + N_{intermolecular\ crosslinker}$

$N_{intermolecular\ crosslinker} = N_{primary\ units} - 1 \approx N_{initiators}$

$\rightarrow N_{branched\ units} \approx N_{intramolecular\ crosslinker} + N_{initiators}$

$\rightarrow N_{branched\ units} / N_{initiators} > 1$ Eq. 3.9

For example in Figure 3.14 (c)

$N_{branched\ units} = 5$, $N_{initiators} = 4$,

$N_{branched\ units} / N_{initiators} = 1.25 > 1$

$N_{intramolecular\ crosslinker} \approx N_{branched\ units} - N_{initiators}$ Eq. 3.10

^{1}H NMR spectroscopy analysis showed that the initiator component ratio is basically equal to the branched unit ratio (39.4% to 40.0%), confirming the formation of hyperbranched structure for polyBDA. The slightly higher ratio of branched unit could be due to secondary intramolecular reaction.

Table 3.3 Polymerization conditions and molecular weight characteristics of the cyclized polyBDA.

	Time (hrs)	M_n[c] (Da)	M_w[c] (Da)	PDI[c]	Vinyl[d] conv.	Branch[e] ratio
Cyclized[a] polyBDA (I:M=1:100)	1.5	1100	1200	1.1	2%	14%
	3.0	1600	1800	1.2	5%	15%
	5.0	2900	3800	1.3	9%	18%
	10.0	10500	24300	2.3	15%	24%
FRP[b] (I:M=1:100)	0.16	Gel				

[a] I/BDA/$CuBr_2$/PMDETA/AA = 1 : 100 : 2.5 : 2.5 : 0.75, Solvent: 2-butanone, [BDA]= 1.44 mol/L, T = 60 °C; [b] I/BDA = 1 : 100, I: 1,1'-azobis-cyclohexane carbonitrile (ACCN), Solvent: 2-butanone, [BDA]= 1.44 mol/L, T = 70 °C; [c] M_n, M_w and PDI are determined by GPC equipped with a refractive index (RI) detector; [d] Vinyl conversion was calculated by ^{1}H NMR and eq. 3.1; [e] Branch ratios were calculated by ^{1}H NMR and eq. 3.6.

A comparison experiment was performed with low initiator to monomer ratio (1:100). GPC traces show that the polymerization process also occurs in two distinct phases (Figure 3.15). At first, the polymer chains display an initial linear-like growth. The increase of molecular weight is linear with monomer conversion and PDI remains low with unimodal molecular distribution. Then, only at much later stages of the polymerization process, chain combination occurs and is accompanied by the rapid increase in M_w

and PDI.

Significant multimodality in the case of HB polyBDA, especially for low and moderate molar masses, is not observed in the case of single cyclized polyBDA. This strongly supports the expected differences in terms of mechanism: in the case of single cyclized polyBDA (almost exclusively intramolecular cyclization), the increase of molar masses is only due to propagation, whereas in the case of HB, it is mainly due to intermolecular combination.

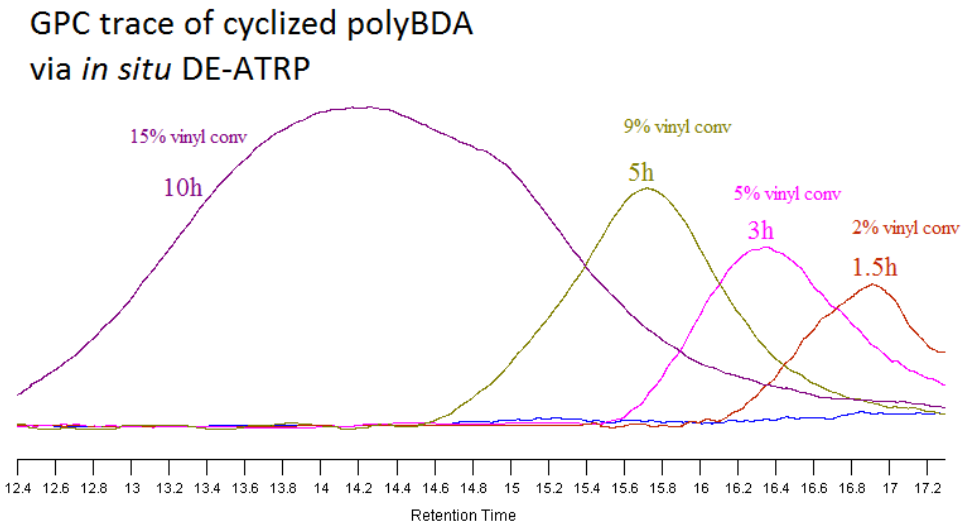

Figure 3.15 Time dependence of the composition of the polymerization mixtures monitored by GPC equipped with a refractive index (RI) detector, showing the unimodal peaks typically at initial stages (<5h) and multimodal peaks appearing later (>5h).

However, a certain proportion of branched units (18%) is formed in the first phase of the reaction (e.g. 5h's sample in Table 3.3 and Figure 3.15, PDI=1.3, Vinyl conversion=9%), which provides evidence for the dominance of cyclization reactions occurring during the linear growth process at the begining of this comparison polymerization.

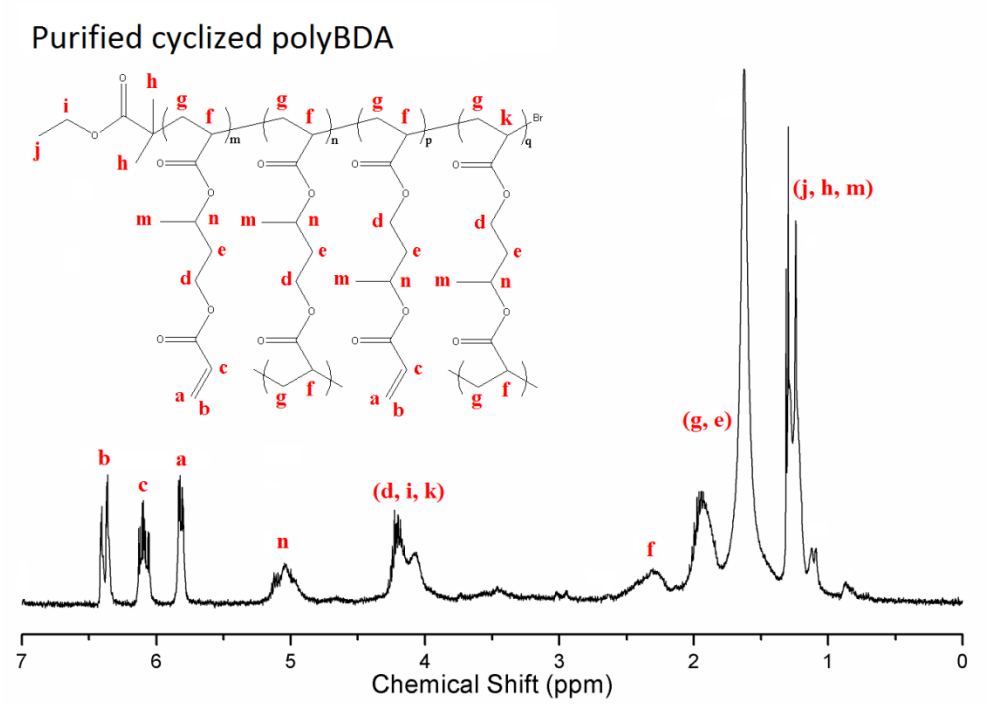

Figure 3.16 ^{1}H NMR spectra of purified cyclized polyBDA (5h product in Figure 3.15). The component ratio of the different units was calculated by eq. 3.3-eq. 3.5 and summarized in Table 3.4. The branched ratio is defined as the ratio of branched BDA units to all the BDA units, as shown in eq. 3.6.

Table 3.4 The component ratio of the different units in the purified 5h's sample of cyclized polyBDA by ^{1}H NMR spectroscopy analysis.

Initiator[a]	Linear BDA[a]	Branched BDA[a]	Degree of Branching[b]
3.7%	78.9%	17.4%	29.6%

[a]The ratio of different units in the polymer is calculated from the Eq. 3.3-Eq. 3.5. [b]Degree of branching is calculated from the Eq. 3.7.

The ^{1}H NMR spectroscopy analysis showed that the initiator component ratio is much lower than the branched unit ratio (3.7% compared to 17.4%), indicating the formation of cyclized structure for polyBDA because more than one crosslinks formed in one primary chain.

3.3.3 Homopolymerization of Other Divinyl Monomers

To verify the universality of this strategy to hyperbranched structures and see whether it can be widely applied to the polymerization of a broad range of MVMs, polymerization of different MVMs, including the derivatives of acrylate, methacrylate and styrene, were implemented with a high initiator/monomer ratio (1:2) in the *in situ* DE-ATRP reaction system. Hyperbranched polymers were synthesized by the homopolymerization of di(ethylene glycol) diacrylate, ethylene glycol dimethacrylate and divinylbenzene (Table 3.5 and Figure 3.17). It can be seen that the homopolymerization of diacrylate resulted in the highest vinyl conversion and highest branch ratio (Table 3.5) whereas the vinyl conversion and branch ratio was relatively low for dimethacrylate (Table 3.5) probably due to the higher reactivity of methacrylate than that of acrylate, which led to a faster linear chain growth and thus advanced the chain combination stage (Figure 3.17 (b)). The polymerization of DVB exhibited a low rate (Figure 3.17 (c)) but the product also possessed a branch ratio of 40% (Table 3.5).

It has been proved here that this approach can be used for the polymerization of different types of multi-vinyl monomers. The approach will provide us a number of possibilities to create a broad range of new highly branched functional polymers with novel properties from a variety of economical and structurally special multi-vinyl monomers.

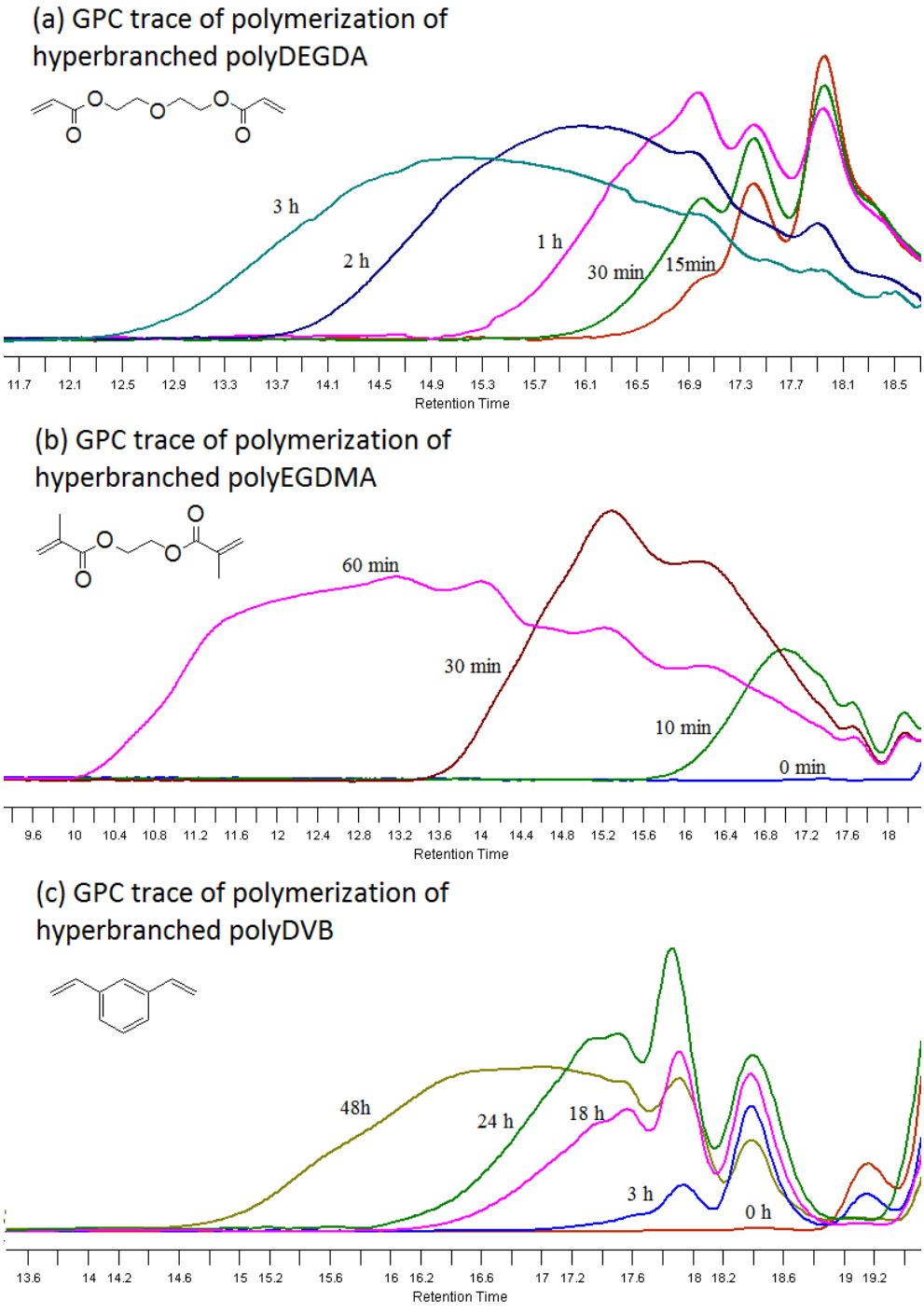

Figure 3.17 GPC trace evolution for polymerizations from different types of divinyl monomers: (a) Polymerization of DEGDA; (b) Polymerization of EGDMA; (c) Polymerization of DVB.

Table 3.5 Polymerization conditions and molecular weight characteristics of polymerizations from different divinyl monomers.

	Time (hrs)	M_n[d] (Da)	M_w[d] (Da)	PDI[d]	Vinyl[e] conv.	Branch[e] ratio
Hyperbranched[a] polyDEGDA	0.25	470	520	1.1	7%	~0%
	0.5	520	630	1.2	18%	~2%
	1	690	1000	1.5	27%	19%
	2	1200	3300	2.7	56%	37%
	3	1900	10400	5.6	70%	66%
Hyperbranched[b] polyEGDMA	0.17	620	680	1.1	8%	~0%
	0.5	1400	2500	1.8	17%	~2%
	1	3100	20800	6.7	30%	30%
Hyperbranched[c] polyDVB	3	250	260	1.0	10%	~0%
	18	400	480	1.2	30%	15%
	24	420	500	1.2	37%	20%
	48	980	2100	2.1	55%	40%

[a] I/DEGDA/$CuBr_2$/PMDETA/AA = 1 : 2 : 0.05 : 0.05 : 0.015, I: ethyl 2-bromoisobutyrate (EBriB), PMDETA: 1,1,4,7,7-pentamethyldiethylenetriamine, AA: L-Ascorbic Acid, solvent: 2-butanone, T = 60 ^oC; [b] I/EGDMA/$CuBr_2$/PMDETA/AA = 1 : 2 : 0.05 : 0.05 : 0.00375, solvent: 2-butanone, T = 60 ^oC; [c] I/DVB/$CuBr_2$/PMDETA/AA = 1 : 2 : 0.05 : 0.05 : 0.025, solvent: toluene, T = 90 ^oC; [d] M_n, M_w and PDI are determined by GPC equipped with a refractive index (RI) detector. [e] Vinyl conversion and branch ratio were calculated by ^1H NMR analysis of original reaction mixtures and precipitated samples.

3.3.4 Homopolymerization of a Disulfide Divinyl Monomer towards a Reductively Degradable HBP

To further prove that our proposed strategy leads to such a highly branched structure, a cleavable polymer was designed and prepared via *in situ* DE-ATRP from a degradable disulfide divinyl monomer

(bis(2-acryloyl)oxyethyl disulphide, DSDA)[36]. Within the DSDA monomer is a disulfide bond that can be cleaved quickly under reducing conditions, thus allowing us to observe the degradation profile and hence determine if a hyperbranced structure (will be degraded into small units), or a cyclized structure (will "untie" into a linear chain) is formed.

In a similar fashion, the DSDA homopolymerization towards a hyperbranched structure was monitored by GPC as shown in Figure 3.18, which presents a similar profile to that obtained for BDA. The molecular weight and PDI at different time interval was summarized in Table 3.6. Vinyl conversion was calculated by eq. 3.11 according to the ^{1}H NMR spectrum shown in Figure 3.19. Vinyl conversion reached 74% at 10 hours without gelation (Table 3.6).

Table 3.6 Polymerization conditions and molecular weight characteristics of the hyperbranched polyDSDA.

	Time (hrs)	M_n[b] (Da)	M_w[b] (Da)	PDI[b]	Vinyl[c] conv.	Branch[d] ratio
Hyperbranched[a] polyDSDA	0.5	600	700	1.1	9%	~0%
	1.5	800	1000	1.3	26%	6%
	3.0	1100	1900	1.7	44%	33%
	6.5	2500	5400	2.2	62%	58%
	10.0	4300	21500	5.0	74%	68%
After purification	10.0	6200	30900	5.0	—	68%
After degradation	10.0	700	1100	1.6	—	—

[a] I/DSDA/$CuBr_2$/PMDETA/AA = 1 : 2 : 0.05 : 0.05 : 0.015, I: ethyl 2-bromoisobutyrate (EBriB), PMDETA: 1,1,4,7,7-pentamethyl diethylenetriamine, AA: L-Ascorbic Acid, Solvent: 2-butanone, [BDA]= 1.44 mol/L, T = 60 °C; [b] M_n, M_w, and PDI are determined by GPC equipped with a refractive index (RI) detector; [c] Vinyl conversion was calculated by ^{1}H NMR as seen in Figure 3.19 and eq. 3.11; [d] Branch ratios of purified polymers were calculated by ^{1}H NMR, as seen in Figure 3.20 and eq. 3.12.

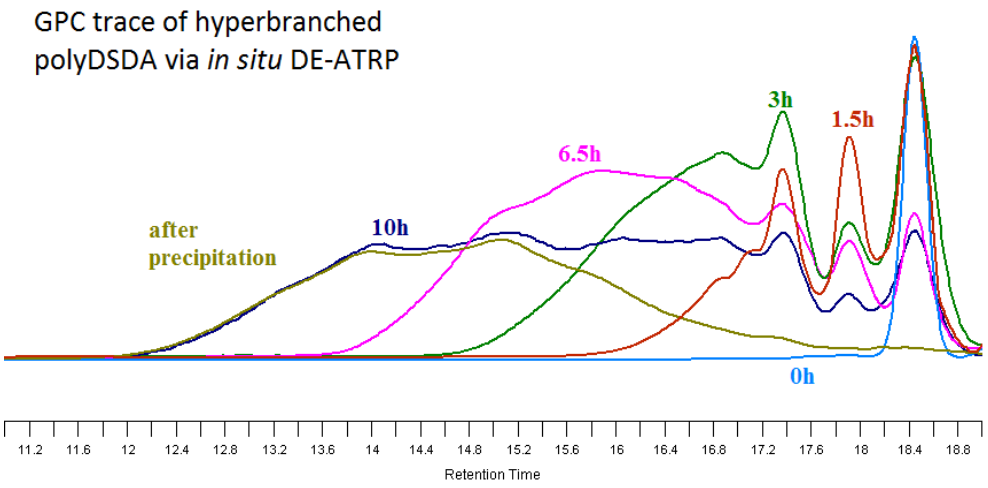

Figure 3.18 Time dependence of the composition of the polymerization mixtures monitored by GPC equipped with a RI detector, indicating that the divinyl monomer firstly underwent a large-scale linear oligomerization (<1.5h) followed by oligomer combination (>1.5h)

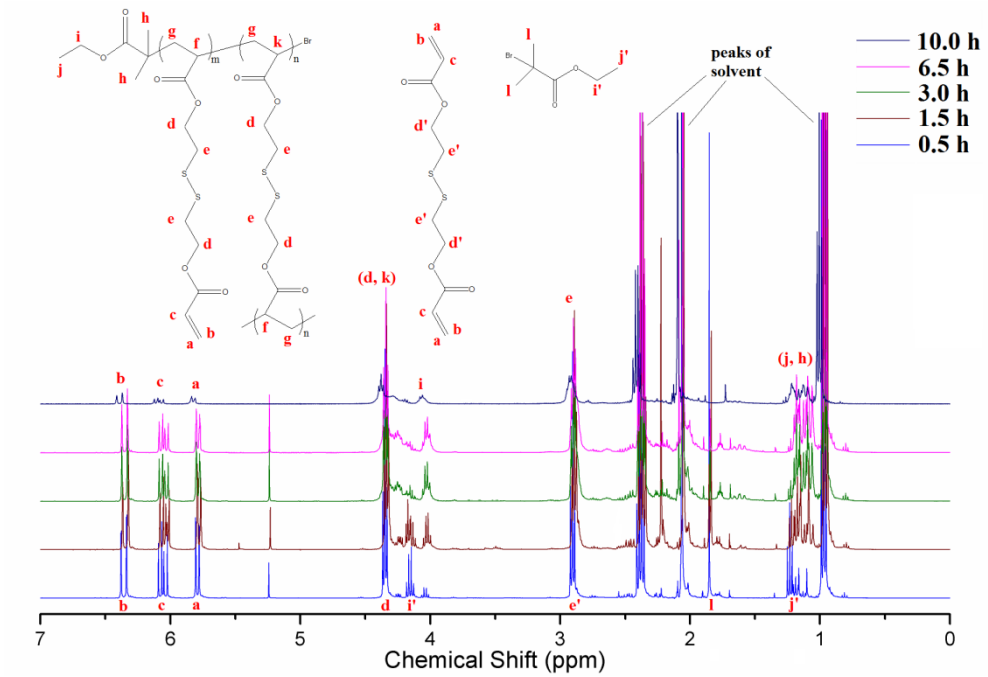

Figure 3.19 ^{1}H NMR spectrum of different periods of polymerization of disulfide-based diacrylate (DSDA) towards hyperbranched structure via in situ DE-ATRP (30% AA of Cu^{II}). The vinyl conversion is defined as the ratio of consumed vinyl groups to all the original vinyl groups, as shown in Eq. 3.11.

$$Vinyl\ conversion = \frac{consumed\ vinyl\ groups}{initial\ vinyl\ groups}$$
$$= 1 - \frac{retained\ vinyl\ groups}{initial\ vinyl\ groups} = 1 - \frac{2 \times Integral\ of\ a}{Integral\ of\ e} \qquad \text{Eq. 3.11}$$

^{1}H NMR spectra for purified hyperbranched polyDSDA (10hrs, M_w=30.9kDa, PDI=5.0) are shown in Figure 3.20. Recently Armes and co-workers developed a quantification method for the intramolecular cyclization by ^{1}H NMR spectrum analysis[37]. However, this quantification method is not suitable for analyzing this new polyDSDA polymers since the proton d (O-CH_2-) overlaps with the proton k and the residue linear unit. Instead, by integration of the initiator end group (proton j and h) and that of the DSDA units (proton of e), we were able to calculate the ratio of initiator units to DSDA units. This ratio was calculated to be 1:1.9, which means that each primary chain consists of only ~1.9 DSDA units. This result proves that the hyperbranched polymer consisted of extremely short primary chains.

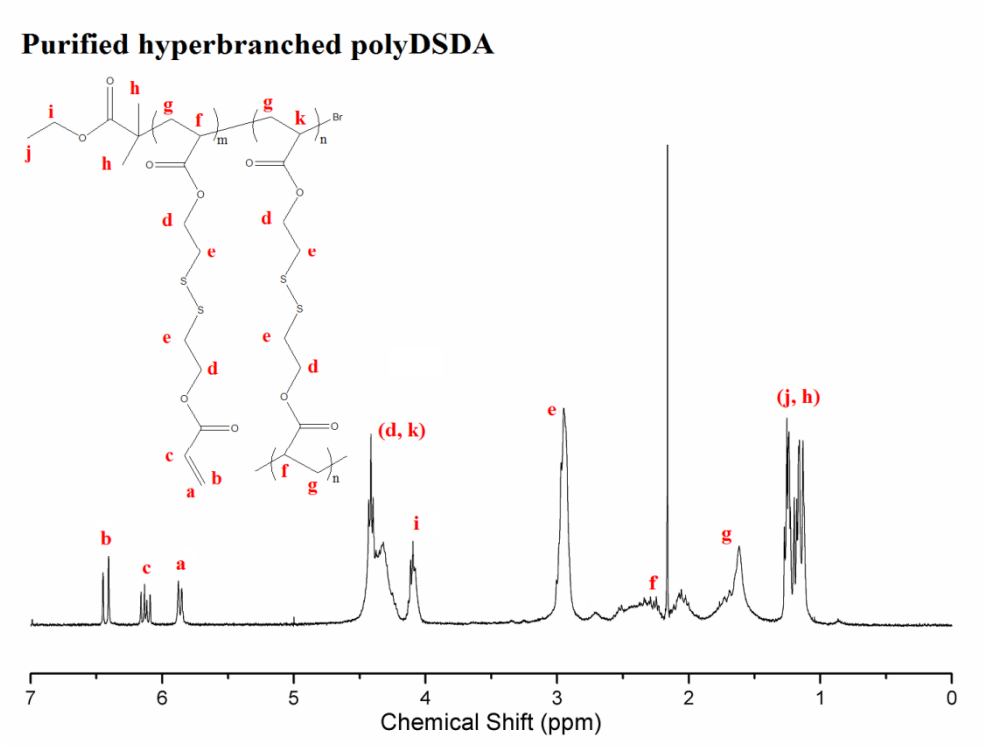

Figure 3.20 ^{1}H NMR spectroscopy of purified hyperbranched polyDSDA (10h product in Figure 3.18). The branched ratio is defined as the ratio of branched DSDA units to all the DSDA units, as shown in Eq. 3.12.

$$Branch\ ratio = \frac{Branched\ \ DSDA\ units}{total\ \ DSDA\ units}$$

$$= 1 - \frac{Linear\ \ DSDA\ units}{total\ \ DSDA\ units} = 1 - \frac{4 \times Integral\ of\ \ a}{Integral\ of\ \ e} \qquad \text{Eq. 3.12}$$

It can be expected that the hyperbranched disulfide polymer, if combined by addition of primary vinyl oligomer, would degrade into oligomers when the intermolecular branch units are broken (Figure 3.21 (a)). In contrast, for the single cyclized polymer, the linear primary chain will still exist after cleavage of the branch units (Figure 3.21 (b)).

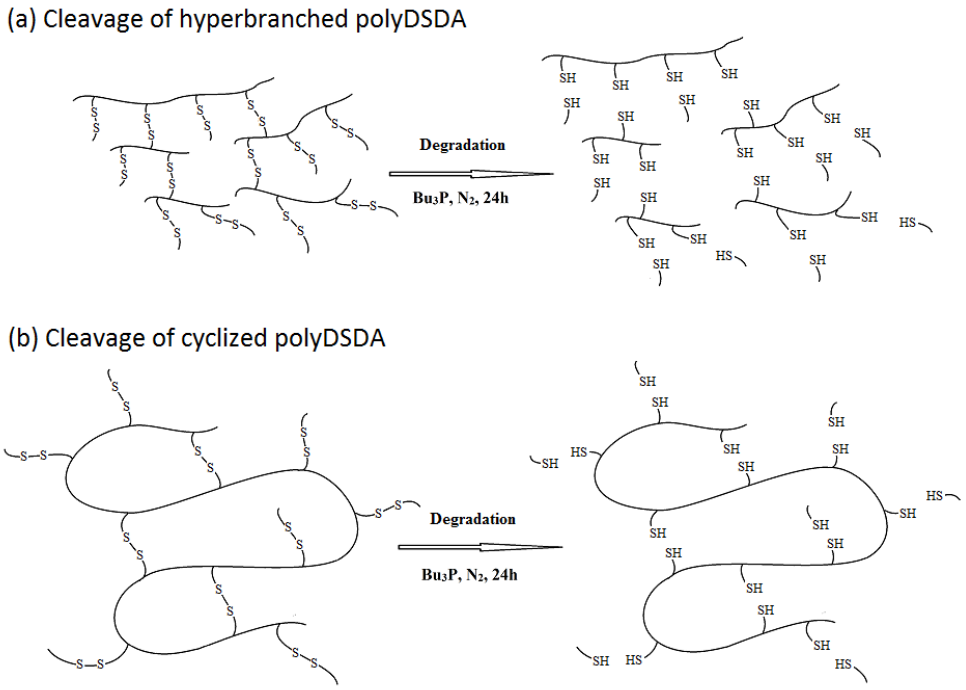

Figure 3.21 Schematic representation of the degradation from polymer to linear primary chains by disulfide bond cleavage, showing that the molecular weight and hydrodynamic size of polymer chains will decrease significantly in hyperbranched polymers, but will only change slightly in single cyclized polymer.

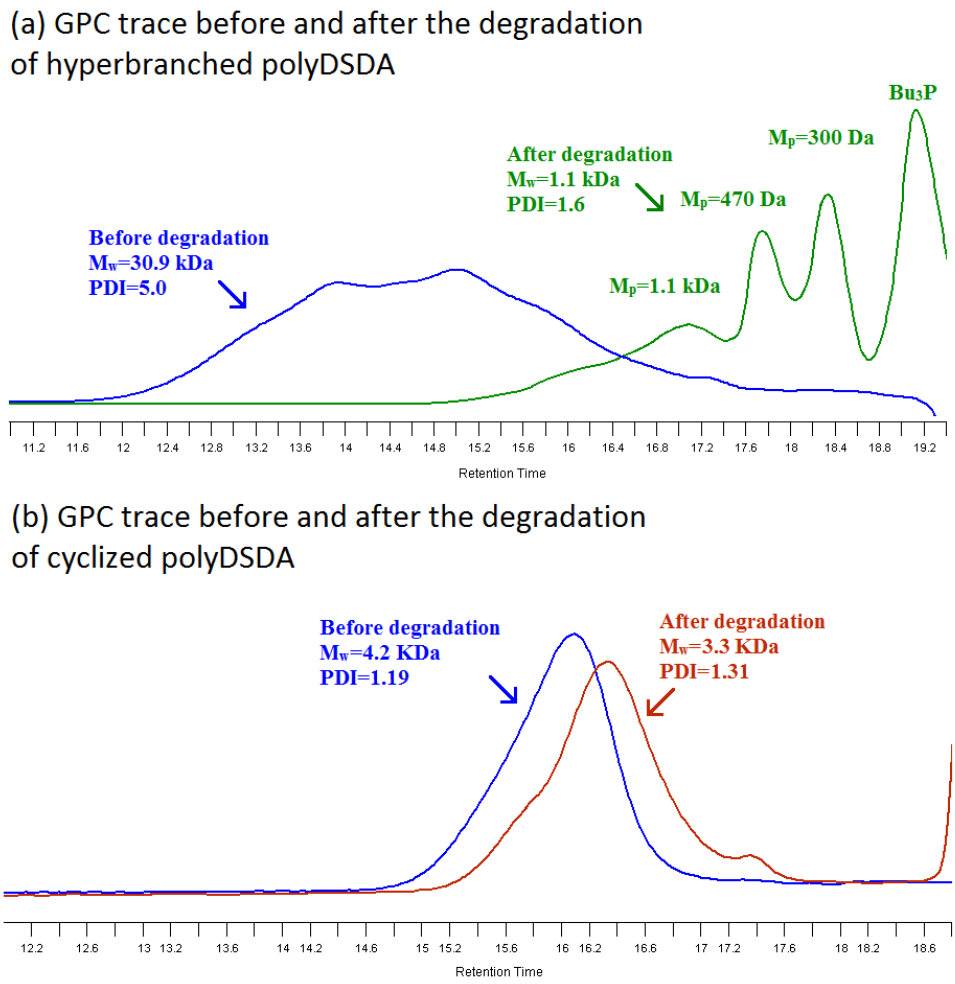

Figure 3.22 GPC trace of the degradation from polymers to linear primary chains by reduction of disulfide bond using tributylphosphine (Bu_3P): (a) Degradation of hyperbranched polyDSDA (synthesized with 1:2 initiator to monomer ratio, purified 10h's polymer in Figure 3.18); (b) Degradation of 'single cyclized' polyDSDA (synthesized with 1:100 initiator to monomer ratio). The GPC trace before and after cleavage of polyDSDA synthesized with a high initiator to monomer ratio proves the hyperbranched structure because the M_w and hydrodynamic size substantially decreased after cleavage (from 31.9 kDa to 1.1 kDa), in contrast, the polyDSDA synthesized with a low initiator to monomer ratio demonstrates only a slight reduction (from 4.2kDa to 3.3 kDa). The vastly different degradation behaviors confirm the large variance between the polymer structures.

The GPC result of the final disulfide polymer before and after degradation confirms our predicted result. The high molecular weight polymer chains were indeed degraded into small chains and the molecular weight showed a very large reduction after degradation (Figure 3.22 (a)). It can be noticed

that the distribution of the cleavage product is broad and multimodal. The components consist of big portions of extremely small molecules and some oligomers. The degradation result provides a profound comparison to the very slight molecular weight reduction observed when the ‘single cyclized’ structure was degraded. It is clearly proved that the polymer prepared by the vinyl oligomer combination approach possessed a highly branched structure and that intermolecular combination reactions are the main contributor to the high branch ratio. ^{1}H NMR spectrums before and after cleavage of both hyperbranched and cyclized polyDSDA are shown in Figure 3.23.

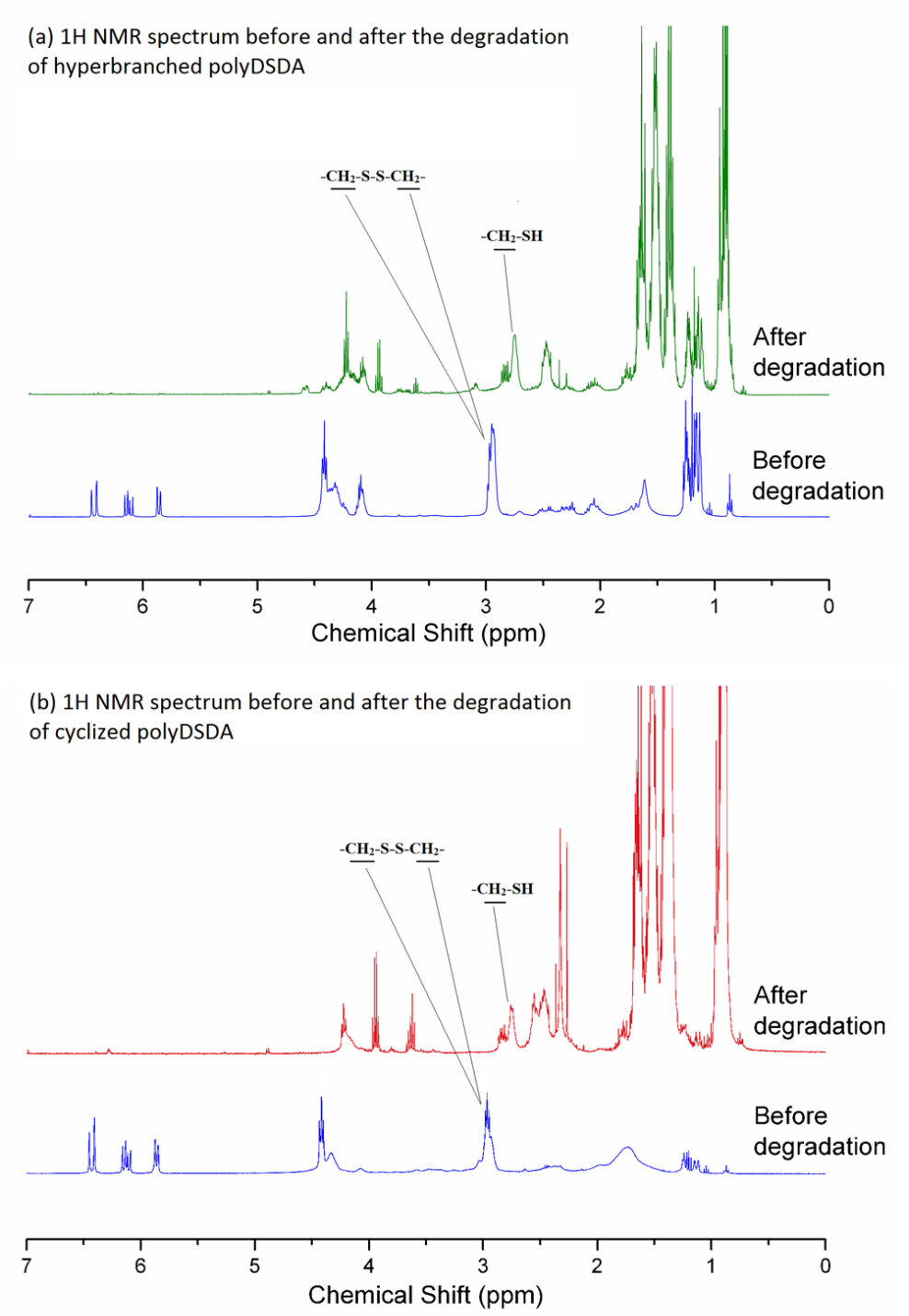

Figure 3.23 ^{1}H NMR spectrums before and after cleavage of the purified hyperbranched and cyclized polyDSDA. The disulfide bond was completely cleaved after 2 h, since the resonance of proton (2.9 ppm) completely disappeared. Peaks of vinyl groups also disappeared, since the vinyl groups were consumed by the newly generated -SH groups.

3.3.5 Discussions

With a deeper analysis of the reaction environments, it becomes less difficult to understand the factors that determine which reaction type will lead to different polymer architectures (as shown in Figure 3.24). More specifically, three parameters, including the growth boundary (kinetic chain length), the chain dimension and the chain concentration, are all taken into account. A relatively small growth boundary, which depends on the kinetics chain length, strictly confines the small number of monomers added to an active center and thus keeps the polymer chains growing in a limited space. In this way, unlike what happens in free radical polymerization (FRP), the formation of huge polymer chains and large-scale combination at the early reaction stages are avoided. Therefore, a small growth boundary, which can be achieved by *in situ* DE-ATRP, is the basic prerequisite for the formation of either the maximal hyperbranched structure or the 'single cyclized' structure. So under this condition of a small growth boundary, different chain dimensions and concentrations will lead to distinct reaction types. A low ratio of initiator to monomer would result in the formation of longer chains but with a lower chain concentration, which would no doubt increase the chance of intramolecular reactions due to the high local/spatial vinyl concentration within the growth boundary. Although the opportunity for intermolecular reactions can rise as the polymer chains grow, this probability at the early stage of reaction can be neglected because of the low chain concentration. That is why a 'single cyclized' polymer can form as the main product. However, in contrast, a high initiator concentration not only diminishes the chain dimension during the linear-growth phase and thus suppresses the intramolecular cyclization, but also it increases the chain concentration in the system so that pendent vinyl groups in one chain are more likely to fall into growth boundary of another chain. After the monomers massively convert to short chains, the intermolecular combination increases and allows the formation of hyperbranched structures with a high density of branching and vinyl functional groups.

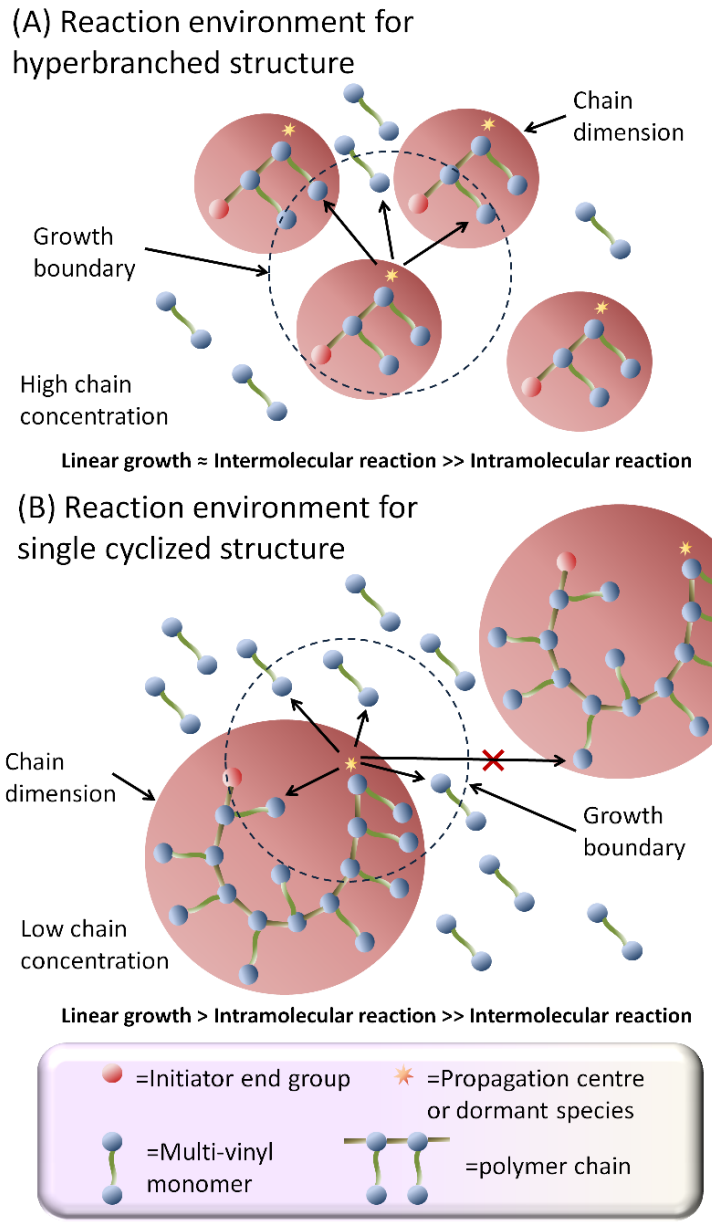

Figure 3.24 Formation of different structures via *in situ* DE-ATRP: (a) Formation of hyperbranched structure; (b) Formation of 'single cyclized' structure. Three parameters are considered: the growth boundary (dotted circle), chain dimension (red shaded part) and chain concentration. The growth boundary, which confines the possible number of vinyl groups reacted within its active lifetime during the propagation process, could change the selectivity of vinyl groups attacked by the propagation centre. The probability of intermolecular combination decreases with distance between an active propagation centre and another polymer chain, which is strongly dependent on the chain dimension and chain concentration.

It is demonstrated here that MVM homopolymerization can be kinetically oriented so as to favor very different polymer architectures with two possible extreme topologies: either single cyclized or hyperbranched polymers, whether cross-linking consists exclusively in intramolecular or intermolecular reactions, respectively. Whereas the intermolecular formation of a cross-link would cause the number of primary chains per polymer molecule to increase, a cyclic sub-structure would result from the intramolecular reaction, thus called cyclization. It should be remember here that a network, which can be defined topologically by the existence of several paths between constitutional units through the structure, would necessarily imply both types of cross-linking reactions. In particular, it is important to distinguish HB structures presented in this contribution from nanogels[38], which can be defined as swollen polymer networks with a size under 100 nm and can be therefore considered as soluble highly branched polymers too: the formation of nanogels implies a contribution of cyclizations, whereas HB are achievable through intermolecular cross-linking only. Up to now, no analytical technique can provide a direct distinction between HB polymers and nanogels, which exhibit similar behaviors. The nature of the topology can be deduced indeed from the combination of the analysis of the products with the knowledge of initial parameters which directly impose key structural characteristics, such as the initial initiator concentration imposing the primary chains concentration, *etc.* In the present contribution, even if intramolecular events can't be totally ruled out (a few cyclization reactions may occur), the experimental conditions implemented clearly favor the formation of HB polymers. This is strongly supported by the GPC analyses of products prepared using the disulfide cross-linker: an important shift towards lower molecular weights is observed after cleavage (no significant modification is expected if intramolecular cross-links are cleaved). A supplementary argument is the primary chains length, which is so short here that it necessarily excludes any significant contribution of cyclizations: if two primary chains are already linked through a cross-link, there are no more enough available monomer units to enable the formation of a second cross-link between them.

3.4 Conclusions

It has been shown here that by using the kinetic control theory to manipulate chain growth conditions, we can design two clearly different polymer structures, including a veritable hyperbranched polymer with a high branch ratio of 66% and a large amount of vinyl functional groups. It can be foreseen that this new strategy for preparation of hyperbranched polymers could open up the field to the polymerization of a very wide range

multifunctional vinyl monomers or combinations of comonomers in any proportion. We envisage that a broad range of new highly branched functional polymers with novel properties will be obtained from a variety of economical and structurally special multi-vinyl monomers, which will have important applications in a variety of different fields.

3.5 References

1. Jikei, M.; Kakimoto, M. Hyperbranched polymers: a promising new class of materials. *Progress in Polymer Science* **2001,** *26* (8), 1233-1285.
2. Frechét, J. M. J.; Hawker, C. J.; Gitsov, I.; Leon, J. W. Dendrimers and hyperbranched polymers: Two families of three-dimensional macromolecules with similar but clearly distinct properties. *Journal of Macromolecular Science-Pure and Applied Chemistry* **1996,** *A33* (10), 1399-1425.
3. Yan, D. Y.; Zhou, Y. F.; Hou, J. Supramolecular self-assembly of macroscopic tubes. *Science* **2004,** *303* (5654), 65-67.
4. Matyjaszewski, K. Architecturally complex polymers with controlled heterogeneity. *Science* **2011,** *333* (6046), 1104-1105.
5. Frechet, J. M. J. Functional polymers and dendrimers - reactivity, molecular architecture, and interfacial energy. *Science* **1994,** *263* (5154), 1710-1715.
6. Voit, B. Hyperbranched polymers - All problems solved after 15 years of research? *Journal of Polymer Science Part A-Polymer Chemistry* **2005,** *43* (13), 2679-2699.
7. Gao, C.; Yan, D. Hyperbranched polymers: from synthesis to applications. *Progress in Polymer Science* **2004,** *29* (3), 183-275.
8. Frechét, J. M. J.; Henmi, M.; Gitsov, I.; Aoshima, S.; Leduc, M. R.; Grubbs, R. B. Self-condensing vinyl polymerization - an approach to dendritic materials. *Science* **1995,** *269* (5227), 1080-1083.
9. Matyjaszewski, K.; Gaynor, S. G.; Müller, A. H. E. Preparation of hyperbranched polyacrylates by atom transfer radical polymerization .2. Kinetics and mechanism of chain growth for the self-condensing vinyl polymerization of 2-((2-bromopropionyl)oxy)ethyl acrylate. *Macromolecules* **1997,** *30* (23), 7034-7041.
10. Matyjaszewski, K.; Gaynor, S. G.; Kulfan, A.; Podwika, M. Preparation of hyperbranched polyacrylates by atom transfer radical polymerization .1. Acrylic AB* monomers in "living" radical polymerizations. *Macromolecules* **1997,** *30* (17), 5192-5194.
11. Matyjaszewski, K.; Gaynor, S. G. Preparation of hyperbranched polyacrylates by atom transfer radical polymerization .3. Effect of reaction conditions on the self-condensing vinyl polymerization of

2-((2-bromopropionyl)oxy)ethyl acrylate. *Macromolecules* **1997,** *30* (23), 7042-7049.
12. Baskaran, D. Hyperbranched polymers from divinylbenzene and 1,3-diisopropenylbenzene through anionic self-condensing vinyl polymerization. *Polymer* **2003,** *44* (8), 2213-2220.
13. Gong, F. H.; Tang, H. L.; Liu, C. L.; Jiang, B. B.; Ren, Q.; Yang, Y. Preparation of hyperbranched polymers through ATRP of in situ formed AB* monomer. *Journal of Applied Polymer Science* **2006,** *101* (2), 850-856.
14. Costello, P. A.; Martin, I. K.; Slark, A. T.; Sherrington, D. C.; Titterton, A. Branched methacrylate copolymers from multifunctional monomers: chemical composition and physical architecture distributions. *Polymer* **2002,** *43* (2), 245-254.
15. Isaure, F.; Cormack, P. A. G.; Graham, S.; Sherrington, D. C.; Armes, S. P.; Butun, V. Synthesis of branched poly(methyl methacrylate)s via controlled/living polymerizations exploiting ethylene glycol dimethacrylate as branching agent. *Chemical Communications* **2004,** (9), 1138-1139.
16. Gao, H.; Miasnikova, A.; Matyjaszewski, K. Effect of cross-linker reactivity on experimental gel points during ATRcP of monomer and cross-linker. *Macromolecules* **2008,** *41* (21), 7843-7849.
17. Gao, H. F.; Matyjaszewski, K. Synthesis of functional polymers with controlled architecture by CRP of monomers in the presence of cross-linkers: From stars to gels. *Progress in Polymer Science* **2009,** *34* (4), 317-350.
18. Konkolewicz, D.; Gray-Weale, A.; Perrier, S. The structure of randomly branched polymers synthesized by living radical methods. *Polymer Chemistry* **2010,** *1* (7), 1067-1077.
19. Liu, B. L.; Kazlauciunas, A.; Guthrie, J. T.; Perrier, S. Influence of reaction parameters on the synthesis of hyperbranched polymers via reversible addition fragmentation chain transfer (RAFT) polymerization. *Polymer* **2005,** *46* (17), 6293-6299.
20. Oh, J. K.; Siegwart, D. J.; Lee, H.-i.; Sherwood, G.; Peteanu, L.; Hollinger, J. O.; Kataoka, K.; Matyjaszewski, K. Biodegradable nanogels prepared by atom transfer radical polymerization as potential drug delivery carriers: Synthesis, biodegradation, in vitro release, and bioconjugation. *Journal of the American Chemical Society* **2007,** *129* (18), 5939-5945.
21. Poly, J.; Wilson, D. J.; Destarac, M.; Taton, D. Synthesis of poly(vinyl acetate) nanogels by xanthate-mediated radical crosslinking copolymerization. *Macromolecular Rapid Communications* **2008,** *29* (24), 1965-1972.
22. Poly, J.; Wilson, D. J.; Destarac, M.; Taton, D. A comprehensive investigation into "controlled/living" chain growth crosslinking copolymerization including a back to basics modeling. *J. Polym. Sci. Pol. Chem.* **2009,** *47* (20), 5313-5327.
23. Rosselgong, J.; Armes, S. P.; Barton, W. R. S.; Price, D. Synthesis of

branched methacrylic copolymers: comparison between RAFT and ATRP and effect of varying the monomer concentration. *Macromolecules* **2010,** *43* (5), 2145-2156.
24. Flory, P. J. Molecular size distribution in three dimensional polymers. I. Gelation. *Journal of the American Chemical Society* **1941,** *63*, 3083-3090.
25. Stockmayer, W. H. Theory of molecular size distribution and gel formation in branched polymers II General cross linking. *Journal of Chemical Physics* **1944,** *12* (4), 125-131.
26. Stockmayer, W. H.; Jacobson, H. Gel formation in vinyl-divinyl copolymers. *Journal of Chemical Physics* **1943,** *11* (8), 393-393.
27. Walling, C. Gel formation in addition polymerization. *Journal of the American Chemical Society* **1945,** *67* (3), 441-447.
28. Yu, Q.; Zhu, Y.; Ding, Y.; Zhu, S. Reaction behavior and network development in RAFT radical polymerization of dimethacrylates. *Macromolecular Chemistry and Physics* **2008,** *209* (5), 551-556.
29. Yu, Q.; Zhou, M.; Ding, Y.; Jiang, B.; Zhu, S. Development of networks in atom transfer radical polymerization of dimethacrylates. *Polymer* **2007,** *48* (24), 7058-7064.
30. Zheng, Y.; Newland, B.; Tai, H.; Pandit, A.; Wang, W. Single cyclized molecule structures from RAFT homopolymerization of multi-vinyl monomers. *Chemical communications (Cambridge, England)* **2012,** *48* (25), 3085-7.
31. Zheng, Y.; Cao, H.; Newland, B.; Dong, Y.; Pandit, A.; Wang, W. 3D single cyclized polymer chain structure from controlled polymerization of multi-vinyl monomers: beyond Flory-Stockmayer theory. *Journal of the American Chemical Society* **2011,** *133* (33), 13130-13137.
32. Wang, W.; Zheng, Y.; Roberts, E.; Duxbury, C. J.; Ding, L.; Irvine, D. J.; Howdle, S. M. Controlling chain growth: A new strategy to hyperbranched materials. *Macromolecules* **2007,** *40* (20), 7184-7194.
33. Koh, M. L.; Konkolewicz, D.; Perrier, S. A simple route to functional highly branched structures: RAFT homopolymerization of divinylbenzene. *Macromolecules* **2011,** *44* (8), 2715-2724.
34. Rosselgong, J.; Armes, S. P.; Barton, W.; Price, D. Synthesis of highly branched methacrylic copolymers: observation of near-ideal behavior using RAFT polymerization. *Macromolecules* **2009,** *42* (16), 5919-5924.
35. Yang, H.-J.; Jiang, B.-B.; Huang, W.-Y.; Zhang, D.-L.; Kong, L.-Z.; Chen, J.-H.; Liu, C.-L.; Gong, F.-H.; Yu, Q.; Yang, Y. Development of branching in atom transfer radical copolymerization of styrene with triethylene glycol dimethacrylate. *Macromolecules* **2009,** *42* (16), 5976-5982.
36. Li, Y. T.; Armes, S. P. Synthesis and chemical degradation of branched vinyl polymers prepared via ATRP: Use of a cleavable disulfide-based branching agent. *Macromolecules* **2005,** *38* (20), 8155-8162.

37. Rosselgong, J.; Armes, S. P. Quantification of intramolecular cyclization in branched copolymers by H-1 NMR spectroscopy. *Macromolecules* **2012,** *45* (6), 2731-2737.
38. Aleman, J.; Chadwick, A. V.; He, J.; Hess, M.; Horie, K.; Jones, R. G.; Kratochvil, P.; Meisel, I.; Mita, I.; Moad, G.; Penczek, S.; Stepto, R. F. T. Definitions of terms relating to the structure and processing of sols, gels, networks, and inorganic-organic hybrid materials (IUPAC Recommendations 2007). *Pure and Applied Chemistry* **2007,** *79* (10), 1801-1827.

Chapter Four

Synthesis of Water Soluble PEG-based Hyperbranched Polymers through Vinyl Oligomer Combination towards Biocompatible Hydrogels

Parts of this chapter have been published in:

Zhao, T., Zhang, H., Zhou, D., Gao, Y., Dong, Y., Greiser, U., Tai, H., Wang, W. 'Water Soluble Hyperbranched Polymers from Controlled Radical Homopolymerization of PEG Diacrylate' *RSC ADVANCES* **2015**, 5, 33823-33830.

4.1 Introduction

4.1.1 Hydrogels for Wound Healing

Hydrogels are hydrophilic polymer networks which can absorb from 10% up to thousands of times their dry weight in water. Hydrogels have been of great interest to biomaterial scientists for many years because of their hydrophilic character and potential to be biocompatible. Hydrogels based on both natural and synthetic polymers have continued to be of interest for encapsulation of cells[1, 2, 3, 4] and most recently such hydrogels have become especially attractive to the new field of wound healing as matrices for regenerating tissues or as skin substitutes. They provide a simple delivery procedure, minimize the patients' discomfort and reduce the scar formation as well as the infection risk[5]. These hydrogels can be applied to any wound size, shape or cavity with minimized invasive surgery, and then *in-situ* form a three-dimensional (3D) water content polymer network via physical or chemical cross-linking, which mimics precisely the mechanical and swelling/shrinking properties of the native tissue.[6]

The use of hydrogels in wound healing can date back to late 70s or early 80s. Hydrogels act as a moist wound dressing material and have the ability to absorb and retain the wound exudates along with the foreign bodies, such as bacteria, within its network structure[7]. In addition, hydrogels have been found to promote fibroblast proliferation by reducing the fluid loss from the wound surface and protect the wound from external noxae necessary for rapid wound healing. Hydrogels help in maintaining a micro-climate for biosynthetic reactions on the wound surface necessary for cellular activities. Fibroblast proliferation is necessary for complete epithelialisation of the wound, which starts from the edge of the wound. Since hydrogels help to keep the wound moist, keratinocytes can migrate on the surface. Hydrogels may be transparent, depending on the nature of the polymers, and provide cushioning and cooling/soothing effects to the wound surface. The main advantage of the transparent hydrogels includes monitoring of the wound healing without removing the wound dressing. The process of angiogenesis can be initiated by using semi-occlusive hydrogel dressings, which is initiated due to temporary hypoxia. Angiogenesis of the wound ensures the growth of granulation tissue by maintaining adequate supply of oxygen and nutrients to the wound surface. Hydrogel sheets are generally applied over the wound surface with backing of fabric or polymer film and are secured at the wound surface with adhesives or with bandages.

4.1.2 PEG-based Hydrogels

Poly(ethylene glycol) (PEG), otherwise known as poly(oxyethylene) or poly(ethylene oxide) (PEO), is one of the most widely used hydrogels in medicine and biomedicine. Hydrogels based on its derivatives-polyethylene glycol methacrylate (PEGMA), polyethylene glycol dimethacrylate (PEGDMA) and polyethylene glycol diacrylate (PEGDA) - are likewise widely applied. PEG hydrogels provide a unique niche for cell encapsulation, as they are highly biocompatible to the cells under proper polymerization conditions.[8] Through co-polymerization with other macromolecules, multiple functional moieties are readily introduced to suppress or promote cell survival and function.

While various methods of gelation (e.g. physical, ionic, or covalent interactions) can be used to form PEG gels, chemically or covalently-crosslinking leads to relatively stable hydrogel structures with tunable physicochemical properties such as permeability, molecular diffusivity, equilibrium water content, elasticity, modulus, and degradation rate[9, 10] (Figure 4.1). Furthermore, the introduction of degradable linkers into the covalent crosslinks permits the fabrication of well-defined network structures with tailorable properties in time.

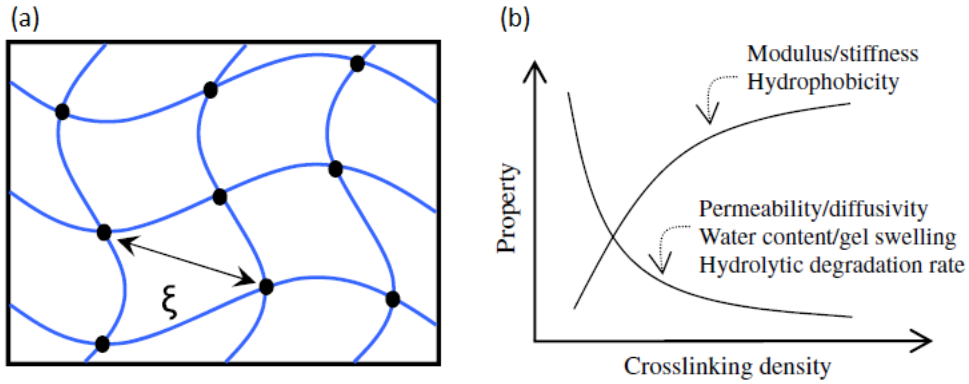

Figure 4.1 (a) Simplified crosslinked hydrogel structure. Black dots represent crosslinking point; ξ represents mesh size of the gel. (b) Hydrogel property as a function of gel crosslinking density.

Lin and Anseth discussed methods of PEG hydrogel formation[11]. They conclude that the synthesis of covalently crosslinked PEG gels falls into one of the following categories, according to the crosslinking reaction mechanism:[12] chain-growth, step-growth, or mixed-mode chain and step growth (Figure 4.2). Figure 4.2 (a) illustrates the network structure resulting

from the chain-growth polymerization of macromolecular PEG precursors. Typically, these networks are formed from functional PEG molecules, such as PEGDMA. Polymerization is initiated by reactive centers, such as radicals, generated from thermal energy, redox reactions, or the photo-cleavage of initiator molecules. These free radicals propagate through unsaturated vinyl bonds on the PEG macromolecular monomers and chain polymerization occurs. The propagation of free radicals through multiple carbon-carbon double bonds on the constituting PEG monomers results in covalently crosslinked, high molecular weight kinetic chains. The functionalities of the chain-growth polymerized hydrogels can be expanded through the copolymerization of other functional (meth)acrylated macromers. One disadvantage of chain-growth polymerization, compared to step-growth mechanism, is that it can lead to lower conversion of the functional groups. Therefore, when it is used in *in situ* polymerization, un-reacted monomers and/or functional groups remaining in the body may cause local inflammatory reaction or systematic immune response.[13] Furthermore, hydrogels made from chain-growth polymerization usually contain certain network non-idealities[14] that may adversely affect drug release performance and material properties.

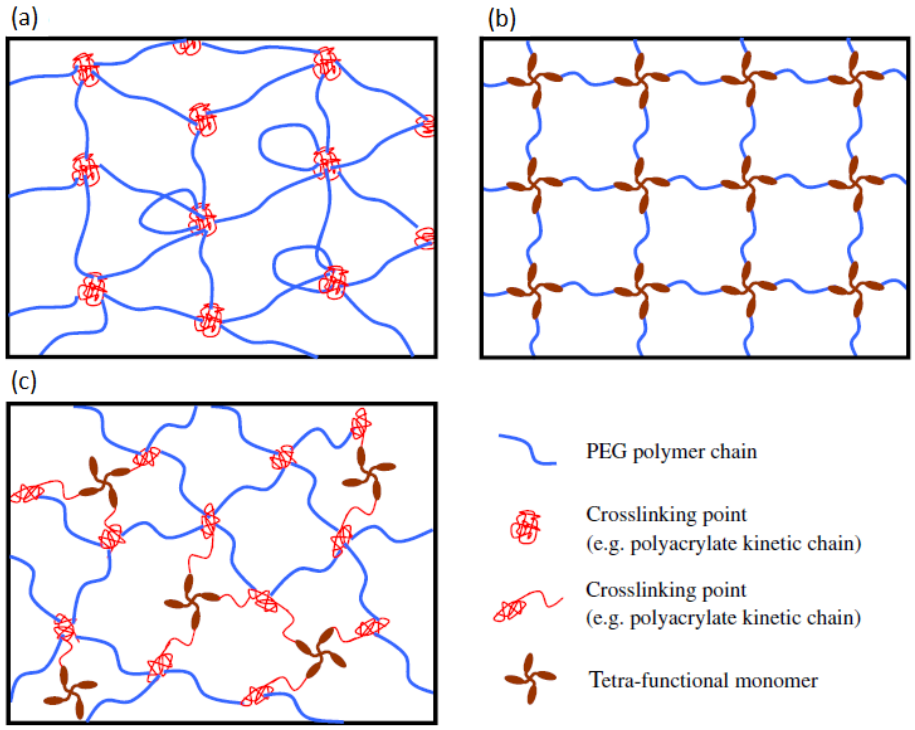

Figure 4.2 Schematic structures of PEG hydrogels formed via: (a) chain-growth, (b) step-growth, and (c) mixed-mode step and chain growth polymerization.

Of all the chain polymerization schemes, photopolymerization is one of the preferable ways to fabricate hydrogels. Hydrogels formed via photopolymerizations usually take minutes to complete, and hence, avoid persistent exposure of biomolecules to thermal energy - a condition generally not suitable for *in situ* encapsulation of fragile proteins and cells. The ability of photopolymerizations to produce stable hydrogel networks mildly and rapidly provides a convenient and efficient method for a variety of wound healing applications.

The step-growth gelation occurs when at least two multifunctional monomers with mutually reactive chemical groups are reacted together in either stoichiometric balanced or imbalanced ratio, and the average monomer functionality is greater than 2. This conjugation reaction can not only be performed under ambient conditions without the use of free-radical initiators, it also produces fewer structural defects during network formation[15] (Figure 4.2 (b)), which permits more precise control over the gel crosslinking density and subsequent material properties. Hubbell and colleagues developed a series of degradable hydrogels formed via step-growth Michael-type addition reaction between acrylated star PEG polymer and dithiol.[16, 17, 18, 19] The degradation products of these gels do not produce high molecular weight kinetic chains, which may not only exceed the glomerular filtration limit but may also induce host inflammatory or immune response. From the standpoint of protein delivery, Michael-type addition reactions decrease possible protein damage due to propagating free radicals as occurred in chain-growth polymerizations, but the presence of thiol groups may reduce the native disulfide bonds of the encapsulated proteins and cause protein denaturation, leading to decreased bioactivity and increased immunogenicity.

In addition to chain-growth and step-growth mechanisms, PEG hydrogel networks can also be formed from mixed-mode polymerizations that exhibit characteristics between chain and step-growth polymerizations as shown in Figure 4.2 (c).[20, 21, 22] This rapid gelation of mixed-mode polymerization overcomes the long polymerization time needed in most of the Michael-type addition reaction. Furthermore, functional macromers, such as peptides, can be incorporated at lower concentrations.[21, 22] Anseth, Bowman and their coworkers have developed a new type of PEG hydrogels based on the mixed-mode polymerization of acrylated monomers and multifunctional thiols.[20, 23, 24, 25, 26] In this approach, solutions with different molar ratios of thiol to acrylate groups were prepared, and the polymerization kinetics were examined either with or without the presence of initiators. Differing from thiol-acrylate Michael addition reaction, thiol-acrylate photopolymerization involves chain transfer of growing polymer chains to thiol monomers.[25] The

polymerization rates and acrylate conversion increased in the presence of photoinitiators, as more thiol groups were added. Unlike chain-growth photopolymerization, the use of initiator is not required in mixed-mode photopolymerizations; the initiator free mechanism has been studied by others.[24, 26] The network structure that results from this mechanism is directly impacted by the ratio of complimentary reactive groups. As the ratio of thiol to acrylate groups increases, the networks transition from being chain-like to more step-like. In the case of degradable mixed-mode hydrogels, the changes in material properties during degradation, such as swelling, can also be controlled by variations in thiolacrylate ratios. This change further permits the control of the molecular weight distributions of the degradation products, which is favorable in many wound healing applications because the degradation products can be naturally eliminated by renal filtration. Finally, spatial and temporal control is possible with the mixed-mode photopolymerization reactions.

4.1.3 Aims and Hypotheses

Based on vinyl oligomer combination approach demonstrated in the chapter 3, the aim of this chapter was to develop a PEG-based hyperbranched polymer as a precursor of a photo-crosslinkable hydrogel system, which could support fibroblast cells growth and proliferation, with the potential use as a bioactive temporary hydrogel dressing for wound healing applications.

Compared to the photo-crosslinking of small multi-vinyl monomers, one advantage of using the multivinyl polymer precursor is that there will be no concern about the un-reacted monomers remaining in the body which may cause local inflammatory reaction or systematic immune response[13]. Another advantage is that the hyperbranched polymer precursor synthesized by controlled radical polymerization may reduce the network defects or non-idealities in hydrogels[14] that may adversely affect mechanical properties, moist maintenance properties, swelling performance and other wound healing properties. Furthermore, the crosslinking efficiency could be faster for the multifunctional hyperbranched polymer than the small monomers because of their huge molecular size and abundant vinyl groups. The hypotheses of this chapter are as below:

1. PEG-based hyperbranched polymers with high degree of branching, high content of vinyl functional groups and high monomer conversion can be achieved by homopolymerization of PEG diacrylate monomers without gelation via vinyl oligomer combination strategy.

2. The high content of vinyl functional groups will lead to an efficient photo-crosslinking property and can be adjusted by varying the polymer composition.

3. PEG-based polymer composition should not result in toxicity to cells.

In this study, two poly(ethylene glycol) diacrylates (PEGDA) ($PEGDA_{575}$, average M_n=575; $PEGDA_{700}$ average M_n=700) having different lengths of PEG spacers (n =10, 13, respectively, as shown in Figure 4.3) were homopolymerized in a concentrated solution ([PEGDA] = 60% w/v) via *in situ* DE-ATRP to produce a series of water-soluble hyperbranched polymers. The polymerization will undergo a slow vinyl propagation process of divinyl monomers followed by a polycondensation or coupling of reactive oligomers. The relative propensities for intermolecular propagating/cross-linking reactions and intramolecular cyclization were assessed using gel permeation chromatography (GPC)/viscosity and ^{1}H NMR measurements. Finally, the concentration-dependent phase transition behaviors of the obtained poly($PEGDA_{575}$)s were discovered and evaluated.

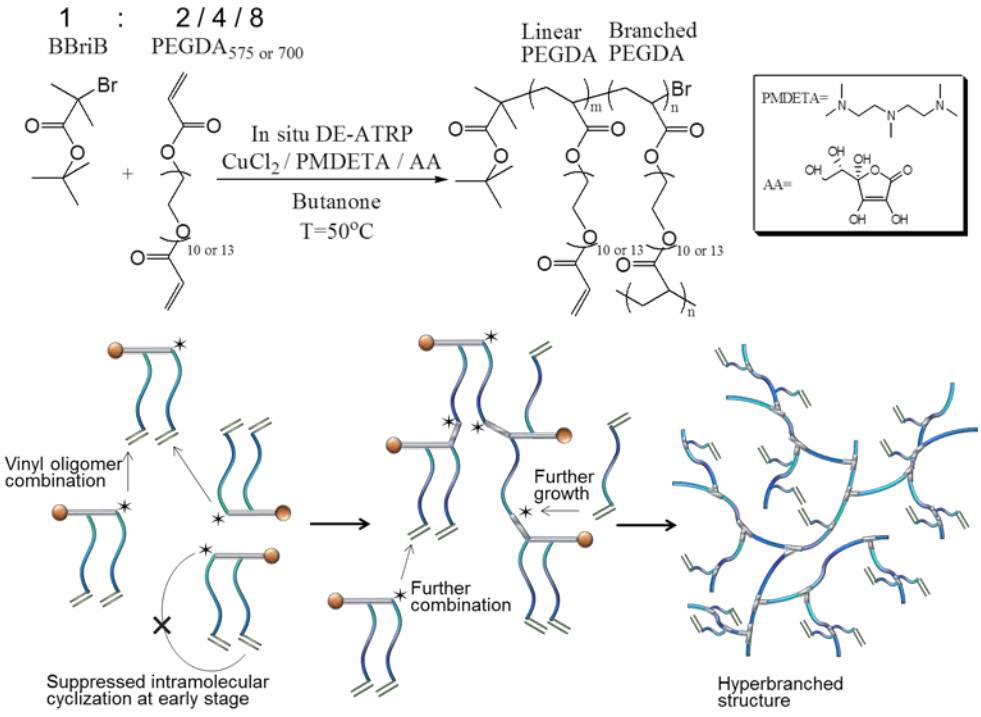

Figure 4.3 Homopolymerization of poly(ethylene glycol) diacrylate through vinyl oligomer combination strategy and a schematic mechanism of the reaction towards a hyperbranched structure.

4.2 Experimental

4.2.1 Materials

Poly(ethylene glycol) diacrylate ($PEGDA_{575}$ and $PEGDA_{700}$, 98% Sigma-Aldrich), tert-butyl bromoisobutyrate (BBriB, 98%, Aldrich), pentamethyldiethylenetriamine (PMDETA, 99%, Aldrich), copper (II) chloride ($CuCl_2$, 97%, Aldrich), L-ascorbic acid (AA, 99%, Aldrich), d-chloroform (99.8%, Aldrich), 2-butanone (HPLC grade, Aldrich), chloroform (HPLC grade, Aldrich), n-hexane (ACS reagent grade, Aldrich) and diethyl ether (ACS reagent grade, Aldrich) were used as received.

4.2.2 Synthesis of Hyperbranched Poly(PEGDA)s

The polymers were prepared in two-neck round bottom flasks. 2-butanone, $CuCl_2$ (67.3 mg, 1 equiv) and PMDETA (173 mg, 2 equiv) were added into the flask. PEGDA monomer were added for different initiator-to-monomer ratios: poly($PEGDA_{575}$) 1:2 (BBriB 4.46g, 40 equiv and $PEGDA_{575}$ 23g, 80 equiv); poly($PEGDA_{575}$) 1:4 (BBriB 2.23g, 20 equiv and $PEGDA_{575}$ 23g, 80 equiv); poly($PEGDA_{575}$) 1:8 (BBriB 1.12g, 10 equiv and $PEGDA_{575}$ 23g, 80 equiv); poly($PEGDA_{700}$) 1:2 (BBriB 4.46g, 40 equiv and $PEGDA_{700}$ 28g, 80 equiv); poly($PEGDA_{700}$) 1:4 (BBriB 2.23g, 20 equiv and $PEGDA_{700}$ 28g, 80 equiv); poly($PEGDA_{700}$) 1:8 (BBriB 1.12g, 10 equiv and $PEGDA_{700}$ 28g, 80 equiv). Oxygen was removed by bubbling argon through the solutions for 20 mins. AA solution (173µl of 0.1 mg/µl AA/H_2O solution, 0.2 equiv) was pipetted into the flasks under positive pressure of argon before the flask was immersed in a pre-heated oil bath at 50˚C. The solution was stirred at 800 rpm and the polymerization was conducted at 50˚C in an oil bath for the required reaction time. The experiment was stopped by opening the flask and exposing the catalyst to air. The solution was then diluted with THF and precipitated into a large excess of cold diethyl ether to remove the monomers. The precipitated mixture was dried under laminar flow then re-dissolved in acetone, followed by three times of passing through an Al_2O_3 column. The mixture was then dried under vacuum.

4.2.3 Characterization Method

Molecular weight determination by gel permeation chromatography (GPC): Small samples were withdrawn from the reaction at specific time

intervals using a glass syringe with luer needle under positive pressure of argon. These aliquots were then diluted in chloroform and filtered through an Al_2O_3 pipette for chromatography followed by a 0.4μm filter before analysis. The molecular weight and molecular weight distribution of each sample was determined using a GPC PL-50 (Agilent) instrument with triple detectors (RI, viscosity and LS). Chromatography was performed with two sequential columns (30 cm PL gel Mixed-C columns) at 40°C using chloroform as eluent with a flow rate of 1 ml/min. The RI and viscosity detector were calibrated with a series of 12 near-monodisperse PMMA standards (M_p from 690 to 1,944,000 $g \cdot mol^{-1}$, Agilent).

Nuclear magnetic resonance (NMR) spectroscopy: The polymers were dissolved in $CDCl_3$ for ^1H NMR analysis. ^1H NMR analysis was carried out on a S4 300 MHz Bruker NMR with MestReNova processing software. The chemical shifts were referenced to the lock chloroform (7.26 ppm). The ^1H NMR spectrum confirmed the presence of each monomer in the polymer structure and the presence of free vinyl groups.

Phase transition temperature measurement: The phase transition temperatures were determined in water by turbidity measurement on a temperature-controlled UV-vis spectrometer (Beckman DU-800). The light transmittance of polymer aqueous solutions of different concentrations was measured with a wavelength of 500 nm at temperatures from 5 to 70 ^oC (heating rate = 0.5 ^oC/second). The data were collected every 2 seconds. The phase transition temperatures were defined as the temperature point corresponding to 90% transmittance of aqueous solution during the heating process.

4.2.4 Preparation of Photo-crosslinked Hydrogels

The polymer solution was mixed with the photoinitiator Irgacure 2959[27] to reach a final concentration of 30% (w/v) of polymer and 0.2% (w/v) of photoinitiator, and cured with a spot-curing UV light source (OmniCure S1000, LumenDynamics Group Inc.) equipped with a filter in the range of 320 to 390 nm. This wavelength range has been previously used to promote the encapsulation of cells in photocurable materials, with minimal cytotoxicity[28]. The UV crosslinking process was carried out in a 96-well plate with 50 μl of polymer/ photoinitiator solution in each well. The curing time was 30 seconds. The light intensity was 0.38W/cm^2 unless otherwise specified.

4.2.5 Cytotoxicity Assessment

2D culture of 3T3 mouse fibroblast cell line was utilized for the cytotoxicity assessment. 5,000 cells and Dulbecco's Modified Eagle's Medium (DMEM, Sigma) were seeded into each well of a 96-wells culture plate with or without the photo-crosslinked hydrogels. After one, three and five days of incubation at 37 ^{o}C and 5% CO_2, alamarBlue® reduction method was used to assess cell metabolic activity. The absorbance at the lower wavelength filter (550 nm) was measured followed by the higher wavelength filter (595 nm) via a thermo scientific Varioskan Flash Plate Reader. The following equations were used to calculate the percentage of cell viability:

AO_{LW} = absorbance of oxidized form of alamarBlue® along at lower wavelength;

AO_{HW} = absorbance of oxidized form of alamarBlue® along at higher wavelength;

Calculated correlation factor:

$$Ro = AO_{LW} / AO_{HW} \quad \text{Eq. 4.1}$$

Calculated the percentage of reduced alamarBlue®:

$$AR_{LW}\ \% = (A_{LW} - A_{HW} \times Ro) \times 100 \quad \text{Eq. 4.2}$$

4.2.6 Statistical Analysis

Comparisons between multiple groups were analyzed via one way-ANOVA using GraphPad Prism 5 software. Differences between two data sets were considered significant when $p < 0.05$.

4.3 Results and Discussions

4.3.1 Synthesis and Characterization of The PEG-based HBPs

To facilitate the intermolecular branching, the molar ratios of initiator to divinyl monomer were set as 1:2, 1:4 and 1:8 for both $PEGDA_{575}$ and $PEGDA_{700}$. The reaction conditions and the molecular weight information of

the polymers at different time points were listed in Table 4.1. It is known that in ATRP reaction, a high initiator concentration will lead to a shift in equilibrium towards the active radicals. And this usually results in a high concentration of radicals which terminate efficiently, leaving an excess of X-Cu^{II}, known as the persistent radical effect (PRE). To eliminate the termination, large amount of Cu^{II} was introduced initially to stabilize the equilibrium and keep the radical concentration low. Therefore, despite of the high initiator concentration, most of the initiators were in their dormant state because of the enhanced deactivation. Meanwhile, 20% of reducing agent and extra amount of ligand was used to (re)generate Cu(I) and thus maintained the reaction rate to an acceptable level. The polymer chain growth was monitored using GPC at regular time intervals during the reaction (Figure 4.4 and Figure 4.5). The traces showed similar evolution of molecule growth in the reaction system. Multimodal peaks at the early stage (before 1.5h) indicate the formation of monoadducts of monomer and initiator as well as a certain portion of oligomers. The appearance of more broadened peaks at later stages suggests that the combination of lower molecular weight oligomers became the dominant reaction pathway. It is likely that at later stages of the reaction, when most of the monomers were already consumed, the reaction conditions were more favorable for statistical branching rather than for linear growth. Living character of the growing chains was demonstrated by a peak shift in the GPC trace from oligomers to larger molecules throughout the reaction, while molecular weights and the polydispersity index increased significantly (Table 4.1), indicating the formation of a hyperbranched structure. It can be seen from the GPC trace that the monomer conversion is high (Figure 4.4 and Figure 4.5), especially for the higher ratio of initiator to monomer (1:2 and 1:4). By precipitation in diethyl ether, the monomers and some lower molecular weight polymers were removed, leaving only the highly branched polymers with higher average molecular weight (as seen from the insertion of Figure 4.4 and 4.5). Thus, the molecular weight of the final products (Table 4.2) is significantly higher than that monitored during the reactions (Table 4.1).

Table 4.1 Molecular weight of poly(PEGDA)s at different time points during the polymerization processes, monitored by GPC RI detector.

Diacrylate	I:M [a]	Time	Conv. [b]	$M_{n, RI}$	$M_{w, RI}$	PDI
$PEGDA_{575}$	1:2	1.5h	68%	2.7k	5.2k	1.9
		3.0h	88%	4.7k	15.7k	3.3
		4.5h	96%	85k	122.5k	14.5
	1:4	1.5h	59%	2.7k	4.2k	1.6
		3.0h	80%	4.7k	12.2k	2.6
		4.5h	89%	7.0k	38.1k	5.4
		6.0h	94%	11.2k	107.4k	9.6
	1:8	1.5h	39%	2.6k	3.7k	1.5
		3.0h	59%	4.4k	8.8k	2.0
		4.5h	72%	6.3k	16.9k	2.7
		6.0h	77%	8.4k	39.8k	4.8
$PEGDA_{700}$	1:2	1.5h	47%	3.0k	4.1k	1.4
		3.0h	83%	4.8k	10.1k	2.1
		4.5h	91%	6.7k	22.9k	3.4
	1:4	1.5h	28%	2.8k	3.4k	1.2
		3.0h	68%	5.8k	11.9k	2.1
		4.5h	79%	7.6k	21.6k	2.8
		6.0h	93%	14.0k	89.2k	6.4
	1:8	1.5h	15%	2.7k	3.0k	1.1
		3.0h	47%	5.3k	9.0k	1.7
		4.5h	64%	7.3k	15.1k	2.1
		6.0h	71%	10.0k	32.3k	3.2

[a] [M]/[I]/[$CuCl_2$]/[PMDETA]/[AA] = 80/x(=40; 20; 10)/1/2/0.2, M: polyethylene glycol diacrylate, I: tert-Butyl α-bromoisobutyrate (BBriB), PMDETA: 1,1,4,7,7-pentamethyldiethylenetriamine, AA: L-Ascorbic Acid, Solvent: 2-butanone; [b] Monomer conversion is determined by the integration of polymer and monomer peaks in the GPC-RI trace.

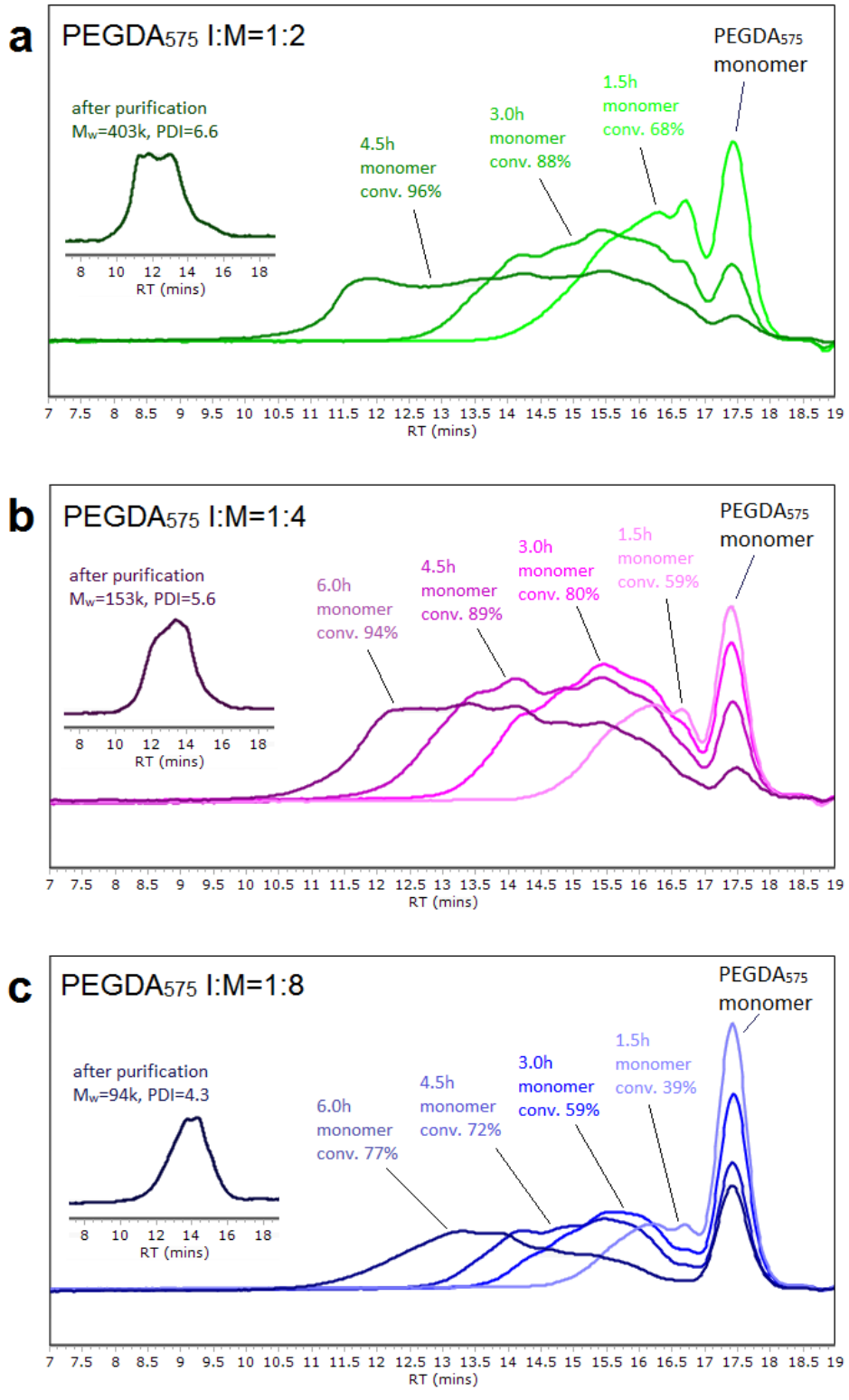

Figure 4.4 Time dependence of the composition of the polymerization mixture for the poly(PEGDA$_{575}$) syntheses, as monitored by GPC. The inserts are the GPC traces of the final product after purification.

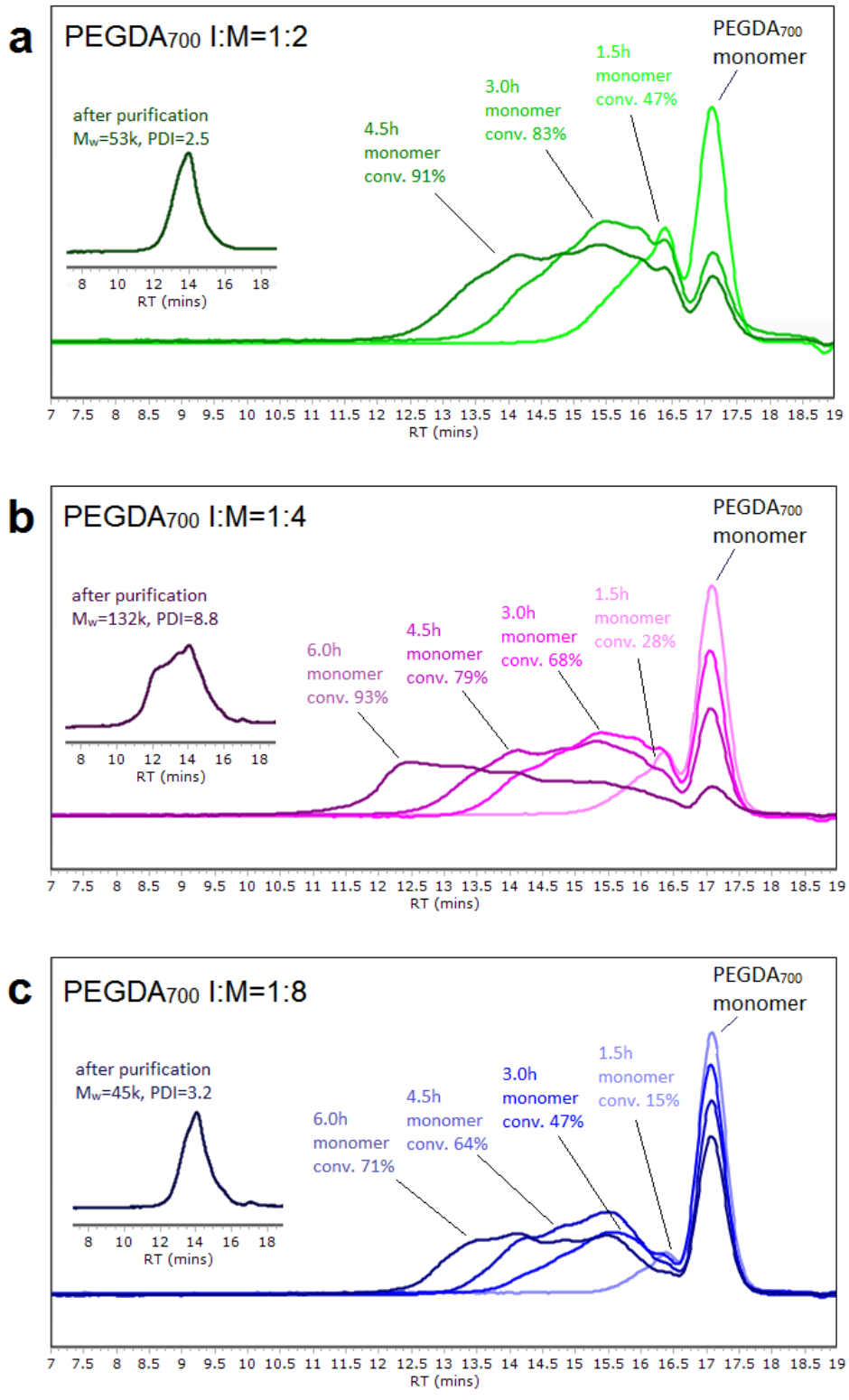

Figure 4.5 Time dependence of the composition of the polymerization mixture for the poly(PEGDA$_{700}$) syntheses, as monitored by GPC. The inserts are the GPC traces of the final product after purification.

Table 4.2 Homopolymerization of PEGDA via in situ DE-ATRP, using tert-Butyl α-bromoisobutyrate as initiator and 2-butanone as solvent with a diacrylate concentration of 60% w/v at 50˚C.

	Diacrylate	I:M [a]	Time	Monomer Conv. [b]	Yield [c] (%)	M_w (M_w/M_n) GPC-RI [d]	M_w (M_w/M_n) GPC-vis [d]	Vinyl content [e]	Branch ratio [e]	Initiator content [f]	α [g]
1		1:2	4.5h	95.6%	68%	403 k (6.6)	531 k (16.1)	37.3%	62.7%	41.1%	0.40
2	$PEGDA_{575}$	1:4	6h	94.1%	65%	153 k (5.6)	279 k (14.5)	52.7%	47.3%	27.8%	0.34
3		1:8	6h	76.9%	54%	94 k (4.3)	177 k (11.7)	61.8%	38.2%	19.0%	0.32
4		1:2	4.5h	90.5%	45%	53 k (2.5)	71 k (4.9)	40.7%	59.3%	44.2%	0.35
5	$PEGDA_{700}$	1:4	6h	93.2%	50%	132 k (8.8)	184 k (11.1)	56.6%	43.4%	29.5%	0.41
6		1:8	6h	70.9%	46%	45 k (3.2)	65 k (3.8)	67.6%	32.4%	21.5%	0.33

[a] [M]/[I]/[$CuCl_2$]/[PMDETA]/[AA] = 80/x(=40; 20; 10)/1/2/0.2, M: polyethylene glycol diacrylate, I: tert-Butyl α-bromoisobutyrate (BBriB), PMDETA: 1,1,4,7,7-pentamethyldiethylenetriamine, AA: L-Ascorbic Acid, Solvent: 2-butanone; [b] Monomer conversion is determined by the integration of polymer and monomer peaks in the GPC-RI trace; [c] Diethyl ether-insoluble part; [d] M_n, M_w are determined by GPC equipped with triple detectors using PMMA as standards in chloroform; [e] Calculated by ^{1}H NMR as seen in Figure 4.7 and Figure 4.8 and Eq. 4.3-4.4; [f] Mole ratio of initiator/PEGDA unit, calculated by ^{1}H NMR as seen in Figure 4.7 and Figure 4.8 and Eq. 4.5; [g] Mark-Houwink exponent α.

In order to develop a useful method for effective preparation of branched polymers, it is necessary to find a condition for the use of a higher monomer concentration. Our attempts have demonstrated that both high monomer conversion and hyperbranched polymer structure could be obtained by homopolymerization of diacrylates with high ratio of initiator at a high monomer concentration (60% w/v).

The determination of the molecular weight of branched polymers is complicated by the fact that the hydrodynamic volume for a given molecular weight differs tremendously from that of a linear sample. Therefore, the use of a linear calibration curve in GPC leads to erroneous results. This problem can be overcome by the use of mass-sensitive online detectors, such as a light scattering detector or a viscosity detector using the universal calibration principle. In this study, the characterization of the purified products was summarized in Table 4.2. Characterization of the obtained poly(PEGDA)s was conducted by GPC/RI and GPC/viscosity to overcome the erroneous results caused by different hydrodynamic volumes of molecules in different solvents. The weight-average molecular weights for all of the poly(PEGDA)s - as determined by GPC/viscosity - are apparently higher than those obtained from GPC/RI (Table 4.2), indicating that the products possess highly branched structures rather than linear structures.

The Mark-Houwink plots for the obtained poly(PEGDA)s and a linear counterpart (Figure 4.6) show that as the molecular weight increases, the viscosity of the obtained poly(PEGDA)s increases less than that of the linear one. The Mark-Houwink exponents of poly(PEGDA)s are significantly low (α=0.3~0.4), indicating a more compact dense structure.

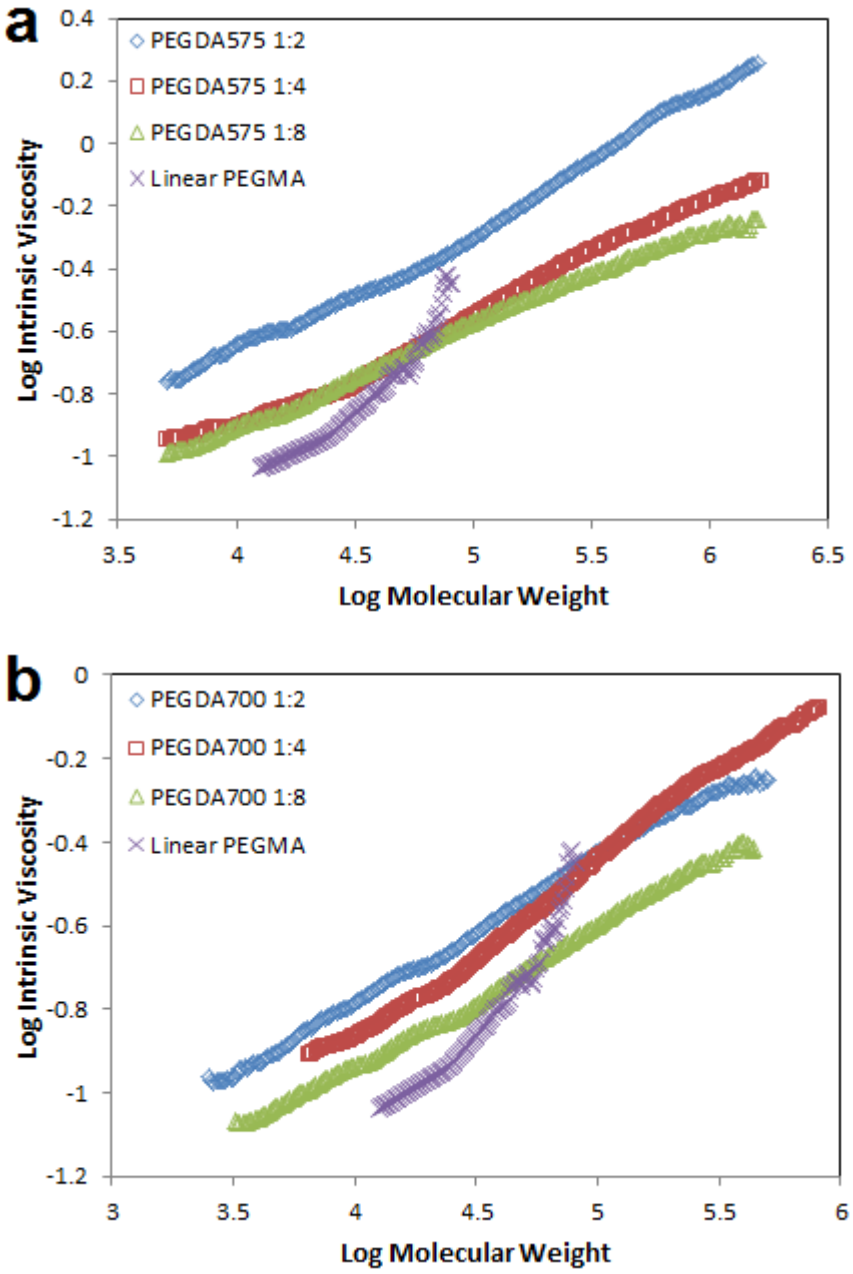

Figure 4.6 Mark-Houwink plots for the polymers obtained by homopolymerization of (a) $PEGDA_{575}$ and (b) $PEGDA_{700}$ with different initiator-to-monomer ratios. The Mark-Houwink plots of a linear polymer from ATRP of poly(ethylene glycol) methyl ether acrylate (polyPEGMA, M_n=48k, PDI=1.24) is given for comparison. The Mark-Houwink exponents of poly(PEGDA)s are significantly low (α=0.3~0.4), indicating a more compact dense structure compared to the linear analogue.

^{1}H-NMR analysis for the poly(PEGDA)s (Figure 4.7, Figure 4.8 and Eq. 4.3-4.5) demonstrates the existence of a high amount of vinyl functional groups at characteristic peaks between 6.5 ppm and 5.7 ppm. The vinyl content and branch ratio is outlined in Table 4.2. The vinyl content decreases reasonably with increasing the initiator-to-monomer ratio because more vinyl groups are consumed by the addition to the halogen-containing initiator at the early stage and by the chain combination at the later stage. The calculations also showed that these polymers possess a high branch ratio, which is the highest for poly($PEGDA_{575}$) 1:2 (62.7%, Table 4.2). This value indicates that ~6 branching unit exists for every 10 PEGDA units linked together in a -C-C- chain.

The initiator contents of the polymers were also summarized in Table 4.2. The ratios of the initiator/PEGDA units were generally proportional to their initial feed ratios. The polymers with initial feed ratios of 1:4 and 1:8 contain higher initiator contents than the theoretical contents due to the high initiation efficiency and the incomplete conversion of PEGDA monomers. In contrast, the polymers with initial feed ratios of 1:2 contain lower initiator contents than the theoretical contents possibly because of the consumption of initiator from the termination reaction at the early stage due to the high initiator concentration. The initiator content in the polymer products is lower than the content of the branching unit for all the poly(PEGDA)s, indicating that more than one connection per primary chain exists and that there is still a certain number of ‘loops’ existing in the polymer products. The formation of the ‘loops’ could be attributed to the secondary intramolecular reaction at later stages when the local concentration of both pendent vinyl and initiation site increased. The flexibility of the PEGDA units and the increasing mobility of macromolecules at later stage might also account for the intramolecular reaction. The proportion of the ‘loops’ in the polymer can be calculated as the proportion of the branching units over the initiator units. It is noteworthy that the proportions of ‘loops’ in poly($PEGDA_{575}$)s (~20%) are higher than that in poly($PEGDA_{700}$)s (~15%), giving the speculation that the diacrylate with shorter lengths of PEG spacers may induce more intramolecular reaction due to higher local concentration of pendent vinyl groups. Free vinyl groups were also left within the poly(PEGDA)s (Figure 4.7 and Figure 4.8), thus providing a photo-crosslinking capability or an opportunity for a range of post functionalization.

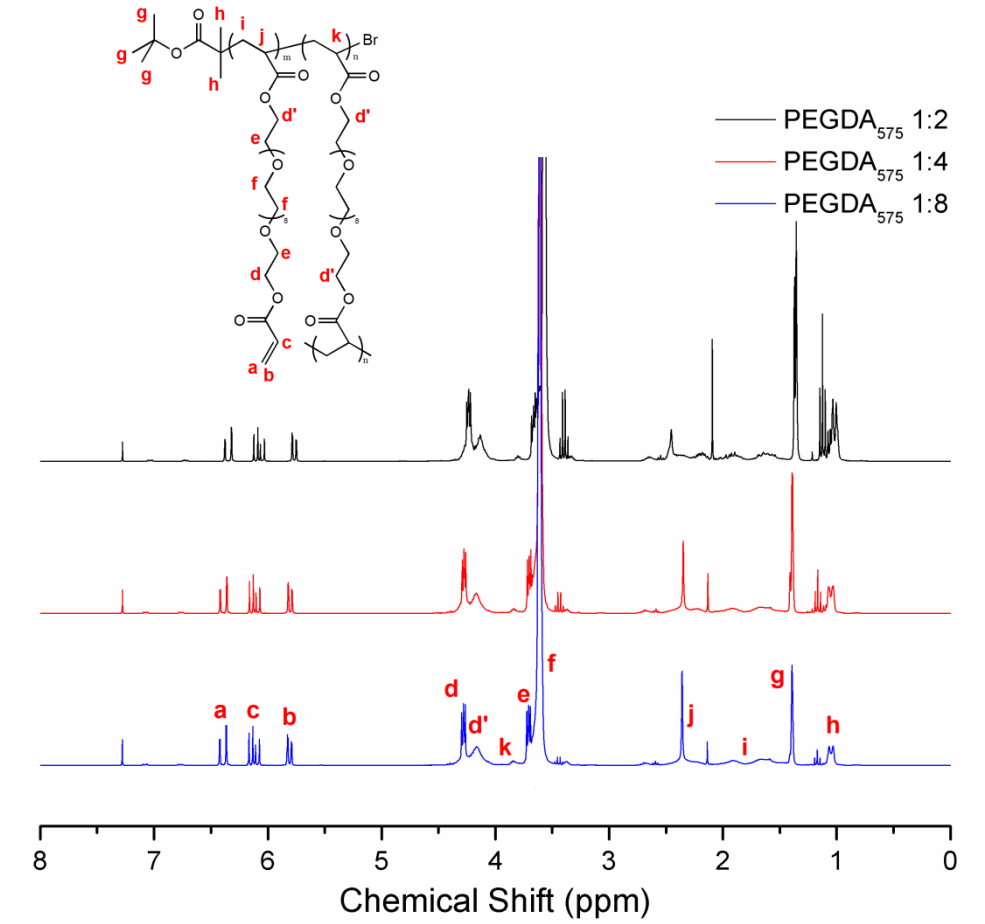

Figure 4.7 ^{1}H NMR spectroscopy of purified polymers obtained by homopolymerization of $PEGDA_{575}$ with different initiator-to-monomer ratios. The poly(PEGDA)s composition was determined by integrating a, d, d' and g peaks (Figure 4.7). Eq. 4.3-4.5 outline the calculations.

$$\text{Vinyl content (mol\%)} = \frac{a}{(d+d')/4} \qquad \text{Eq. 4.3}$$

$$\text{Branch ratio (mol\%)} = 1-\frac{a}{(d+d')/4} \qquad \text{Eq. 4.4}$$

$$\text{Initiator content (mol\%)} = \frac{g/9}{(d+d')/4} \qquad \text{Eq. 4.5}$$

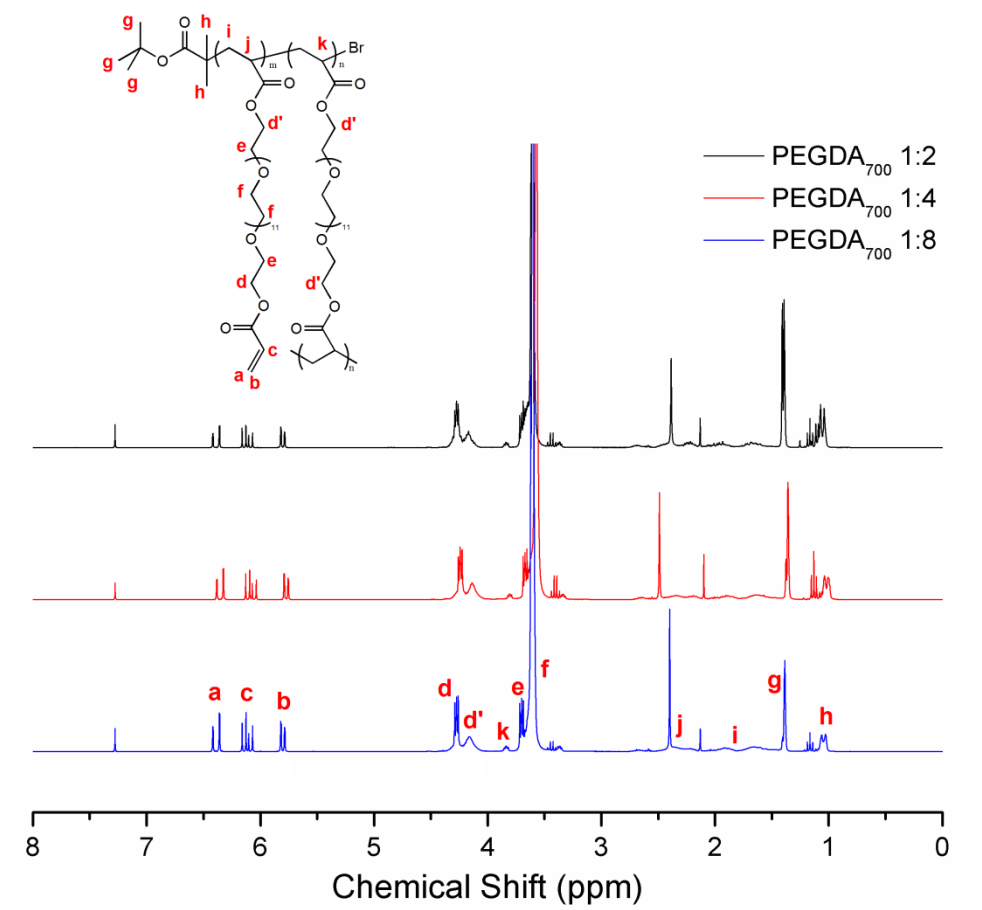

Figure 4.8 ^{1}H NMR spectroscopy of purified polymers obtained by homopolymerization of PEGDA$_{700}$ with different initiator-to-monomer ratios. The poly(PEGDA)s composition was determined by integrating a, d, d' and g peaks (Figure 4.8). Eq. 4.3-4.5 outline the calculations.

4.3.2 Thermoresponsive Behavior of Poly(PEGDA$_{575}$)

Both poly(PEGDA$_{575}$)s and poly(PEGDA$_{700}$)s were soluble in polar solvents (including water and methanol) as well as in many organic solvents (e.g. THF and chloroform). The products obtained from PEGDA$_{700}$ show good solubility in aqueous solution due to the longer PEG chains which can provide a higher hydrophilicity to the molecules, whereas the products from PEGDA$_{575}$ were found to exhibit a reversible thermoresponsive property in distilled water. It is worth mentioning that unlike the phase transition of some linear PEG-PLGA-PEG or PEG-PCL-PEG polymer, which could turn the whole solution into an immobile state or a physical gel, the phase transition behavior for these poly(PEGDA$_{575}$)s is more like a precipitation process followed by a phase separation into binary layers, especially at low concentration. This phenomenon could be attributed to the hyperbranched

structure which shows lower viscosity and has less interaction with the solvent than the linear structure. So when the environment is favored for the phase transition, these less entangled hyperbranched molecules tend to be separated out from their original solutions.

The thermally induced phase transition behavior in water was monitored by raising the temperature from 5 to 70˚C and measuring the temperature at the onset of cloudiness. It is well known that thermoresponsive polymer chains in solution adapt an expanded coil conformation and that they collapse at phase transition temperature to form compact globules. The globules aggregate in the absence of mechanisms that reduce surface tension, subsequently causing turbidity and the formation of visible particles. Many previous studies have explored the phase transition temperature for PEG based polymers in a low polymer concentration (typically 0.2% w/v). However, we found that the reversible phase transition temperature of our poly($PEGDA_{575}$)s is also strongly dependent on polymer concentration[29].

As shown in Figure 4.9 (a), the lower critical solution temperatures (LCSTs) for the poly($PEGDA_{575}$)s with different initiator/monomer ratio (1:2, 1:4 and 1:8) appear at the polymer concentration of ~2.5% w/v. The LCST values are 9˚C, 21˚C and 31˚C for poly($PEGDA_{575}$) 1:2, poly($PEGDA_{575}$) 1:4 and poly($PEGDA_{575}$) 1:8, respectively. The initiator end group and the carbon-carbon backbone are hydrophobic components, whereas the PEG chains are hydrophilic components. The difference in LCST could be mainly attributed to the different hydrophobic/hydrophilic composition of the products, since more PEGDA units would enhance the polymer-water hydrogen bonding interaction and thus expand the temperature range of miscibility, whereas more initiator end group or longer backbone would lower the LCSTs by bringing higher thermodynamic cost of solvation.

It can be noted that the phase transition temperature for all of the three poly($PEGDA_{575}$)s changed with a similar trend, but with different changing rates. The poly($PEGDA_{575}$) 1:4 increased dramatically from 21˚C to 65˚C with the polymer concentration raised from 2.5% to 60% w/v. However, the increase is more gentle for the poly($PEGDA_{575}$) 1:2 and the poly($PEGDA_{575}$) 1:8. It is known that the phase transition temperature of a polymer is dependent upon a series of factors affecting solubility. And it has been reported that increasing molecular weight (MW) tends to depress the phase transition temperature and broadens the phase transition lines due to an increasing energy cost of solvation. This could explain why the poly($PEGDA_{575}$) 1:2 which has a M_w of 403kDa shows a more steady line than the poly($PEGDA_{575}$) 1:4 which has a M_w of 153kDa. This tendency is well confirmed in Figure 4.9 (b), in which the phase transition behavior of

poly(PEGDA$_{575}$) 1:4 with different MW were studied. The polymers were prepared at different time points of polymerization and summarized in Table 4.3. The branch ratios for these polymers were similar but the molecular weight showed a significant difference. As can be seen in Figure 4.9 (b), with an increase in MW, the phase transition temperature drops slightly at each polymer concentration and the phase transition line becomes broader.

The poly(PEGDA$_{575}$) 1:8 also showed a steady change of phase transition temperature despite of having the lowest MW. This could be attributed to the longer hydrophobic backbone in the poly(PEGDA$_{575}$) 1:8. It can be noted that the phase transition temperature for the poly(PEGDA$_{575}$) 1:8 is maintained between 30˚C to 40˚C for a wide range of concentration. This phase transition property around body temperature holds great potential for biomedical applications in various areas such as smart hydrogels and drug delivery.

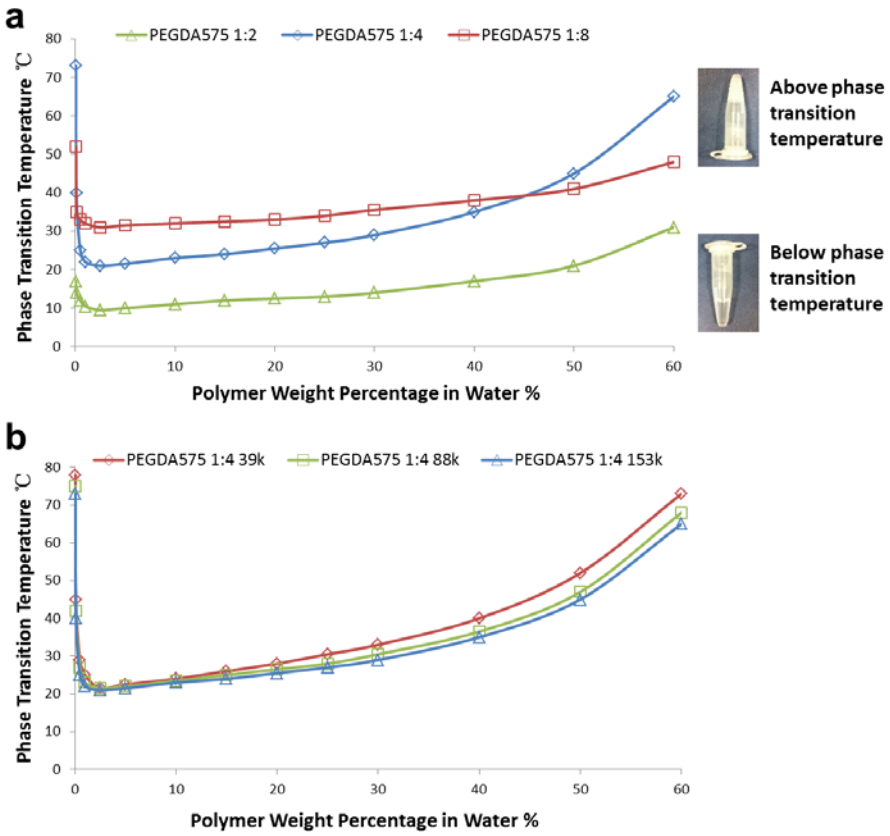

Figure 4.9 Thermoresponsive properties of the obtained homopolymers of PEGDA$_{575}$: (a) Phase transition temperature of the poly(PEGDA$_{575}$)s in distilled water at different concentrations. (b) Comparison of phase transition temperature of the poly(PEGDA$_{575}$)s 1:4 obtained at different times of polymerization with different molecular weight.

Table 4.3 Molecular weight of purified poly($PEGDA_{575}$) 1:4 at different reaction time, monitored by GPC-RI detector. These polymers were used for the phase transition study.

Polymer	Time	M_w(kg/mol) (M_w/M_n)[a]	Branch ratio (%) [b]	Initiator content (%) [b]	Initiator content (% of PEGDA unit)[b]
poly($PEGDA_{575}$) 1:4	3.0h	39 (1.9)	40.7	32.1	29.7
	4.5h	88 (2.9)	43.9	30.2	28.6
	6.0h	153 (5.6)	47.3	27.8	27.8

[a] M_n, M_w are determined by GPC equipped with an RI detector using PMMA as standards in chloroform; [b] Calculated by ^{1}H NMR of the purified polymers.

4.3.3 Photo-crosslinked Hydrogels and Cytotoxicity Assessment

The hyperbranched poly(PEGDA)s (final concentration 30%, w/v) was mixed with the photoinitiator Irgacure 2959 (final concentration 0.2%, w/v)[27] and cured with a spot-curing UV light source (OmniCure S1000, LumenDynamics Group Inc.) equipped with a filter in the range of 320 to 390 nm. This wavelength range has been previously used to promote the encapsulation of cells in photocurable materials, with minimal cytotoxicity[28]. The UV crosslinking process was carried out in a 96-well plate with 50 µl of polymer/ photoinitiator solution in each well. Gelation was observed within 15 seconds of UV curing. To facilitate a more sufficient gelation and minimize the unreacted vinyl groups, the curing time was set as 30 seconds. The light intensity was 0.38W/cm^2 unless otherwise specified.

AlamarBlue assay was implemented for the cytotoxicity assessment of the hydrogels and 3T3 mouse fibroblast cells were evaluated. The UV crosslinked hydrogels were washed 5 times with DMEM medium before the cell seeding. 5,000 of 3T3 mouse fibroblast cells were seeded onto the hydrogel surface in each well of a 96-well tissue culture plate. 100µl of DMEM medium was then added to each culture well. A blank well without hydrogels was treated with the same procedure and analyzed as a control. The alamarBlue® reduction method was used to assess changes in cell viability after one, three and five days.

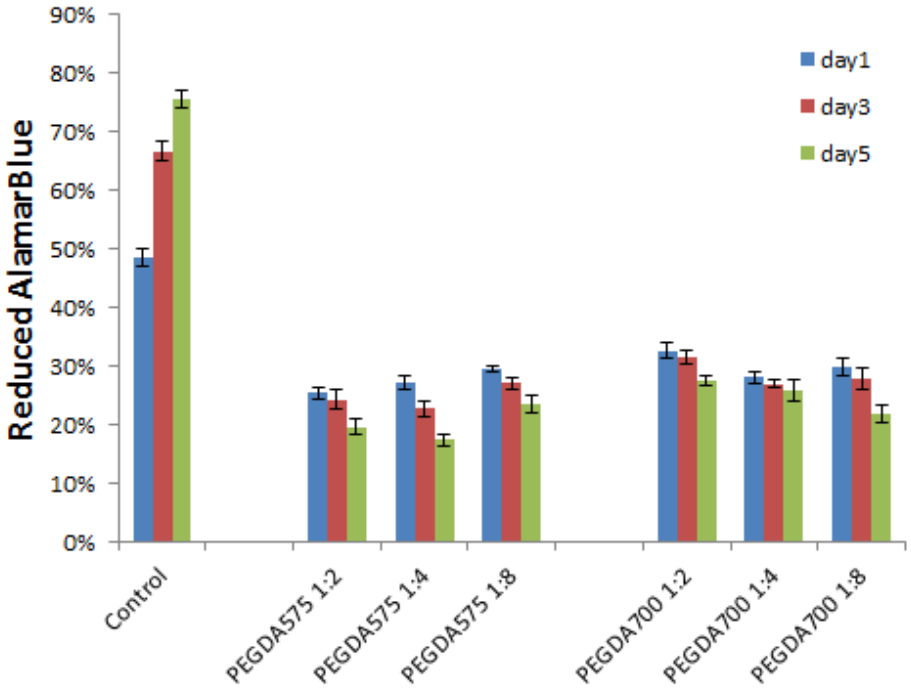

Figure 4.10 Cell metabolic activity assessment of 3T3 cells after one, three and five days 2D culture on poly(PEGDA) photo-crosslinked hydrogels using alamarBlue® assay. Cells on the blank culture plate were used as the control. The cell concentration was 5,000 per well on the 96-well plate. Note: there is significant difference of cell viability between the control and the hydrogels but no significant difference was found between the hydrogels crosslinked from different polymers after one, three and five days (mean ± SD, n = 3, $p < 0.05$).

The results (Figure 4.10) showed that compared to the plate-cultured cells, the cells on the hydrogels can maintain more than half of their metabolic activities after one day culture. However, it didn't show evidence of cell proliferation on any of the hydrogels since the metabolic activities for cells on all of hydrogels reduced after three and five days. Observation from the microscope showed that the cells maintained round shapes during the period of testing, indicating that the cells didn't spread on the surface of the hydrogels. This could be the reason for the reduction of the cell metabolic activities. The hydrogels formed from poly($PEGDA_{700}$) showed a slightly lower toxicity than that from poly($PEGDA_{575}$), indicating that longer PEG spacers in the hydrogel is more benign for the cell survival. Generally, it can be concluded that there is significant difference of cell viability between the control and the hydrogels but no significant difference was found between the hydrogels crosslinked from different polymers after one, three and five days, indicating that all of the hydrogel is affecting the cellular metabolism

to varying extents.

4.4 Conclusions

In this chapter, a series of water soluble hyperbranched polymers was prepared by homopolymerization of PEGDA through vinyl oligomer combination. High monomer conversions (up to 96%) and hyperbranched polymer structure were both achieved by increasing the ratio of initiator/monomer, which results in a high chain concentration and a smaller chain dimension before the crosslinking reaction occurs. The poly($PEGDA_{700}$)s show good solubility in aqueous solution whereas the poly($PEGDA_{575}$)s show a characteristic thermoresponsive property, which is highly dependent on the polymer concentration and the polymer composition.

These PEG-based hyperbranched vinyl functional polymers were used as photo-crosslinkable precursors for the formation of PEG-based hydrogels and manifested efficient UV curing properties (within 15 seconds). The fabricated hydrogels showed capability to maintain most of the 3T3 cell viability, but are unable to support the cell proliferation. However, these hydrogels still possess the potential of further modification on their surface due to the existence of multiple functional groups such as halogen and isobutyrate groups from the initiator, and may exhibit improved surface environment for cell growth.

4.5 References

1. Gin, H.; Dupuy, B.; Baquey, A.; Baquey, C.; Ducassou, D. Lack of responsiveness to glucose of microencapsulated islets of langerhans after 3 weeks inplantation in the rat influence of the complement. *Journal of Microencapsulation* **1990,** *7* (3), 341-346.
2. Matthew, H. W.; Salley, S. O.; Peterson, W. D.; Klein, M. D. Complex coacervate microcapsules for mammalian-cell culture and artificial organ development. *Biotechnology Progress* **1993,** *9* (5), 510-519.
3. Hsu, F. Y.; Tsai, S. W.; Wang, F. F.; Wang, Y. J. The collagen-containing alginate/poly(L-lysine)/alginate microcapsules. *Artificial Cells Blood Substitutes and Immobilization Biotechnology* **2000,** *28* (2), 147-154.
4. Sefton, M. V.; May, M. H.; Lahooti, S.; Babensee, J. E. Making microencapsulation work: conformal coating, immobilization gels and in vivo performance. *Journal of Controlled Release* **2000,** *65* (1-2), 173-186.
5. Hou, Q. P.; De Bank, P. A.; Shakesheff, K. M. Injectable scaffolds for

tissue regeneration. *Journal of Materials Chemistry* **2004,** *14* (13), 1915-1923.
6. Overstreet, D. J.; Dutta, D.; Stabenfeldt, S. E.; Vernon, B. L. Injectable hydrogels. *Journal of Polymer Science Part B-Polymer Physics* **2012,** *50* (13), 881-903.
7. Pal, K.; Banthia, A. K.; Majumdar, D. K. Polymeric hydrogels: characterization and biomedical applications. *Designed Monomers and Polymers* **2009,** *12* (3), 197-220.
8. Bryant, S. J.; Nuttelman, C. R.; Anseth, K. S. Cytocompatibility of UV and visible light photoinitiating systems on cultured NIH/3T3 fibroblasts in vitro. *Journal of Biomaterials Science-Polymer Edition* **2000,** *11* (5), 439-457.
9. Lin, C.-C.; Metters, A. T. Hydrogels in controlled release formulations: Network design and mathematical modeling. *Advanced Drug Delivery Reviews* **2006,** *58* (12-13), 1379-1408.
10. Peppas, N. A.; Bures, P.; Leobandung, W.; Ichikawa, H. Hydrogels in pharmaceutical formulations. *European Journal of Pharmaceutics and Biopharmaceutics* **2000,** *50* (1), 27-46.
11. Lin, C.-C.; Anseth, K. S. PEG hydrogels for the controlled release of biomolecules in regenerative medicine. *Pharmaceutical Research* **2009,** *26* (3), 631-643.
12. Rydholm, A. E.; Bowman, C. N.; Anseth, K. S. Degradable thiol-acrylate photopolymers: polymerization and degradation behavior of an in situ forming biomaterial. *Biomaterials* **2005,** *26* (22), 4495-4506.
13. Fournier, E.; Passirani, C.; Montero-Menei, C. N.; Benoit, J. P. Biocompatibility of implantable synthetic polymeric drug carriers: focus on brain biocompatibility. *Biomaterials* **2003,** *24* (19), 3311-3331.
14. Metters, A. T.; Anseth, K. S.; Bowman, C. N. A statistical kinetic model for the bulk degradation of PLA-b-PEG-b-PLA hydrogel networks: Incorporating network non-idealities. *Journal of Physical Chemistry B* **2001,** *105* (34), 8069-8076.
15. Malkoch, M.; Vestberg, R.; Gupta, N.; Mespouille, L.; Dubois, P.; Mason, A. F.; Hedrick, J. L.; Liao, Q.; Frank, C. W.; Kingsbury, K.; Hawker, C. J. Synthesis of well-defined hydrogel networks using Click chemistry. *Chemical Communications* **2006,** (26), 2774-2776.
16. Rizzi, S. C.; Ehrbar, M.; Halstenberg, S.; Raeber, G. P.; Schmoekel, H. G.; Hagenmueller, H.; Mueller, R.; Weber, F. E.; Hubbell, J. A. Recombinant protein-co-PEG networks as cell-adhesive and proteolytically degradable hydrogel matrixes. Part II: Biofunctional characteristics. *Biomacromolecules* **2006,** *7* (11), 3019-3029.
17. Rizzi, S. C.; Hubbell, J. A. Recombinant protein-co-PEG networks as cell-adhesive and proteolytically degradable hydrogel matrixes. Part 1: Development and physicochernical characteristics. *Biomacromolecules*

2005, *6* (3), 1226-1238.
18. Elbert, D. L.; Pratt, A. B.; Lutolf, M. P.; Halstenberg, S.; Hubbell, J. A. Protein delivery from materials formed by self-selective conjugate addition reactions. *Journal of Controlled Release* **2001,** *76* (1-2), 11-25.
19. van de Wetering, P.; Metters, A. T.; Schoenmakers, R. G.; Hubbell, J. A. Poly(ethylene glycol) hydrogels formed by conjugate addition with controllable swelling, degradation, and release of pharmaceutically active proteins. *Journal of Controlled Release* **2005,** *102* (3), 619-627.
20. Rydholm, A. E.; Reddy, S. K.; Anseth, K. S.; Bowman, C. N. Controlling network structure in degradable thiol-acrylate biomaterials to tune mass loss behavior. *Biomacromolecules* **2006,** *7* (10), 2827-2836.
21. Salinas, C. N.; Anseth, K. S. Mixed mode thiol-acrylate photopolymerizations for the synthesis of PEG-peptide hydrogels. *Macromolecules* **2008,** *41* (16), 6019-6026.
22. Salinas, C. N.; Anseth, K. S. The enhancement of chondrogenic differentiation of human mesenchymal stem cells by enzymatically regulated RGD functionalities. *Biomaterials* **2008,** *29* (15), 2370-2377.
23. Cramer, N. B.; Bowman, C. N. Kinetics of thiol-ene and thiol-acrylate photopolymerizations with real-time Fourier transform infrared. *Journal of Polymer Science Part A-Polymer Chemistry* **2001,** *39* (19), 3311-3319.
24. Cramer, N. B.; Scott, J. P.; Bowman, C. N. Photopolymerizations of thiol-ene polymers without photoinitiators. *Macromolecules* **2002,** *35* (14), 5361-5365.
25. Cramer, N. B.; Davies, T.; O'Brien, A. K.; Bowman, C. N. Mechanism and modeling of a thiol-ene photopolymerization. *Macromolecules* **2003,** *36* (12), 4631-4636.
26. Cramer, N. B.; Reddy, S. K.; Cole, M.; Hoyle, C.; Bowman, C. N. Initiation and kinetics of thiol-ene photopolymerizations without photoinitiators. *Journal of Polymer Science Part A-Polymer Chemistry* **2004,** *42* (22), 5817-5826.
27. Williams, C. G.; Malik, A. N.; Kim, T. K.; Manson, P. N.; Elisseeff, J. H. Variable cytocompatibility of six cell lines with photoinitiators used for polymerizing hydrogels and cell encapsulation. *Biomaterials* **2005,** *26* (11), 1211-1218.
28. Khetan, S.; Guvendiren, M.; Legant, W. R.; Cohen, D. M.; Chen, C. S.; Burdick, J. A. Degradation-mediated cellular traction directs stem cell fate in covalently crosslinked three-dimensional hydrogels. *Nature Materials* **2013,** *12* (5), 458-465.
29. Cheng, S. Z. D. *Phase transitions in polymers: The role of metastable states* 2008. p 1-307.

Chapter Five

Synthesis of Highly Branched Degradable Functional Poly(dimethylaminoethyl methacrylate-co-bis(2-acryloyl)oxyethyl disulphide) as Efficient Gene Vector

Most parts of this chapter have been published in:

Zhao, T., Zhang, H., Newland, B., Aied, A., Zhou, D., Wang, W. 'Significance of branching for transfection: synthesis of highly branched degradable functional poly(dimethylaminoethyl methacrylate) by vinyl oligomer combination' *ANGEWANDTE CHEMIE INTERNATIONAL EDITION*, **2014**, 53(24), 6095-6100**.**

5.1 Introduction

5.1.1 Poly(dimethylaminoethyl methacrylate) Based Polymers as Gene Vectors

The notion that the macromolecular structure of non-viral gene vectors alters their transfection efficacy has inspired numerous novel designs of 3D polymeric structures, such as globular dendrimers,[1] micelle block copolymers,[2] star-shaped,[3] randomly branched[4] or cyclized[5] copolymers, for both transfection enhancement and cytotoxicity reduction. Although the "gold standard" branched poly(ethyleneimine) (PEI) generally shows high transfection, its associated high cytotoxicity (IC50=~30 μg/ml)[6] is a major drawback and has been a driving force for PEI modification[7, 8] or explorations of other vectors.

With a buffering capacity (pK_a=7.5) and less cytotoxicity than PEI,[6] poly(dimethylaminoethyl methacrylate) (PDMAEMA) is a promising gene delivery system as the design and precise synthesis is possible in a relatively simple manner using DMAEMA as a vinyl monomer. Controlled molecular weights, well-defined chain ends, and different macromolecular architectures (such as block, star, graft and knot) could be easily achieved using controlled/living radical polymerization (CRP) techniques like atom transfer radical polymerization (ATRP)[9] and reversible addition fragmentation chain transfer (RAFT).[10] However, most of the designs on PDMAEMA have led to the formation of long non-degradable carbon-carbon chains during the chain growth polymerization. Therefore, the cytotoxicity of PDMAEMA based vectors maintains at a relatively high level[11, 12] and modifications such as PEGylation, aiming at reducing cytotoxicity, are usually accompanied with a loss of transfection.[13, 14] The introduction of a hydrophobic segment (i.e. polycaprolactone) significantly improved the transfection efficiency,[15] however, multiple steps were required for the preparation, and the transfection level was still much lower than commercial transfection agents. Compared to the numerous studies on linear or block PDMAEMA, the study of 3D branched PDMAEMA is still comparatively rare.[4] Although a branched DMAEMA/ethylene glycol dimethacrylate (EGDMA) copolymer has shown comparable transfection capability to commercial agents and a much higher level than its linear counterpart,[4] the effect of PDMAEMA branching structure on transfection efficiency has not yet been fully understood and explored. Moreover, the study did not address issues such as degradation or functionalization.

As a potential alternative to dendrimers, hyperbranched (HB) polymers hold simpler and more cost-effective synthesis as well as a high range of functionality. Based on the Chapter 2 and 3, a facile approach, so called 'vinyl oligomer combination', has been developed for the preparation of HB polymer from multi-vinyl monomers (MVMs) via chain growth polymerization.[16] By kinetic control and statistical manipulation, HB structures consisting purely of extremely short primary C-C chains were obtained. This strategy allowed us to predict that it could, in principle, be applied to a copolymerization system.

Therefore, on the basis of this strategy, this chapter will report the preparation of a series of highly branched DMAEMA/bis(2-acryloyl)oxyethyl disulphide (DSDA) copolymers via 'vinyl oligomer combination' approach and *in situ* DE-ATRP technology. High initiator/DMAEMA ratios (1/8~1/32) were employed in order to supply a high concentration of initial short primary chains, which could enhance intermolecular combination and thus lead to a highly branched structure.

5.1.2 Aims and Hypotheses

The logic for hypothesizing that this highly branched structure would lead to greater performance is 2-fold: first, by the creation of a 3D branched structure with multiple functional groups for DNA interaction and, second, by efficient intracellular cleavage of disulphide bond[17, 18, 19] for low cytotoxicity.

The aim was therefore to assess if the degradable branched PDMAEMA-DSDA can supersede the linear PDMAEMA in terms of both transfection capability and lower toxicity. Also, commercially available transfection vectors (25k bPEI, Xfect, and polyamidoamine (PAMAM) dendrimer) were used as comparable samples. The branched PDMAEMA-DSDA with similar molecular weight but varying degrees of branching were synthesized. After end-capping the vinyl groups with functional molecules, these polymers were studied on different cell types, showing that the highly branched PDMAEMA-DSDA is superior to the linear PDMAEMA.

5.2 Experimental

5.2.1 Materials

The monomers 2-(dimethylamino)ethyl methacrylate (DMAEMA), ethylene glycol dimethacrylate (EGDMA), acryloyl chloride (≥97%) and 2-hydroxyethyl disulfide (90%) were purchased from Sigma Aldrich. Bis(2-acryloyl)oxyethyl disulfide (DSDA, ≥95%) was synthesized according to literature. Ethyl 2-bromoisobutyrate (EBriB, 98%, Aldrich), pentamethyldiethylenetriamine (PMDETA, 99%, Aldrich), copper(II) chloride ($CuCl_2$, 97%, Aldrich), L-ascorbic acid (AA, 99%, Aldrich), 3-Morpholinopropylamine (MPA, 98%, Aldrich), *d*-Chloroform (99.8%, Aldrich), tetrahydrofuran (THF, HPLC grade, Fisher) and *n*-hexane (ACS reagent grade, Fisher), diethyl ether (ACS reagent grade, Fisher), dichloromethane (ACS reagent grade, Fisher), dimethylformamide (DMF, HPLC grade, Fisher) were used as received. For polyplex characterization and performance, agarose (for electrophoresis, Aldrich), SYBR® Safe Gel stain (invitrogen), BioLux™ Gaussia Luciferase Assay Kit (New England Biolabs), alamarBlue® (Invitrogen) were used as received according to protocols.

5.2.2 Preparation of The Bis(2-acryloyl)oxyethyl Disulfide (DSDA) Monomer

2-hydroxyethyl disulfide (9.79 ml) and TEA (22.25 ml) were added in a two-necked round bottom flask, with chloroform (200 ml) as solvent. Acryloyl chloride (25.8 ml) was then added dropwise under the argon protection. The flask was sealed and the mixture was stirred in an ice bath for 24hrs. The by-produced salt was removed by filtering under reduced pressure followed by 6 times of washing with sodium carbonate aqueous solution (Na_2CO_3, 0.1M). Then the solution was evaporated to smaller volume and passed through a basic alumina column with DCM as eluents. The obtained product of bis(2-acryloyl)oxyethyl disulfide was determined by ^1H NMR in $CDCl_3$: 2.84 ppm t (4H), 4.45 ppm t (4H), 5.80 ppm d (2H), 6.05 ppm q (2H), 6.43 ppm d (2H).

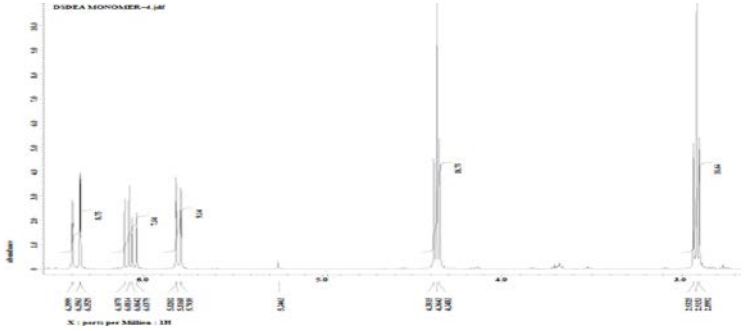

5.2.3 Synthesis and Functionalization of The Poly(DMAEMA-co-DSDA) (PD-DS) Polymers

Polymer synthesis: The polymers were prepared in two-necked round bottom flasks. THF (10 ml), $CuCl_2$ (26.89 mg, 1 equiv) and PMDETA (34.66 mg, 1 equiv) were added into the flask. Monomers were added in the following ratios for each of the three polymers: PD_{32}-$DS_{1.5}$ (EBriB 0.24g, 6.25 equiv, DMAEMA 6.29g, 200 equiv, and DSDA 0.49g, 9.38 equiv); PD_{16}-DS_2 (EBriB 0.49g, 12.5 equiv, DMAEMA 6.29g, 200 equiv, and DSDA 1.31g, 25 equiv); PD_8-$DS_{2.5}$ (EBriB 0.98g, 25 equiv, DMAEMA 6.29g, 200 equiv, and DSDA 3.28g, 62.5 equiv); Oxygen was removed by bubbling argon through the solutions for 20 mins. AA solution (100µl of 70.4 mg/ml AA/THF solution, 0.2 equiv) was pipetted into the flasks under positive pressure of argon before the flask was immersed in a preheated oil bath at 50 ^oC. The solution was stirred at 800 rpm and the polymerization was conducted at 50 ^oC in an oil bath for the desired reaction time. The experiment was stopped by opening the flask and exposing the catalyst to air. This was then diluted with THF and precipitated into a large excess of cold hexane/diethyl ether (10:7 v/v) to remove the monomers. The precipitated mixture was dried under laminar flow then redissolved in THF followed by three times of passing through an Al_2O_3 column. The mixture was then dried under vacuum.

Post functionality of the PD-DS polymers: The three PD-DS polymers were redissolved in THF to make a concentration of 100mg/ml. Then 10 times more excessive mole of MPA than the vinyl groups of the polymers was dissolved in same volume of THF. The two solutions were mixed together and stirred for 24h. Then the MPA was removed by three times of precipitation against a large excess of cold hexane/diethyl ether (10:7 v/v). The mixture was then dried under vacuum.

Reduction cleavage of the PD-DS polymers and subsequent analysis: 0.1g of purified PD-DS polymers were dissolved in 1ml of distilled H_2O followed by adding 1ml of 20mM L-glutathione H_2O solution. The mixture was stirred at room temperature for 1 h and freeze dried for further analysis.

5.2.4 Polymer Characterization Method

Molecular weight determination by size exclusion chromatography. Small samples were withdrawn from the reaction at specific time intervals

using a glass syringe with luer needle under positive pressure of argon. These were then diluted in DMF and filtered through an Al_2O_3 pipette for chromatography followed by a 0.2μm filter before analysis. The molecular weight and molecular weight distribution of each sample was determined using a Varian 920-LC instrument with a refractive index detector (RI). Chromatograms were run at 60 °C using DMF as eluent with a flow rate of 1 ml/min. The machine was calibrated with linear poly(methyl methacrylate) standards.

Nuclear magnetic resonance (NMR) spectroscopy. The polymer was dissolved in $CDCl_3$ for ^1H NMR analysis and all chemical shifts are reported in ppm relative to TMS. The NMR spectrum confirmed the presence of each monomer in the polymer structure and the presence of free vinyl groups.

5.2.5 Polyplex Characterization

Cell secreted Gaussia princeps luciferase plasmid (pCMV-GLuc) was obtained from New England Biolabs UK, and its expansion, isolation and purification was performed using the Giga-Prep (Qiagen) kit as per protocol. UV spectroscopy (NanoDrop™ ND1000 Spectrophotometer, Thermo Scientific) and gel electrophoresis were used to confirm plasmid purity. The nanoparticle formed *via* the electrostatic attraction between the DNA and cationic polymer, termed “polyplex” was characterized by these two methods. However, firstly these were formed at various polymer/plasmid (w/w) ratios, by mixing the polymer in serum free media with the G-luciferase plasmid for 30 minutes prior to use. An agarose gel (1% agarose in Tris-borate-EDTA (TBE) buffer, with SYBR®Safe DNA stain) was made up to analyze at which weight ratio polyplex formation would occur. 5μl of each polymer/plasmid solution (DNA concentration of 50 $\mu g \cdot ml^{-1}$) were added along with 5μl loading dye to each well and subjected simultaneously to 80mV for up to an hour. For size and charge determination (Malvern Instruments Zetasizer (Nano-2590)), solutions of various polymer/plasmid weight ratios were made up as explained above but in distilled water.

5.2.6 Cell Culture

Human cervical cancer cells (HeLa) and human adipose derived stem cells (hADSC, passage 5 (Invitrogen)) were grown in Dulbecco modified Eagle's minimal essential medium (DMEM) with 10% fetal bovine serum (FBS)

and 1% Penicillin/Streptomycin (P/S) at 37°C with 5% CO_2 using standard cell culturing techniques. Normal human keratinocytes (NHK) were grown in KGM™ keratinocyte growth medium and KGM™ BulletKit™ with 5% fetal bovine serum (FBS) at 37°C with 5% CO_2 using standard cell culturing techniques.

5.2.7 Luciferase Transfection and AlamarBlue® Reduction

Under usual cell culture sterile conditions cells were seeded in 96 well plates at a density of 50,000 cells/ml 24 hours prior to the addition of the polyplexes (formed with 1µg of pDNA per well). After the incubation at 37^{o}C and 5% CO_2 the cell culture media was replaced with polyplex solutions of varying weight ratios made up as described above, in serum containing media. A control of cells that were subject to the same treatment, but received plasmid alone, were also performed as well as the comparative controls of commercially available transfection agents. After 48 hours of incubation, analysis of the luciferase activity was performed as per the provided protocol, which, for this secreted luciferase means analysis of the cell supernatant, and subsequent plotting of luciferase activity directly in terms of relative light units (RLU). This renders the cells that received the polyplexes free for cytotoxicity analysis, which was performed using the alamarBlue® reduction method. To perform this assay, the cells are first washed three times with Hanks Balanced salt solution (HBSS) followed by addition of 10% alamarBlue® in (HBSS). Cell metabolism causes the blue alamarBlue® solution to be reduced, turning pink in the process which can be followed as a change in absorbance according to protocol. Briefly the alamarBlue® solution from each well is transferred to a fresh flat bottomed 96-well plate for absorbance measurements at 550nm and 590nm via a thermo scientific Varioskan Flash Plate Reader. The following equations were used to calculate the percentage of cell viability:

AO_{LW} = absorbance of oxidized form of alamarBlue® along at lower wavelength;

AO_{HW} = absorbance of oxidized form of alamarBlue® along at higher wavelength;

Calculated correlation factor:

$$Ro = AO_{LW} / AO_{HW} \qquad \text{Eq. 5.1}$$

Calculated the percentage of reduced alamarBlue®:

AR_{LW} % = (A_{LW} - A_{HW} × Ro) × 100 Eq. 5.2

Calculated the percentage of cell metabolic activity:

Cell activity % = (AR_{LW}[Samples] / AR_{LW}[Cells along]) × 100 Eq. 5.3

Although the reduction method is a measure of cell metabolism, it is an indicator of cell viability if compared to the cells that receive no polymer (absorbance values normalized and plotted as 100% viable). As only live cells can reduce the alamarBlue® solution any decrease in reduction capability is denoted as a loss of viability. All luciferase and alamarBlue® reduction experiments were performed in quadruplicate with margin of error shown as plus or minus the standard deviation.

5.2.8 Green Fluorescent Protein (GFP) Expression

The expression of the internally expressed pCMV-GFP green fluorescent protein plasmid (New England Biolabs UK, also obtained as described earlier) was used to assess polymer transfection in terms of the percentage of cells transfected. Cells were seeded in 4-well chamber slides (for fluorescent microscopy analysis) at 100,000 cells/ml, 24 hours prior to the same treatment as outlined earlier, but with 2µg of plasmid GFP instead of luciferase. Three chamber slides per group were viewed with an Olympus BX51 epifluorescence microscope fitted with an OlympusDP70 digital CCD camera, using a PlanFl 40x/0.75 NA air objective (Mason Technologies, Dublin, Ireland). Digital images were captured using ImagePro (v5.0, Media Cybernetics, Inc.).

5.2.9 Statistical Analyses

Statistical analyses were performed using GraphPad Prism (v.5, GraphPad Software, San Diego, CA, USA). D'Agostino and Pearson omnibus normality tests were used to determine normal distribution. Where normal distribution was evident, a one-way ANOVA was performed, followed by Turkey's post hoc test. P values < 0.05 were considered to be statistically significant. Stars indicate a statistically significant beneficial difference between PD-DS polymers and the linear PDMAEMA control. All transfection/cytotoxicity experiments were performed in quadruplicate unless otherwise stated with error bars indicating ± standard deviation.

5.3 Results and Discussions

5.3.1 Synthesis and Characterization of The Poly(DMAEMA-co-DSDA) Polymers

Figure 5.1 outlines the design and synthesis of the $PDMAEMA_x$-$DSDA_y$ (termed as PD_x-DS_y below) polymers. The initial molar ratio for initiator: DMAEMA: DSDA was set at 1: x: y. Varying the component ratios can allow for a range of degrees of branching. The reaction system in this chapter could be classified into the controlled radical crosslinking copolymerization (CRCC), in which a single vinyl monomer is copolymerized with a multi-vinyl cross-linker via controlled/living methods.[20, 21] However, there are mainly two significant features for our reaction system which are different from the traditional one.

Firstly, the initial molar ratio of cross-linker to initiator is more than 1. In the traditional CRCC, the portion of cross-linker is usually lower than that of the initiator, since it is widely accepted that critical gelation happens when the average number of cross-linkage (cross-linker with both vinyl groups reacted) per primary chain exceeds unity if the primary chains are uniform. This hypothesis has been confirmed in various experiments.[22, 23, 24, 25] According to this hypothesis, the reaction systems in this chapter will eventually lead to cross-linked networks before a complete monomer conversion is reached. However, if the monomer conversion is kept incomplete and some of the divinyl cross-linker does not fully react, or is consumed by intramolecular cyclization, gelation may not be observed. The benefit for a higher ratio of cross-linker is that much more highly branched structures could be achieved and pendent vinyl groups could be reserved in the product, acting as a universal chemical group for various functioning. The acrylate based cross-linker was used here for the ease of Michael addition to the amine groups on the functional molecules.

The second feature is that the molar ratio of initiator to vinyl monomer is relatively high (1/8~1/32) compared to the traditional protocol (1/50~1/100).[23] This high ratio was adopted for the purpose of shortening the primary chains and enhancing their intermolecular combination, by which highly branched structures are favoured. If the linkages between primary chains are cleavable in a specific environment, the polymer product will have the potential of fragmenting into small pieces of oligomers which are more easily removed or processed by cells and the organism.

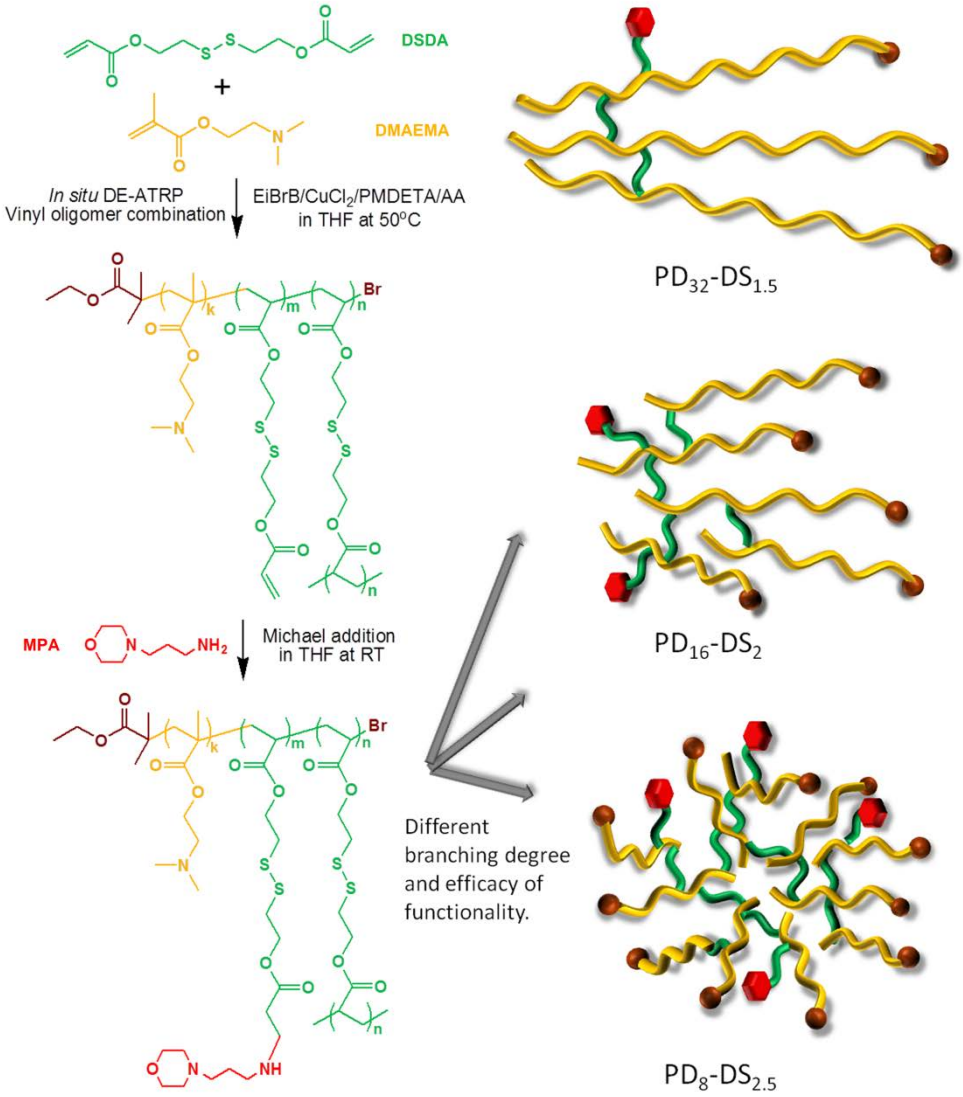

Figure 5.1 Illustration of the controlled radical crosslinking copolymerization via *in situ* DE-ATRP and a post-functionalization process, alongside a graphical representation of the formation of structures of different branching degrees. The efficacy of functionalization depends on the content of the pendent vinyl groups.

The reaction process was followed by GPC analysis of samples extracted during the reaction, as described in Table 5.1. Figure 5.2 shows the typical GPC traces for the synthesis of the three polymers, illustrating similar evolution of molecule growth in the reaction system. Highly symmetrical and unimodal peaks at 2 hours indicate the controlled nature of growth. The molecular weight distributions were also narrow for all the polymers at 2 hours (M_w/M_n<1.4), indicating the formation of predominantly linear chains with rare branching. As the reaction progresses, both molecular weight and

polydispersity increases gradually because of the increased participation of divinyl DSDA at higher monomer conversion. The peaks at 5 hours become slightly asymmetric with the left side spread a little, indicating the formation of moderate branching molecules. The right sides of peaks at 5 hours were in parallel to those of the corresponding peaks at 2 hours, thus manifesting the living feature of reaction. The peaks at 20 hours spread dramatically due to large scale of intermolecular branching between primary chains when the critical overlap concentration is reached. Above this conversion threshold, the barriers to intermolecular reaction are significantly reduced, thus the branching becomes a priority. After precipitation, the small linear chains and the monomers were removed, leaving only the highly branched products. In this way, the interference of linear molecules was cleared.

There are also some subtle differences in the evolution of molecular weight when the molar ratio of initial reactants varies. As shown in Figure 5.2, the lower molar ratio of initiator to vinyl monomer (PD_{32}-$DS_{1.5}$) led to a faster molecular weight increase at the linear growth period. However, the higher content of divinyl cross-linker of PD_8-$DS_{2.5}$ promoted the intermolecular combination reaction and thus resulted in a stronger exponential increase of molecular weight during the later stage.

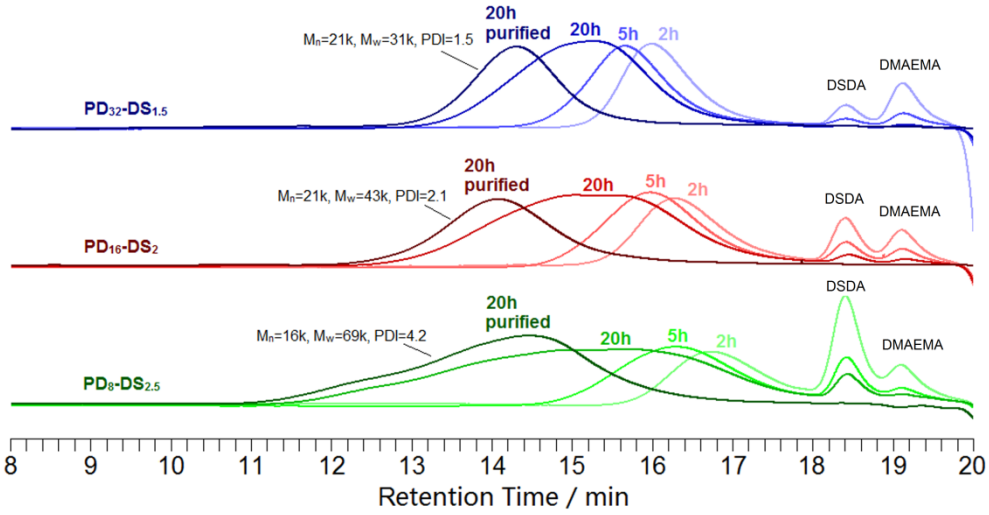

Figure 5.2 Time dependence of the composition of the polymerization mixtures for the three PDx-DSy syntheses, monitored by GPC equipped with a refractive index (RI) detector, showing subtly different reaction pathways.

Table 5.1 Polymerization conditions and molecular weight characteristics of the polymers with different monomer feed ratios.

	Time	M_n [e] kDa	M_w [e] kDa	M_w/M_n [e]	Conversion [f] (%)
PD_{32}-$DS_{1.5}$ [a]	2h	3.2	4.4	1.36	74.8
	5h	4.2	6.8	1.60	90.3
	20h	6.8	15.6	2.29	98.3
	purified [d]	20.9	31.1	1.49	-
PD_{16}-DS_2 [b]	2h	2.3	3.1	1.35	69.2
	5h	3.1	5.1	1.67	83.8
	20h	5.4	18.1	3.36	96.0
	purified [d]	20.9	43.0	2.06	-
PD_8-$DS_{2.5}$ [c]	2h	1.5	2.0	1.34	49.8
	5h	2.3	4.0	1.78	75.6
	20h	4.4	35.7	8.16	90.8
	purified [d]	15.7	69.4	4.42	-

[a] I/DMAEMA/DSDA/$CuCl_2$/PMDETA/AA = 1: 32: 1.5: 0.16: 0.16: 0.032, I: ethyl 2-bromoisobutyrate (EBriB), PMDETA: 1,1,4,7,7-pentamethyldiethylenetriamine, AA: L-Ascorbic Acid, Solvent: THF, [DMAEMA]= 2 mol/L, T = 50 °C; [b] I/DMAEMA/DSDA/$CuCl_2$/PMDETA/AA = 1: 16: 2: 0.08: 0.08: 0.016, Solvent: THF, [DMAEMA]= 2 mol/L, T = 50 °C; [c] I/DMAEMA/BADS/$CuCl_2$/PMDETA/AA = 1: 8: 2.5: 0.04: 0.04: 0.008, Solvent: THF, [DMAEMA]= 2 mol/L, T = 50 °C; [d] Purification was done by three times of precipitation against hexane/diethyl ether (10:7 v/v) followed by two times of passing through a Al_2O_3 column; [e] M_n, M_w and PDI are determined by GPC equipped with a refractive index (RI) detector; [f] Conversions were calculated by the integration of peak area from GPC.

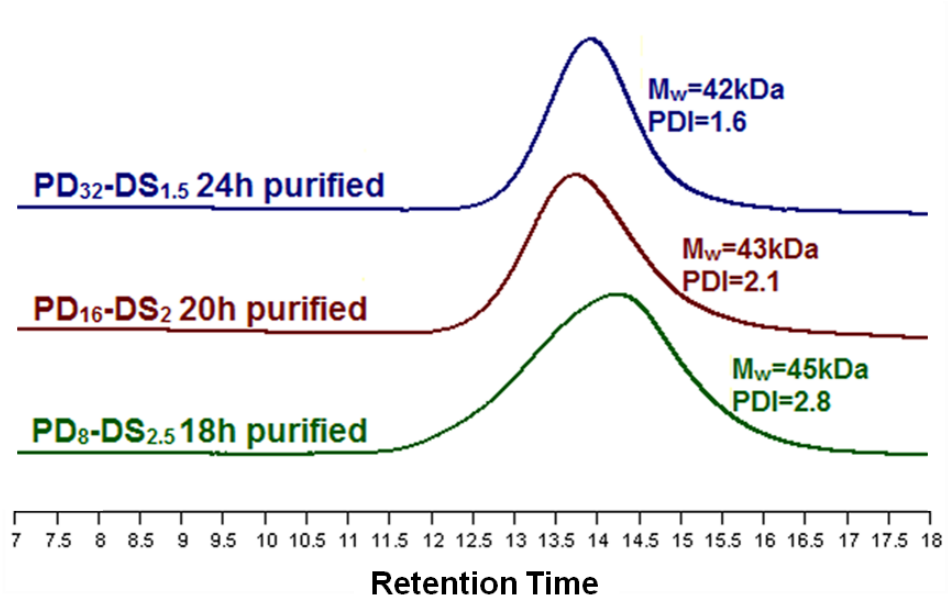

Figure 5.3 GPC traces of the three PD_x-DS_y polymers obtained at different time point with similar M_w.

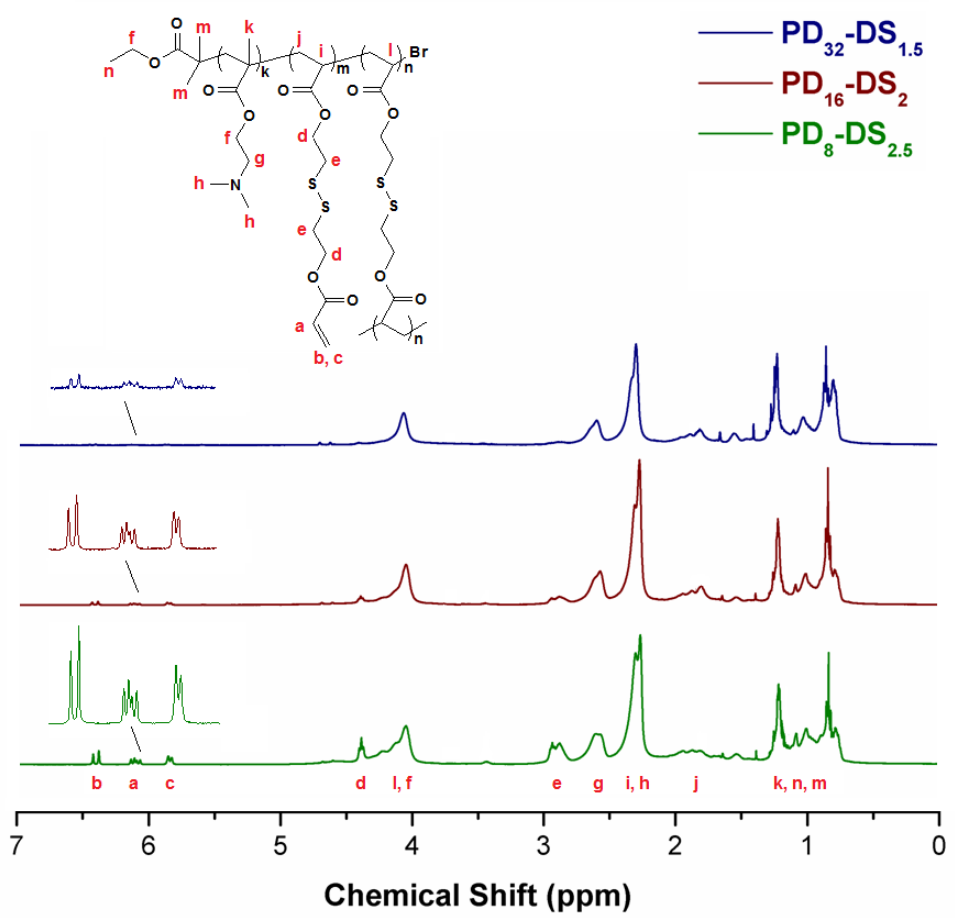

Figure 5.4 ^{1}H NMR spectrum of the three PD_x-DS_y polymers products, showing certain amount of vinyl groups left in those polymers.

To minimize the interference of the effect of molecular weight (well-known to affect the performance of transfection),[3] the reactions were stopped at different time periods (24h for PD_{32}-$DS_{1.5}$, 20h for PD_{16}-DS_2 and 18h for PD_8-$DS_{2.5}$ with the GPC conversion of 98.5%, 96.0% and 87.1% respectively) to obtain similar molecular weights. The GPC trace of the final PD-DS products were shown in Figure 5.3 and their ^{1}H NMR spectrum were shown in Figure 5.4. The weight average molecular weights are 42kDa, 43kDa and 45kDa for PD_{32}-$DS_{1.5}$, PD_{16}-DS_2 and PD_8-$DS_{2.5}$ respectively. The ratios of components for the products were calculated from ^{1}H NMR and were shown in Table 5.2. The units of DMAEMA and DSDA are basically proportional to their initial feed ratio for all the three polymers. The DMAEMA units take a slightly higher ratio, indicating higher reactivity of methacrylate derivative than the acrylate derivative. This difference in reactivity may lead to the different rate of incorporation into the chains. As a result the resulting branched polymer is probably a structure of heterogeneously distributed branches[26] or more like a branched core decorated with PDMAEMA short hairs. Determination of the polymer structure by analysis of the ^{1}H NMR spectroscopy also shows that these polymers possess high degree of branching, with the PD_8-$DS_{2.5}$ holding the highest (9.4%) (Table 5.2), indicating one branching unit exists for every 20 atoms in a -C-C- chain. The initiator content in the polymer products is higher than the content of branching unit, indicating that the divinyl cross-linker were mainly consumed by intermolecular reaction. This means that one connection per primary chain is still not reached and thus the reaction conversion is still under the gelling point. The high conversion could be attributed to the fact that the divinyl cross-linker does not fully react, or is inevitably consumed by intramolecular cyclization at later stages.[27, 28] Free vinyl groups were also left within the polymer structure (as shown in Table 5.2 and Figure 5.4) providing an opportunity for a range of post synthesis functionalizations.

Table 5.2 The composition of the three PD_x-DS_y polymers can be varied by adjusting the monomer feed ratios of the simple "One-Pot" reaction, with high percentage of branching unit and functional vinyl groups.

	Initiator (%)	DMAEMA (%)	DSDA (%)	Branch unit /Total (%)	Vinyl unit /Total (%)	Vinyl conc. (mmol/g)
PD_{32}-$DS_{1.5}$	3.0	92.7	4.3	2.7	1.6	0.10
PD_{16}-DS_2	5.8	85.4	8.8	5.3	3.5	0.21
PD_8-$DS_{2.5}$	10.9	70.1	19.0	9.4	9.6	0.53

All of the three purified polymers were endcapped with 3-Morpholinopropylamine (MPA) via Michael addition between the unreacted acrylate moieties on those polymers and primary amine of MPA. The Morpholino structures were recently introduced into a poly(β-aminoester) which exhibited good performance of transfection.[29] Figure 5.5 shows the ^{1}H NMR spectrum of PD_8-$DS_{2.5}$ before and after the endcapping. It can be seen that all the vinyl groups are consumed and the typical peaks for MPA chemical structure appear after the endcapping, indicating a good connection of MPA to the polymer.

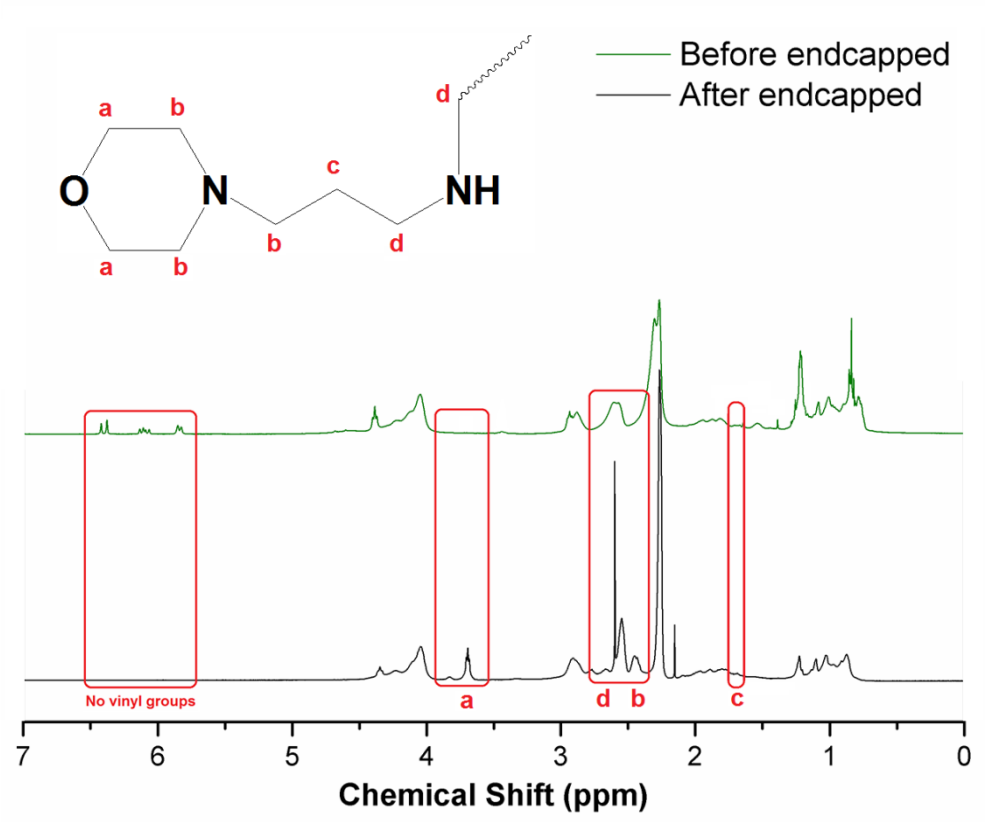

Figure 5.5 ^{1}H NMR spectrum of PD_8-$DS_{2.5}$ before and after Michael addition of the primary amine on the MPA and vinyl group on the polymer, showing a successful functionalization.

5.3.2 Degradation Test of The Poly(DMAEMA-co-DSDA) Polymers

The highly branched structures were also confirmed by the cleavage of the disulphide bonds, which undergo fast reduction upon the addition of 20 mM glutathione. As shown in Figure 5.6 (a), if a typical highly branched structure was being formed, exposing the polymer to glutathione would result in cleavage of the branching units, including those used as intermolecular links, resulting in small fragments of polymer being produced. It can be imagined that a polymer comprised of shorter primary chains as well as a higher degree of branching would be cleaved into smaller pieces. The three PD-DS polymers were analyzed for their M_w and PDI before and after being subjected to 1 h of glutathione treatment. Significant reduction in M_w occurred for all the polymers (Figure 5.6 (b)), confirming that this structure is comprised predominantly of short primary chains. The PD_8-$DS_{2.5}$, synthesized with the highest ratio of initiator to monomer and the highest amount of disulphide crosslinker, shows the most significant M_w

reduction from 45k to 1k, perfectly following the design of shortening the primary chains. This efficient degradation capability is supposed to have potential in reducing cytotoxicity, since high cytotoxicity is usually induced by high molecular weight foreign molecules, which are too difficult for cells to metabolize or exocytose.

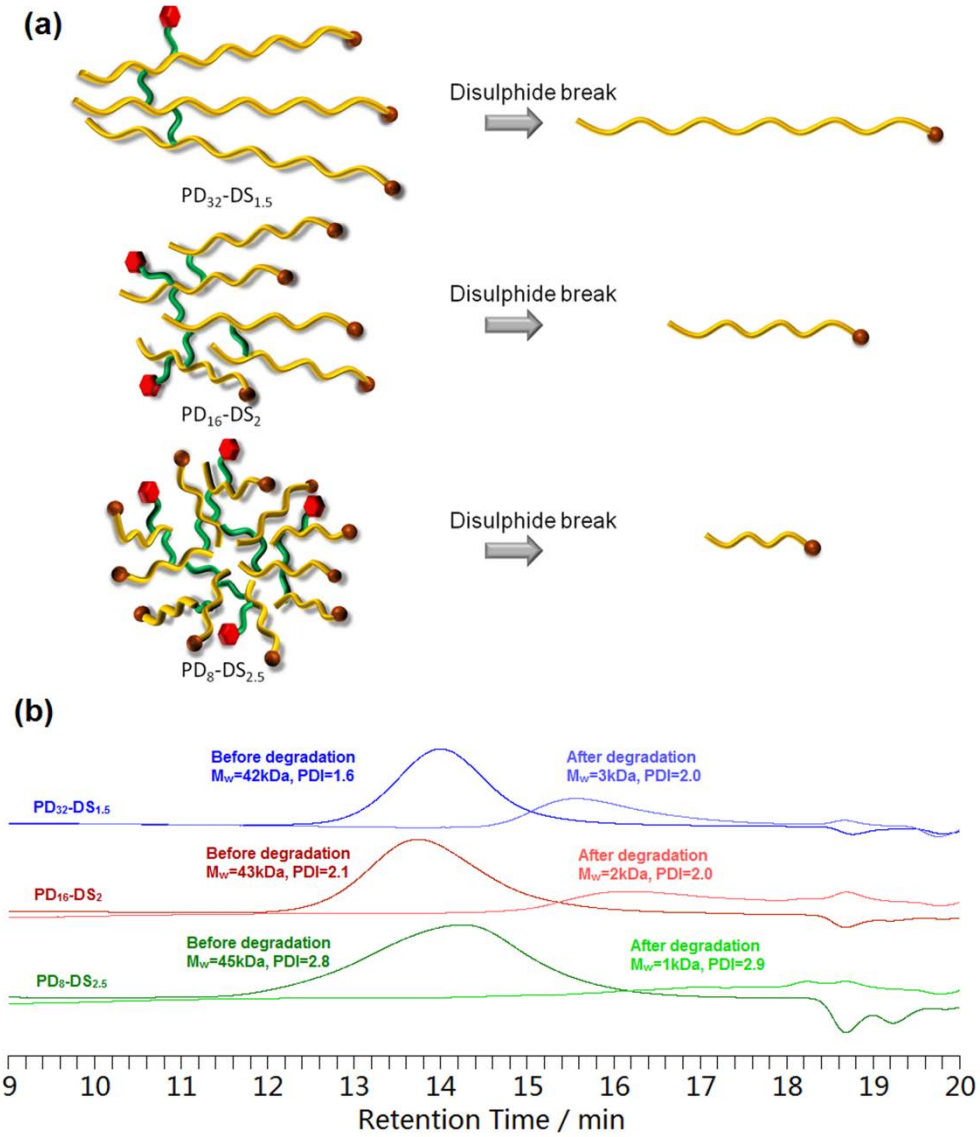

Figure 5.6 Degradation of the three PD_x-DS_y polymers: (a) Graphical representations of the degradations of structures with different branching degrees; (b) GPC traces of the three PD_x-DS_y polymers before and after 1 hours treatment of 20mM glutathione, showing a significant molecular weight reduction.

5.3.3 Characterization of the polymer/DNA complexes

The polymer/DNA interaction (polyplex) characterization was firstly

performed by agarose gel electrophoresis as shown in Figure 5.7. It can be seen that the critical complex formation weight ratios for PD_{32}-$DS_{1.5}$, PD_{16}-DS_2 and PD_8-$DS_{2.5}$ were around 0.4, 0.6 and 0.8, respectively. This could be attributed to the difference of DMAEMA contents, which lead to different positive charge density of these polymers. Another possible reason is that less branched molecules possess higher flexibility and thus need less entropy change for DNA binding compared to the rigid highly branched molecules.

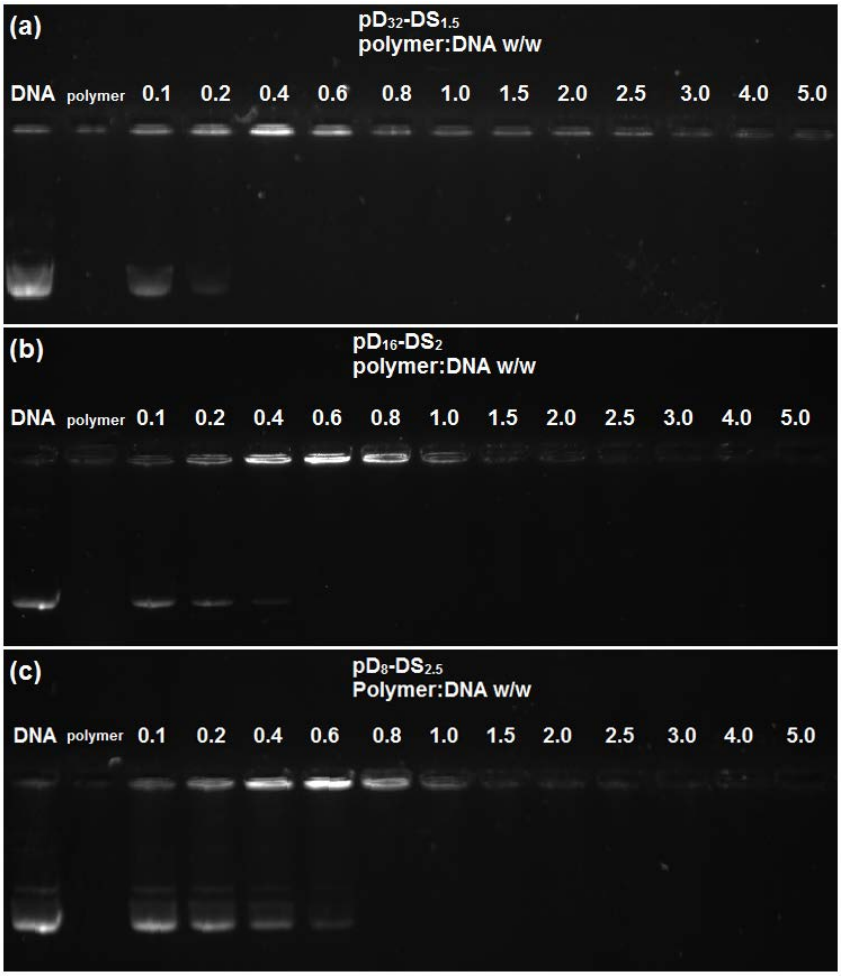

Figure 5.7 The polymer/DNA interaction characterization by gel electrophoresis, showing that (a) PD_{32}-$DS_{1.5}$ complexes DNA at a ratio of 0.4:1 (w/w); (b) PD_{16}-DS_2 complexes DNA at a ratio of 0.6:1 (w/w) and (c) PD_8-$DS_{2.5}$ complexes DNA at a ratio of 0.8:1 (w/w);

Polyplex size and charge characterization was then carried out as shown in Figure 5.8. Three polymer/plasmid weight ratios of 1:1, 3:1 and 5:1 were chosen to form polyplexes. All the polyplexes formed by the PD-DS polymers exhibited decrease in size and increase in surface potential as the

weight ratio of polymer/DNA increased. The particle sizes range from 50nm to 200nm with the PD_8-$DS_{2.5}$ polyplexes showing the largest sizes. This is possibly due to the increasing hydrophobicity caused by the higher amount of DSDA units. All the surface potential of the polyplex particles exhibit positive values. It is interesting to note that the surface potentials of the polyplexes show different increasing rates, with the PD_8-$DS_{2.5}$ polyplexes growing the fastest, indicating different manners of DNA binding between polymers and DNA.

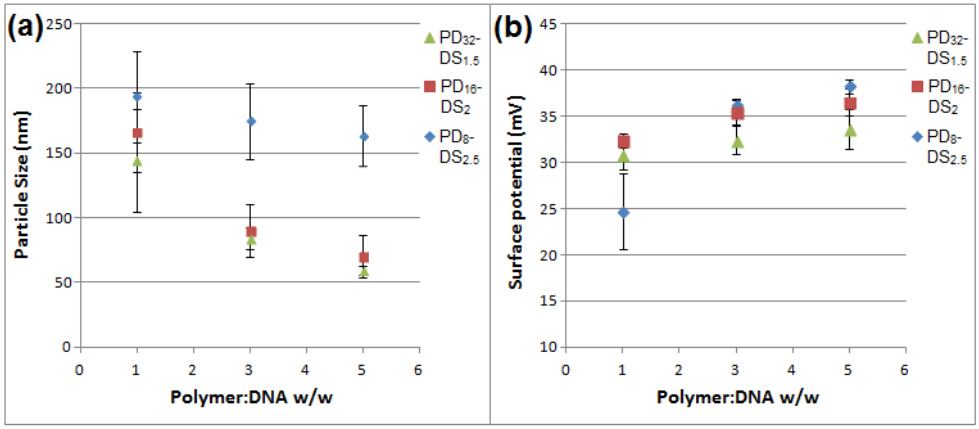

Figure 5.8 Size and surface potential of the three PD_x-DS_y/DNA polyplexes at different weight ratios: (a) particle size; (b) surface potential. As the weight ratio of polymer/DNA increases, the particle size decreases and the surface potential increases for all the polyplexes.

5.3.4 Transfection and cell viability study

The transfection capability of the three polymers was assessed by the secreted G-luciferase protein assay on HeLa cells (Figure 5.9 (a)). In each G-luciferase study, three polymer/plasmid weight ratios of 1:1, 3:1 and 5:1 were tested for all the PD-DS polymers together with the linear PDMAEMA (44kDa) and non-degradable branched $PDMAEMA_8$-$EGDMA_{2.5}$ (labeled as PD_8-$E_{2.5}$ in Figure 5.9) as comparison. To estimate the real transfection capability of the highly branched PD-DS and their commercial prospects, commonly used polymer transfection agents, such as PEI, Superfect and Xfext, were used as the positive control throughout these studies according to the manufacturers' protocol. The subsequent effect on cell viability of those commercial agents and polymers with different weight ratios were also plotted (Figure 5.9 (b)). The alamarBlue® reagent was used to measure any reduction in cell metabolic activity, normalized to indicate cell viability by plotting as a percentage of the control cells.

It can be seen from Figure 5.9 (a) that highly branched PD-DS polymers exhibited far higher transfection capabilities than did the linear PDMAEMA when the polymer/plasmid weight ratio is above 3. Meanwhile, the transfection capability increased with the branching intensifying from PD_{32}-$DS_{1.5}$ to PD_{8}-$DS_{2.5}$, showing strong effect of changing the degree of branching on the transfection performance. Despite complete complexation of the plasmid occurring at polymer/plasmid weight ratios below 1, highest transfection was observed at weight ratios above 3, possibly because of the smaller particle size observed at the higher ratio, and sufficient positive charge to aid membrane translocation. The degradable PD_{8}-$DS_{2.5}$ also showed higher transfection capability than did the non-degradable PD_{8}-$E_{2.5}$ polymer with similar degree of branching. Contributing factors could be the higher cytotoxicity associated with the non-degradable PD-E polymers as shown in Figure 5.9 (b). It has to be mentioned that the PD-E may not be the best candidate for comparison as the similar reactivity of the methacrylate on DMAEMA and EGDMA could result in a homogeneous branch distribution different from that of the PD-DS polymer. Cell metabolic activity analysis of the polymers (and comparisons) was performed using HeLa cells exposed to different concentrations for 48 hours. As the concentration increased (by increasing polymer plasmid ratio), reduced cell viability was seen for all polymers. On the other hand, PD-DS polymers show much lower adverse effect on cells, with the PD_{8}-$DS_{2.5}$ showing cell metabolic activities above 90% even at the high weight ratio of 5.

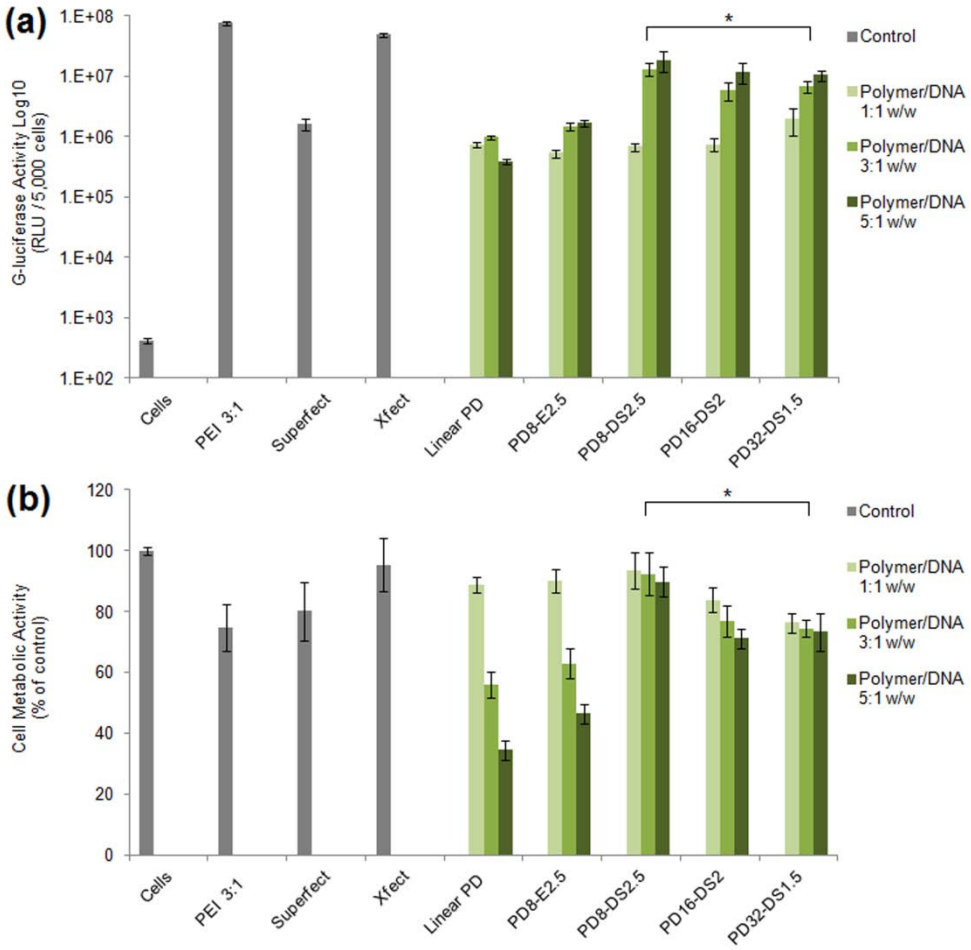

Figure 5.9 G-luciferase transfection and cytotoxicity analysis on HeLa cells after 48 hours incubation: The branched PD_x-DS_y polymers manifest more favorable transfection properties in terms of transfection ability (a) and cytotoxicity (b) than the linear PDMAEMA (n=6, 5,000 cells and 1µg of pDNA per well, error bars indicate ± standard deviation, and asterisks indicate a significant difference from linear PDMAEMA).

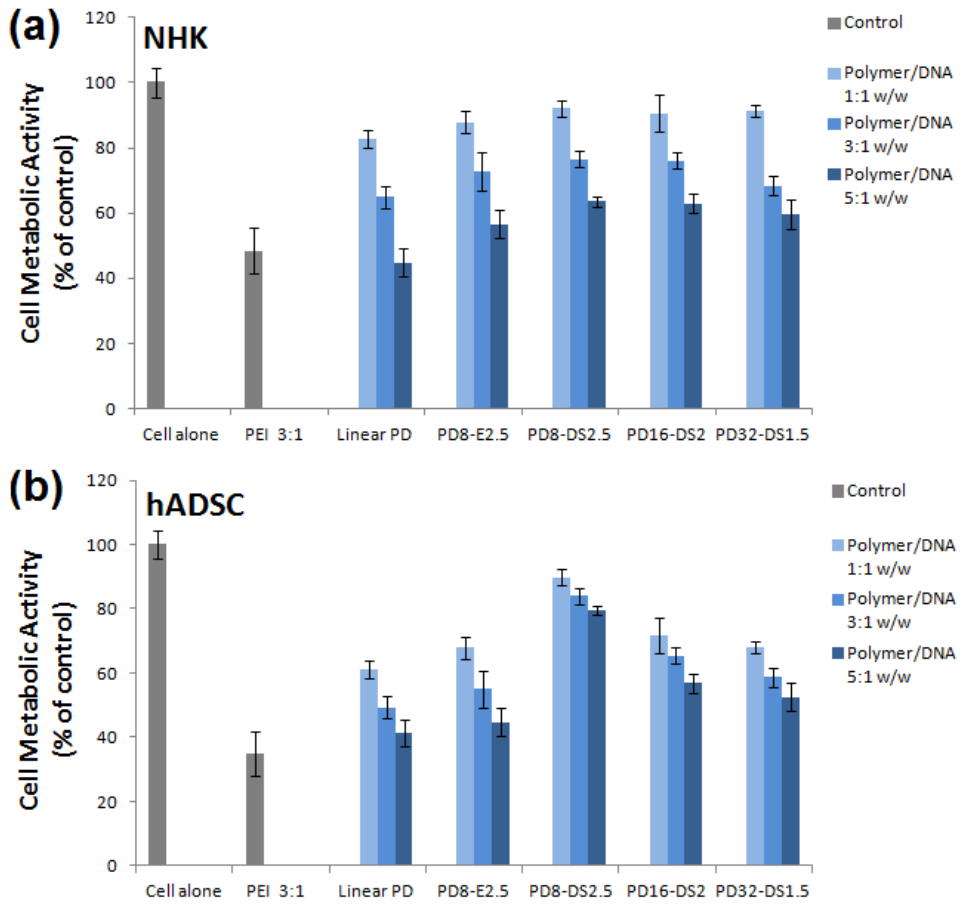

Figure 5.10 Cytotoxicity analysis by alamarBlue assay on NHK (a) and hADSC (b) cells after 48 hours incubation, error bars indicate ± standard deviation.

The cytotoxicity test was also performed on different cell lines (normal human keratinocyte (NHK) and human adipose stem cell (hADSC)), showing a similar trend of influences on cells (Figure 5.10). This is extremely promising since high transfection capability and low cytotoxicity could be achieved at the same time by bringing a high degree of branching with degradation capability to PDMAEMA. It is worth noted that different cell types showed sensitivities to different factors. The NHKs were more sensitive to the high dose of transfection agents but showed less variance of cell metabolic activity with different transfection agents. Whereas, the hADSCs were more sensitive to the type of transfection agents and the highly degradable PD_8-$DS_{2.5}$ showed the least influence on the metabolic activity of the hADSCs.

Fluorescent microscopy imaging of GFP expression was also used to confirm the transfection on different cell types, including HeLa (Figure 5.11), NHK (Figure 5.12) and hADSC (Figure 5.13). The GFP expression of HeLa cells is qualitatively in accordance with the G-luciferase expression. Large areas of cells can be transfected with widespread GFP expression throughout the cell cytoplasm when PD_8-$DS_{2.5}$ is used as the transfection agent. Meanwhile, most of the cells stayed alive after 48h transfection without changing the medium post transfection, revealing low cytotoxicity. The NHKs maintained in good viabilities after 48h only with low polymer/DNA weight ratio (1:1) added. This is quite in accordance with the alamarBlue results shown in Figure 5.10. The transfection efficiency on NHKs did not show huge variance between different PD-DS polymers. Good cell compatibility of PD_8-$DS_{2.5}$ was also observed for hADSC cells, though transfection efficacy was much lower for this cell type.

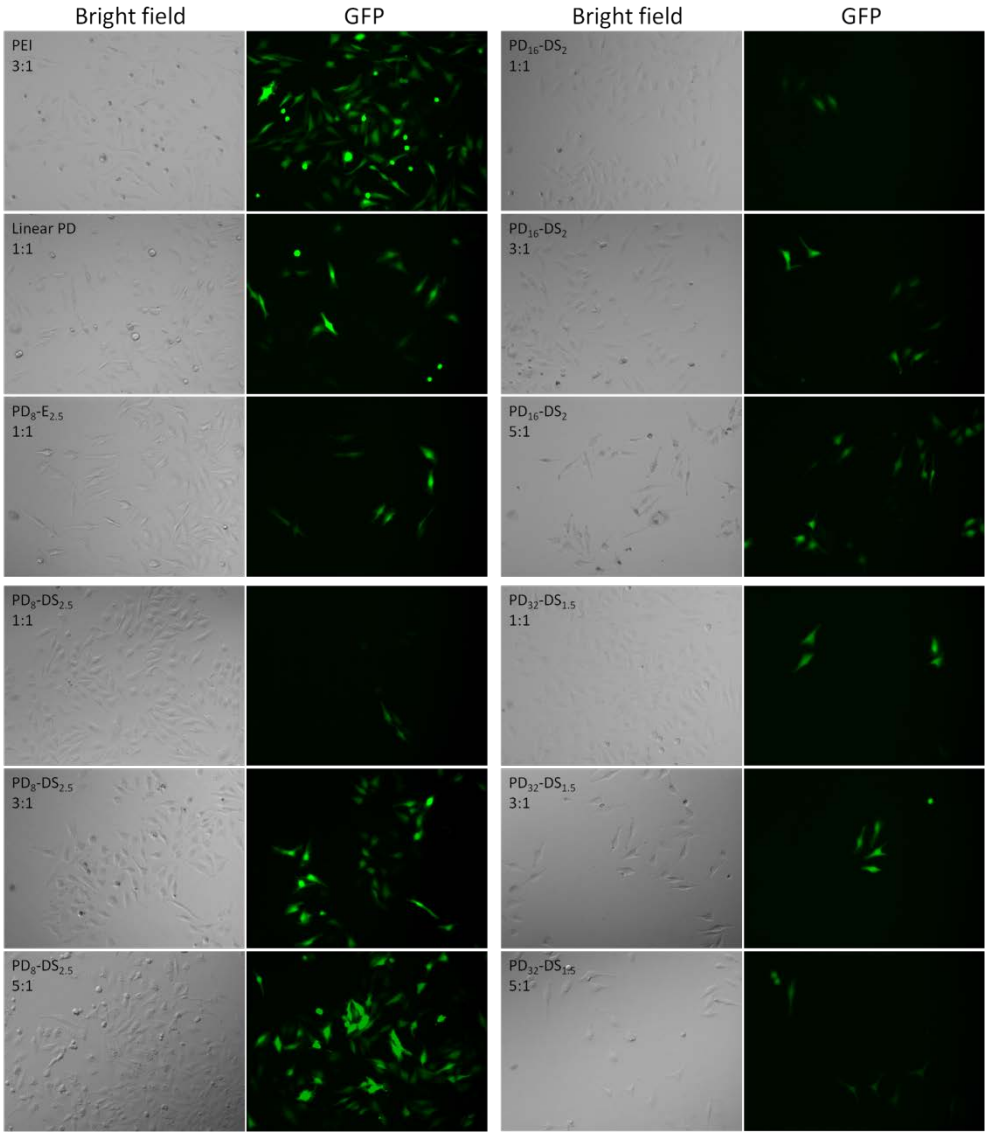

Figure 5.11 Fluorescent microscopy images of HeLa cells incubated for 48 h with GFP polyplexes comprised of the three PD_x-DS_y polymers in comparison to the linear PDMAEMA (44kDa) and non-degradable branched PD_8-$E_{2.5}$ as well as the commercial 25kDa bPEI. The ratios embedded in the photos stand for the polymer/DNA weight ratio.

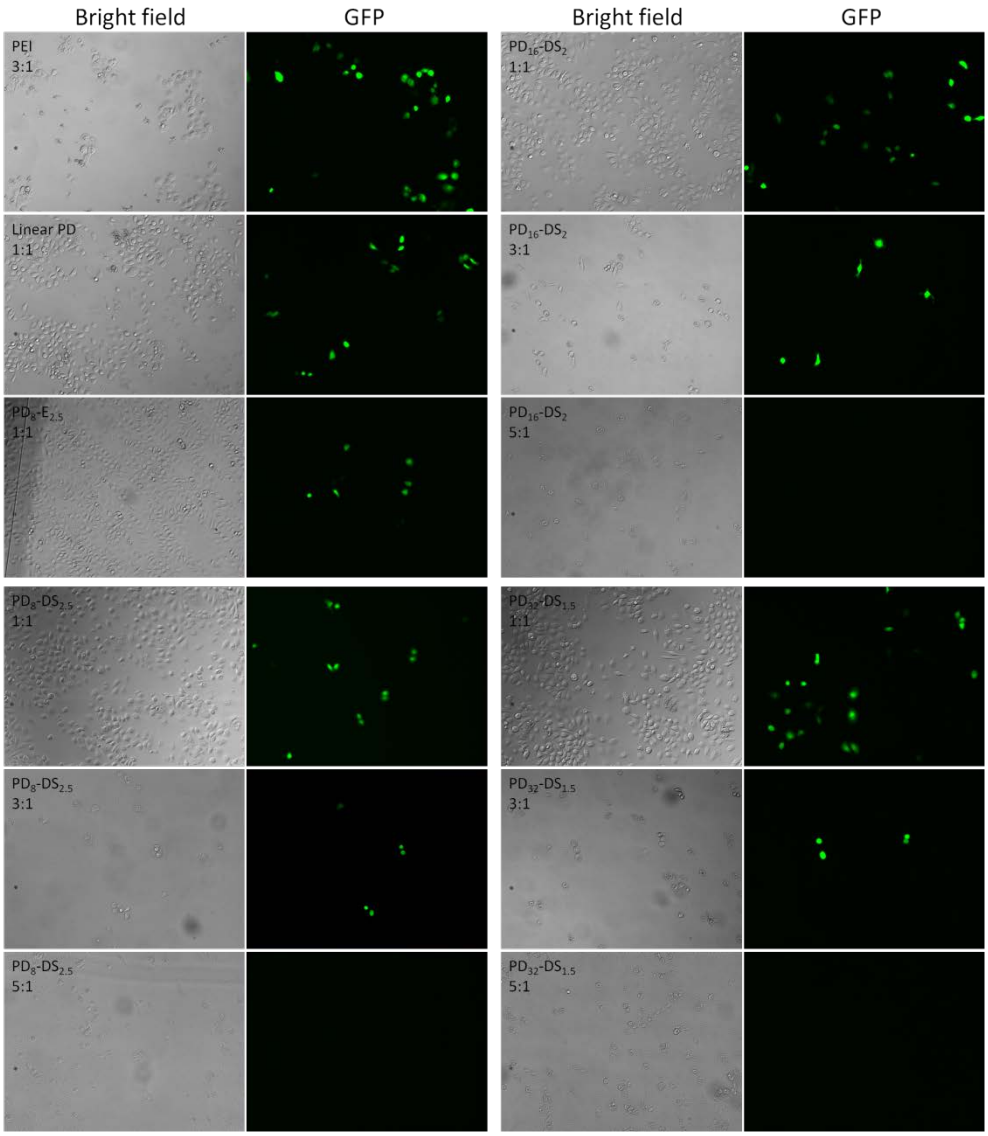

Figure 5.12 Fluorescent microscopy images of NHK cells incubated for 96 h with GFP polyplexes comprised of the three PD_x-DS_y polymers in comparison to the linear PDMAEMA (44kDa) and non-degradable branched PD_8-$E_{2.5}$ as well as the commercial 25kDa bPEI. The ratios embedded in the photos stand for the polymer/DNA weight ratio.

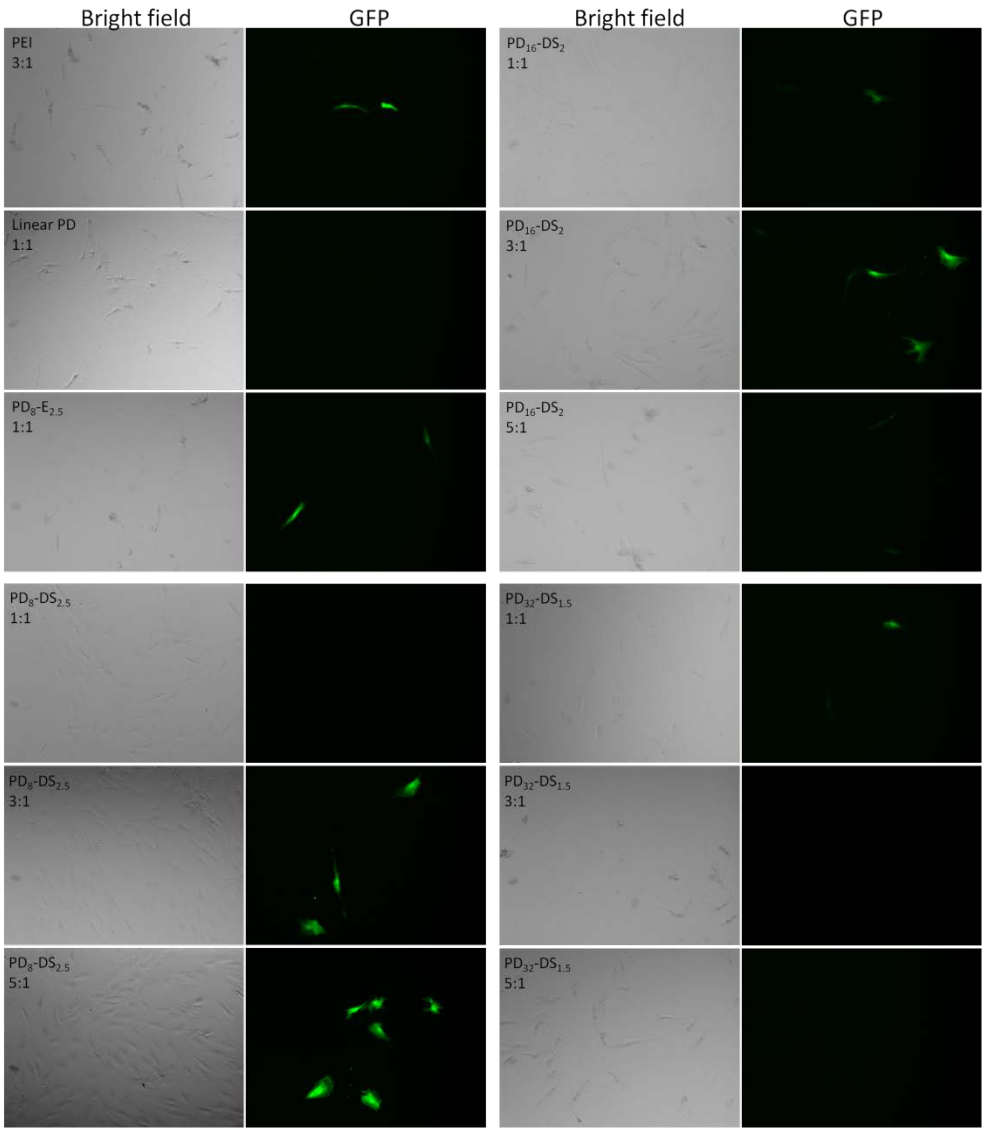

Figure 5.13 Fluorescent microscopy images of hADSC cells incubated for 96 h with GFP polyplexes comprised of the three PD_x-DS_y polymers in comparison to the linear PDMAEMA (44kDa) and non-degradable branched PD_8-$E_{2.5}$ as well as the commercial 25kDa bPEI. The ratios embedded in the photos stand for the polymer/DNA weight ratio.

5.4 Conclusions

In conclusion, highly branched degradable PD-DS copolymers consisting of short primary chain molecules were synthesized and proved to be effective *in vitro* gene delivery agents. The special structure and components of

PD-DS copolymers provides a strong capability for post-functionalization or labeling as well as an efficient degradation property. The highly branched copolymers also offer different patterns of interaction between the polymer and plasmid DNA, and lead to a general profile of comparable transfection capability to the leading commercial transfection agents. By adjusting the degree of branching and the length of primary chain molecules, lower cytotoxicity was also achieved, thus rendering the PD-DS copolymers a more attractive alternative to the linear PDMAEMA. This strategy towards highly branched degradable structures, previously unachievable theoretically and experimentally, will open new avenues for the field of gene delivery.

5.5 References

1. Esfand, R.; Tomalia, D. A. Poly(amidoamine) (PAMAM) dendrimers: from biomimicry to drug delivery and biomedical applications. *Drug Discov. Today* **2001,** *6* (8), 427-436.
2. Zhu, C. H.; Jung, S.; Luo, S. B.; Meng, F. H.; Zhu, X. L.; Park, T. G.; Zhong, Z. Y. Co-delivery of siRNA and paclitaxel into cancer cells by biodegradable cationic micelles based on PDMAEMA-PCL-PDMAEMA triblock copolymers. *Biomaterials* **2010,** *31* (8), 2408-2416.
3. Synatschke, C. V.; Schallon, A.; Jerome, V.; Freitag, R.; Muller, A. H. E. Influence of polymer architecture and molecular weight of poly(2-(dimethylamino)ethyl methacrylate) polycations on transfection efficiency and cell viability in gene delivery. *Biomacromolecules* **2011,** *12* (12), 4247-4255.
4. Newland, B.; Tai, H.; Zheng, Y.; Velasco, D.; Di Luca, A.; Howdle, S. M.; Alexander, C.; Wang, W.; Pandit, A. A highly effective gene delivery vector-hyperbranched poly(2-(dimethylamino)ethyl methacrylate) from in situ deactivation enhanced ATRP. *Chemical Communications* **2010,** *46* (26), 4698-4700.
5. Newland, B.; Zheng, Y.; Jin, Y.; Abu-Rub, M.; Cao, H.; Wang, W.; Pandit, A. Single cyclized molecule versus single branched molecule: A simple and efficient 3D "knot" polymer structure for nonviral gene delivery. *Journal of the American Chemical Society* **2012,** *134* (10), 4782-4789.
6. Agarwal, S.; Zhang, Y.; Maji, S.; Greiner, A. PDMAEMA based gene delivery materials. *Materials Today* **2012,** *15* (9), 388-393.
7. Joralemon, M. J.; McRae, S.; Emrick, T. PEGylated polymers for medicine: from conjugation to self-assembled systems. *Chemical Communications* **2010,** *46* (9), 1377-1393.
8. Yu, J.-H.; Quan, J.-S.; Kwon, J.-T.; Xu, C.-X.; Sun, B.; Jiang, H.-L.; Nah, J.-W.; Kim, E.-M.; Jeong, H.-J.; Cho, M.-H.; Cho, C.-S. Fabrication of

a novel core-shell gene delivery system based on a brush-like polycation of alpha, beta-poly (L-aspartate-graft-PEI). *Pharmaceutical Research* **2009,** *26* (9), 2152-2163.
9. Plamper, F. A.; Schmalz, A.; Penott-Chang, E.; Drechsler, M.; Jusufi, A.; Ballauff, M.; Mueller, A. H. E. Synthesis and characterization of star-shaped Poly(N,N-dimethylaminoethyl methacrylate) and its quaternized ammonium salts. *Macromolecules* **2007,** *40* (16), 5689-5697.
10. Sahnoun, M.; Charreyre, M. T.; Veron, L.; Delair, T.; D'Agosto, F. Synthetic and characterization aspects of dimethylaminoethyl methacrylate reversible addition fragmentation chain transfer (RAFT) polymerization. *Journal of Polymer Science Part A-Polymer Chemistry* **2005,** *43* (16), 3551-3565.
11. Rawlinson, L.-A. B.; O'Brien, P. J.; Brayden, D. J. High content analysis of cytotoxic effects of pDMAEMA on human intestinal epithelial and monocyte cultures. *Journal of Controlled Release* **2010,** *146* (1), 84-92.
12. Samsonova, O.; Pfeiffer, C.; Hellmund, M.; Merkel, O. M.; Kissel, T. Low molecular weight pDMAEMA-block-pHEMA block-copolymers synthesized via RAFT-polymerization: Potential non-viral gene delivery agents? *Polymers* **2011,** *3* (2), 693-718.
13. Mathew, A.; Cao, H.; Collin, E.; Wang, W.; Pandit, A. Hyperbranched PEGmethacrylate linear pDMAEMA block copolymer as an efficient non-viral gene delivery vector. *International Journal of Pharmaceutics* **2012,** *434* (1-2), 99-105.
14. Rungsardthong, U.; Deshpande, M.; Bailey, L.; Vamvakaki, M.; Armes, S. P.; Garnett, M. C.; Stolnik, S. Copolymers of amine methacrylate with poly(ethylene glycol) as vectors for gene therapy. *Journal of Controlled Release* **2001,** *73* (2-3), 359-380.
15. Chang, L.; Deng, L.; Wang, W.; Lv, Z.; Hu, F.; Dong, A.; Zhang, J. Poly(ethyleneglycol)-b-poly(epsilon-caprolactone-co-gamma-hydroxyl-epsi l on-caprolactone) bearing pendant hydroxyl groups as nanocarriers for doxorubicin delivery. *Biomacromolecules* **2012,** *13* (10), 3301-3310.
16. Zhao, T.; Zheng, Y.; Poly, J.; Wang, W. Controlled multi-vinyl monomer homopolymerization through vinyl oligomer combination as a universal approach to hyperbranched architectures. *Nature Communications* **2013,** *4*.
17. Tsarevsky, N. V.; Matyjaszewski, K. Combining atom transfer radical polymerization and disulfide/thiol redox chemistry: A route to well-defined (bio)degradable polymeric materials. *Macromolecules* **2005,** *38* (8), 3087-3092.
18. Li, Y. T.; Armes, S. P. Synthesis and chemical degradation of branched vinyl polymers prepared via ATRP: Use of a cleavable disulfide-based branching agent. *Macromolecules* **2005,** *38* (20), 8155-8162.
19. Wang, L.; Li, C. M.; Ryan, A. J.; Armes, S. P. Synthesis and peptide-induced degradation of biocompatible fibers based on highly

branched poly(2-hydroxyethyl methacrylate). *Advanced Materials* **2006,** *18* (12), 1566-1570.
20. Gao, H. F.; Matyjaszewski, K. Synthesis of functional polymers with controlled architecture by CRP of monomers in the presence of cross-linkers: From stars to gels. *Progress in Polymer Science* **2009,** *34* (4), 317-350.
21. Bannister, I.; Billingham, N. C.; Armes, S. P.; Rannard, S. P.; Findlay, P. Development of branching in living radical copolymerization of vinyl and divinyl monomers. *Macromolecules* **2006,** *39* (22), 7483-7492.
22. Gao, H.; Li, W.; Matyjaszewski, K. Synthesis of polyacrylate networks by ATRP: Parameters influencing experimental gel points. *Macromolecules* **2008,** *41* (7), 2335-2340.
23. Rosselgong, J.; Armes, S. P.; Barton, W. R. S.; Price, D. Synthesis of branched methacrylic copolymers: comparison between RAFT and ATRP and effect of varying the monomer concentration. *Macromolecules* **2010,** *43* (5), 2145-2156.
24. Gao, H. F.; Miasnikova, A.; Matyjaszewski, K. Effect of cross-linker reactivity on experimental gel points during ATRcP of monomer and cross-linker. *Macromolecules* **2008,** *41* (21), 7843-7849.
25. Gao, H.; Polanowski, P.; Matyjaszewski, K. Gelation in living copolymerization of monomer and divinyl cross-linker: comparison of ATRP experiments with monte carlo simulations. *Macromolecules* **2009,** *42* (16), 5925-5932.
26. Shinoda, H.; Matyjaszewski, K. Improving the structural control of graft copolymers. Copolymerization of poly (dimethyl siloxane) macromonomer with methyl methacrylate using RAFT polymerization. *Macromolecular Rapid Communications* **2001,** *22* (14), 1176-1181.
27. Rosselgong, J.; Armes, S. P. Quantification of intramolecular cyclization in branched copolymers by H-1 NMR spectroscopy. *Macromolecules* **2012,** *45* (6), 2731-2737.
28. Zheng, Y.; Cao, H. L.; Newland, B.; Dong, Y. X.; Pandit, A.; Wang, W. X. 3D single cyclized polymer chain structure from controlled polymerization of multi-vinyl monomers: Beyond Flory-Stockmayer theory. *Journal of the American Chemical Society* **2011,** *133* (33), 13130-13137.
29. Eltoukhy, A. A.; Chen, D.; Alabi, C. A.; Langer, R.; Anderson, D. G. Degradable terpolymers with alkyl side chains demonstrate enhanced gene delivery potency and nanoparticle stability. *Advanced Materials* **2013,** *25* (10), 1487-1493.

Chapter Six

Summary and Future Directions

6.1 Summary

This chapter summarizes the research results and overall conclusions of the thesis in the following four main parts: 1) ATRA reaction study for good kinetic control of multi-vinyl monomer homopolymerization; 2) development of the vinyl oligomer combination strategy as a universal approach to hyperbranched polymers; 3) synthesis of PEG-based hyperbranched polymers by vinyl oligomer combination towards photo-crosslinkable hydrogels and 4) synthesis of highly branched degradable cationic polymers by vinyl oligomer combination towards efficient gene delivery agents.

6.1.1 ATRA Reaction Study for Good Kinetical Control of Homopolymerization of Multi-vinyl Monomer

The objective of chapter 2 is to establish the optimal, well-controlled reaction system for ATRP of vinyl monomers, especially in the presence of a large amount of initiator. It is hypothesized that if a vinyl monomer can achieve a high yield of mono-addition in an ATRA reaction, it will also support a good ATRP under the same condition. Based on this objective and hypothesis, different copper-catalyzed ATRA reactions (including normal ATRA, ARGET-ATRA and *in situ* DE-ATRA) were initially evaluated through the addition of chloroform to mono-vinyl monomers (styrene and methyl methacrylate). Both, high conversion and high monoadduct yield, were obtained in the *in situ* DE-ATRA system in the presence of initial Cu^{II} and a low portion of reducing agent. The ATRA reaction in the presence of Cu^{I} catalyst at 100 ppm proceeded less efficiently but still allows a good control for the formation of monoadduct. In contrast, FRP and ARGET-ATRA could not achieve the preparation of monoadduct under either of the following reaction conditions - absence of Cu^{I} or presence of Cu^{II} with excess AA. High initial Cu^{II} concentration and low proportion of reducing agent are beneficial for a high, constant reaction rate and are essential for a well-controlled ATRA reaction.

After the evaluation of the ATRA on the mono-vinyl monomer, an attempt was made to accomplish the homopolymerization of divinyl monomers. It is hypothesized that if a strategy can be obtained to form a high yield of the monoadduct, this method could then be applied to the polymerization of divinyl monomers to produce HBPs with an ideal dendritic structure - a

short primary chain length and a high number of functional end groups. To verify this hypothesis, homopolymerization of two divinyl monomers (EGDMA and DVB) were studied. Utilizing the optimized ATRA reaction system (*in situ* DE-ATRA), the chain growth of divinyl monomers was minimized and the polymerization was driven towards branching. In this way, hyperbranched poly-EGDMA and poly-DVB were prepared with a high branch ratio and a high number of vinyl functional groups. These promising, initial results were then improved and further developed in the following experiments as a universal approach to functional hyperbranched polymers.

6.1.2 Development of Vinyl Oligomer Combination Strategy as a Universal Approach to HBPs

Based on the evaluation of the *in situ* DE-ATRA and the study of the polymerization of divinyl monomers in chapter 2, chapter 3 developed a universal approach, a so called 'vinyl oligomer combination', which allows the successful design of hyperbranched polymer architectures from commercially available multi-vinyl monomers. By introducing a high ratio of initiator to monomer and good kinetic control, hyperbranched polymers were synthesized that consist purely of extremely short primary chains and abundant vinyl functional groups. The structure is fundamentally distinct from the architecture produced by any previous method (*e.g.* polycondensation, 'Strathclyde synthesis', CRCC or even SCVP).

The polymerization process of diacrylate monomers was carefully studied using GPC, NMR, GC and MS analysis. We have provided solid evidence to demonstrate that it is possible to kinetically and statistically control and tailor the hyperbranched structure during the homopolymerization of multi-vinyl monomers in a concentrated polymerization system. It has been shown that by manipulation of the chain growth condition, the di-vinyl monomers can be built up into two clearly different polymer structures. One is a 'single cyclized' structure, which is linked repeatedly, wrapping around itself in an interlaced pattern, creating a very dense but soluble structure; the other one is a veritable hyperbranched structure which is composed of approximately 70% branched units with the remaining 30% retaining the potential of branching or further addition of functional groups.

The derivatives of methacrylate and styrene were also employed and successfully used for the polymerization towards hyperbranched polymers. This provides us with a number of possibilities to create a broad range of

new highly branched functional polymers with novel properties from a variety of economical and structurally special multi-vinyl monomers. This new approach demonstrates great advantages for the synthesis of hyperbranched polymers for industrial applications through its sheer simplicity, monomer possibilities and high yield.

6.1.3 Synthesis of PEG-based HBPs by Vinyl Oligomer Combination towards Photo-crosslinkable Hydrogels

The objective of this part was to develop a PEG-based hyperbranched polymer as a precursor of a photo-crosslinkable hydrogel system with the potential use as a bioactive temporary hydrogel dressing for wound healing applications.

Based on the vinyl oligomer combination strategy developed in the chapter 3, two poly(ethylene glycol) diacrylates (PEGDA) with different lengths of PEG spacers were homopolymerized in a concentrated solution ([PEGDA] = 60% w/v) via *in situ* DE-ATRP to produce a series of water-soluble hyperbranched polymers. The polymerization will undergo a slow vinyl propagation process of divinyl monomers followed by a polycondensation or coupling of reactive oligomers. High monomer conversions (up to 96%) and hyperbranched polymer structure were both achieved by increasing the ratio of initiator/monomer, which results in a high chain concentration and a smaller chain dimension before the crosslinking reaction occurs.

The hyperbranched structure was verified by the comparison of Mark-Houwink plots and molecular weights determined by RI and viscometer. The relative propensities for intermolecular propagating/cross-linking reactions and intramolecular cyclization were assessed using ^{1}H NMR measurements.

The poly($PEGDA_{700}$)s show good solubility in aqueous solution whereas the poly($PEGDA_{575}$)s show a characteristic thermoresponsive property, which is highly dependent on the polymer concentration and the polymer composition. LCST was determined by testing the phase transition temperature of different polymer concentration. It was found that the LCST value decreases with an increased hydrophobicity. These data suggest that LCST value can be easily adjusted to the required temperature between 9 and 31˚C by controlling the hydrophilic-hydrophobic balance.

These PEG-based hyperbranched vinyl functional polymers were used as

photo-crosslinkable precursors for the formation of PEG-based hydrogels and resulted in efficient UV curing properties (within 15 seconds). The fabricated hydrogels were used for 2D culture of 3T3 cells and showed capability to maintain high cell viability of these cells.

6.1.4 Synthesis of Highly Branched Degradable Cationic Polymers by Vinyl Oligomer Combination towards Efficient Gene Delivery Agents

The notion that the macromolecular structure of non-viral gene vectors alters their transfection efficiency has inspired numerous novel designs of 3D polymeric structures. Compared to the numerous transfection studies on linear or block PDMAEMA, the study of 3D branched PDMAEMA is still comparatively rare. The objective was therefore to synthesize highly branched PDMAEMAs with degradation properties and to assess if the degradable highly branched PDMAEMA can supersede the linear PDMAEMA in terms of both transfection capability and lower toxicity.

On the basis of the vinyl oligomer combination approach developed and described in the previous chapters, this part successfully transferred and applied the approach to a copolymerization system and reported the preparation of a series of highly branched DMAEMA/bis(2-acryloyl)oxyethyl disulphide (DSDA) copolymers via 'vinyl oligomer combination' approach and *in situ* DE-ATRP technology. High initiator/DMAEMA ratios (1/8~1/32) and high initiator/DSDA ratios (1/2.5~1/1.5) were employed in order to supply a high concentration of initial short primary chains, which could enhance intermolecular combination and thus lead to a highly branched structure.

We hypothesized that this highly branched structure would lead to greater performance because a 3D branched structure with multiple functional groups for DNA interaction is created and because the efficient intracellular cleavage of disulphide bond will result in low cytotoxicity.

Three polymers with different initial component ratio (PD_{32}-$DS_{1.5}$, PD_{16}-DS_{2}, PD_{8}-$DS_{2.5}$) were synthesized to reach a similar molecular weight. The polymerization process was also monitored by GPC, showing that the lower molar ratio of initiator to DMAEMA monomer (PD_{32}-$DS_{1.5}$) led to a faster molecular weight increase at the linear growth period whereas the higher content of divinyl cross-linker of PD_{8}-$DS_{2.5}$ resulted in a stronger

exponential increase of molecular weight during the later stage.

The special structure and components of PD-DS copolymers provides a strong capability for post-functionalization or labeling as well as an efficient degradation property. After end-capping the vinyl groups with functional molecules, these polymers were studied on different cell types, showing that the highly branched PD-DS is superior to the linear PDMAEMA with some polyners showing comparable transfection capability to the commercial DNA vectors (bPEI (25k), Xfect, and polyamidoamine (PAMAM)). By adjusting the degree of branching and the length of primary chain molecules, lower cytotoxicity was also achieved, thus rendering the PD-DS copolymers a more attractive alternative to the linear PDMAEMA. This strategy towards highly branched degradable structures, previously unachievable theoretically and experimentally, will open new avenues for the field of gene delivery.

6.2 Limitations

The studies described in chapter 2 evaluated different copper-catalyzed ATRA reaction systems. However, the study mainly focused on one commonly used ligand (PMDETA). It has been reported that the ligand plays a significant role in determining the rate constant of the equilibrium in the copper-catalyzed ATRA reaction[1]. Changing the ligand could induce different performance of ATRA reactions, resulting in different monoadduct yields and monomer conversions. Also, there are still several ATRA systems that remain to be evaluated, including ICAR ATRA (with conventional initiator (I-I), metal complex in the higher oxidation state (Cu^{II}/Ligand) and monomer added at the beginning of reaction) and SR&NI ATRP (with conventional initiator (I-I), alkyl halide (R-X), metal complex in the higher oxidation state (Cu^{II}/Ligand) and monomer added at the beginning of reaction). The ICAR ATRA has recently been proved to be a very efficient method to achieve a high yield of monoadduct at low copper catalyst concentration[2]. Thus, it is worth to explore effects of different ligands and reaction systems and further optimize the ATRA reactions.

The main drawback of the vinyl oligomer combination approach for the development of hyperbranched polymers described in chapter 3 is the wide polydispersity (PDI) of the products obtained. Even though the first stage of linear propagation is controlled, the chain combination in the later stage is quite complicated since the mixture in the reaction could be more complex than the polycondensation. It is known that most of the natural polymers are monodispersed. In general, a low PDI is a prerequisite for the use of

polymer in pharmaceutical applications. A PDI value below 1.1 indicates a homogenous polymer preparation that provides reliable, persistent residence time in the body[3]. Therefore, the polydispersity could be an important index for biological research and applications. Currently, it is still challenging to obtain hyperbranched polymers with low PDI in a single step reaction. However, by using advanced purification and separation methods, such as membrane dialysis, gradient precipitation, size exclusion chromatography and ultrafiltration, the molecular weight distribution can be optimized toward biomedical grades. The separated, well defined hyperbranched polymers and their properties could be another interesting subject of research. Another feature of the vinyl oligomer combination approach is that it requires a large amount of initiator in the reaction and thus leaves an abundance of initiator end-groups in the polymer product. These initiator end-groups have advantages and disadvantages. In experimental settings that include polymers with similar properties to the monomers or that study the effect of the monomers, these end-groups could interfere and therefore need to be removed. However, these end-groups could bring new properties and possibilities for post-functionalization. Modification could be applied to the initiator before polymerization or after the polymer is synthesized.

In chapter 4, the photo-crosslinking method was used to fabricate hydrogels. However, some drawbacks limit the applications of the photo-crosslinked systems in clinical such as the extra equipment that is needed in a clinical setting, the dosage and safety concerns of applying UV radiation[4, 5, 6]. Furthermore, the hydrogel evaluation only focused on the cell viability test. Some important properties, such as swelling, degradation, were not systematically studied. In addition, the hydrogel showed limited cell-adherent properties as do most of the PEG-based hydrogels. To overcome these limitations, several modified approaches could be performed with the polymer and hydrogel system, some of which are discussed in the following section as “future directions”.

In chapter 5, despite the successful *in vitro* study of the PDMAMEA-DSDA copolymers, *in vivo* experiments need to be carried out in order to evaluate the efficacy of the polymers for clinical applications.

6.3 Future Directions

6.3.1 Kinetic Modeling and Simulation of Vinyl Oligomer Combination

Recently, computational simulation has become one of the major tools in polymer science that helps understanding the molecular structure and dynamics of the polymer chains. It can be applied to study complex gelation processes under various conditions, predicting molecular weight, molecular weight distribution, degree of branching and gelling point. The gelation in the simulated system depends not only on the parameters used but also on the applied model. A statistical theory was developed by Flory[7, 8, 9] and Stockmayer[10, 11, 12] (F-S theory) to predict the gel point. In F-S theory, the gel point based on monomer conversion is influenced by the initial molar ratio of cross-linker to initiator, the initiation efficiency and polydispersity of primary chains. However, the statistical model takes into account only the concentration of involved reagents and did not consider the space and instantaneous growth boundary concept of the polymerization. Thus, a new model which includes the kinetic parameters should be studied in the future. The new kinetic model can help to better understand and predict the experimental gelation process. Also, the Monte Carlo model which has been used to simulate controlled radical copolymerization[13] or the thread-button model[14] which is very similar to the di-vinyl monomer polymerization can be very helpful to the theoretical simulation.

6.3.2 Bioactive Modification of PEG-based Hydrogels

PEG-based hydrogels usually display minimal or no biological functionality due to their non-adhesive and non-degradable nature.[15] Therefore, much effort has been devoted to develop the bioactive modified PEG-based hydrogels that mimic the natural ECM environment.[16, 17, 18, 19]

In Chapter 4, PEG-based hyperbranched polymers with high degree of acrylate functionality have been developed by vinyl oligomer combination. The high content of active vinyl groups provides these polymers with the capability of rapid cross-linking either via Michael-type addition reaction at physiological conditions or via photo-initiated polymerization. Compared with the commercially available PEG-based acrylate functional monomers (e.g. PEGDA) or polymers (e.g. 4-arm-PEG-Acr), these new PEG-based

polymers exhibit advantages such as higher vinyl content, flexible and well-controlled polymer structure and ease of production via one-step reaction. Therefore, a number of bioactive modifications, such as cell adhesive peptides, cleavable crosslinkers, fluorescent molecule and antibodies can be performed based on this acrylate functional polymer for specific purposes.

6.3.3 Optimizing Polymeric Vectors for Improved Transfection

The polymeric materials seem to be rather promising candidates for gene delivery. The synthetic strategies to prepare novel-structured polymers in a controlled manner and possibility of subsequent functionalization offer great opportunities to prepare gene carriers with tailored properties. Despite the success of *in vitro* studies for the developed PD-DS polymers, *in vivo* experiments need to be carried out to further evaluate the efficacy for clinical applications. Although numerous gene vectors have been developed in recent decades, their translation into clinical trials has been slow. This is mainly due to the insufficient knowledge of the physicochemical and biological properties during the various phases of the transfection process. Our developed polymers possess numerous functional groups which can be used to link the tracing molecules. This could help us to improve our understanding of transfection pathways and the fate of nanoparticle/polymer *in vitro* and *in vivo*.

Leal[20] recently reported the development of cationic liposome siRNA complexes with a novel cubic phase nanostructure that exhibited efficient silencing with low toxicity. This finding underscores the importance of understanding interactions between gene complex nanostructure and cell components for the development of gene vectors. By changing our polymer structure, we could probably tune the nanostructure of the polyplex and this could open up new directions for the design of gene carriers.

In addition, primary and stem cells are much harder to transfect than immortalized cells due to their slow proliferation rate and higher extracellular matrix deposition.[21] However, transfection studies on these cell types are very important since primary cells are more representative of the main functional component of the tissue from which they are derived in comparison to immortalized or tumor derived cell lines and stem cells, such as embryonic and induced pluripotent stem cells hold great potential for disease treatment because they can differentiate into any cell type.[22] Thus, it

is important to focus the vector design and optimization on the cellular uptake and nuclear import mechanisms of primary and stem cells. This will inevitably increase the transfection of non-viral vectors in the clinic.

Furthermore, the more recently emerged gene silencing strategy that delivers siRNA into the cells takes benefit from existing expertise in plasmid DNA transfer. However, the delivery of siRNA has predominantly utilized agents most of which were developed for plasmid DNA delivery. DNA and RNA are different in physicochemical properties, for example, the size, the affinity of cation, the stiffness of the strand (resistance to condensation), *etc*. Plasmid DNA needs to be transported into the nucleus for gene expression, while siRNA only needs to be transferred across the plasma membrane to reach its target in the cytoplasm. The optimal carriers may be different for these two applications and polymeric gene vectors should be specifically developed for siRNA delivery.

6.4 References

1. Balili, M. N. C.; Pintauer, T. Kinetic studies of the initiation step in copper catalyzed atom transfer radical addition (ATRA) in the presence of free radical diazo initiators as reducing agents. *Inorganic Chemistry* **2010,** *49* (12), 5642-5649.
2. Pintauer, T.; Matyjaszewski, K. Atom transfer radical addition and polymerization reactions catalyzed by ppm amounts of copper complexes. *Chemical Society Reviews* **2008,** *37* (6), 1087-1097.
3. Veronese, F. M.; Pasut, G. PEGylation, successful approach to drug delivery. *Drug Discovery Today* **2005,** *10* (21), 1451-1458.
4. Hoare, T. R.; Kohane, D. S. Hydrogels in drug delivery: Progress and challenges. *Polymer* **2008,** *49* (8), 1993-2007.
5. Kwon, I. K.; Matsuda, T. Photo-iniferter-based thermoresponsive block copolymers composed of poly(ethylene glycol) and poly(N-isopropylacrylamide) and chondrocyte immobilization. *Biomaterials* **2006,** *27* (7), 986-995.
6. Potta, T.; Chun, C.; Song, S.-C. Dual cross-linking systems of functionally photo-cross-linkable and thermoresponsive polyphosphazene hydrogels for biomedical applications. *Biomacromolecules* **2010,** *11* (7), 1741-1753.
7. Flory, P. J. Molecular size distribution in three dimensional polymers. I. Gelation. *Journal of the American Chemical Society* **1941,** *63*, 3083-3090.
8. Flory, P. J. Molecular size distribution in three dimensional polymers. II. Trifunctional branching units. *Journal of the American Chemical Society* **1941,** *63*, 3091-3096.

9. Flory, P. J. Molecular size distribution in three dimensional polymers. III. Tetrafunctional branching units. *Journal of the American Chemical Society* **1941,** *63*, 3096-3100.
10. Stockmayer, W. H. Theory of molecular size distribution and gel formation in branched polymers II General cross linking. *Journal of Chemical Physics* **1944,** *12* (4), 125-131.
11. Stockmayer, W. H.; Jacobson, H. Gel formation in vinyl-divinyl copolymers. *Journal of Chemical Physics* **1943,** *11* (8), 393-393.
12. Stockmayer, W. H. Theory of molecular size distribution and gel formation in branched-chain polymers. *Journal of Chemical Physics* **1943,** *11* (2), 45-55.
13. Bannister, I.; Billingham, N. C.; Armes, S. P. Monte Carlo modelling of living branching copolymerisation of monovinyl and divinyl monomers: comparison of simulated and experimental data for ATRP copolymerisation of methacrylic monomers. *Soft Matter* **2009,** *5* (18), 3495-3504.
14. Yan, D. Y.; Zhou, Z. P. Theoretical study on the linking process of divinyl compounds with living precursors .1. Uniform precursor chains. *Macromolecular Theory and Simulations* **1997,** *6* (6), 1211-1235.
15. Lee, J. H.; Lee, H. B.; Andrade, J. D. Blood compatibility of polyethylene oxide surfaces. *Progress in Polymer Science* **1995,** *20* (6), 1043-1079.
16. Cushing, M. C.; Anseth, K. S. Hydrogel cell cultures. *Science* **2007,** *316* (5828), 1133-1134.
17. Lutolf, M. P. Spotlight on hydrogels. *Nature Materials* **2009,** *8* (6), 451-453.
18. Lutolf, M. P.; Hubbell, J. A. Synthetic biomaterials as instructive extracellular microenvironments for morphogenesis in tissue engineering. *Nature Biotechnology* **2005,** *23* (1), 47-55.
19. Tibbitt, M. W.; Anseth, K. S. Hydrogels as extracellular matrix mimics for 3D cell culture. *Biotechnology and Bioengineering* **2009,** *103* (4), 655-663.
20. Leal, C.; Bouxsein, N. F.; Ewert, K. K.; Safinya, C. R. Highly efficient gene silencing activity of siRNA embedded in a nanostructured gyroid cubic lipid matrix. *Journal of the American Chemical Society* **2010,** *132* (47), 16841-16847.
21. Gniadecki, R. Regulation of keratinocyte proliferation. *General Pharmacology* **1998,** *30* (5), 619-622.
22. Massumi, M.; Hoveizi, E.; Baktash, P.; Hooti, A.; Ghazizadeh, L.; Nadri, S.; Pourasgari, F.; Hajarizadeh, A.; Soleimani, M.; Nabiuni, M.; Khorramizadeh, M. R. Efficient programming of human eye conjunctiva-derived induced pluripotent stem (ECiPS) cells into definitive endoderm-like cells. *Experimental Cell Research* **2014,** *322* (1), 51-61.

Appendices

A. Sample Preparation for Gel Permeation Chromatography

1. While bubbling under argon, draw out 100μl from polymer solution during or after polymer reaction using a glass syringe.
2. Dilute the sample in 2 ml dimethylformamide (DMF) or tetrahydrofuran (THF) depending on the GPC eluent.
3. Pass the diluted sample through aluminum oxide and cotton wool to remove the copper.
4. Filter the solution through 0.2μm filter to protect GPC columns.
5. Run GPC for 35 minutes.

B. Sample Preparation for Proton Nuclear Magnetic Resonance

1. Polymer is re-suspended in Deuterium Oxide (or Chloroform-D) to a final concentration of 5mg/ml
2. This solution is then pipetted into special ^{1}H NMR tubes
3. The ^{1}H NMR spectrum is analysed using the DELTA processing software

C. Sample Preparation for Zetasizer

1. Weigh out 2mg of the polymer and re-suspend in distilled water to make 0.2mg/ml stock solution
2. Make up 0.02mg/ml of DNA (GFP or G-luciferase) stock solution
3. Make up the following polymer to DNA ratios: 1:1, 3:1, 5:1, at the same DNA concentration (0.01mg/ml)
4. A minimum of 1ml is required to fill a standard potential or size measurement tube
5. Measure using Zetasizer Nano-ZS90

D. Experimental Protocol for Agarose Gel Electrophoresis

Materials needed: Agarose
TAE Buffer
6X Sample Loading Buffer
DNA ladder standard
Electrophoresis chamber
Power supply
Gel casting tray and combs
DNA stain

TAE Buffer: 4.84 g Tris Base
1.14 ml Glacial Acetic Acid
2 ml 0.5M EDTA (pH 8.0)
Bring the total volume up to 1L with water
Add Tris base to ~900 ml H_2O. Add acetic acid and EDTA to solution and mix. Pour mixture into 1 L graduated cylinder and add H_2O to a total volume of 1 L.

6X Sample Loading Buffer:
1 ml sterile H_2O
1 ml glycerol
~ 0.05 mg bromophenol blue to make the buffer deep blue
SYBR®Safe DNA gel stain

Preparing the agarose gel:

1. Measure 0.7 g Agarose powder and add it to a 100 ml TAE Buffer
2. Melt the agarose in a microwave or hot water bath until the solution becomes clear. Usually 2 minutes in microwave.
3. Let the solution cool to about 50-55°C, swirling the flask occasionally to cool evenly.
4. Add 10μl of SYBR®Safe DNA stain when solution has cooled to ~ 40°C
5. Place the combs in the gel casting tray.
6. Pour the melted agarose solution into the casting tray and let cool until it is solid (appear as milky white solution).
7. Place the gel in the electrophoresis chamber.
8. Add TAE Buffer so that there is about 2-3 mm of buffer over the gel.

Loading and running the gel

1. Add 6 μl of 6X Sample Loading Buffer to each 25 μl sample
2. Record the order each sample will be loaded on the gel, controls and ladder.
3. Carefully pipette 20 μl of each sample/Sample Loading Buffer

mixture into separate wells in the gel.
4. Pipette 10 µl of the DNA ladder standard into at least one well
5. Connect the positive electrode to the positive inlet (red) and negative electrode to the negative inlet (black).
6. Run the gel at 80V for 30-45 minutes depending the size of the DNA
7. Bubbles should be seen rising from both sides of the chamber indicating that the setup is working.
8. The bands should be visible and checked every 10 minutes.
9. Visualize the bands under short wave bypass on G-Box.

E. Experimental Protocol for Cell Splitting

1. Pre-warm trypsin to 37°C in water bath
2. Sterilize all equipment, flasks, pipettes and falcon tubes before placing them in the culture hood
3. Remove culture media and wash cells once with Hanks buffer
4. Add 6 ml of pre-warmed trypsin to the flask and incubate for 2 minutes

Note: incubation time is cell type dependent.

F. Experiemental Protocol for Cell Freezing and Thawing

1. Pre-warm growth media in 37°C water bath
2. Thaw frozen cells in water bath until only $3/4^{th}$ of the cells are in solution
3. Quickly spry with 70% IMS and place in culture hood
4. After the solution is completely thawed, pipette the complete cell suspension into a 15ml tube
5. Slowly add the pre-warmed media into the 15ml tube and centrifuge at 1200rpm for 5 minutes.
6. Discard

G. Experimental Protocol for 2D Cell Seeding on Hydrogel Surface

1. All performance in hood
2. Prepare polymer solution of poly(PEGDA) in DMEM serum media at certain concentration

3. Prepare the photoinitiator Irgacure 2959 solution in PBS
4. Mix polymer solution and photoinitiator Irgacure 2959 solution to reach a final concentration of 30% (w/v) of polymer and 0.2% (w/v) of photoinitiator
5. Transfer mixture into 96-well plate (25 µl per well).
6. Photocrosslink the solution with a UV light source (OmniCure S1000, LumenDynamics Group Inc.) for 30 seconds.
7. Wash gel by HBSS, 10 min in incubator 3 times
8. Wash gel by culture media, 20 min in incubator 2 times
9. Split, count cells and concentrate/dilute cell suspension to 50,000 cell/ml in culture media (DMEM+1%PS+10%FBS)
10. Add 100 µl (about 5,000 cell per well for 96 well-plate or 4 well-slides) cell suspension on the gel surface
11. Leave plate in incubator for 2-4 h to let cell attach on the gel
12. Culture in incubator, change media every 1-2 days

H. Experimental Protocol for Transfection of Cultured Cells: (96-well Plate)

Cells should be transfected when they are 60-80% confluent

1. Prepare 0.2 µg/µl of polymer stock solution in distilled water

Note: When using commercial transfection agents follow protocol provided by manufacturer

2. Prepare 0.02 µg/µl of DNA in DMEM serum/growth medium.
3. Mix DNA with Polymer to obtain certain ratio of polymer:DNA

For higher ratios use more polymers.

4. Vortex the solution and incubate at RT for 15 minutes.
5. Add the 100 µl of polyplex solution to the cells and incubate at 37°C, 5% CO_2 for 4 hours.
6. After the incubation period. Remove the polyplex solution from the cells and wash cells and add pre-warmed serum/growth medium.
7. Incubate the cells for 48 hours and measure protein expression

I. Experimental Protocol for AlamarBlue® Protocol for Cell Viability: (96-well Plate)

1. Prepare alamarBlue® working solution by adding 800 µl of the alamarBlue® to 10 ml of Hanks buffer.

2. Remove growth media from the cells and wash once with Hanks buffer
3. Add 1 ml of alamarBlue® working solution to each well and incubate at culture conditions for 1-4 hours.
4. Pipette out 100 µl of the solution into a clear 96-well plate after the time has elapsed.
5. Measure absorbance at ex: 550nm and em: 595nm
6. Subtract the absorbance values of Hank's balanced salt solution only from the absorbance values of the alamarBlue® in Hank's balanced salt solution (ratio 1:9).

Refer to Alamar Blue® guidelines for instructions on calculating reduction values.

J. Conference Proceedings

- Aied, A., **Zhao, T.**, Mauerer, E., South, A., Carroll, O., Greiser, U., Pandit, A., Wang, W., 'Knotted Polymer Structures: Efficient Nucleic Acid Delivery Agents'. *Podium presentation* at the 25th European Conference on Biomaterials, Madrid, Spain, Sep. 8^{th}-13^{th} 2013

K. Peer-reviewed Articles

- **Zhao, T.**, Zhang, H., Newland, B., Aied, A., Zhou, D., Wang, W. 'Significance of branching for transfection: synthesis of highly branched degradable functional poly(dimethylaminoethyl methacrylate) by vinyl oligomer combination' *ANGEWANDTE CHEMIE INTERNATIONAL EDITION*, 2014, 53(24), 6095-6100**.**
- **Zhao, T.**, Zheng, Y., Poly, J., Wang, W. 'Controlled multi-vinyl monomer homopolymerization through vinyl oligomer combination as a universal approach to hyperbranched architectures' *NATURE COMMUNICATIONS*, 2013, 4, article number: 1874.
- Zheng, Y., **Zhao, T.**, Newland, B., Poly, J., Wang, W. 'Controlled homopolymerization of multi-vinyl monomers: dendritic polymers synthesized via an optimized ATRA reaction' *CHEMCAL COMMUNICATIONS*, 2013, 49, 10124-10126. **(Joint first author)**

- Wang, D., **Zhao, T.**, Zhu, X., Yan, D., Wang, W. 'Bioapplications of hyperbranched polymers' *CHEMICAL SOCIETY REVIEWS*, 2014, Advance Article, **DOI:** 10.1039/C4CS00229F
- Newland, B., Aied, A., Pinoncely, A. V., Zheng, Y., **Zhao, T.**, Zhang, H., Niemeier, R., Dowd, E., Pandit, A., Wang, W. 'Untying a nanoscale knotted polymer structure to linear chains for efficient gene delivery in vitro and to the brain' *NANOSCALE*, 2014, 6, 7526-7533.
- Kennedy, R., Hassan, W., Tochwin, A., **Zhao, T.**, Dong, Y., Wang, Q., Tai, H., **Wang, W.** 'In situ formed hybrid hydrogels from PEG based multifunctional hyperbranched copolymers: a RAFT approach' *POLYMER CHEMISTRY*, 2014, 5 (6), 1838-1842.
- Zhang, H., Bré, L., **Zhao, T.**, Zheng, Y, **Wang, W.** 'Mussel-inspired hyperbranched poly (amino ester) polymer as strong wet tissue adhesive' *BIOMATERIALS*, 2014, 35, 711-719.
- Zhang, H., Bre, L., **Zhao, T.**, Newland, B., Da Costa, M., **Wang, W.** 'A biomimetic hyperbranched poly (amino ester)-based nanocomposite as a tunable bone adhesive for sternal closure' *JOURNAL OF MATERIALS CHEMISTRY B*, 2014, 2, 4067-4071.
- Cao, H., Dong, Y., Aied, A., **Zhao, T.**, Chen, X., Wang, W., Pandit, A., 'Acetal-linked branched poly(dimethyl-aminoethyl methacrylate) as an acid cleavable gene vector with reduced cytotoxicity' *CHEMICAL COMMUNICATIONS*, 2014, 50, 15565-15568.